THE EFFECTS OF CHANGES IN ENGINE GEOMETRY ON THE BREATHING AND COMBUSTION IN A SPARK IGNITION ENGINE

by

Hugh Anthony Newlyn, BSc(Eng), CEng, MIMechE.

Thesis submitted for the degree of Doctor of Philosophy of the Council for National Academic Awards.

School of Mechanical and Production Engineering,
Leicester Polytechnic,
Leicester.

May 1982

In collaboration with

Weslake & Company,
Rye,
Sussex.

ACKNOWLEDGEMENTS

I would like to express my gratitude to the following:

Professor D.J. Picken for his support and supervision;

Mr. B.T. Pritchard-Lovell of Weslake & Co., for his continued assistance;

Dr. P.C. Few for his advice;

Mr. R. Smith of the technical staff in the School of Mechanical and Production Engineering for his assistance with the project.

CONTENTS

CHAPTER 7 - CONCLUSIONS AND SUGGESTIONS FOR FURTHER WORK

ABSTRACT

The effects of changes in engine geometry on the breathing and combustion processes in a spark ignition engine have been investigated.

It has been shown that a survey of engine geometry can readily illustrate design limitations in three areas : Fluid dynamic, Mechanical and Thermodynamic, and so reduce the extent of investigation available to the designer.

The induction performance has been analysed mathematically and comparisons made with experimental work.

The results indicate that an assessment of the effect of changes of geometry can be made using empirical relationships without complex mathematics.

An attempt has been made to relate the turbulent to laminar flame speed ratio to the engine's physical parameters. These results compare well with previously published work by other workers.

Aim of the programme:

The aim of the programme was to investigate the effects of engine geometry changes on the breathing and combustion efficiency in a spark ignition engine.

The work is intended to indicate the relative benefits or penalties of changes in engine geometry with the object of assessing the requirements for lean burn operation.

Proposal:

The current emphasis on engine fuel economy and exhaust emissions have emphasised the need for a deeper understanding of the combustion process in the S.I. engine.

It has been shown that combustion chamber surface to volume ratio is a major factor when considering hydrocarbon emissions (Ref. 7, 57, 58).

Burn rate, and hence NO_x emissions, are a function of the inflamed volume characteristics of the combustion chamber. (Ref. 20, 53, 55).

A detailed knowledge of the chamber geometry is essential if the emission characteristics of a design is to be assessed. The burn rate will also be influenced by the turbulence in the combustion chamber as indicated by the turbulent burning velocity, U_T. The dependence of the burning velocity on the turbulence level is usually related to the turbulent intensity u' (Ref. 43, 44, 49). This, however, is an internal characteristic of the in-cylinder conditions and not within the designer's ability to predict.

As all pre-ignition turbulence is a function of the induction system and engine cylinder geometry in conjunction with the piston motion, it should be possible to relate the burning velocity to the engine geometry. Under this premise an attempt has been made to investigate the breathing and combustion characteristics of a spark ignition engine as influenced by changes in engine geometry.

Programme objectives:

The project was approached with certain objectives in mind, namely:

(i) In the geometry and breathing analysis, special reference be made to the 4 valve/cylinder configuration and the input data to the programme be kept to a minimum to enable a true comparison to be made.

The result was to input three items of data, the bore/stroke ratio, the valve included angle and the swept volume.

(ii) The results of the breathing performance analysis should be useable, and not rely entirely on complex computations. To attain this end, the computer calculations were validated experimentally and then the results related to those predicted by empirical expressions developed by other research workers (Ref. 13, 14).

(iii) The prediction of the combustion events should be related to geometrical data to enable a broad survey to be made.

(iv) Validation of the results of the combustion calculations be made by comparison to work done on the CFR (Co-ordinating Fuel Research) engine.

As this engine has a zero squish and low swirl combustion chamber, use of the spherically radiating flame front intersecting with a right cylinder would be applicable. By this means the range of experimental evidence to compare with the theoretical predictions could be broadened beyond that possible for an individual worker.

NOMENCLATURE

The nomenclature used is defined in the text or given in the associated figures.

CHAPTER 1

REVIEW OF PREVIOUS WORK

CHAPTER 1 - REVIEW OF PREVIOUS WORK

1.1 Effects of engine geometry on engine performance:

The geometric configuration of an engine will control all aspects of its performance, including the mechanical efficiency, thermodynamic efficiency and specific power output. The term 'geometry' will include major design features such as the swept volume, number of cylinders and more detailed considerations like the combustion chamber shape and induction system detail. This work deals with geometric effects on the ability of the engine to induce charge and the possible effects on its subsequent combustion characteristics.

The major reference work on engine configuration is by Taylor (Ref. 1), who calls on many sources to give a broad based discussion on the influence of various engine geometry changes on performance. Much of the discussion is related to the effects on volumetric efficiency, and by using an analogy with the steady flow process and the principles of dimensional analysis, Taylor produces a relationship for the volumetric efficiency.

$$\eta_v = \phi\left\{\frac{u}{a}, \frac{P_e}{P_i}, \frac{aL}{u}, \frac{T_i C_p}{FQ_c}, \frac{T_c C_p}{FQ_c}, F, R_1 \text{ --- } R_n\right\}$$

where, η_v = volumetric efficiency

u = a characteristic velocity

P_e = exhaust pressure

P_i = inlet pressure

a = sonic velocity at inlet

ρ = inlet density

μ = inlet viscosity

T_i = inlet temperature

T_c = coolant temperature

S = stroke

F = fuel/air ratio

Q_c = heat of combustion of fuel

The ratio $\frac{u}{a}$ is termed the 'Mach index' and $\frac{aL\rho}{\mu}$ the Reynolds number.

The terms R_1 --- R_n are engine design ratios related to the gas flow through the engine and will include such things as the compression ratio.

As no account is taken here of the inlet valve timing and valve lift, these quantities must be incorporated into the characteristic velocity u. This is done using the mean inlet flow coefficient which is a function of the inlet tract design, valve lift and valve opening period.

A new dimensionless group is derived, still termed the 'inlet Mach index' or Gulp factor, and is defined as:

$$Z = \frac{1}{n}\left[\frac{B}{D}\right]^2 \frac{V_p}{2C_m a}$$

where, B = cylinder bore

D = inlet valve diameter

n = number of inlet valves

V_p = mean piston speed

C_m = mean inlet flow coefficient

The parameter Z is suggested as a design tool and it is stated that "engines should be designed, if possible, so that Z does not exceed 0.5".

This is because, as Z exceeds 0.5, the volumetric efficiency falls rapidly due to pressure loss through the inlet valve. It should be noted that the analysis of Z is related to operation without dynamic effects in the induction and exhaust process, and with small valve overlap, 20^{o} or less being stated as normal. This is certainly not the case with high speed engines using dynamic effects.

The Reynolds number, being a measure of the relative inertia and viscous forces, has little influence on the volumetric efficiency as the viscous forces are too small to affect the flow under normal operating circumstances. This was confirmed using three geometrically similar engines.

An attempt to take into account the dynamic aspect of the flow processes in the engine was made by King (Ref. 2).

Several assumptions are made in deriding the use of 'inlet mach index', but the basic point that is missed is that in the derivation of Z no attempt is made to include inertia effects and hence it cannot give an absolute comparison of breathing capabilities under true operating conditions. Its value lies in determining the relative operating condition of an engine.

A refinement to the use of the Gulp factor was suggested by Fututani and Watanabe (Ref. 3) who suggested the introduction of volumetric efficiency and valve opening period. Their definition of a mean inlet mach number, 'Mim', was

$$Mim = \frac{180\eta_v}{\theta_{ic} - \theta_{io}} \cdot Z.$$

This, however, cannot be used as a design tool as η_v is unknown. They suggest that with η_v = 100% the value of Mim so calculated is a better index for predicting engine speed at which volumetric efficiency decreases.

The relationships between combustion characteristics and the engine configuration are far more complex and interrelated and it is unlikely that any simple expressions can be found that will give a true indication of the combustion characteristics.

It is apparent from the observations and experience of very high speed engines, Nakamura (Ref. 4) that the burning velocity in an engine can be related to the engine rotational speed. Exactly what the intermediate relationships are that bring about this phenomena are difficult to assess.

In addition to engine speed the burning velocity can also be influenced by the combustion chamber geometry in the form of squish areas and chamber compactness.

Use of a simple dimensionless group like the Reynolds number in the intake pipe to relate engine speed to burning velocity proved to be inadequate as shown by Taylor (Ref. 5) and some additional information related to the combustion chamber geometry should be considered.

Actual combustion performance must include thermal efficiency and exhaust emissions. Combustion chamber surface to volume ratio will become an important consideration in this respect as it directly affects the hydrocarbon emissions and thermal efficiency as shown by Siewert and Scheffler (Ref. 6, 7).

References to further work on combustion characteristics is given in Chapter 6.

1.2 Poppet valve steady flow

The analysis presented in this thesis of the intake and exhaust events is that of a quasi-steady condition, where pipe and cylinder states are assumed steady for a finite period, usually one or two degrees of crank angle rotation.

In order to be able to determine the increment of flow during this period, the characteristics of the valve and port at any given valve lift and pressure conditions are required. This information is usually presented in the form of a discharge coefficient. This discharge coefficient C_d is defined as the ratio of the 'effective area' of a frictionless nozzle that would pass the same flow under the same conditions relative to a datum area. This datum area is arbitrary and care must be taken when comparing results to make sure that the same reference area has been used.

Various reference areas have been used (Ref. 8, 9, 10). The three most common being:

(i) A fixed reference area, either the valve curtain area at a lift of one quarter the valve diameter or the valve throat area.

(ii) A varying area equal to the valve curtain area.

(iii) A three stage area related to certain intervals of valve lift as defined by Kastner et al (Ref. 8). This has been done to relate to the three states of flow through the valve as the valve lift is increased.

Woods (Ref. 9) investigated the flow through dual, vertical exhaust valves and the reference area used in this analysis was the area at the minimum port diameter.

The definition of the discharge coefficient becomes:

$$C_d = \frac{A_E}{n \times \frac{\pi}{4} D_T^2}$$

where A_E = effective area

n = number of valves

D_T = Valve throat diameter

A review of the results of tests on various inlet and exhaust valve arrangements is given by Annand & Roe (Ref. 10). These results have been related to the valve curtain area and illustrate the flow regimes more effectively than when a fixed reference area is used. The effect of pressure ratio on the discharge coefficient is demonstrated in the paper by Woods and Khan (Ref. 11). An approximation to this can be obtained by use of the expression derived by Annand (Ref. 10). This has been corrected for use with a fixed reference area and is given in Chapter 3.

Comparison of the data presented by Woods and Khan on inflow through an inlet valve and outflow indicate very little change in the effective area, and it was decided to use the same characteristics for inflow and outflow for both intake and exhaust valves.

1.3 Wave action in the intake duct

There are basically two approaches available in determining the effect of induction pipe dynamics on the filling of the

cylinder (i) treatment of the system as a resonator and (ii) a solution to the momentum and continuity equations describing the condition in the duct.

The first of these presents a simple useful way of determining peaks in the induction performance if a suitable model can be described.

The work by Vorum (Ref. 12) treats the induction cycle as two distinct parts. Firstly, with the valve open the system acts like a Helmholtz resonator with the kinetic mass of gas in the pipe reacting with the static mass in the cylinder. Secondly, when the valve is closed the pipe is isolated and resonates as an organ pipe. The concept of the organ pipe resonator is used by Yagi et al (Ref. 13) with claimed success if synchronization of a pressure pulse, with top dead centre (t.d.c.) in the valve open period, is achieved. This is discussed in Chapter 5 where some doubt is thrown on the selection of t.d.c. as the synchronization point.

The series of articles on induction ramming by Broome (Ref. 14) attempts to derive design relationships that will predict peaks in the volumetric efficiency curves due to wave effects in, and the inertia of, the induction pipe air mass. Two parameters are produced, the wave ram parameter θ_t, which is half the period of the intake pipe expressed in crankshaft degrees, and a dimensionless inertial ram parameter ϕ_t which is related to θ_t by the expression

$$\phi_t = \theta_t^2 \quad \frac{V_{cyl}}{V_{pi}}$$

V_{cyl} = swept volume

V_{pi} = intake pipe volume

Design graphs are given indicating areas of optimum wave and inertial ram conditions. The concept of an inertia ram parameter is also used in Ref. 13, and is termed the 'inertia supercharge index'.

The two papers by Broome and Yagi et al are further discussed in Chapter 5 and form the basis for comparison with the current analysis. The more detailed computational analysis giving a pressure-time history of events in the induction pipe and cylinder is based on work by Benson et al (Ref. 15), and are described in the paper by Blair and Coulburn (Ref. 16). Boundary conditions, when the intake valve is open, are as derived in Annand & Roe (Ref. 10) and used by Prosser (Ref. 17). The derivation of the equations and the method of solution by the method of characteristics is given in Chapter 5

1.4 Combustion modelling

The increase in activity in mathematical modelling applied to internal combustion engines in the past 10 - 15 years has been a direct result of the exhaust emissions legislation and pressures for increased fuel economy. The largest category of models has been termed phenomenological models and can be said to be composed of separate physically based submodels of important identifiable phenomena. These models are built on a 1st Law of Thermodynamics formulation, where time or engine crank angle is the only really independent variable, and as such are sometimes referred to as zero-dimensional. This is

to be contrasted with the detailed multi-dimensional models which attempt to give detailed geometry - dependent, spatial resolution of state variables such as fluid velocity, temperature, species, etc.

Within the main model, sub-models are required in order to describe the following phenomena, (i) turbulent flame propagation, (ii) heat transfer, (iii) hydrocarbon emissions, and (iv) knock. Within this thesis an attempt has been made to relate the first phenomena to engine geometry.

One approach to modelling of burnrate can be expressed as:

$$\frac{dmb}{dt} = \rho A_f U_T$$

where ρ is the unburnt gas density, A_f is a flame front area and U_T is the turbulent burning velocity.

The assumptions required here are:

(i) An assumed flame front geometry, and,

(ii) specification of U_T.

A spherical flame front is commonly employed and U_T has been related to the laminar flame speed by a constant, i.e:

$$U_T = K U_L$$

where K is often directly related to engine speed. This type of expression is consistent with the observed linear relationship between turbulent intensity and engine speed, and has been used successfully by many research workers (Ref. 18, 19, 20). This technique does, however, require a value of K to be determined for a particular engine by tests and it does assume constant turbulent intensity during compression of the unburnt charge. Or, U_T can only vary at a given engine speed due to

changes in U_L. This model has not been found to be very successful during the ignition delay period or for variations in spark timing.

An alternative approach to burnrate modelling has been the turbulent entrainment model developed by Blizard & Keck (Ref. 21) and later extended by Tabaczynski et al (Ref. 22). The original proposals, later modified by McCuston, Lavoie and Kauffman (Ref. 23), assume that the turbulent fluid is composed of a series of discrete eddies of characteristic radius ℓ_e that are entrained by the flame front at an entrainment velocity U_e. The eddies burn at the laminar flame speed U_L in a characteristic eddy burn-up time. $\tau_b = \ell_e / U_L$

A more detailed eddy structure was proposed by Tabaczynski which envisaged an individual eddy to be composed of dissipative eddies of the Taylor microscale (λ) order, where laminar combustion dominates, separated by rod-like, stringy regions of a highly dissipative nature, of an order defined by the Kolmogorov scale (η). Within these very fine structures burning is assumed instantaneous and the rate of propagation of ignition sites is $u' + U_L$, where u' is the turbulent intensity and U_L the laminar flame speed.

A relationship between the turbulent scales and the turbulent intensity for isotropic turbulence is given by Andrews et al (Ref. 24) as:-

$$\frac{\lambda^2}{\ell_e} = 48.64 \frac{\nu}{u'}$$

where ν is the kinematic viscosity.

This reference also defines a Reynolds number, based on the Taylor microscale (R_λ) and an expression for the Kolmogorov scale η.

$$R_\lambda = \frac{u' \lambda}{\nu}$$

$$\eta = \lambda 15^{-\frac{1}{4}} R_\lambda^{-\frac{1}{2}}$$

Representative values are shown in Fig. 1.4/1. It is also stated that the large eddies are of a size comparable to that of the width of the flow and are anisotropic, which has important considerations when considering chamber height and compactness.

Changes in the eddy integral scale and the turbulent intensity are accommodated in the combustion model by use of the density changes and the results gave the correct trends in combustion duration and ignition delay period.

This work was developed by Tabaczynski, Trinker and Shannon (Ref. 25) who attempted to provide a smooth transition between the ignition delay period and the fully developed turbulent burning region. Assumptions were made relating the turbulent intensity to mean piston speed and experimental verification carried out on an engine with a 4 valve/cylinder configuration. Discrepancies were found between theoretically predicted mass fraction burnt plots and experimental results. This was explained as being due to the assumption of the flame front area being generated spherically from a point of ignition in a cylinder having a right circular cylinder geometry.

This approximation is acceptable with long duration combustion but will cause discrepancies when the duration is short with relatively small piston movement. Accurate prediction of laminar flame speed is another area of difficulty.

Further development of the turbulent entrainment model was carried out by Hires et al (Ref. 26) who developed expressions for ignition delay period and combustion duration. The expression for ignition delay is derived from the assumption that it is proportional to the time to burn a turbulent eddy, expressed as the characteristic eddy burn-time τ_b.

$$\Delta t_{ig} = C_1 \tau_b$$

The expression derived is given in Chapter 6 and contains a constant which is stated as unique to an engine geometry but independent of engine operating conditions. The expressions developed in the reference were related to the laminar flame speed U_L, the turbulent intensity u', the integral scale ℓ_e and the Taylor microscale λ. To investigate geometry changes these quantities need to be replaced by engine design parameters.

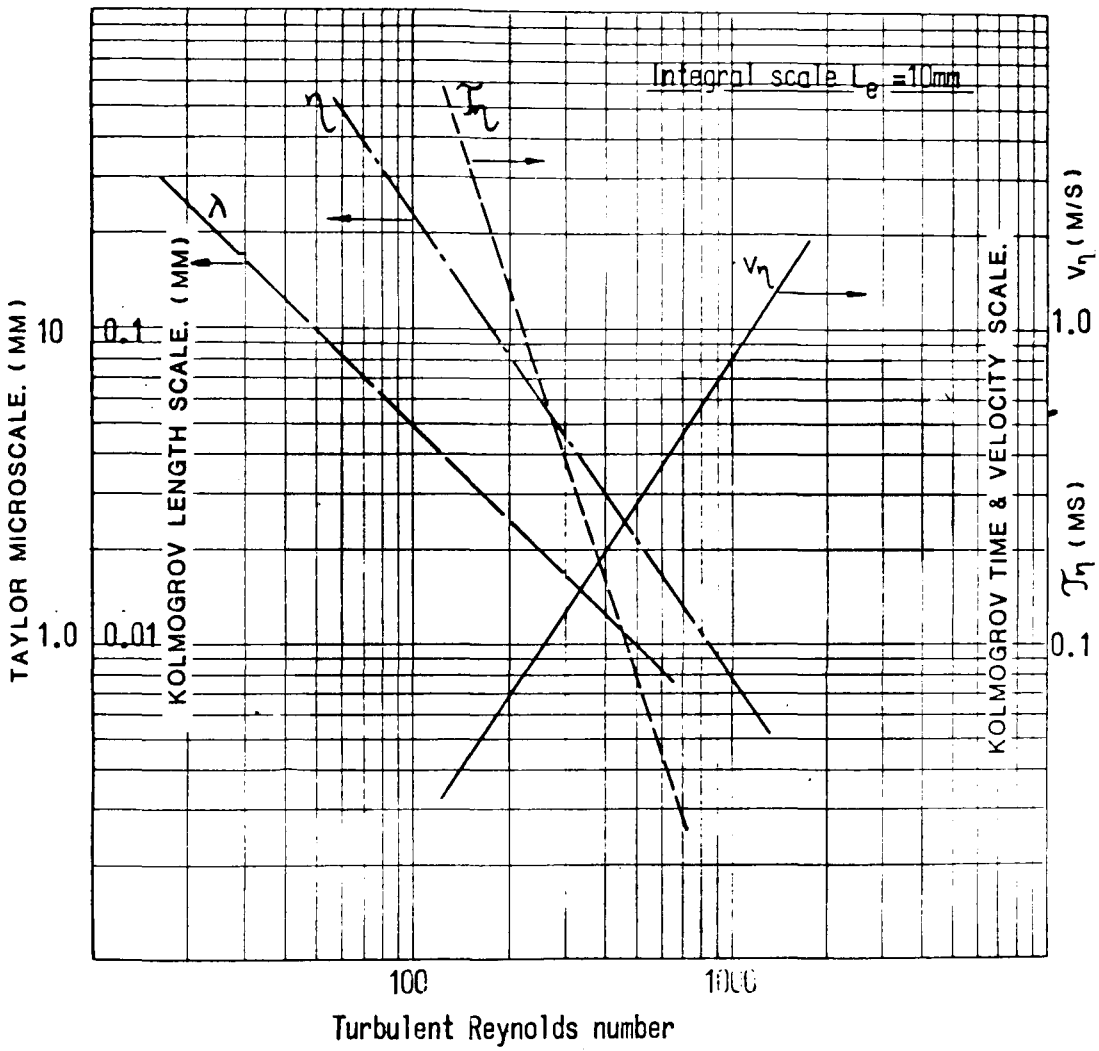

(FIG 1.4/1) Graph of the Taylor microscale and related Kolmogrov scales for an integral scale of 10mm (comparable to the height of a combustion chamber). From Ref 24.

CHAPTER 2

INVESTIGATION INTO THE GEOMETRY OF THE 4-VALVE/CYLINDER CONFIGURATION

2. CHAPTER 2 - INVESTIGATION INTO THE GEOMETRY OF THE 4-VALVE/CYLINDER CONFIGURATION

2.1 Introduction:

The 2-inlet/ 2-exhaust pent-roof combustion chamber design dates back to 1912 and has since then been mainly confined to racing engines. A historical review of the design is given in Appendix A1.

The adoption of the design for racing purposes is mainly due to the excellent breathing capabilities of the design which are necessary in order to obtain a high b.m.e.p. The design has additional advantages beneficial to operation at high speed, exhibiting a high burn rate. It has a compact combustion chamber with a centrally located spark plug.

The ability to produce a high burn rate is one that is now becoming increasingly important in production engines when operating with a lean mixture.

It is possible that the economic disadvantage of the 4-valve design could be outweighed by its thermodynamic performance.

2.1.1 Discussion of 4-valve/cylinder configuration

Benefits from the use of the pent-roof configuration are evident in four areas:

1) Air consumption
2) Thermal loading
3) Valve gear dynamics
4) Thermal efficiency.

The most obvious benefit of using 2-inlet valves as opposed to a single valve is in the potentially greater inlet flow area available.

Taking the dimensions given in three references gives the following relationships between inlet valve diameter D_I and the cylinder bore B.

		2-valve	4-valve
(i)	Taylor (Ref. 5)	$D_I = 0.44B$	$D_I = 0.33B$
		% increase in 4-valve curtain area over the 2-valve = 13%	
(ii)	Barnes-Moss (Ref. 27)	$D_I = 0.49B$	$D_I = 0.36B$
		% increase = 8%	
(iii)	Annand & Roe (Ref. 10)	$D_I = 0.485B$	$D_I = 0.39B$
		% increase = 29%	

These figures assume that the valve lift/diameter ratio is kept constant. If the lift is maintained at that for the large valve the figures become even more beneficial, being 50%, 47% and 61% respectively. This comparison is purely based on the flow area available. An added advantage occurs when the mean discharge coefficient is examined.

The 2-inlet valve configuration exhibits an enhanced mean inlet discharge coefficient over the case of two isolated valves of the design. Reference to the results in Section 3.5 shows that with a maximum lift set at an $L/_D$ ratio of 0.25,

the dual-valve layout gives an improvement of 11.8% over two isolated valves. If the $L/_D$ ratio is increased to 0.3 the benefit is now 12.9%. Thus the effective inlet valve area available is increased by this amount over the figures previously quoted, making the dual-inlet valve design more attractive with regard to air consumption. In this context the 4-valve pent-roof chamber also benefits from the use of dual-exhaust valves, since smaller valves represent shorter heat flow paths.

Cooling of the exhaust valves is further enhanced by the fact that the perimeter available for heat transfer is increased in the same ratio as the basic flow area. As it is estimated that about 75% of the heat loss from the valve is through the seat, this is particularly advantageous.

The final benefit resulting from the use of dual-valves comes from the dynamics of the valve train. Whilst the use of dual-valves does not necessarily lead to a reduction in valve gear mass, it does reduce the valve gear characteristic speed (S_V).

This is defined by Taylor (Ref. 5) as:

$$S_v = \frac{V_p \, Q}{\sqrt{n}}$$

where:

V_p = mean piston speed Q = bore/stroke ratio

n = number of inlet or exhaust valves per cylinder, whichever is less.

Hence for the same bore/stroke ratio and piston speed, the valve characteristic speed of a 4-valve design is 0.7 of that of a 2-valve.

Alternatively, the piston speed can be increased without reaching dynamic limitations on the valve gear.

Apart from the multiple valve aspect, the pent-roof chamber also has advantages for thermal efficiency.

The research done by Yagi et al (Ref. 13) on small displacement engines attempts to determine the 'actual combustion efficiency' of several designs of combustion chamber. Actual combustion efficency η^*_{comb} is defined by Yagi as the factor by which the air standard efficiency must be multiplied in order to obtain the actual indicated thermal efficiency.

The data presented shows that the pent-roof chamber is comparable to the hemispherical chamber, having η^*_{comb} between 74.5 to 76.5%. The wedge chamber is shown as 73 to 75% and the bath tub 70 to 71.5% This is almost certainly due to the excellent surface to volume ratio of the pent-roof and hemispherical chambers.

2.2 Modelling of the combustion space and spherical flame front

2.2.1 Cylinder head configuration

The basic model for the combustion space was developed after considering several existing cylinder heads of the 4-valve/cylinder configuration and attempting to incorporate the common features.

The basic model consists of two intersecting planes, one containing the inlet valves and the other the exhaust valves. It was assumed that the inlet and exhaust valves were arranged in the fore and aft direction and had a relative included angle, ϕ, which was one of the basic design parameters (Fig. 2.2.1/1). The angular displacement of the two valve planes was calculated using a ratio of inlet to exhaust valve insert diameter, and assuming that the width of the valve planes was proportional in this ratio.

The actual space occupied by valve inserts is related to the valve plane width by a stated amount and the valve inserts are assumed to be arranged at the top of the planes to provide as much freeboard as possible to minimise the interference of the valves with the piston. The actual spacing of the valves is controlled by the limit placed on the size of the bridge pieces between adjacent inlet

and exhaust valve seat inserts and between the two inlet and two exhaust inserts, and cylinder bore clearance.

The size of the bridge pieces that is acceptable under normal conditions has been determined from manufacturing and operating experience and is quoted as a function of inlet valve seat insert diameter (Table 2·1) The value used was 0.07 IID (Inlet Insert Diameter) which is conservative and allows the use of a 14 mm plug. In the case of a racing engine, in order to maximise inlet valve area, the bridge piece can be reduced to 0.055 IID, but this is an absolute minimum and would probably entail the use of a 10 mm plug.

Using this basic data, the size, position and angular displacement of the inlet and exhaust valve seat inserts can be determined. The volume contained by the two included valve planes, the bore and the cylinder head face can be calculated and is the basic combustion space.

In order to produce a realistic combustion chamber it is necessary to allow for the curvature round the perifery. The radius of this curvature was assumed to be the height of the sloping plane at that point on the bore, measured from the cylinder head face. The equations used for determining these basic volumes and surface areas are given in Appendix A2.

The two other constituents of the combustion space are the piston top to cylinder head face volume and the valve pockets in the piston crown.
For all the analysis of the 4-valve/cylinder engine configuration, only flat-topped pistons were considered. The main reason for this was mathematical convenience. Allied to this was the fact that it has proved to be a satisfactory design in practice and allows a full range of compression ratios to be obtained with satisfactory inlet duct geometry. The piston top to cylinder head face volume presents no problem, requiring only the constant K2 to be defined for the clearance at TDC. This can later be modified to allow for piston movement (K22).
The valve pocket volume presents more difficulty as the pockets, if they exist, can be either, (i) full valve cutouts, where at the maximum proximity of the valve and piston the full valve head is recessed into the piston crown, or (ii) partial cutouts, where only a part of the valve interferes with the piston crown. The cutouts for both inlet and exhaust can be any combination of these three conditions and this must be determined before the correct routine can be used in the analysis.
The condition at the maximum proximity of the valves and piston is determined by the piston

movement and the cam characteristics. The equations used for determining the valve pocket volumes and surface areas are shown in Appendix A2.

The valve and valve port geometry for both the inlet and exhaust sides is based on the empirical relationships supplied by Weslake and Company Ltd., of Rye, Sussex, hereafter referred to as Weslakes, which have been derived from their extensive experience of 4-valve/cylinder designs.

2.2.2 Flame front geometry and associated burnt and unburnt region surfaces and volumes

In order to use a burn rate combustion model with the expressions

$$\delta R = U_T \, dt \quad \text{and} \quad \delta M_b = \delta V_f \rho$$

where U_T = entrainment velocity;

δV_f = incremental increase in enflamed volume due to δR,

it is necessary to be able to determine the enflamed volume at any flame radius.

The most common flame front geometry used in burn rate models is that of a sphere radiating from the point of ignition, the flame front being that area cut off by the boundaries of the cylinder head and piston surface. Justification for the use of this model can be found in work done by Curry (Ref. 28) and James (Ref. 18), using ionization probes and

Rashidi (Ref. 29) using photography. Both Curry and Rashidi used the CFR engine which has a zero squish combustion chamber with low swirl. The Renault engine used by James is also zero squish with little swirl.

The flame pattern indicated from these tests is a circular one radiating from the point of ignition. The ignition point in these engines is located to one side of the chamber. As the flame approaches the far side of the chamber there appears to be a flattening of the flame front and a deviation from the circular pattern; this is probably due to non-uniform compression of the unburnt charge ahead of the flame and the proximity of the bare wall at the edges. In the case of a centrally located spark plug this would not occur and the assumption of a spherical flame front would be applicable up to the chamber wall. Data on the flame progression in engines of the 4-valve/cylinder configuration is limited.

The experimental work of Kumagai and Kudo on flame studies in high speed spark ignition engines (Ref. 30) and Nakamura (Ref. 4) both used small displacement 4-valve/cylinder engines. The flame progression was monitored by ionization gaps placed on the central plane along the apex of the valve planes.

The ignition point was varied in Kumagai et al's work, being at the side for the engine speed tests, and then central for subsequent mixture ratio and ignition timing tests.

Some anomilies exist in the relationship between total flame travel time and engine speed. The initial results indicate a reduction in terms of degrees of crank angle with increasing speed, whereas the latter results show an increase in travel time. This could possibly be related to the differing enflamed volume characteristics of the two spark plug positions. An example of this effect is shown in Fig. 6.6/14 which is for a cylindrical chamber. Together with this difference, the characteristics of the burnt volume surface area should be studied.

Nakamuras work used a central ignition point and as such is similar to the previously discussed paper.

Harrow (Ref. 31) produced some flame speed results but there is no indication in this, or in the two previous papers, of flame front geometry, and hence no indication that deviation from a spherical geometry should be considered for this type of engine.

All the above work was of an experimental nature, with no attempt at a theoretical analysis.

However, Tabaczynski et al (Ref. 25) used a

turbulent flame propagation model to predict events in a 4-valve/cylinder spark ignition engine. He did however assume the flame front (enflamed volume) characteristics to be those of a central plug located in a cylindrical combustion chamber, as used by Blizard & Keck (Ref.21) given in Appendix A5. The difference between this and the characteristic for a 4-valve geometry based on the present assumptions are shown in Fig. 2.2.2/1. The difference between the two characteristics could result in the discrepancy shown in the theoretical and experimental curves of mass fraction burnt, this would be most evident in the results relating to the effects of equivalence ratio.

The flame front area characteristic affects the rate at which unburnt charge is engulfed,

i.e. $$\frac{dm_e}{dt} = \rho_u \; A_e \; (u' + U_L)$$

where, m_e = mass engulfed into the flame front

ρ_u = density of unburnt charge

A_e = area of the engulfment front

u' = turbulent intensity

U_L = laminar flame speed

The rate of burning is related to the rate of engulfment by:

$$\frac{dm_b}{dt} = \frac{m_e - m_b}{\tau}$$

where, m_b = burnt mass

τ = characteristic eddy burn time

i.e. $\tau = \lambda / U_L$

λ = Taylor micro-scale

So the effects of equivalence ratio appear in the laminar flame in two regions, (i) the characteristic eddy burn time and, (ii) the rate of engulfment. The flame front characteristic has a direct effect on the rate of engulfment whereas the laminar flame speed's effect is only in relation to its contribution to $(u' + U_L)$. Thus, accurate prediction of A_e is, in this case, more important then U_L.

2.2.2-1 Basic geometry of the enflamed volume

The basic geometry used in determining the enflamed volume is shown in Fig. 2.2.2/2. The computer program uses the nomenclature indicated in the figure. There are three limits at which the equations change:-

(i) Intersection of the flame with the piston crown R>R1,

(ii) Intersection with the radiused edge R>R2,

(iii) Beyond the extent of the valve planes R>R3.

Of these limits R2 and R3 are fixed at any set

geometry but R1 is dependent on the piston position.

The equations used for determining the enflamed volume at any given radius are shown in Appendix A3.

2.2.2-2 Interaction with the valve pockets

Determination of the flame front area associated with valve pockets at any radius entailed some simplification of the geometry. The area is also dependent on the type of pocket, i.e. full or partial.

The areas for inlet and exhaust sides are calculated separately and consist of the product of an arc length and a mean height. The basic geometry and nomenclature are given in Fig.2.2.2/3.

The flame front area in the valve pocket is only calculated if the radius is within the correct limits. These limits called R5 and R6 in the program are determined dependent upon the type of valve pocket. For example, if CODI>0 an inlet valve pocket exists. If PIN>IID it is a full pocket and R5 and R6 are calculated on this basis.

The equations used are shown in Appendix A3.

2.2.2-3 Burnt and unburnt zone heat transfer areas

The heat transfer area of the burnt gas region was determined in order to achieve a more accurate assessment of the heat loss; this should be

reflected in thermal efficiency comparisons with differing geometries.

The basic burnt zone area is circular where the sphere is cut by the valve planes. The limits of the radius are the same as those used for the flame front calculations.

The equations used are shown in Appendix A4.

2.3 Results of computer calculation of engine geometry

The general opinion amongst research workers (Ref. 7, 57, 58) is that the production of hydrocarbons is due to flame quenching in the proximity of the combustion chamber surface and the crevice regions around the piston top land and any squish areas present. Some reduction of these hydrocarbons occurs due to oxidation in the exhaust process and some due to secondary reaction.

The split between quench zone hydrocarbons and crevice region hydrocarbons depends on speed and load and combustion chamber geometry (Ref.58). However the quench zone hydrocarbons present an area where very little can be done to effect a reduction per unit area.

From work by Daniels (Ref.57) the thickness of the quench layer can be expressed as:-

$$q = K P^{-0.52} T^{-0.56}$$

where K is a constant and P and T are the cylinder pressure and temperature.

Hence the quench zone thickness can nominally only be

reduced by an increase in the pressure and temperature in the cylinder. Both of these effects would tend to increase NO_x production.

In addition the quench effect will also be a function of (a) the combustion chamber surface temperature, (b) the heat transfer coefficient between the gas and the cylinder walls and hence the cylinder turbulence. However, little can be done to reduce the actual thickness of the quench zone.

The fractional emissions in the exhaust gas is, therefore, a function of the ratio of the volume of the quench zone to the volume of the combustion chamber, i.e. the surface/volume ratio of the chamber. The surface/volume ratio also influences the thermal efficiency in that percentage chamber heat loss will be related to the mixture and wall temperatures, the heat transfer coefficient and the heat transfer surface.

The variation of surface to volume ratio with the main chamber geometry parameters is shown in Figs. 2.3/1, 2.3/2 and 2.3/3 for swept volumes of 250cc, 375cc and 500cc respectively.

2.3.1 Effects of engine geometry changes on surface to volume ratio

Referring to Fig. 2.3/1-3 reinforces the conclusions of Scheffler (Ref.7) that to design for a low surface to volume ratio requires a low compression ratio, a low bore/stroke ratio and a

large cylinder displacement.

What is perhaps not so obvious is that the relative improvement in the reduction of surface to volume ratio is dependent on the bore/stroke ratio. For instance, increasing the cylinder size from 250cc to 500cc gives a reduction of 21% on S/V ratio at a bore/stroke ratio of 1·4, whereas at 0.8 the reduction is only 18%. However the higher percentage figure is the result of the S/V ratio falling by 0.1, whereas the lower percentage figure is a fall of only 0.058. Thus even though the percentage savings are of a similar order, the higher bore/stroke ratio saving represents a bigger improvement. These results are indicated in Fig. 2.3.1/1.

Changing the cylinder size without reference to total engine capacity is not truly representative of the actual situation and Fig. 2.3.1/2 shows the benefits of reducing the number of cylinders and, effecting an increase in cylinder size on a 2-litre capacity engine. The surface to volume ratio in this case, with a fixed compression ratio of 12:1, can be reduced by 20% when changing from a 6 to a 4-cylinder engine. Another aspect of the changes in geometry on S/V ratio occurs when considering the increase in compression ratio.

With the current trend towards high compression, high turbulence lean burn engines for economy purposes, this could result in high surface to volume ratios and hence high H.C. emissions. However it can be seen that with this configuration a 2-litre 4-cylinder engine, at a compression ratio of 10:1, would have a valve included angle of 26° and a S/V ratio of 0.298 $^{1}/mm$ at a bore/stroke ratio of 1·4.

For the design of an engine of the same configuration and capacity, but with an increased compression ratio of 12:1, and without detrimental effects on the S/V ratio, this could be achieved by decreasing the B/S ratio to 1.03 and increasing the included angle to 24°. It is true that this would result in a reduction of valve curtain area from 8200 mm^2 to 6800 mm^2 or 17%. But at this reduced valve area the pent-roof cylinder head valve area is only slightly below that for a hemi-spherical head at a bore/stroke ratio at the original 1.4 value, Fig. 2.3.1/3.

This illustrates the ability of the pent-roof 4-valve configuration to provide a compact chamber with low S/V ratio without the penalty of poor breathing performance.

2.3.2 Effects of engine geometry changes on breathing performance

A measure of an engine's ability to consume air can be obtained from a study of the "Mean Inlet Mach Index" or Gulp factor, as defined by Taylor (Ref. 1).

Specific design limits are indicated, Fig. 2.3.2/1-3, if the inlet Mach index factor is plotted against bore/stroke ratio for a constant compression ratio.

Engine speeds can be plotted for a limiting inlet Mach index of 0.5, above which there is a considerable reduction in volumetric efficiency as shown by Taylor and Fukutani (Ref. 1,3).

The above results use a mean inlet discharge coefficient of 0.381 as determined from tests, Fig. 2.3.2/2.

If it is desired to design an engine of 500cc cylinder capacity with as compact a combustion chamber as possible, to minimise the surface to volume ratio and to run at a maximum speed of 8000 rev/min, the minimum bore/stroke ratio is 0.8. At 10,000 rev/min, this minimum becomes 1.13, and for 12,000 rev/min about 1.5. However, if the mean inlet discharge coefficient is reduced, perhaps as the result of inducing more turbulence, a 10% reduction changes these bore/stroke ratios

to 0.94, 1.32 and in excess of 2.0. Similar limitations can be determined for other cylinder capacities.

Another limitation on bore/stroke ratio is mean piston speed. If 4500 ft/min (22.9 m/s) is taken as a maximum limitation on a production engine, the bore/stroke ratio at this limiting piston speed can be expressed as follows:-

$$Q = 6.28 \times 10^{-8} \sqrt{V}\, N^{3/2}$$

where, Q = bore/stroke ratio

V = cylinder capacity (cc)

N = engine speed rev/min

hence, limits of bore/stroke ratio can be calculated. These are shown on the bottom of Fig. 2.3.2/3. With a discharge coefficient of 0.381, the limiting bore/stroke ratio on volumetric efficiency at 8000 rev/min for a 500 cc cylinder is 0.8. With regard to piston speed it is 1.0. So piston speed is the limiting factor on the design bore/stroke ratio. However, if the C_m is reduced by more than 14%, the volumetric efficiency becomes the limit on the selection of bore/stroke ratio. This change over between the two limiting conditions can also be seen with the changing cylinder volume. For example, at 10000 rev/min the cylinder of 500 cc capacity requires a reduction of 13.5% in C_m, the 375 cc capacity needs 11.6% reduction and the

250 cc only 8.1% reduction, so the smaller the capacity the more likely it is to be limited by volumetric efficiency.

TABLE 2·1

CYLINDER HEAD DESIGN RELATIONSHIPS

$$A_t = A_p / 0.77$$

$$d_t = d_p / 0.77$$

$$d_v = d_t + 0.025\, d_t$$

$$d_i = d_t + 0.05\, d_t$$

$$t = 0.055\, d_i \ *$$

$$c = d_i + t$$

where A_t = valve throat area

A_p = port area at upstream end

d_p = port diameter

d_t = throat or min. seat insert dia.

d_v = valve head diameter

d_i = valve seat insert dia.

t = bridge between adjacent valves in same plane

c = centre distance between adjacent valves

* This is an absolute minimum and would probably dictate the use of 10 mm spark plugs.

$t = 0.07\, d_i$ would be a more conservative value.

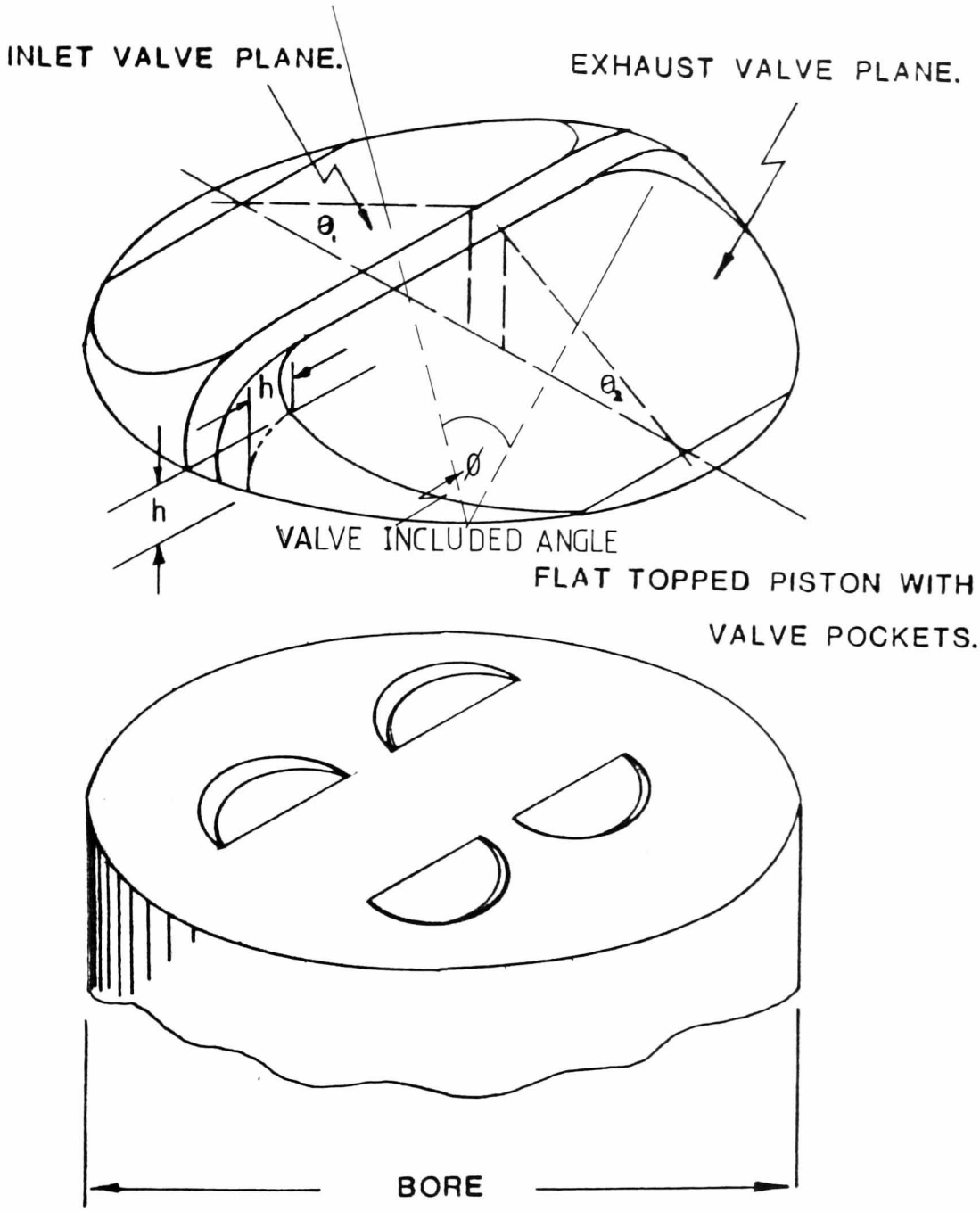

(FIG 2.2.1/1) MODEL USED FOR CYLINDER HEAD ANALYSIS.

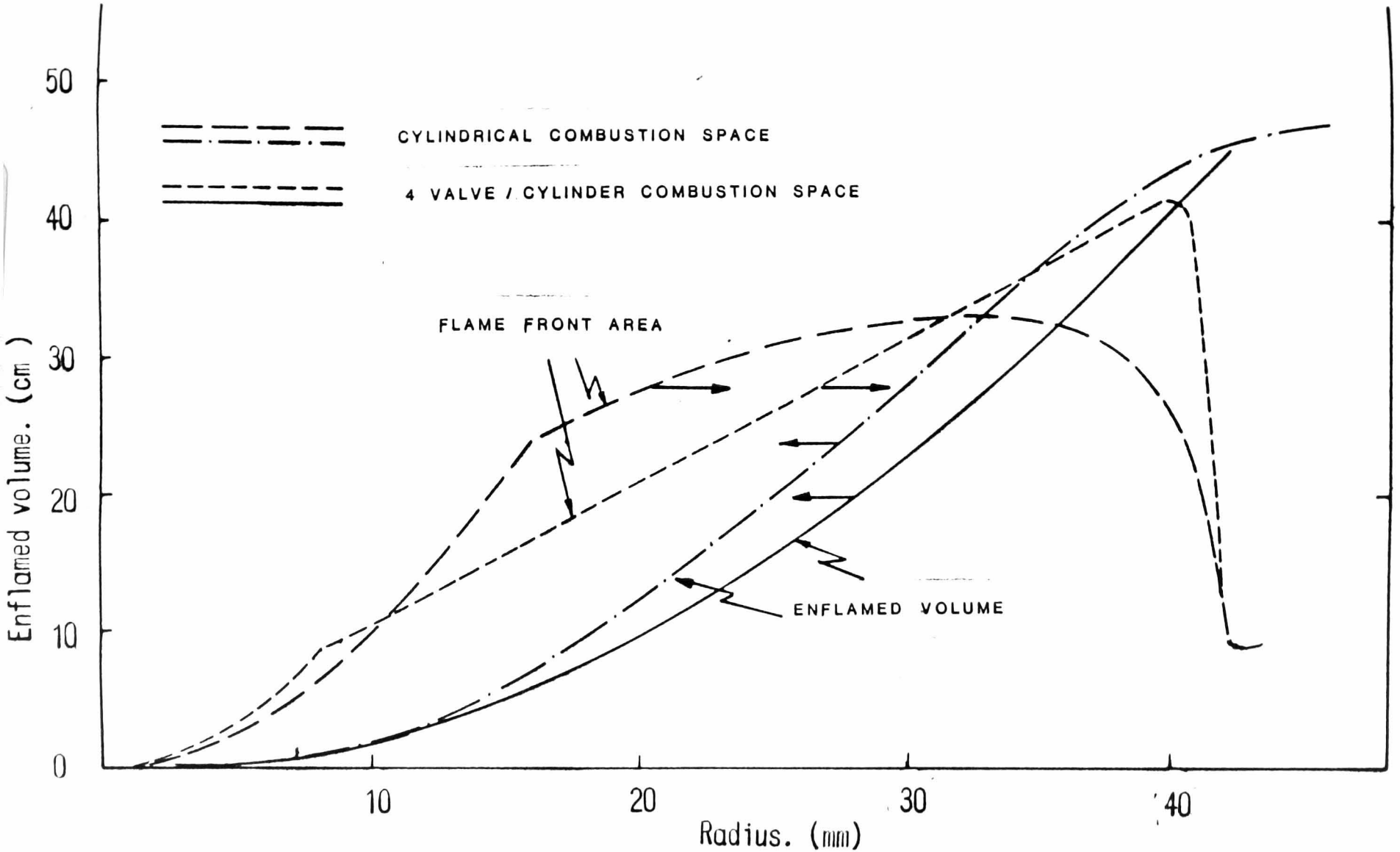

(FIG 2.2.2/1) ENFLAMED VOLUME AND FLAME FRONT AREA AGAINST RADIUS FOR ENGINE CONFIGURATION USED IN REF.25 COMPARED TO 4 VALVE/CYLINDER CONFIGURATION.

FIG 2.2.2/1.

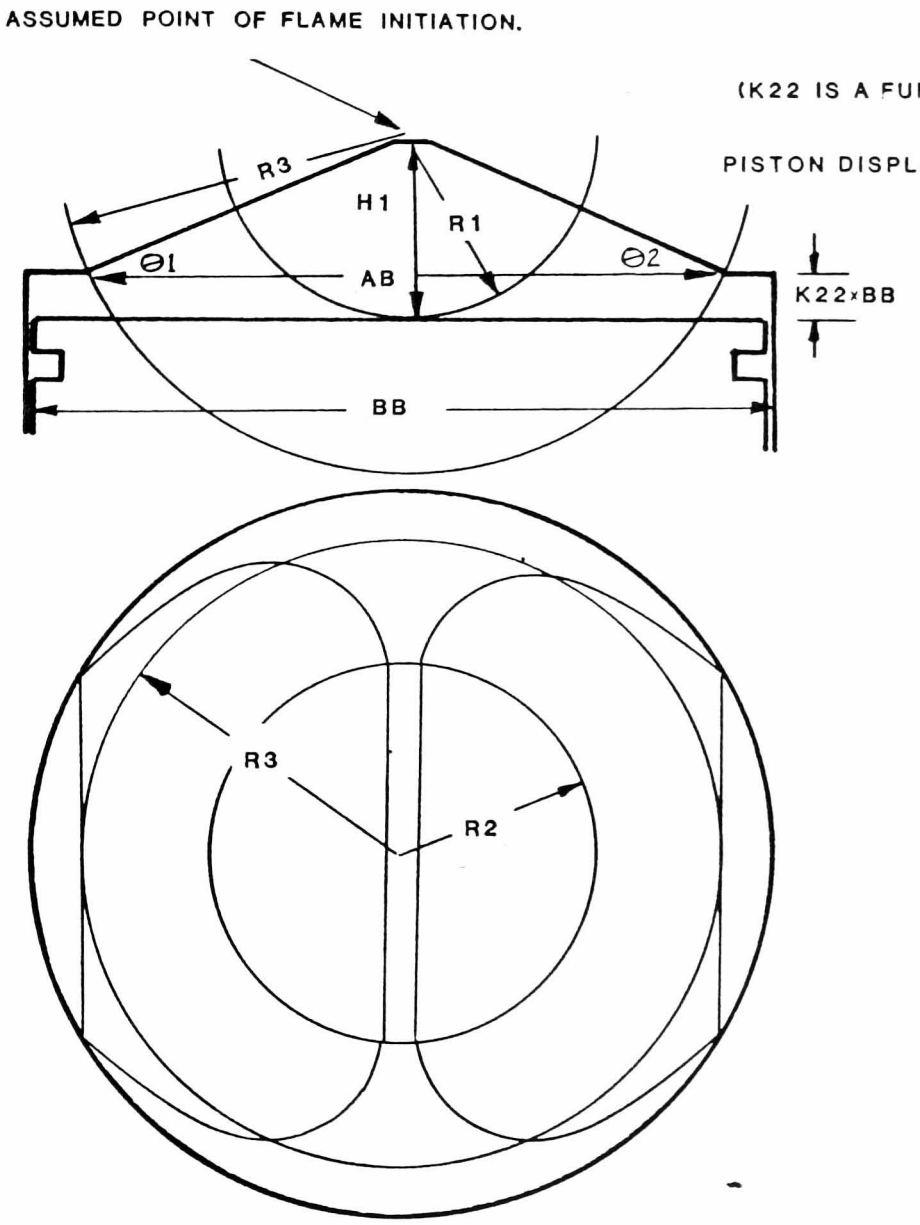

(FIG 2.2.2/2) Basic geometry of enflamed volume.

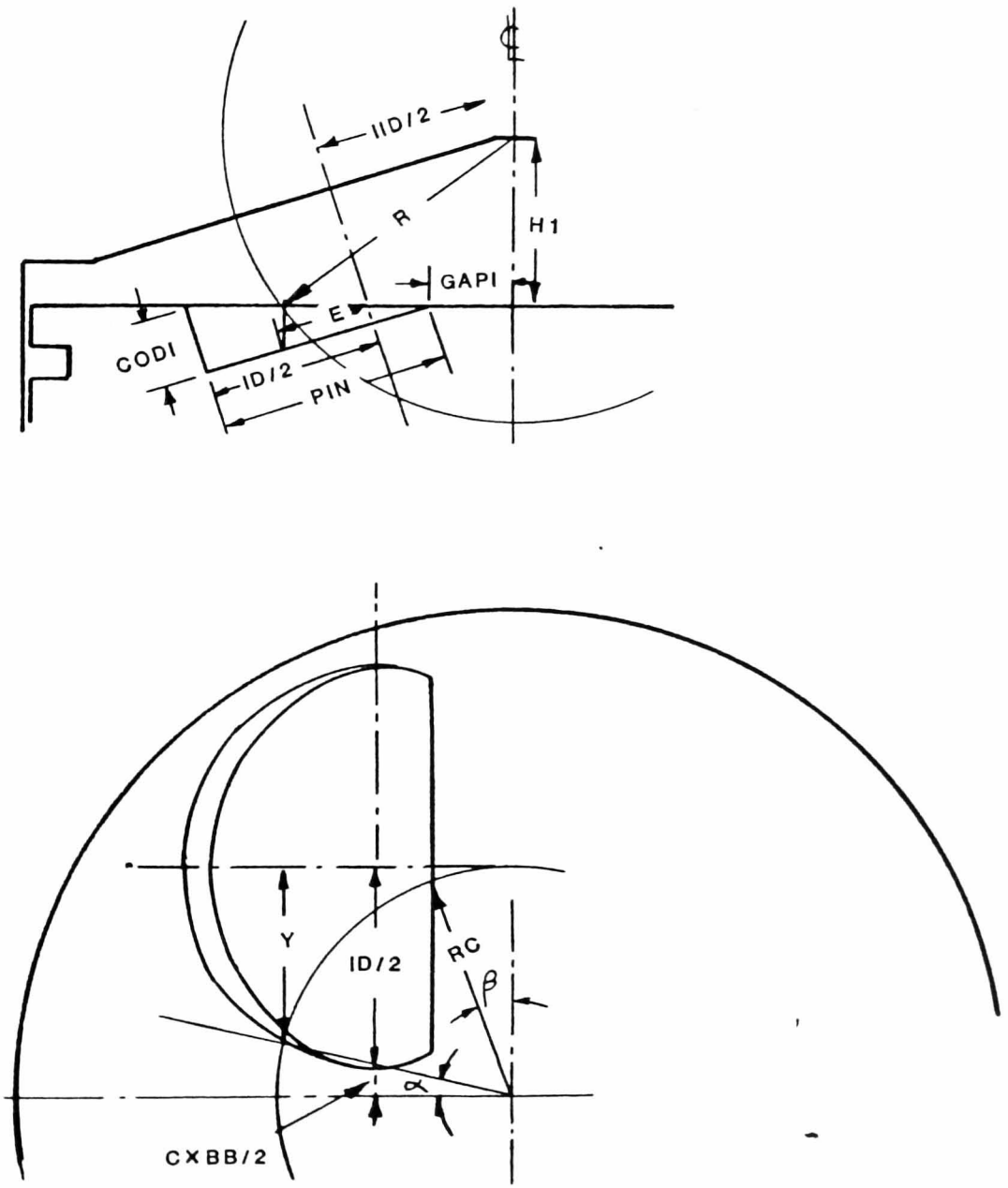

(FIG 2.2.2/3) Valve pocket geometry.
Inlet side.

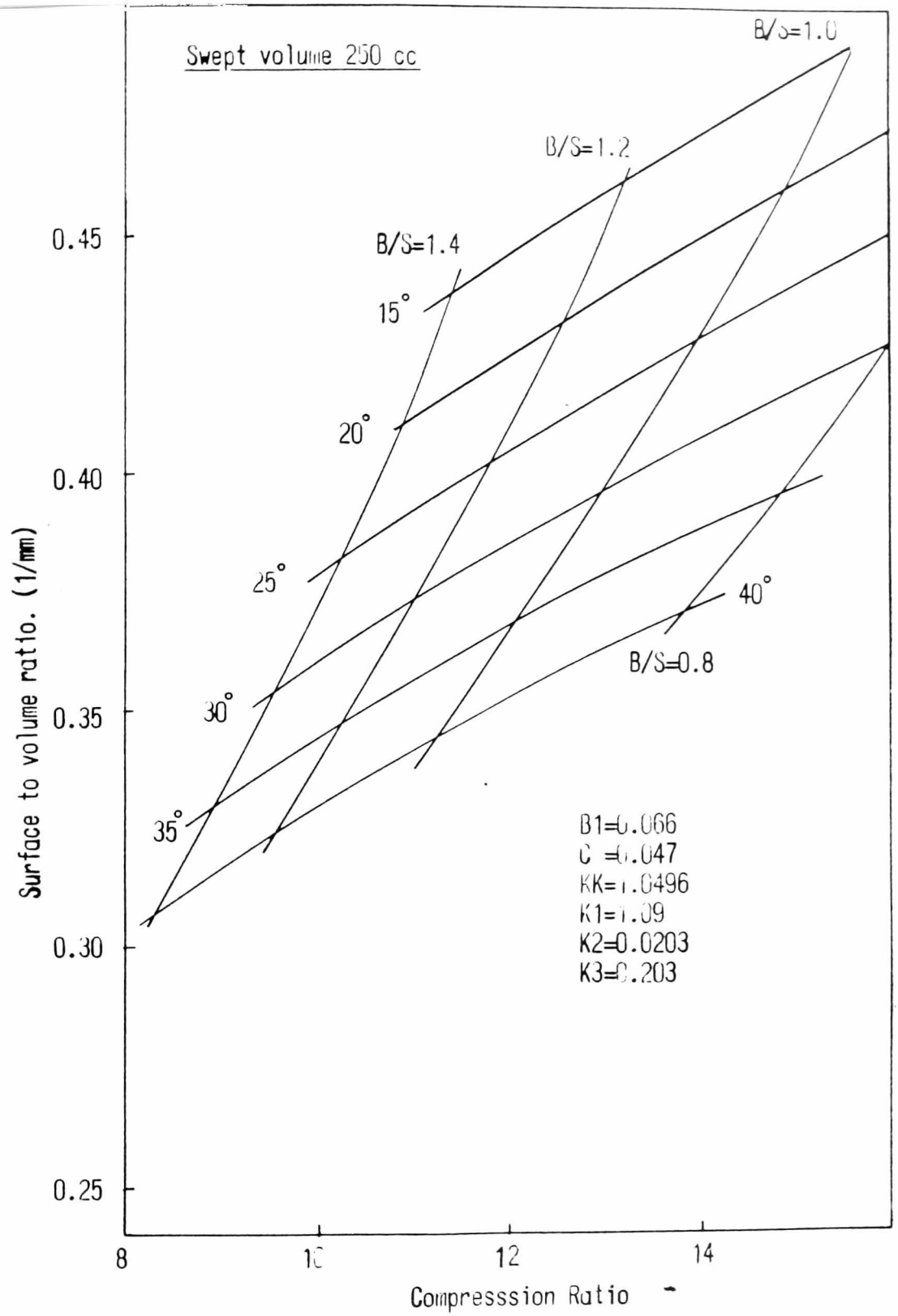

(FIG 2.3/1) SURFACE TO VOLUME RATIO AGAINST COMPRESSION RATIO FOR VARIOUS BORE/STROKE RATIOS AND VALVE INCLUDED ANGLES.

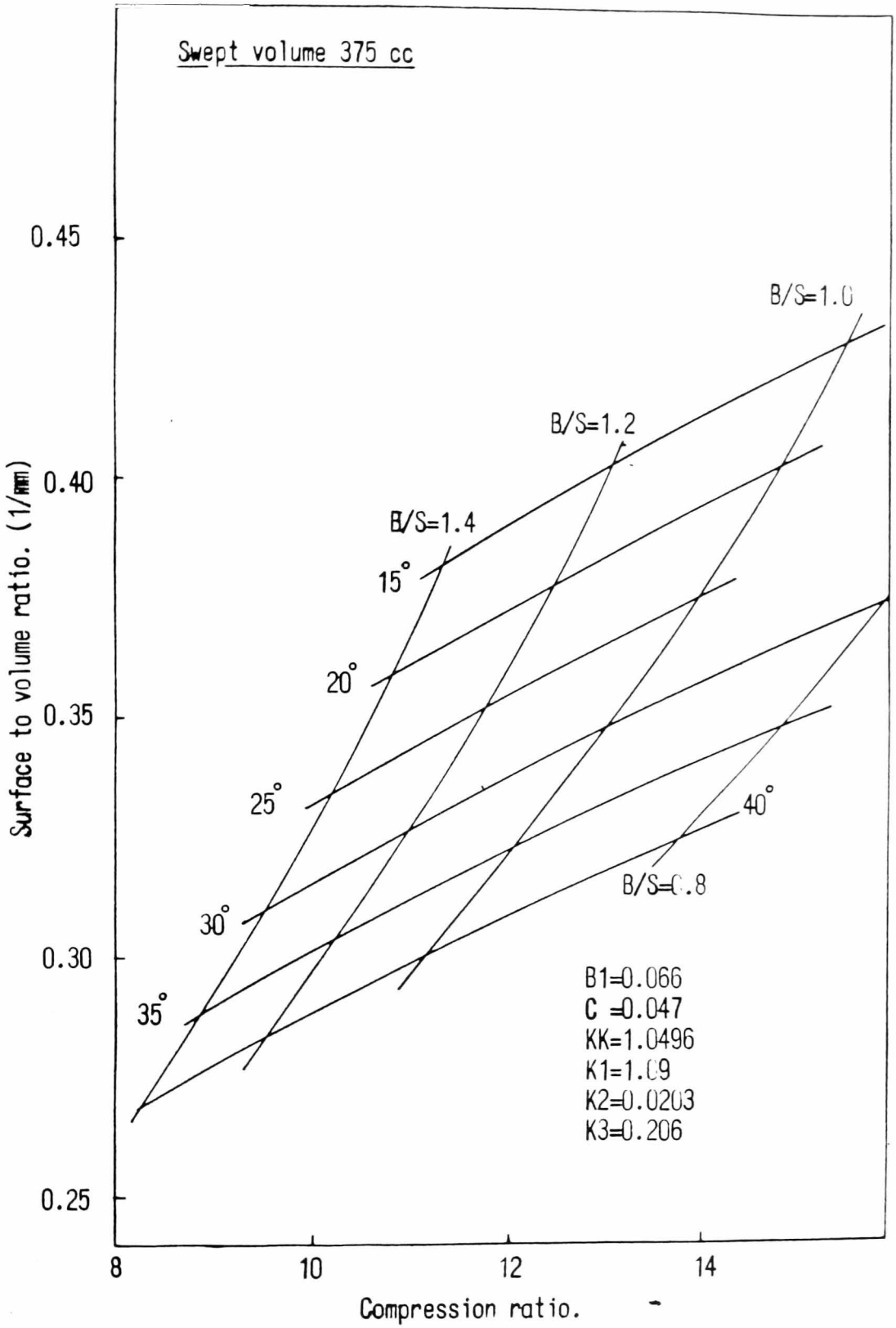

(FIG 2.3/2) SURFACE TO VOLUME RATIO AGAINST COMPRESSION RATIO FOR VARIOUS BORE/STROKE RATIOS AND VALVE INCLUDED ANGLES.

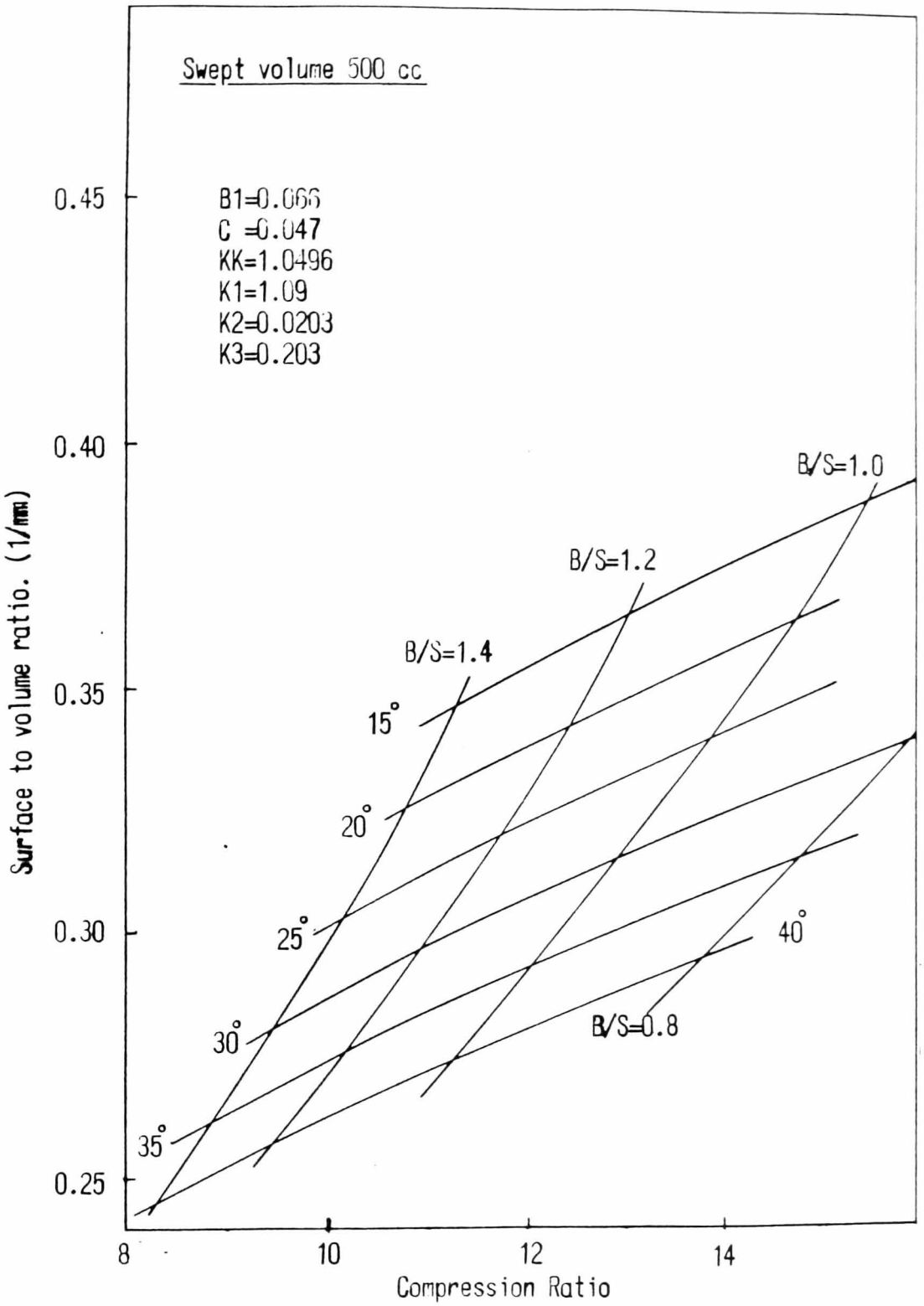

(FIG 2.3/3) SURFACE TO VOLUME RATIO AGAINST COMPRESSION RATIO FOR VARIOUS BORE/STROKE RATIOS AND VALVE INCLUDED ANGLES.

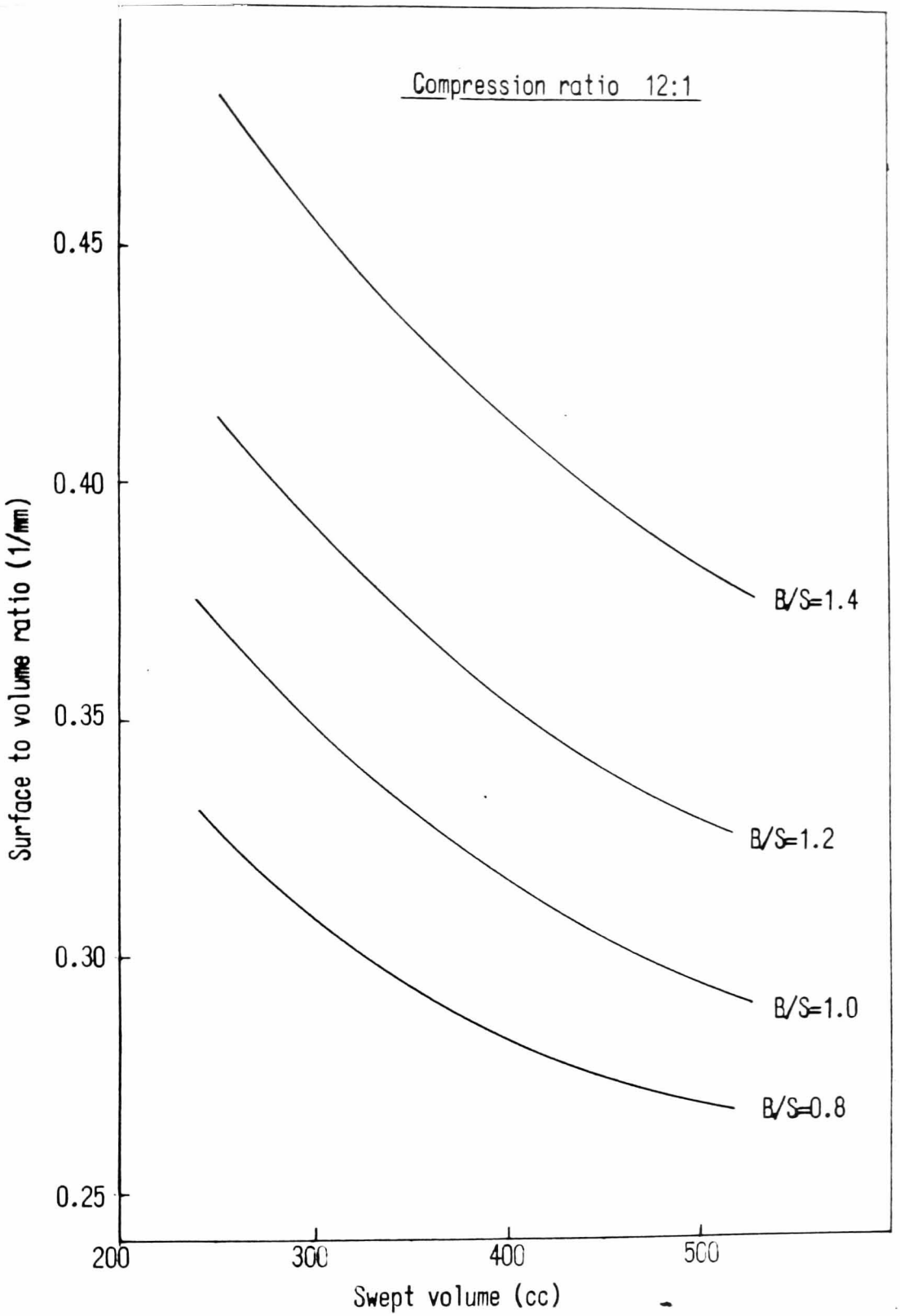

(FIG 2.3.1/1) SURFACE TO VOLUME RATIO AGAINST SWEPT VOLUME FOR VARIOUS BORE/STROKE RATIOS.

FIG 2.3.1/2.

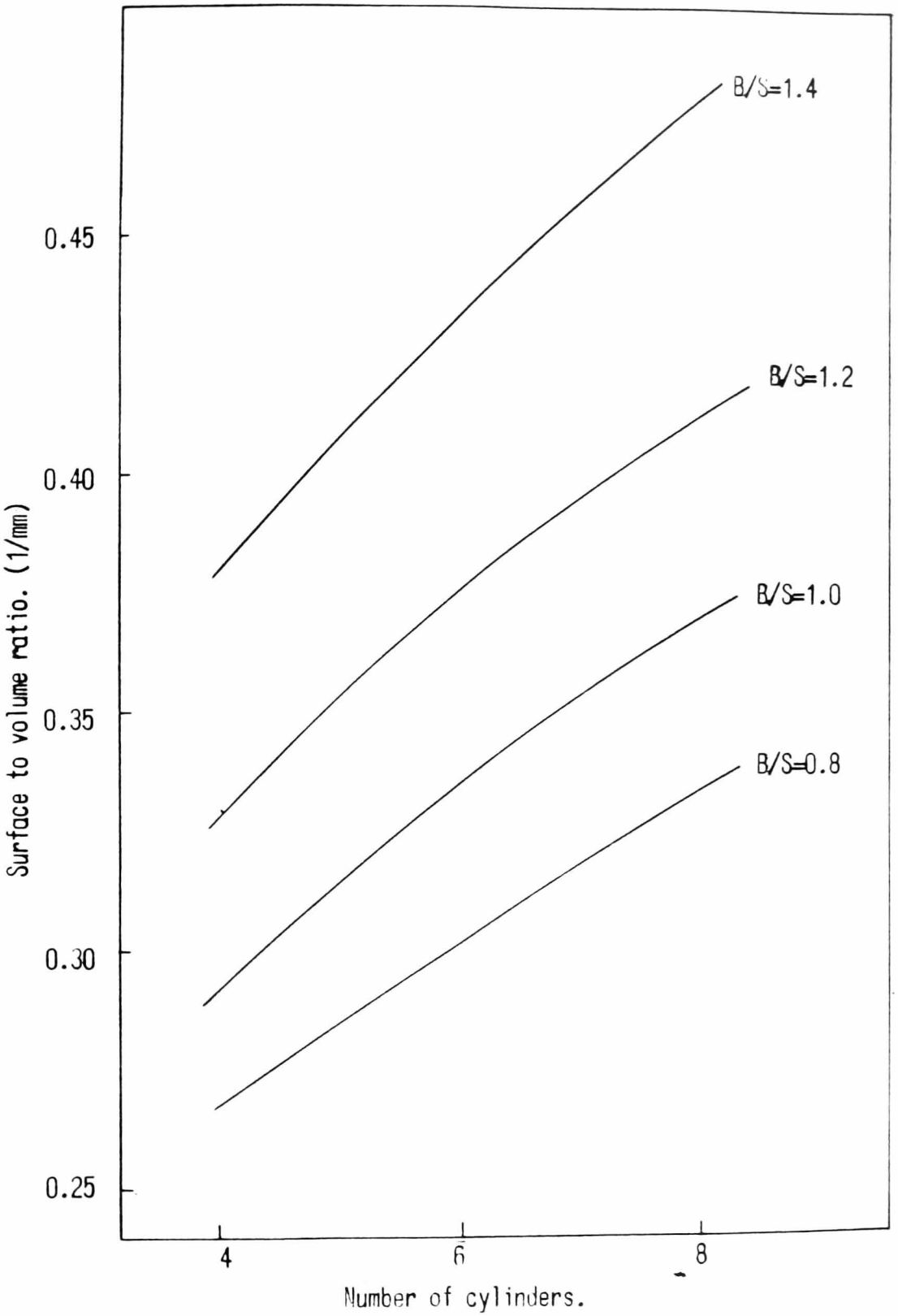

(FIG 2.3.1/2) SURFACE TO VOLUME RATIO AGAINST NUMBER OF CYLINDERS FOR A 2 LITRE ENGINE WITH A 12:1 COMPRESSION RATIO.

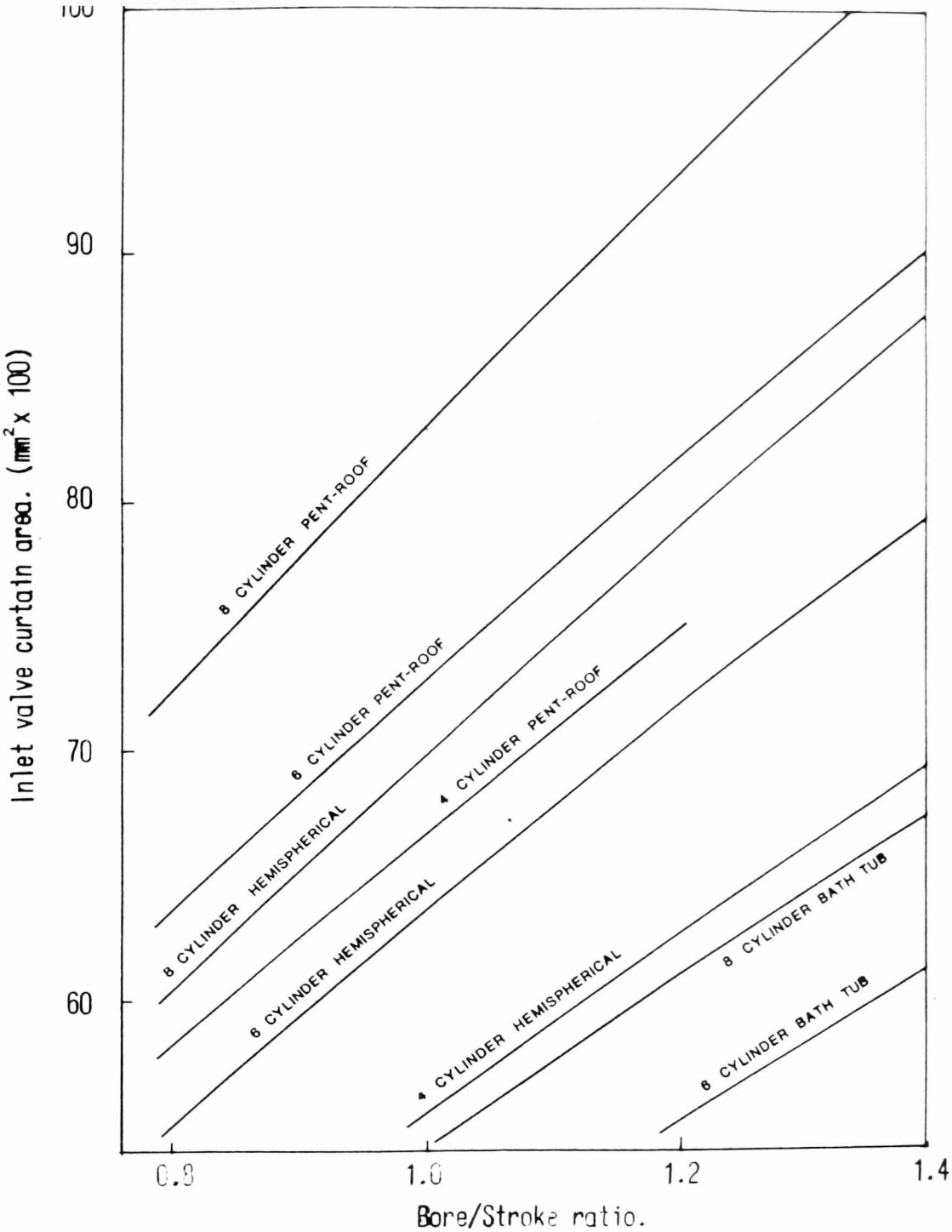

(FIG 2.3.1/3) INLET VALVE CURTAIN AREA AGAINST BORE/STROKE RATIO FOR A 2 LITRE ENGINE.

FIG 2.3.2/1.

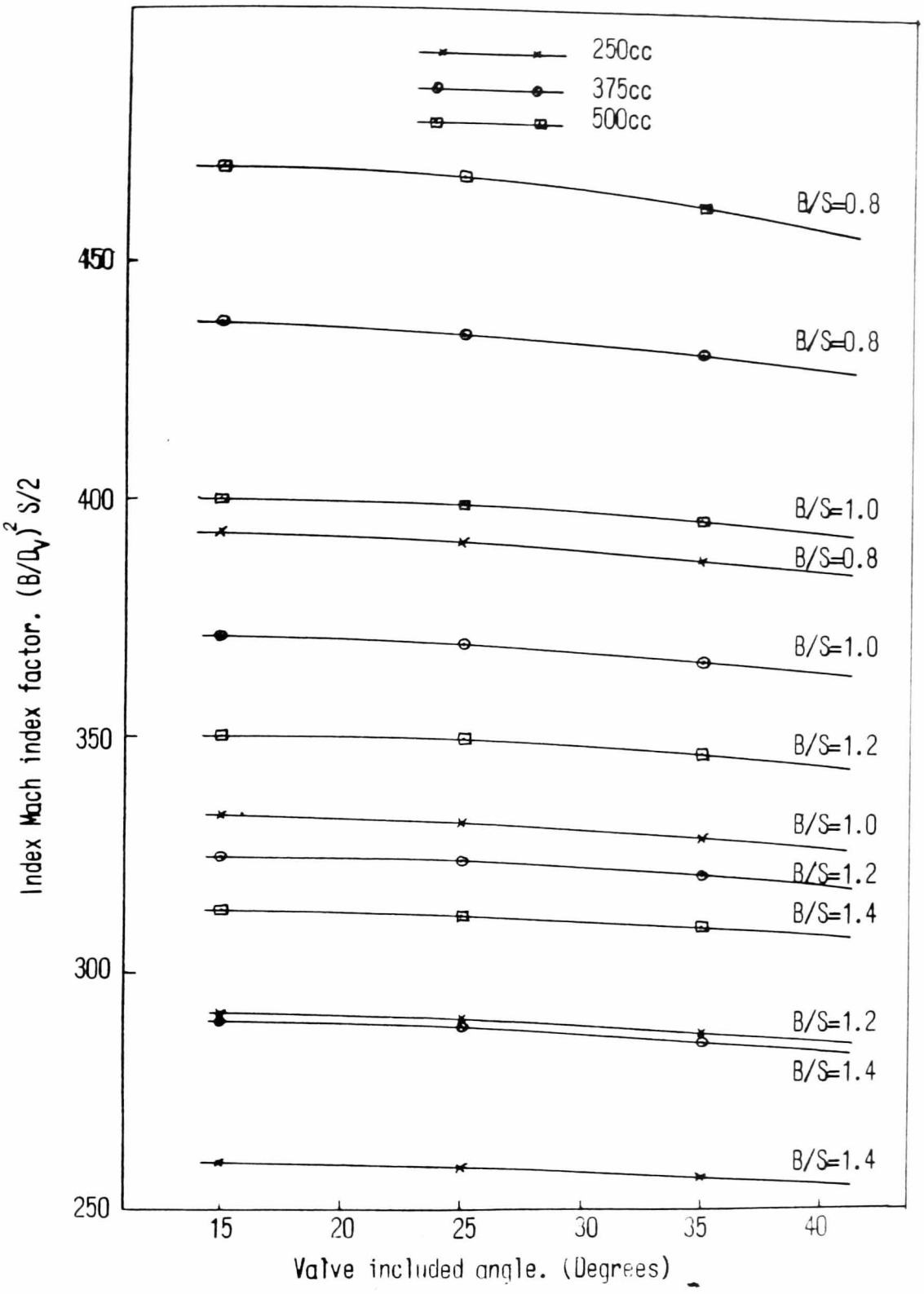

(FIG 2.3.2/1) INLET MACH INDEX FACTOR AGAINST VALVE INCLUDED ANGLE FOR VARIOUS SWEPT VOLUMES AND BORE/STROKE RATIOS.

FIG 2.3.2/2.

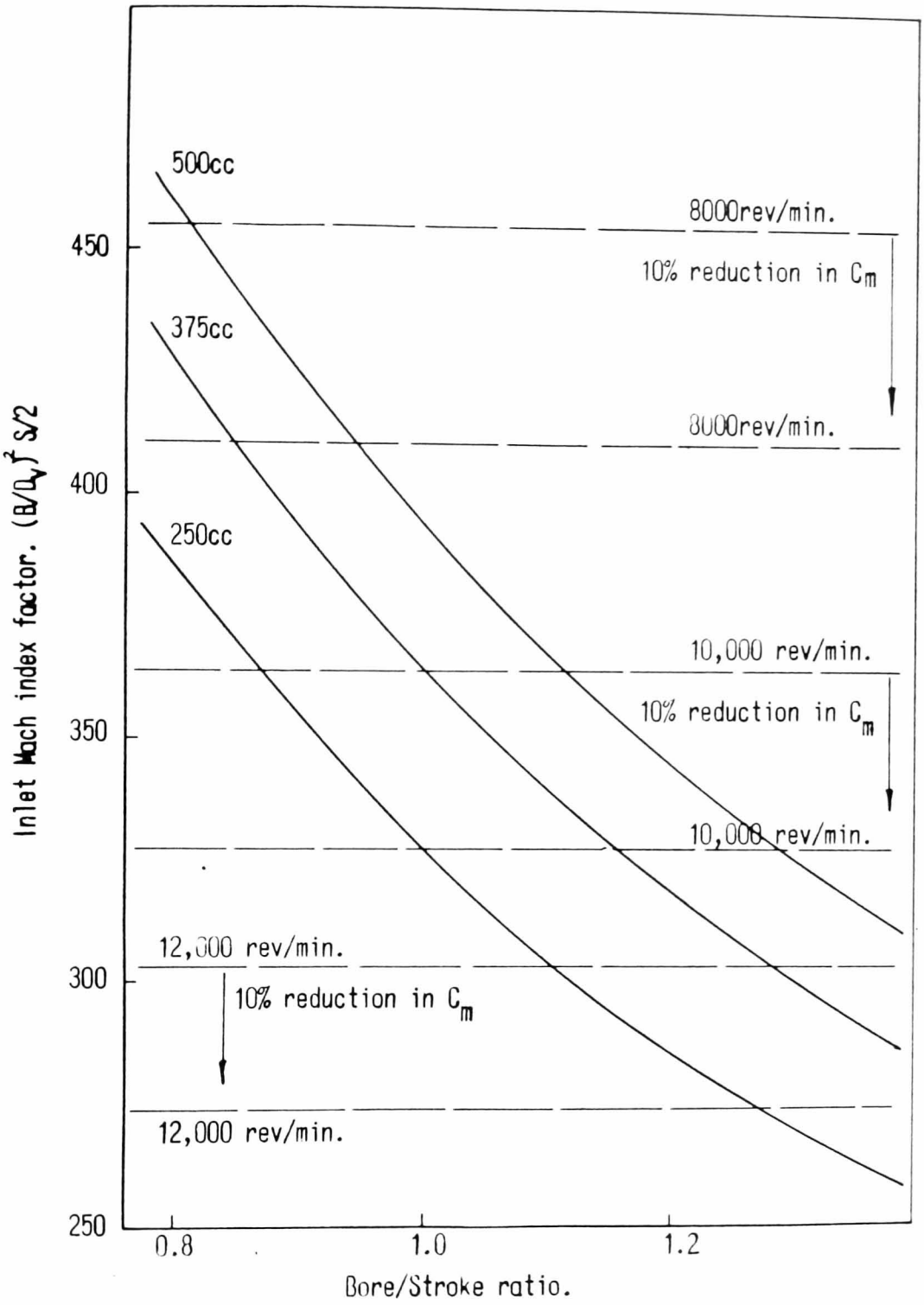

(FIG 2.3.2/2) INLET MACH INDEX FACTOR AGAINST BORE/STROKE RATIO FOR A 40° VALVE INCLUDED ANGLE AND VARIOUS SWEPT VOLUMES.

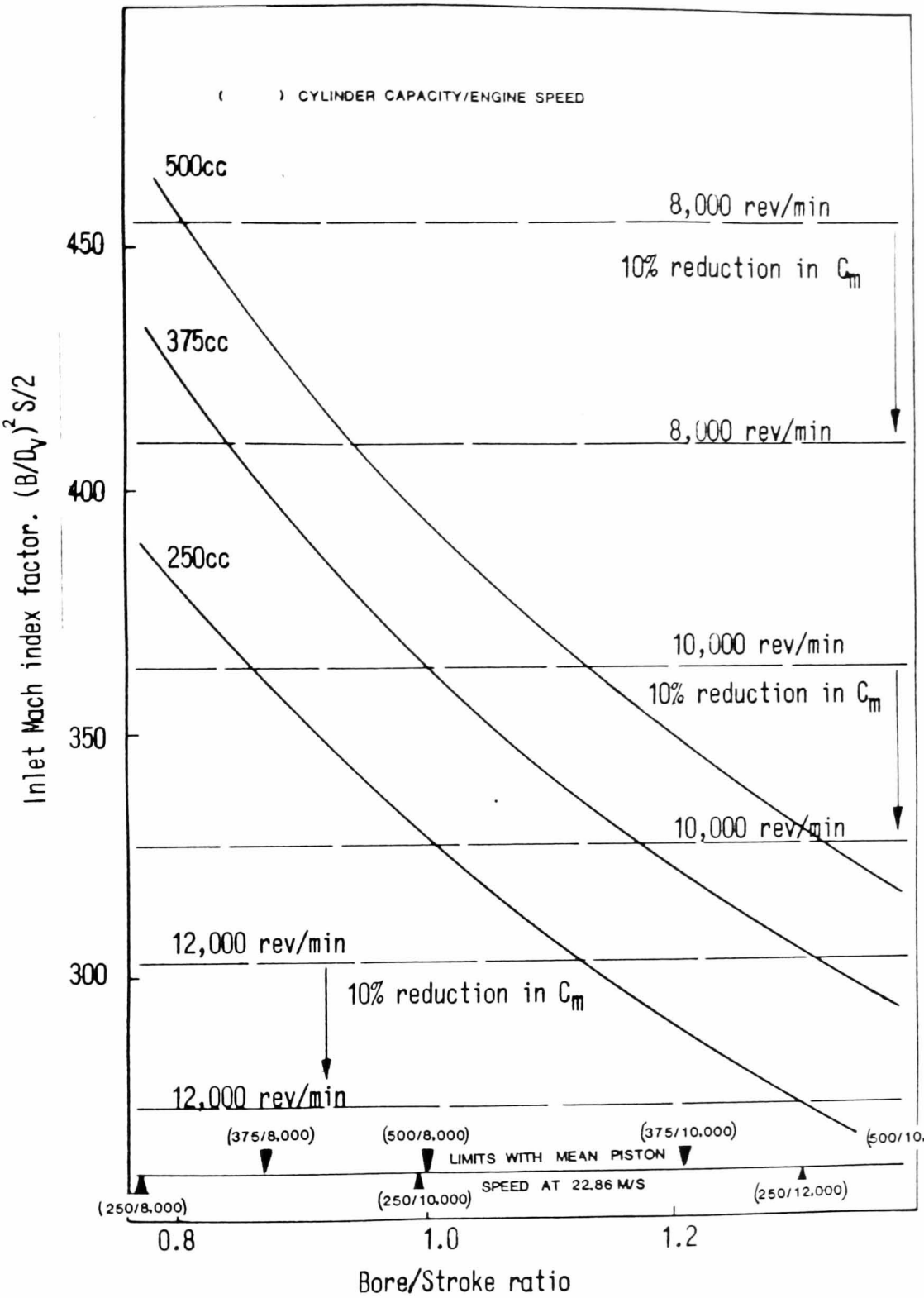

(FIG 2.3.2/3) INLET MACH INDEX FACTOR AGAINST BORE/STROKE RATIO FOR A 12:1 COMPRESSION RATIO AND VARIOUS SWEPT VOLUMES.

CHAPTER 3

STEADY FLOW TESTS ON CYLINDER HEADS

3. CHAPTER 3 - STEADY FLOW TESTS ON CYLINDER HEADS

3.1 Introduction:

When considering the effects of various changes in cylinder head geometry on engine performance, it is necessary to be able to predict accurately the flow through the inlet and exhaust valves at any instant. If this can be done, a quasi-steady analysis can be made of the cylinder filling and emptying abilities of various induction system geometries. With this in view it was decided to carry out steady flow tests on several cylinder heads of pent-roof configuration.

The major geometry difference in the pent-roof design is the valve included angle, and the cylinder heads available did exhibit differing values of this parameter, as can be seen in Table 3.1.

3.2 Theoretical model

The model chosen was the constant pressure model as used by Woods and Khan (Ref.11). This enabled a comparison to be made between the results of Woods (Ref. 9), on dual poppet valves, with the current experimental results.
The paper by Woods was the only one available on flow-through dual valves.

The model presumes isentropic flow from upstream conditions to the valve throat, then if the flow at the throat is subsonic the static pressure remains constant from throat to cylinder in the case of inflow.

Inflow conditions:-

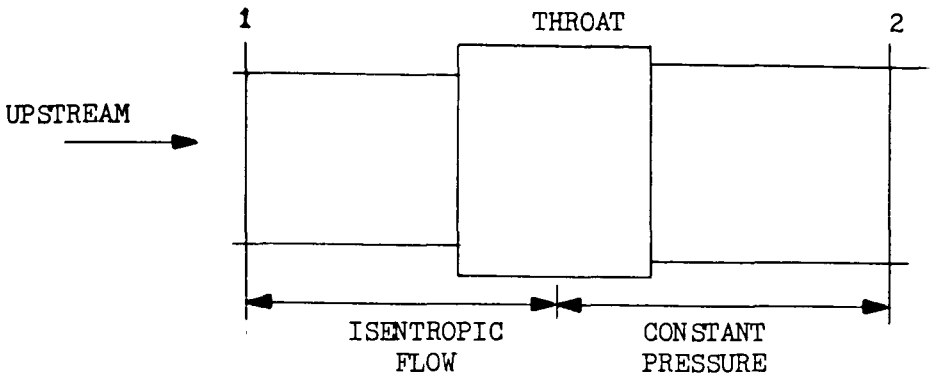

The steady flow energy equation gives:-

$$C_{p_1} T_{1_0} = C_{p_2} T_T + \frac{1}{2} u_T^2 \qquad (1)$$

where the suffix 0 indicates stagnation conditions.

C_p is the specific heat at constant pressure,

T the absolute temperature and u_T the throat velocity.

but, $a_{1_0} = \sqrt{\gamma R T_0}$

and, $T_T = \frac{a_T^2}{\gamma R}$

Substituting and simplifying leads to:-

$$a_{1_0}^2 = a_T^2 + \frac{1}{2} [\gamma - 1] \; u_T^2 \qquad (2)$$

The continuity equation gives:-

$$A_E = \frac{\dot{M}}{\rho_T u_T} \qquad (3)$$

With isentropic flow from upstream to throat:-

$$\frac{P_{1_0}}{P_T} = \left(\frac{\rho_{1_0}}{\rho_T}\right) = \left(\frac{a_{1_0}}{a_T}\right)^{\frac{2}{\gamma - 1}}$$

$$\rho_T = \rho_{1_0} \left(\frac{P_T}{P_{1_0}} \right)^{1/\gamma}$$

and, $$a_T^2 = \left(\frac{P_T}{P_{1_0}} \right)^{\frac{\gamma - 1}{\gamma}}$$

$$u_T = \sqrt{\frac{2}{\gamma - 1} \left[a_{1_0}^2 \left(1 - \left(\frac{P_T}{P_{1_0}} \right)^{\frac{\gamma - 1}{\gamma}} \right) \right]}$$

$$A_E = \frac{\dot{M}}{\rho_{1_0} \left(\frac{P_T}{P_{1_0}} \right)^{1/\gamma} \sqrt{\frac{2}{\gamma - 1} \left[a_{1_0}^2 \left(1 - \left(\frac{P_T}{P_{1_0}} \right)^{\frac{\gamma - 1}{\gamma}} \right) \right]}}$$

which reduces to:-

$$A_E = \frac{\frac{\dot{M}\sqrt{T_{1_0}}}{P_{1_0}} \sqrt{\frac{(\gamma - 1)R}{2\gamma}}}{\left(\frac{P_T}{P_{1_0}} \right)^{1/\gamma} \sqrt{1 - \left(\frac{P_T}{P_{1_0}} \right)^{\frac{\gamma - 1}{\gamma}}}}$$

where A_E is an effective area at the throat.

The valve discharge coefficient or non-dimensional effective area can be defined as:-

$$C_d = \frac{A_E}{\text{Reference area}}$$

The reference area used in this expression is arbitrary, but once chosen must be adhered to rigidly and care must be taken when comparing results that the same reference area has been selected.

The reference area used can be complex, such as that used by Kastner, Williams and White (Ref. 8) who used three regions of L/D and defined separate areas for each region. A much simpler approach is to take either a varying area, such as the valve curtain area as did Annand (Ref. 10), or a fixed area such as the valve diameter as used by Watson (Ref. 36), or the minimum port area or throat area as used by Woods (Ref. 9). For the purpose of comparison, the throat area was used as the reference area.

3.3 Apparatus for steady flow tests

A diagrammatic arrangement of the steady flow test rig is shown in Fig. 3.3/1. The rig consisted of a 100 mm bore heavy duty plastic pipe through which air was drawn, using initially a positive displacement blower attached to a diesel engine and subsequently to a centrifugal fan.
The main length of the pipe was fitted with a bypass valve which could be opened for initial start up of the engine and subsequently used as a control to maintain the pressure downstream of the cylinder head.
Flow was measured using an orifice plate designed to BS 1042 (Ref. 59), placed in the pipe at a distance greater than 16 diameters downstream of the cylinder head.
Pressure downstream of the cylinder head was determined using a water manometer, as was the pressure drop across the orifice plate.

The maximum depression across the inlet ports used in the tests was 30 cm of water (11.8 in H_2O), which was sufficient for most flow work on inlet valve arrangements.

It was found however that when the centrifugal fan was used with the valves fully open, in some cases only 5 cm H_2O pressure drop was available.

The effect of this low pressure ratio on the mean discharge coefficient can be determined using the relationship given in Ref. 10.

Here the discharge coefficient at a pressure ratio can be expressed in terms of the discharge coefficent under incompressible flow conditions, or with a pressure ratio close to unity, the pressure ratio ψ and the critical pressure ratio ψ_c :—

$$C_{d_c} = C_{d_i} + 0.7(1 - C_{d_i})(C_{d_i} - 0.1)(\psi - 1)(\psi_c - 1)$$

and, $$\psi_c = \left(\frac{\gamma + 1}{2}\right)^{\gamma/\gamma - 1}$$

The discharge coefficient here has been related to the valve curtain area, so the expression must be modified when applied to the valve throat area discharge coefficient.

$$C_{d_c} = C_{d_t} \frac{D_T^2}{4 L_V D_V}$$

where, C_{d_c} = discharge coefficient with curtain area as reference.

C_{d_t} = discharge coefficient with throat area as reference

L_V = valve lift

D_V = valve diameter

Taking a particular result on the Ford B.D.A.head.

D_T = 27.71 mm; L_V = 8.5 mm; D_V = 33.2 mm;

C_{d_t} = 0.6211; ψ = 1.0047.

However, at 1 mm valve lift ψ = 1.0153.

If the discharge coefficient is corrected to this pressure ratio.

$$C_{d_c} = 0.6800 \times 0.6211 + 0.625\left(1 - 0.6800 \times 0.6211\right)\left(0.6800 \times 0.6211 - 0.1\right) \times (1.0153 - 1)$$

$$= 0.4241$$

$$C_{d_t} = \frac{0.4241 \times 4 \times 8.5 \times 33.2}{27.71^2} = 0.6235$$

i.e., a difference of 0.38%. Hence it was concluded that the variation in pressure head across the valves at different openings would not significantly affect the results.

Flow was measured using an orifice plate designed to BS.1042, with an area ratio of 0.0992. The mass flow is given by the expression:-

$$W = 2.379\, Z_R . \varepsilon . d^2 \sqrt{H \rho}$$

where, W = mass flow (Kg/Hr)

Z_R = Reynolds number correction factor

ε = expansibility factor

d = orifice diameter (cm)

H = pressure drop (cm H_2O)

ρ = density

The Reynolds number correction factor and the expansibility factor were calculated using curve fits as shown in Figs. 3.3/2-3.

The pressure drop across the orifice plate and the downstream pressure were measured using water manometers. The downstream temperature required a mercury-in-glass thermometer.

Valve opening was achieved by specially designed fixtures for each cylinder head. Care was taken in the measurement of the valve deflection. This is especially important with high speed engine cylinder heads as they require large valve spring forces to retain cam contact at the point of maximum deceleration.

For example the Weslake WR275 springs have a pre-load of 524N with a spring rate of 123 N/mm giving a maximum spring force at 10 mm lift of 1.75 kN.

To eliminate the effects of flexure in the valve operating fixture, the screws were centre-drilled and a steel rod passed through to rest on the valve opening block or cap. The displacement was recorded using a dial test indicator.

3.4 Experimental procedure

The experimental procedure was relatively simple, the greatest difficulty being in the adjustment of the pressure ratio across the valves.

When using the diesel driven blower for the initial tests, the pressure ratio could be kept reasonably constant and adjusted by a change in engine speed or the by-pass valve. However, with the adoption of the centrifugal fan, no adjustment was possible, but as previously mentioned the variation of the pressure ratio should have very little influence on the results.

In order to compare the results with those of single valve configurations, a series of tests was carried out with unequal valve openings.

3.5 Experimental results and discussion

The experimental results were processed using a computer programme.(Appendix A6.) The results of the tests on the four cylinder heads are shown in Fig. 3.5/1-4, in which the discharge coefficient C_d is plotted against the valve lift/valve diameter ratio.

The results are very much as expected, three of the cylinder heads showing virtually identical performance. The fourth, the twin-cylinder head, performs less well, for two reasons. Firstly, the design has a considerably greater angle between the port axis and the cylinder axis (Table 3.2), which would contribute to the losses, and secondly, the port was initially damaged by machining and the repair, perhaps, did not reproduce exactly the original profile. Very little data is available for comparison. Woods (Ref. 9.) carried out tests on twin exhaust poppet valves, but these were only for normal out-flow conditions.

The results he obtained for a cylinder-to-pipe pressure ratio of 1.2 are replotted on Fig. 3.5/1. A comparison between the normal inflow conditions on the inlet valves and the results of Woods' exhaust flow tests is only made on the basis of the work by Woods and Khan (Ref. 11).

At a pressure ratio of 1.4 the results they obtained for single valves show little difference between inflow and outflow. The reduction of C_d by blockage due to the proximity of the valve to the cylinder wall, as illustrated in the graph, is not relevant when using inclined valves as in the pent-roof configuration, in which the valve moves progressively away from the wall.

The work on small displacement Honda engines (Ref. 13) suggests some mean discharge coefficients for inlet valves, varying from 0.3 to 0.45 and, as the $L/_D$ ratio is not specified, nor the presence of any dwell, a comparison is not possible. Comparison with the flow from two single valves is also difficult, as identical conditions upstream of the valve are not possible.

Woods quotes a progressive improvement in effective area of dual valves over that of two single valves above a $L/_D$ ratio of 0.18, with about 13% improvement at an $L/_D$ ratio of 0.4. However, this is with outflow with one valve shut, in which upstream conditions are identical to the dual valve case.

With inflow with one valve shut, losses are bound to occur at the point of division between the two inlet ports when one channel is stagnant. As an attempt to overcome this, tests were carried out with unequal valve openings, as shown in Fig. 3.5/5. The tests consisted of fixing one valve at 1, 2 and 3 mm lift and determining the discharge coefficient with the other valve opened progressively over the normal range 0 to 9 mm.

It was hoped that by extrapolation the discharge coefficient for a single valve only could be obtained, but as can be seen from Fig. 3.5/5, the result by extrapolation gives a lower coefficient than when one valve is shut, so those tests were inconclusive.

The results with two single valves, compared to dual-valves with equal opening, are shown in Fig. 3.5/6., and indicate a progressive improvement over the whole range of $L/_D$ with a gain in effective area of 18% at an $L/_D$ ratio of 0.2.

TABLE 3.1

COMPARISON OF CYLINDER HEAD GEOMETRY

Engine	Bore mm	Inlet valve dia.mm	Exhaust valve dia.mm	Inlet throat dia.mm	Valve included angle	Cylinder capacity cc
Weslake WR 275	86.0	33.5	31.8	26.9	40°	500
Dolomite Sprint	90.3	34.5	30.5	29.8	35°	500
Cosworth Ford BDA	85.7	33.2	28.5	27.7	40°	400
Weslake 2-cylinder	82.5	29.0	24.5	25.5	30°	375

TABLE 3.2

COMPARISON OF INLET TRACT GEOMETRY

Cylinder Head	Port length mm	Port/valve angle	Port/cylinder angle	Distance of separator upstream from valve mm
Weslake WR 275	74	42°	63°	67
Dolomite Sprint	125	40°	59°	100
Cosworth Ford BDA	113	40°	59°	93
Weslake 2-cylinder	109	59°	75°	69

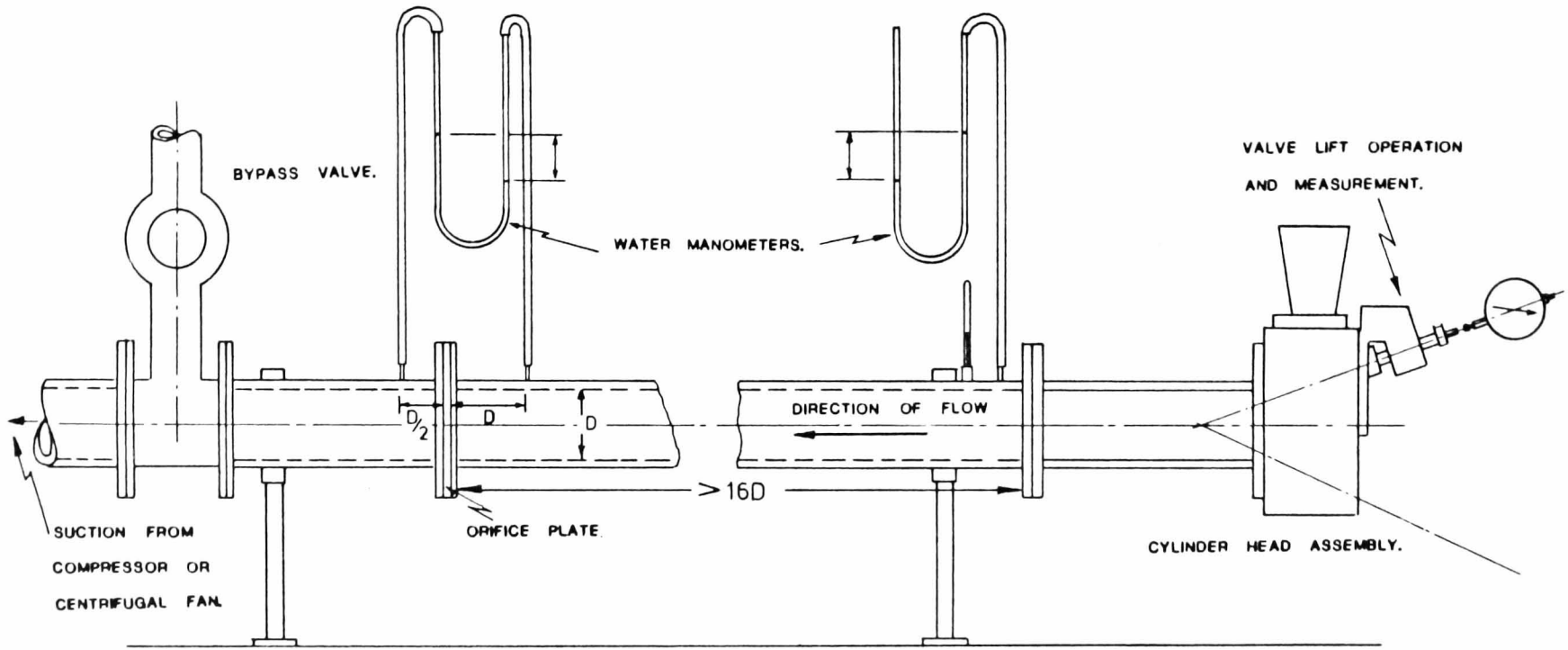

(FIG 3.3/1) Diagrammatical arrangement of steady flow test rig.

FIG 3.3/1.

FIG 3.3/2.

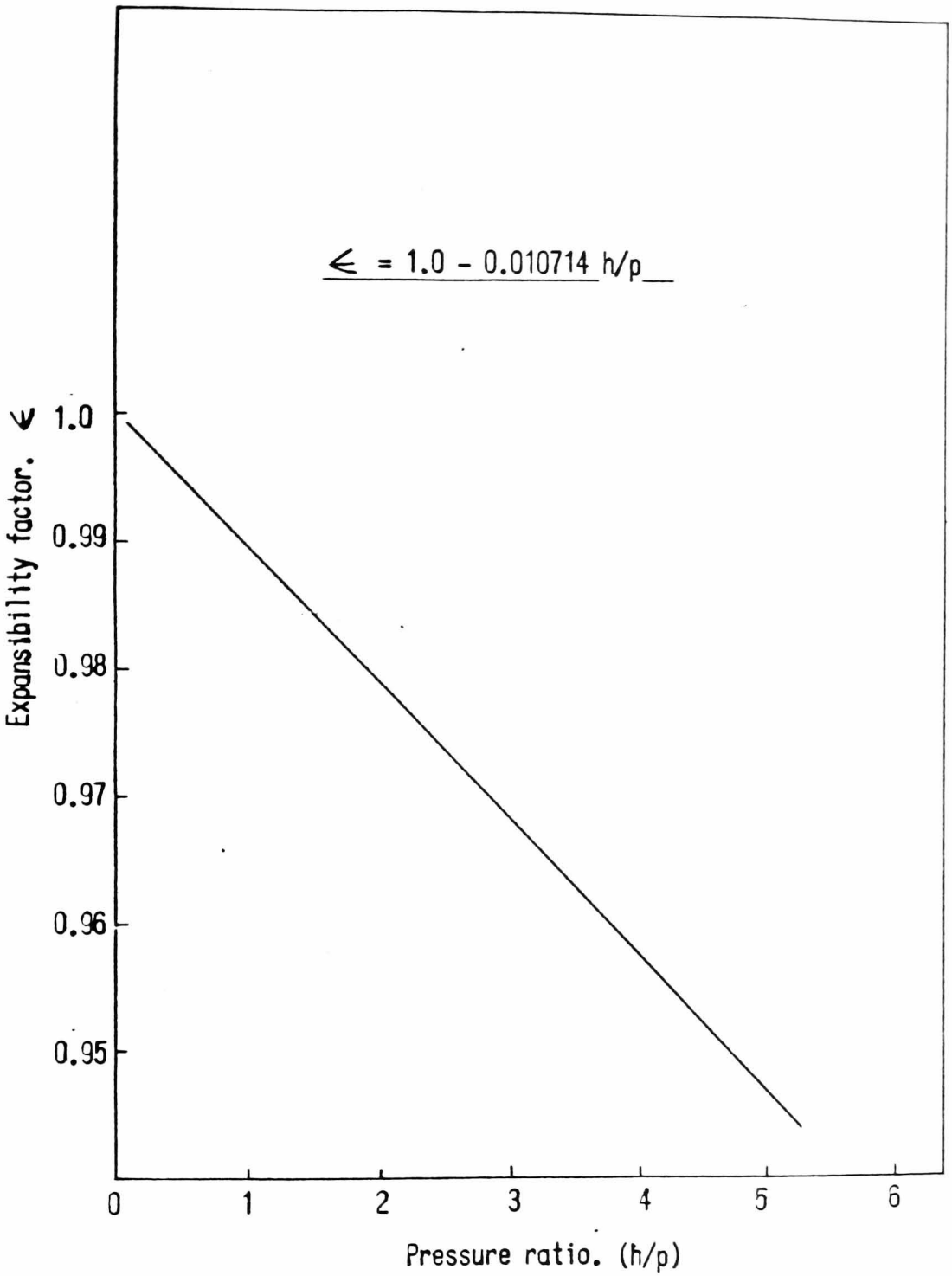

(FIG 3.3/2) EXPANSIBILITY FACTOR AGAINST PRESSURE RATIO FOR AN AREA RATIO OF 0.09765

FIG 3.3/3.

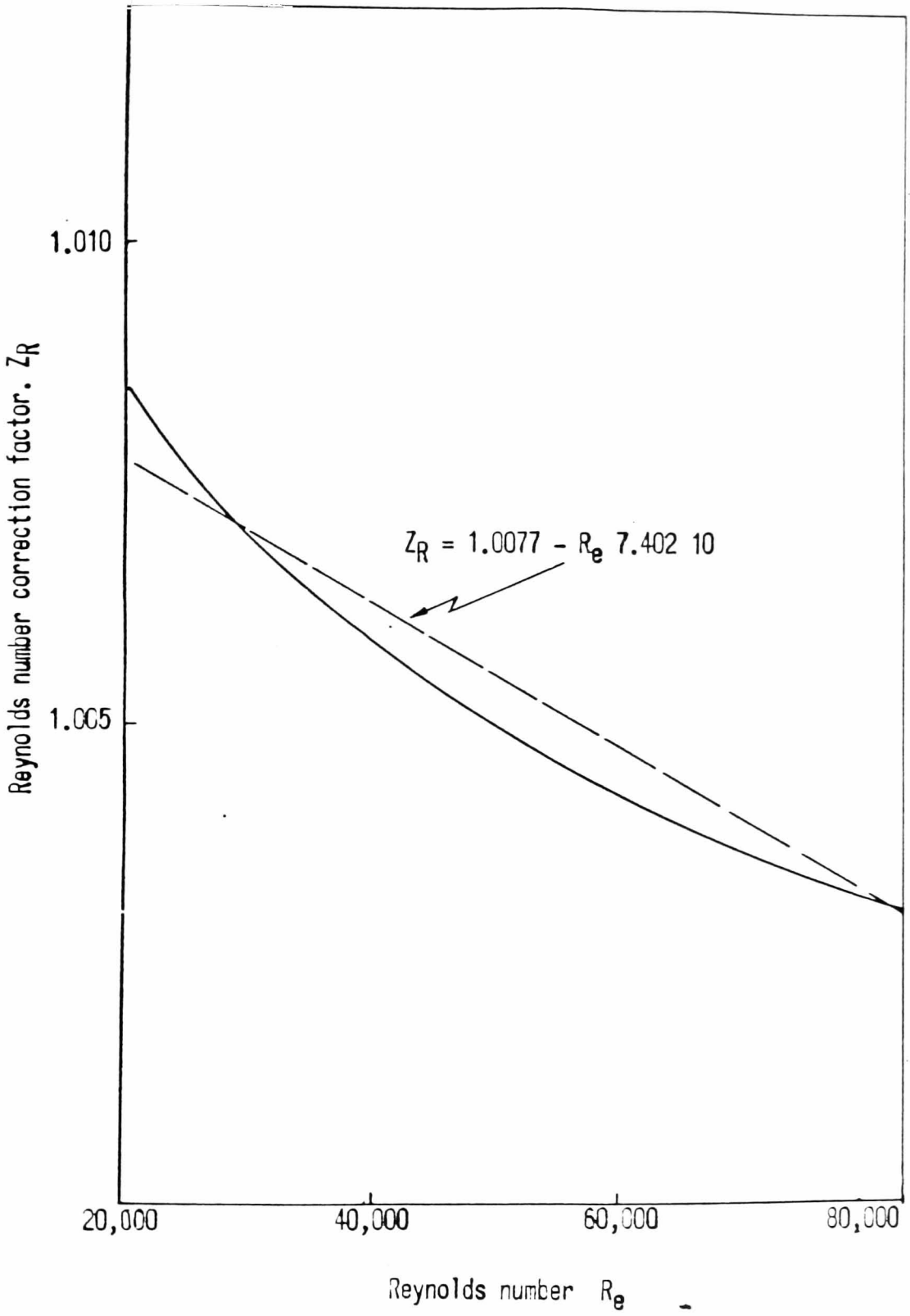

(FIG 3.3/3) REYNOLDS NUMBER CORRECTION FACTOR AGAINST REYNOLDS NUMBER.

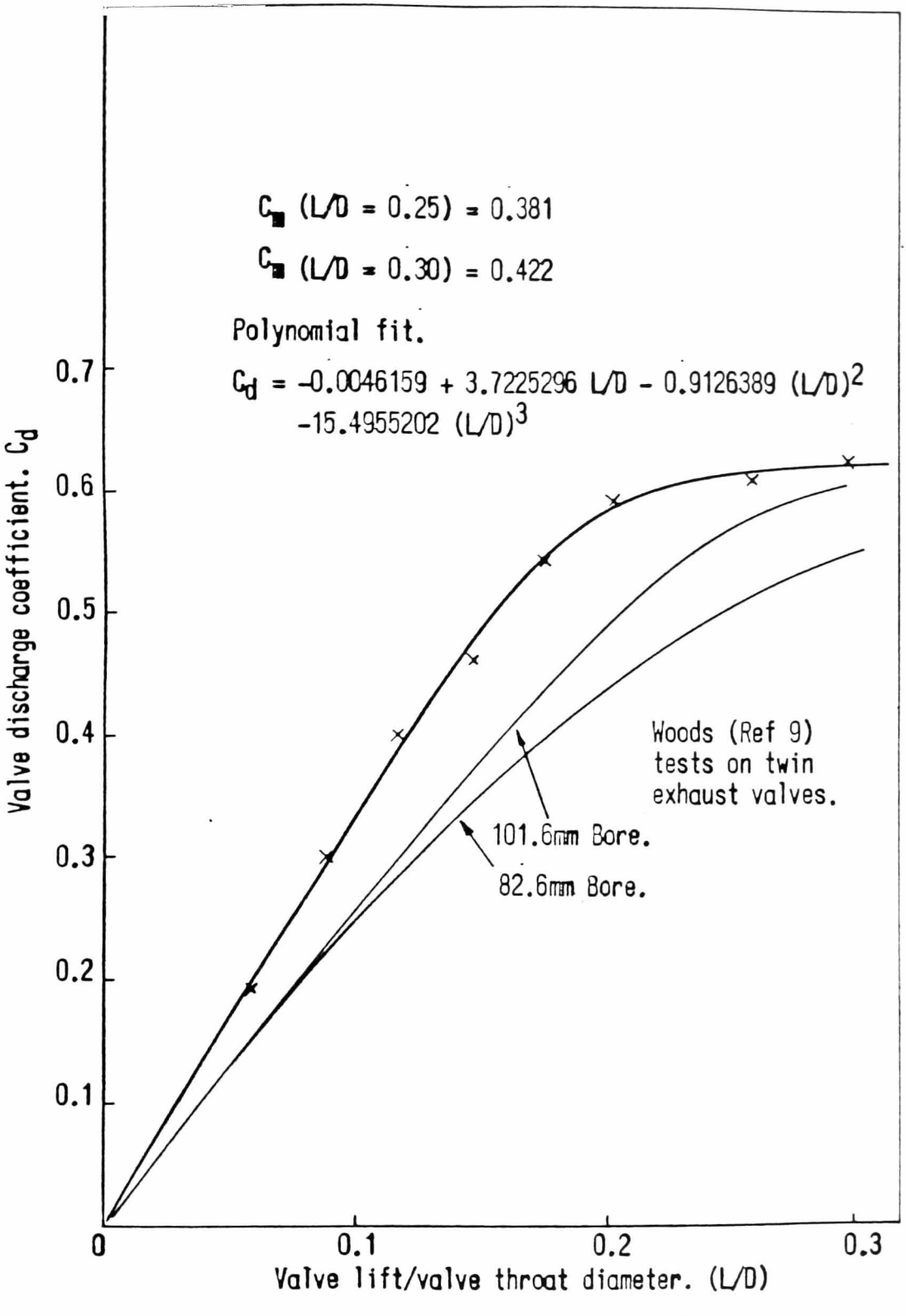

(FIG 3.5/1) INLET VALVE DISCHARGE COEFFICIENT AGAINST LIFT/DIAMETER RATIO FOR THE TRIUMPH DOLOMITE SPRINT CYLINDER HEAD WITH EQUAL VALVE OPENNINGS.

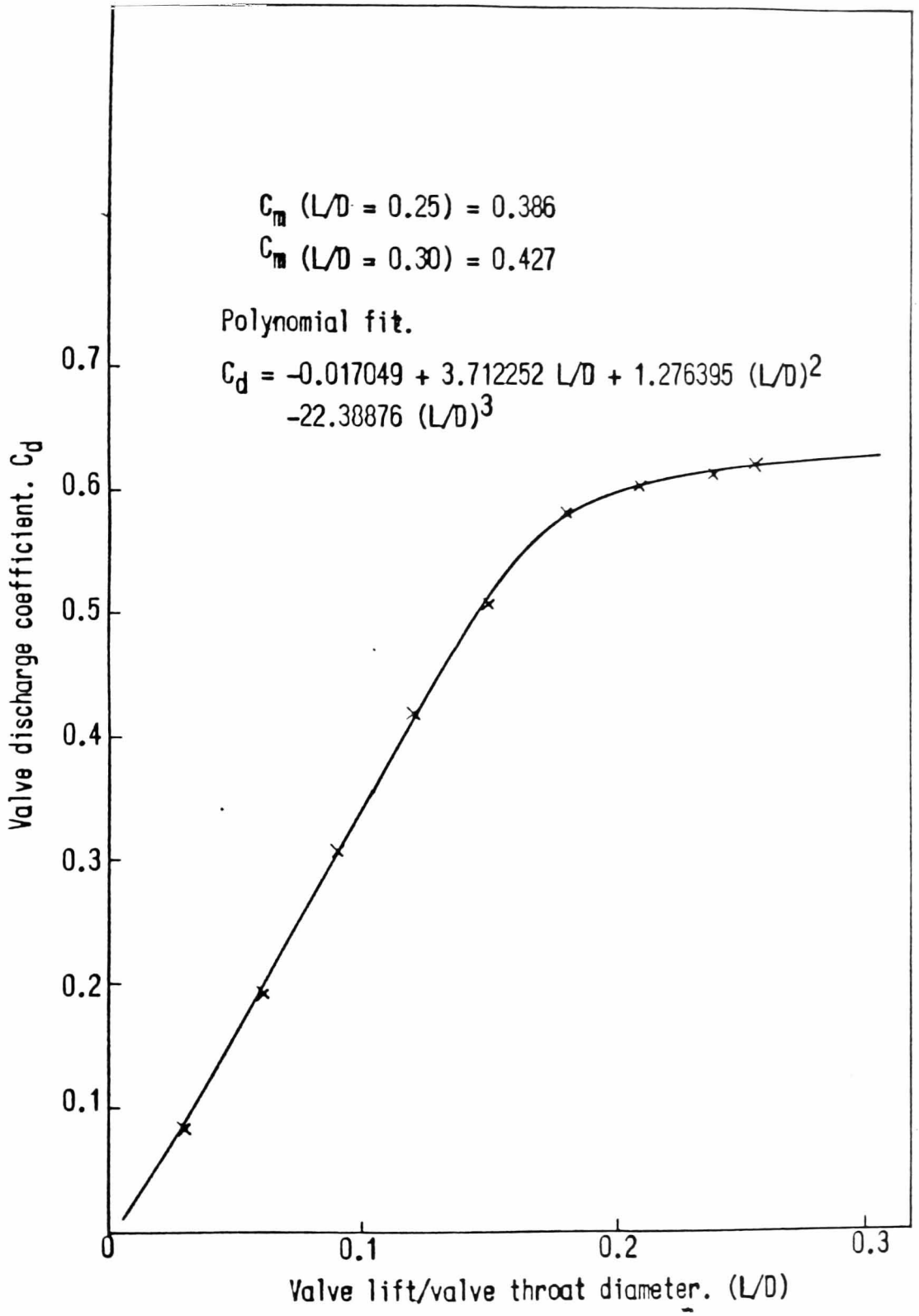

(FIG 3.5/2) INLET VALVE DISCHARGE COEFFICIENT AGAINST LIFT/DIAMETER RATIO FOR THE FORD COSWORTH CYLINDER HEAD WITH EQUAL VALVE OPENNINGS.

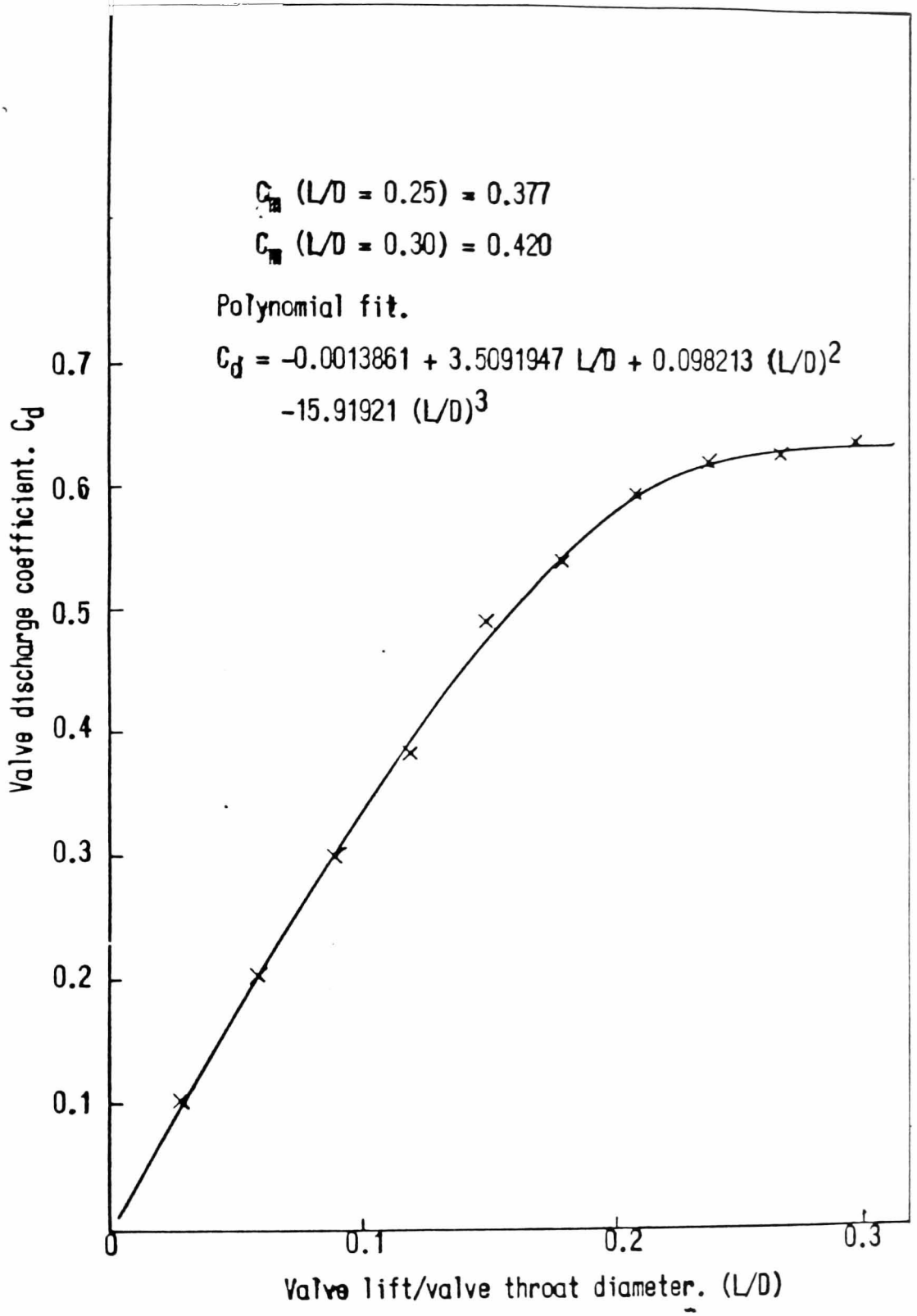

(FIG 3.5/3) INLET VALVE DISCHARGE COEFFICIENT AGAINST LIFT/DIAMETER RATIO FOR THE WESLAKE WR 275 CYLINDER HEAD WITH EQUAL VALVE OPENNINGS.

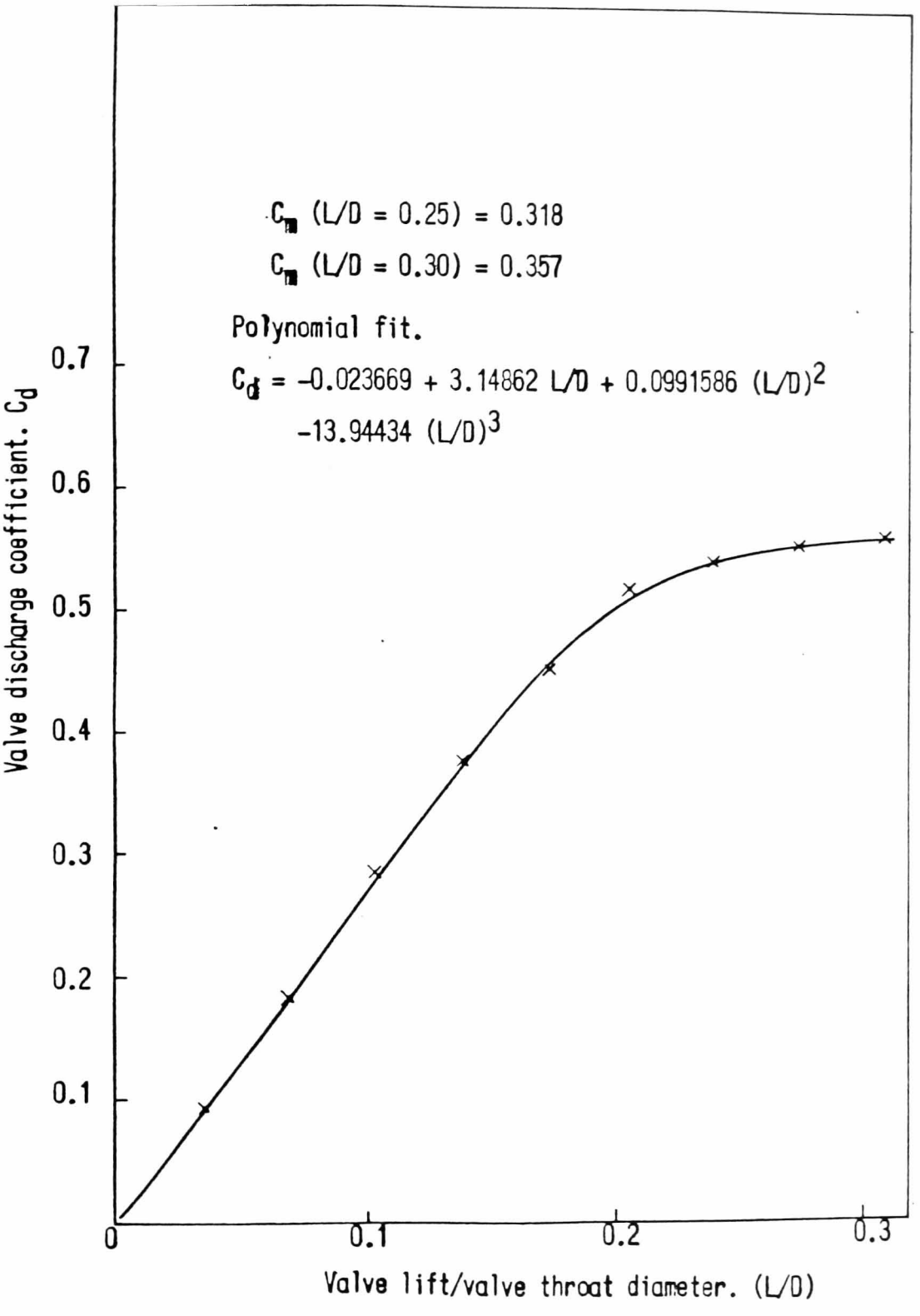

(FIG 3.5/4) INLET VALVE DISCHARGE COEFFICIENT AGAINST LIFT/DIAMETER RATIO FOR THE WESLAKE TWIN CYLINDER ENGINE CYLINDER HEAD WITH EQUAL VALVE OPENNINGS.

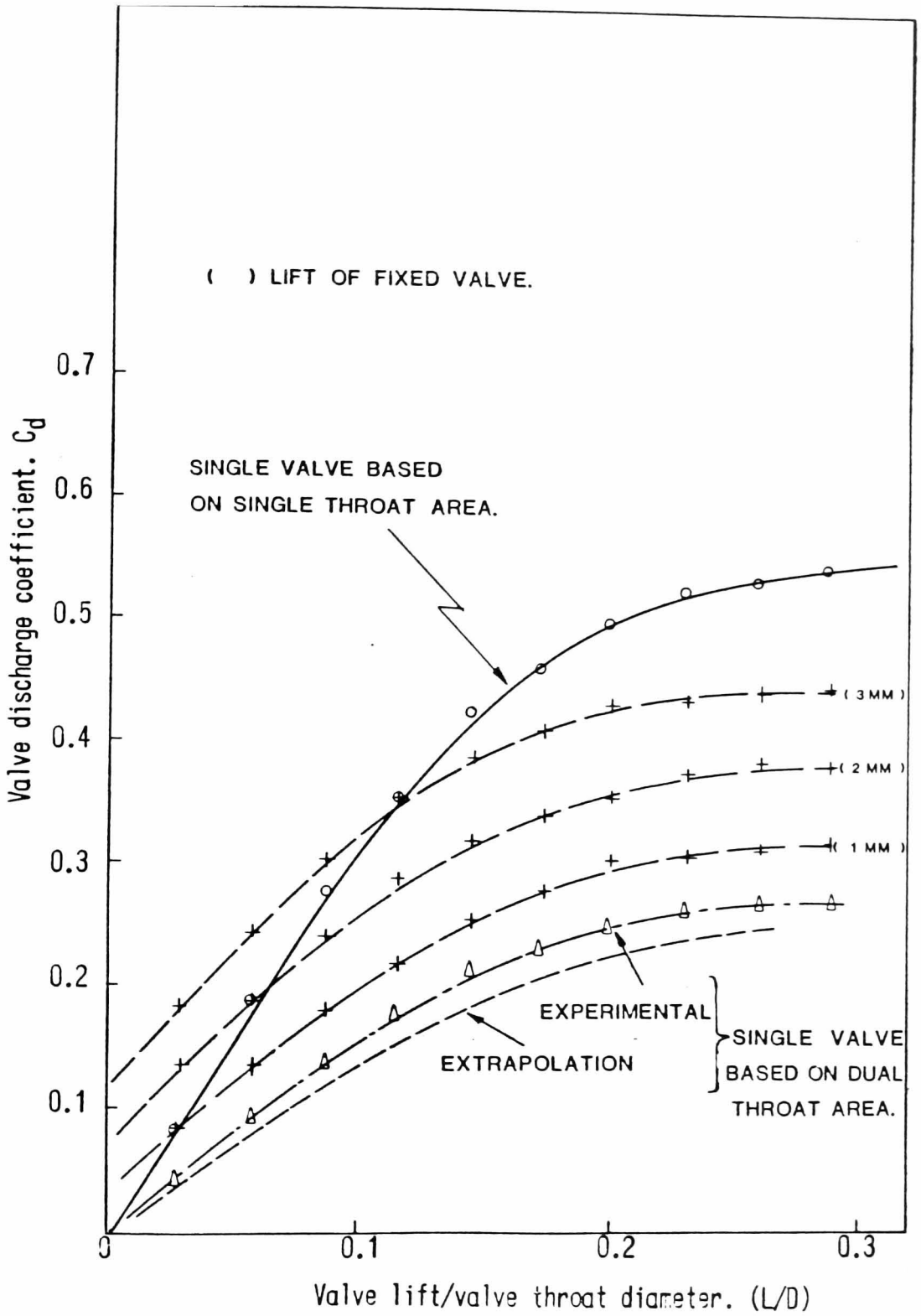

(FIG 3.5/5) INLET VALVE DISCHARGE COEFFICIENT AGAINST LIFT/DIAMETER RATIO FOR THE TRIUMPH DOLOMITE SPRINT CYLINDER HEAD WITH UNEQUAL VALVE OPENNINGS.

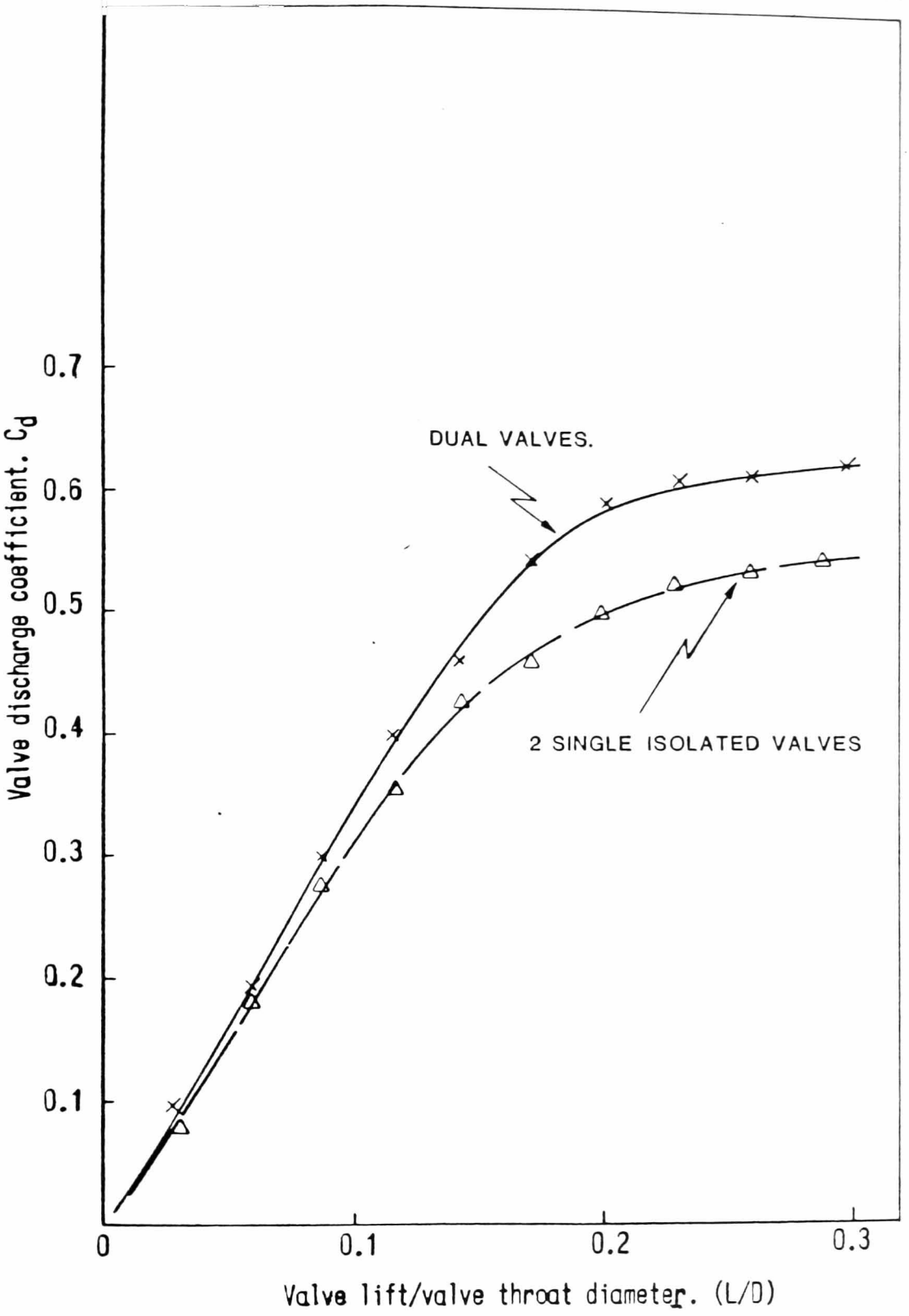

(FIG 3.5/6) INLET VALVE DISCHARGE COEFFICIENT AGAINST LIFT/DIAMETER RATIO FOR THE SPRINT CYLINDER HEAD. COMPARISON BETWEEN DUAL VALVES AND TWO ISOLATED VALVES.

CHAPTER 4

CAM DESIGN

4. CHAPTER 4 - CAM DESIGN

4.1 Introduction

When considering the merits of a cylinder head induction configuration, relative to either volumetric efficiency or to the combustion process, it is essential to be able to predict the valve motion accurately. The limitations imposed on the valve gear by its physical size and operating limits should also be considered. This must be allied to a method for producing a practical cam within the limits of the manufacturing process.

With respect to volumetric efficiency, the valve lift is usually set at one quarter of the valve diameter in order to equate the valve curtain area at full lift to the throat area. It is rarely worthwhile to exceed this value in production engines as the curve of discharge coefficient flattens off in this region (Fig. 3.5/1). This lift can be accommodated with an acceptable valve timing, without excessively high accelerations in the valve train and the attendant high loadings. Possible loss of contact at the nose can also be avoided.

The valve lift appears in the expression developed for the flame speed ratio (Section 6.3.2) as it has been related to the integral turbulent scale or characteristic eddy size.

The valve opening characteristics also affect the quality as well as the quantity of mixture entering the cylinder as encompassed in the mean discharge coefficient, which

also appears in the flame speed ratio expression Section 6.3.2.

The cam used in the Weslake WR275 engine was designed (by the author) using the polydyne method which is described in Appendix A7. This method requires the valve train stiffness to allow for dynamic deflection, and this was determined experimentally.

4.2 Determination of the valve train stiffness

In order to be able to define the correct dynamic and static deflection coefficients for use in the Polydyne method it is necessary to determine the valve train stiffness. Various values have been attributed to both overhead cam and pushrod stiffnesses.

The need to determine experimentally this stiffness value is stated by Watson and Milkins (Ref. 36). Here, a cam was designed using an assumed stiffness of 0.8 of the push rod stiffness. Experiments later showed it to be 0.3 of the push rod stiffness. A great deal of the difference occurred due to the flexure of the rocker shaft fulcrum. This is perhaps an extreme example and is aggravated by the fact that the effective rocker ratio was 1.66 to 1.685, whereas in the Weslake engine the ratio is 1.115.

The two-inlet valve configuration does create some problems in obtaining the displacements and related loads. There is a stiffness between each valve, and it would be incorrect to deflect one rocker finger only.

To overcome this difficulty, the valve train was assumed to be made up of the spring elements as shown below:

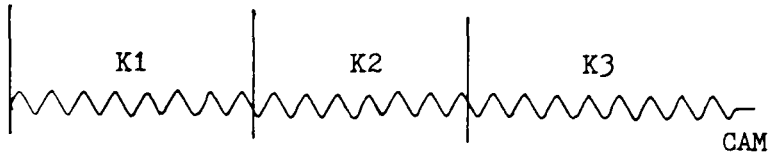

VALVE 1 VALVE 2 ROCKER FULCRUM

$\longrightarrow \delta_1 \quad \longrightarrow \delta_2 \longrightarrow \delta_{3_v} \mid \longrightarrow \delta_3$ Deflections

$\longrightarrow P_1 \quad \longrightarrow P_2 \longrightarrow P_{3_v} \longrightarrow P_3$ Forces

If δ_{3_v} and P_{3_v} refer to displacement and force on the valve side of the Fulcrum:

$$P_{3_v} = P_1 + P_2 \quad \text{and}$$

$$P_3 = P_{3_v} \times RR \qquad (RR = \text{Rocker ratio})$$

$$P_3 = (P_1 + P_2)RR$$

if $K_3 = \dfrac{P_3}{\delta_3}$

$$\delta_3 = \frac{(P_1 + P_2)RR}{K_3}$$

but $\delta_{3_v} = RR \times \delta_3 = \dfrac{(P_1 + P_2)\frac{RR^2}{K_3}}{}$

$$\delta_2 = \frac{P_1 + P_2}{K_3} + \delta_{3_v}$$

$$= \frac{P_1 + P_2}{K_2} + \frac{(P_1 + P_2)}{K_3} RR^2$$

---

and $\delta_1 = \frac{P_1}{K_1} + \frac{(P_1 + P_2)}{K_2} + \frac{(P_1 + P_2)}{K_3} RR^2$

if $P_1 = 0$ (only valve 2 loaded)

$$\frac{P_2}{\delta_2} = \frac{1}{\frac{RR^2}{K_3} + \frac{1}{K_2}}$$

---

if $P_2 = 0$ (only valve 1 loaded)

$$\frac{P_1}{\delta_1} = \frac{1}{\frac{RR^2}{K_3} + \frac{1}{K_2} + \frac{1}{K_1}}$$

Hence, if the valves are loaded separately, and the deflections measured at the particular valve and at the top of the pushrod to obtain K_3, K_1 and K_2 can be determined.

The loads in the system were determined by attaching 5mm, 120Ω aluminium foil strain gauges to the pushrod. These were then connected to a Tinsley Telcon strain bridge. The pushrod was calibrated using a Dartec 1502 screw driven tensile testing machine. Displacements were measured using dial indicators.

The results are shown in Fig. 4.2/1.

From Fig. 4.2/1, K_3 = 15062 N/mm.

A check with the actual pushrod stiffness can be made:-

Push rod dia. = 9.525mm E = 73.5GN/m^2 Length = 160mm.

$$\frac{P}{\delta} = \frac{AE}{L} = \frac{73.5 \times 1000 \times \pi}{160}$$

$$= \underline{32{,}733 \text{ N/mm}}$$

Thus the cam follower contributes considerably to the flexibility from the rocker to the cam. This is one of the disadvantages of using a roller follower that prevents the cam follower guides extending down to the follower base at full lift.

This is the worse condition where, with the valve closed the cam follower extends its maximum distance from the guides.

Loading valve 1 only gives:

$$\frac{P_1}{\delta_1} = 3{,}452 \text{ N/mm at valve.}$$

Loading valve 2 only gives:

$$\frac{P_2}{\delta_2} = 4{,}249 \text{ N/mm at valve.}$$

But, $$\frac{P_2}{\delta_2} = \frac{1}{\frac{1.115^2}{15{,}062} + \frac{1}{K_2}}$$

$$\frac{1}{K_2} = \frac{\delta_2}{P_2} - \frac{1{,}115^2}{15{,}062}$$

$$K_2 = \underline{6{,}544 \text{ N/mm}}$$

and $$\frac{P_1}{\delta_1} = \frac{1}{\frac{RR^2}{K_3} + \frac{1}{K_2} + \frac{1}{K_1}}$$

$$\frac{1}{K_1} = \frac{\delta_1}{P_1} - \frac{\delta_2}{P_2}$$

$$K_1 = \underline{18{,}403} \text{ N/mm}$$

By considering only the torsional stiffness of the rocker shaft, the stiffness K_1 is 34,439 N/mm, so the valve operating fingers reduce the stiffness by about 45%.

Operating condition

During operation the load on the ends of the fingers will be equal, if slight differences in displacement are neglected.

$$P_1 = P_2 = \frac{P_3}{2RR}$$

$$\delta_1 = \frac{P_3}{2RRK_1} + \frac{P_3}{RRK_2} + \frac{P_3}{RR} \cdot \frac{RR^2}{K_3}$$

$$\frac{P_3}{\delta_1} = \left[\frac{1}{\frac{1}{2 \times 1.115 \times 18{,}403} + \frac{1}{1.115 \times 6{,}544} + \frac{1.115}{15{,}062}} \right]$$

$$\frac{P_3}{\delta_1} = 4{,}247 \text{ N/mm}$$

and $$\delta_2 = P_3 \left[\frac{RR}{K_3} + \frac{1}{RRK_2} \right]$$

$$\frac{P_3}{\delta_2} = \frac{1.115}{15{,}062} + \frac{1}{1.115 \times 6{,}544}$$

$$= \underline{4{,}738} \text{ N/mm}$$

This gives an average stiffness of $\underline{4{,}492}$ N/mm, which is only 0.14 of the pushrod stiffness.

4.3 Cam design for the Weslake WRP275 engine

The cam used in the engine has an 83 degree half period angle with a designed maximum valve lift of 10.69 mm (0.421") and was originally to be used with a 1.25 rocker ratio.

The rocker ratio finally used was 1.12, which results in an actual valve lift of 9.525 mm (0.375").

The cam has a 20 deg. constant velocity type ramp with a ramp height of 0.265 mm (0.01044") at the valve.

The ramp velocity is 0.0007 in/deg with an initial acceleration of 0.00008 in/deg^2.

Details of the cam and valve train are given below, and the design performance is shown in Figs. 4.3/1 and 2.

Valve train design data

Maximum cam shaft speed	= 4,906 rev/min
Valve train stiffness	= 4,492 N/mm
Valve spring stiffness (2 valves)	= 123 N/mm
Design rocker ratio	= 1.25
Weight of push rod	= 1.797 N
Weight of rocker	= 2.993 N
Weight of springs (2 valves)	= 0.628 N
Weight of valves (2)	= 1.232 N
Spring preload (2 valves)	= 524 N

Cam design data

Maximum valve lift	= 10.69 mm
Half camshaft period	= 83 deg
Radius of roller follower	= 9.525 mm

Base radius of cam = 12.19 mm

Cam width = 10.16 mm

Polynomial powers: 2, 8, 12, 32, 46.

Ramp data (constant velocity type)

Ramp period = 20 deg

Ramp height = 0.01044 in.

Initial acceleration = 0.00203 mm/deg^2

Constant velocity = 0.01778 mm/deg

The master cam is manufactured ten times full size and created using tangent cuts. This precludes the use of any concavity in the cam profile.

The angular and radial coordinates for tangent manufacture are produced by the program.

FIG 4.2/1.

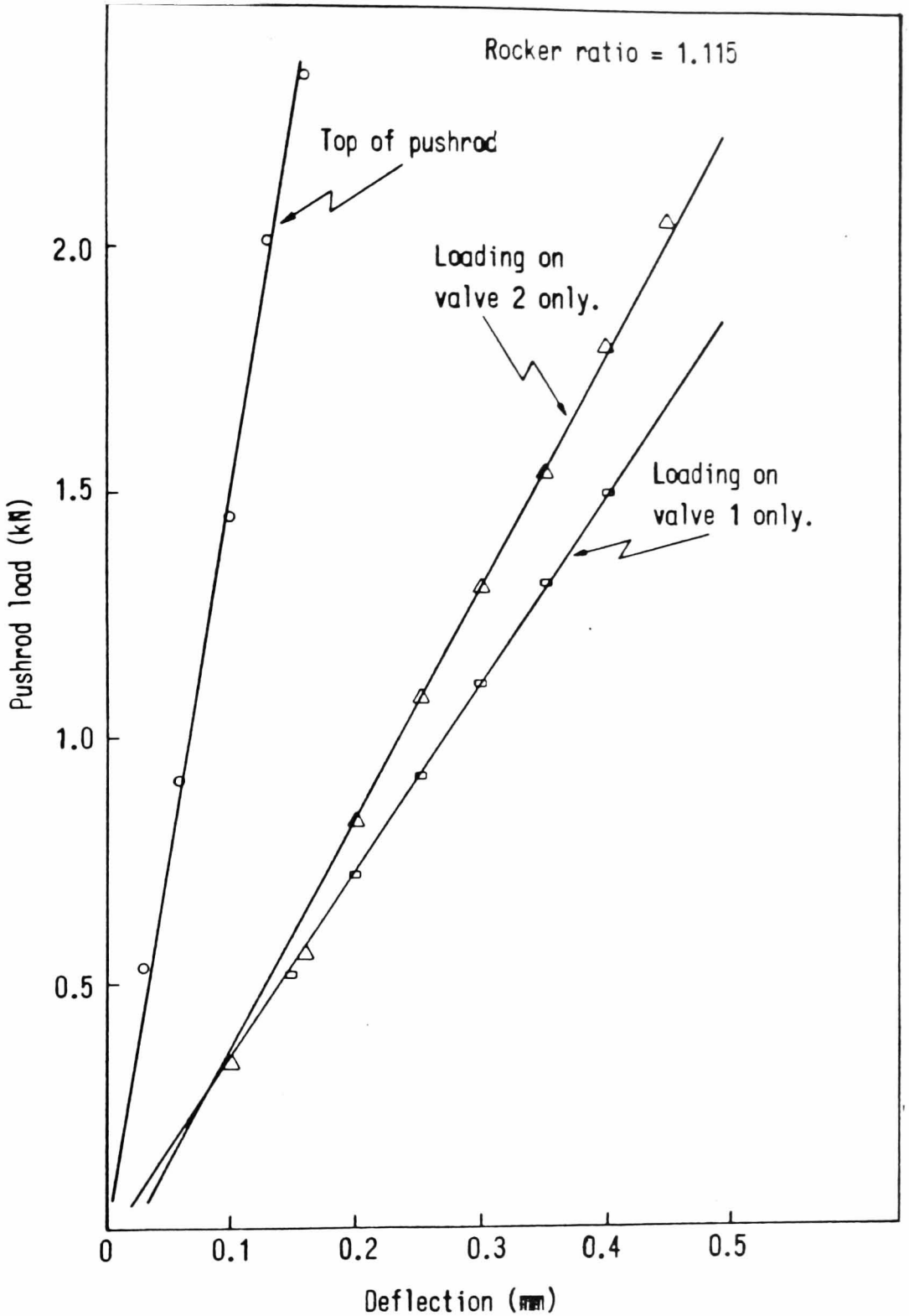

(FIG 4.2/1) FORCE-DISPLACEMENT GRAPH FOR LOADING AT DIFFERENT POINTS IN THE VALVE GEAR.

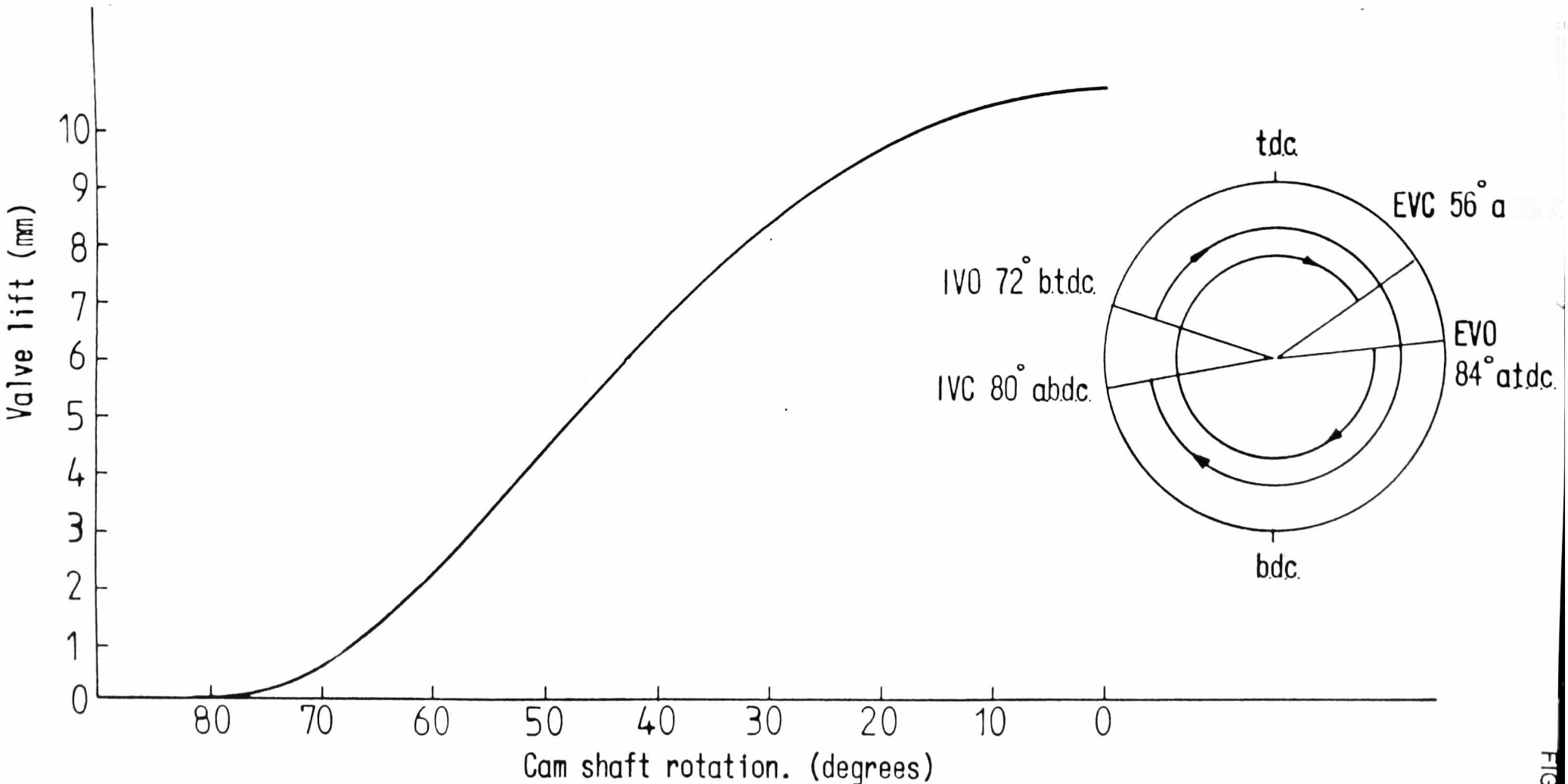

(FIG 4.3/1) Valve lift profile for 83° half period cam as used in engine.

FIG 4.3/1.

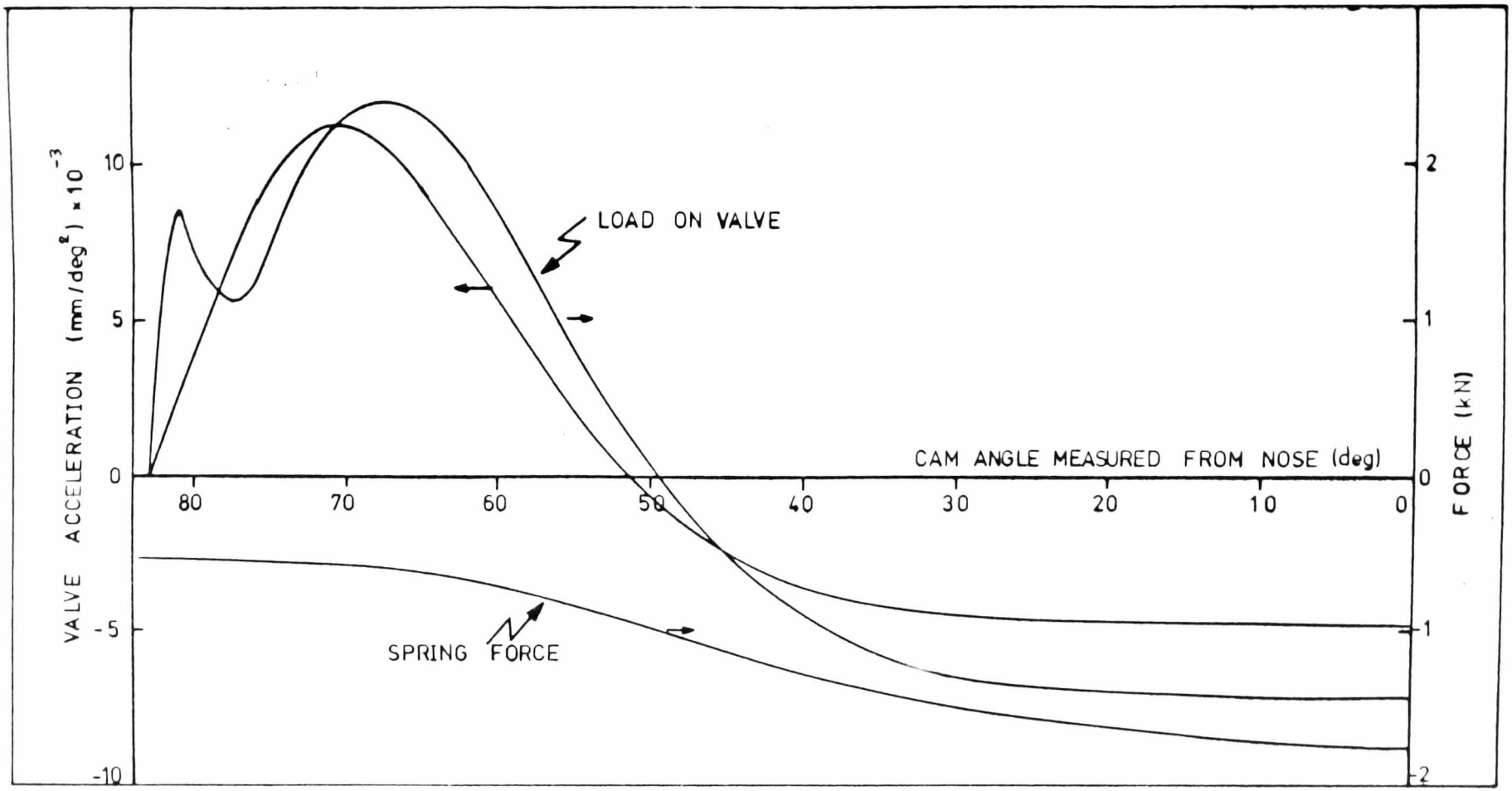

(FIG 4.3/2) Weslake WRP275 camshaft design performance.

FIG 4.3/2.

CHAPTER 5

EFFECTS OF ENGINE GEOMETRY ON INLET PIPE DYNAMICS AND VOLUMETRIC EFFICIENCY

5. CHAPTER 5 - EFFECTS OF ENGINE GEOMETRY ON INLET PIPE DYNAMICS AND VOLUMETRIC EFFICIENCY

5.1 Introduction

In order to produce an effective model of the engine process that will reflect changes in engine and hence inlet tract geometry, it was decided to include the dynamic effects in the induction pipe. This should also enable some future investigations to be carried out into the matching of induction performance with the cam characteristics, especially in the case of inlet valve throttling and reduced valve overlap to control exhaust emissions.

The inlet tract was taken as a straight pipe of constant cross-section with no heat transfer and no friction (i.e. Homentropic flow).

The effect of wave action and gas inertia in the inlet and exhaust systems can considerably enhance the volumetric efficiency of the engine. This is achieved in the case of the inlet tract by arranging for a positive pressure pulse to arrive during the inlet valve opening period. This will enhance the pressure drop across the inlet valve and restrict reverse gas flow. Thus a longer opening period of the inlet valve may be used with consequent improvement in volumetric efficiency.

The timing of the arrival of the pressure pulse will be dependent on the inlet duct length and engine speed. Its magnitude will depend on the 'in cylinder' conditions, valve timing and inlet pipe dimensions.

The basic mechanism involved is as follows:

After exhausting the burnt gases, a depression will occur within the cylinder, before t.d.c. if exhaust tuning has been used.

With opening of the inlet valve this will allow a restricted flow into the cylinder, with the small valve opening. This will result in a depression in the valve region of the pipe. The depression will travel along the inlet tract and be reflected as a compressive pulse from the open end of the pipe. As the valve continues to open this procedure continues and builds up a complex interaction within the pipe, producing a series of positive and negative pressure pulses.

Enhanced filling of the cylinder can take place without reverse flow, if the compressive pulse is timed correctly to arrive when it is most advantageous.

During the period when the inlet valve is closed, the wave action will continue. A compressive pulse will be reflected at the valve as a returning compressive pulse. This will continue whilst the valve is closed, but with a steadily reducing amplitude due to losses.

The period of these residual waves can be calculated from:

$$p = (24LN/a_o)$$

where p is the period in crank angle degrees, L is the effective inlet tract length in metres, N is the engine speed in rev/min and a_o is the local velocity of sound in m/s.

The effective inlet tract length is given by the pipe length + 0.3 x the pipe diameter. As the inlet pipe is taken as constant cross-sectional area and without obstruction, the model is only indicative of the likely wave action in a real engine with wide open throttle. This type of tuning of the inlet duct is sometimes called "inertia supercharging" or "induction ramming". It is very sensitive to speed and can, at certain speeds, lead to a reduction of volumetric efficiency.

5.2 Basic equation for Homentropic Flow with constant cross-sectional area (Ref. 10, 15, 16)

Continuity equation:

Consider a duct of constant cross-section with a local fluid velocity of u, for continuity of mass within an element of length δ_x, the following equation is easily derived.

$$\frac{\partial \rho}{\partial t} + \rho \frac{\partial u}{\partial x} + u \frac{\partial \rho}{\partial x} = 0$$

Eulers momentum equation:

For the length of gas δ_x within the duct the following equations apply:

Total acceleration $\frac{du}{dt} = \frac{\partial u}{\partial t} + u \frac{\partial u}{\partial x}$

Net pressure force is $- \frac{\partial P}{\partial x} \delta_x$

Mass of element $= \rho \delta_x$

Applying Newton's Second Law gives:

$$-\frac{\partial P}{\partial x}\,\delta_x = (\rho\delta_x)\left(\frac{\partial u}{\partial t} + u\frac{\partial u}{\partial x}\right)$$

or $$0 = \frac{1}{\rho}\frac{\partial P}{\partial x} + \frac{\partial u}{\partial t} + u\frac{\partial u}{\partial x}$$

using the relationship $\frac{P}{\rho^{\gamma}}$ = constant for isentropic flow and $a^2 = \frac{\gamma P}{\rho}$, P can be eliminated giving u and ρ as functions of x and t.

The equations become:

$$a\left(\frac{\gamma - 1}{2}\right)\frac{\partial u}{\partial x} + u\frac{\partial a}{\partial x} + \frac{\partial a}{\partial t} = 0 \qquad \text{(continuity equation)}$$

$$u\frac{\partial u}{\partial x} + \frac{\partial u}{\partial t} + \frac{2a}{\gamma - 1}\cdot\frac{\partial a}{\partial x} = 0 \qquad \text{(momentum equation)}$$

A solution to these equations gives:

$$\frac{d_x}{d_t} = u \pm a \qquad \text{(direction conditions)}$$

$$\frac{d_a}{d_u} = \pm\frac{\gamma - 1}{2} \qquad \text{(compatibility conditions)}$$

Integrating the compatibility equation gives:

$$a = -\left(\frac{\gamma - 1}{2}\right)u + n(\text{constant})$$

or $$n = a + \left(\frac{\gamma - 1}{2}\right)u$$

a constant for waves moving in one direction and

$$m = a - \left(\frac{\gamma - 1}{2}\right)u$$

for waves moving in the opposite direction.

So we have a direction condition that the wave velocity

is $u \pm a$. If we take a set of axes of t vertically and x horizontally we can plot a position diagram.

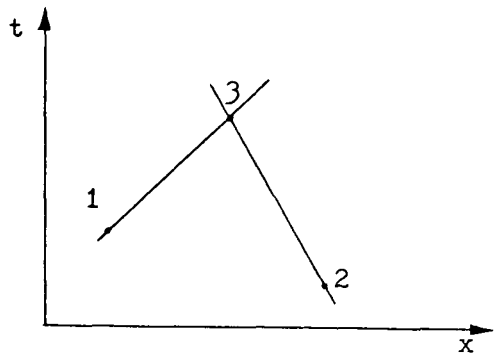

Taking two points on such a position diagram 1 and 2, the conditions at 3 can easily be found.

Along the rightward moving curve $\frac{d_x}{d_t} = u_1 + a_1$

(always +ve as $a > u$).

$$a_1 + \frac{(\gamma - 1)}{2} u_1 = n = \text{constant}$$

Along the leftward moving curve $\frac{d_x}{d_t} = u_2 - a_2$

and $a_2 + \frac{(\gamma - 1)}{2} = m$ constant

However at the intersection point both m and n must equal $a_3 + \frac{(\gamma - 1)}{2} u_3$, hence a_3 and u_3 can be found and P_3.

This is the basis of the method of characteristics.

The curves from 1 and 2 being the "characteristic curves".

5.3 Application of the method of characteristics to the Inlet Duct

5.3.1 General equations and method

The method used to determine the effect of the interaction of the pressure pulses in the inlet duct, is the familiar one of splitting the pipe into a series of equal length sections.

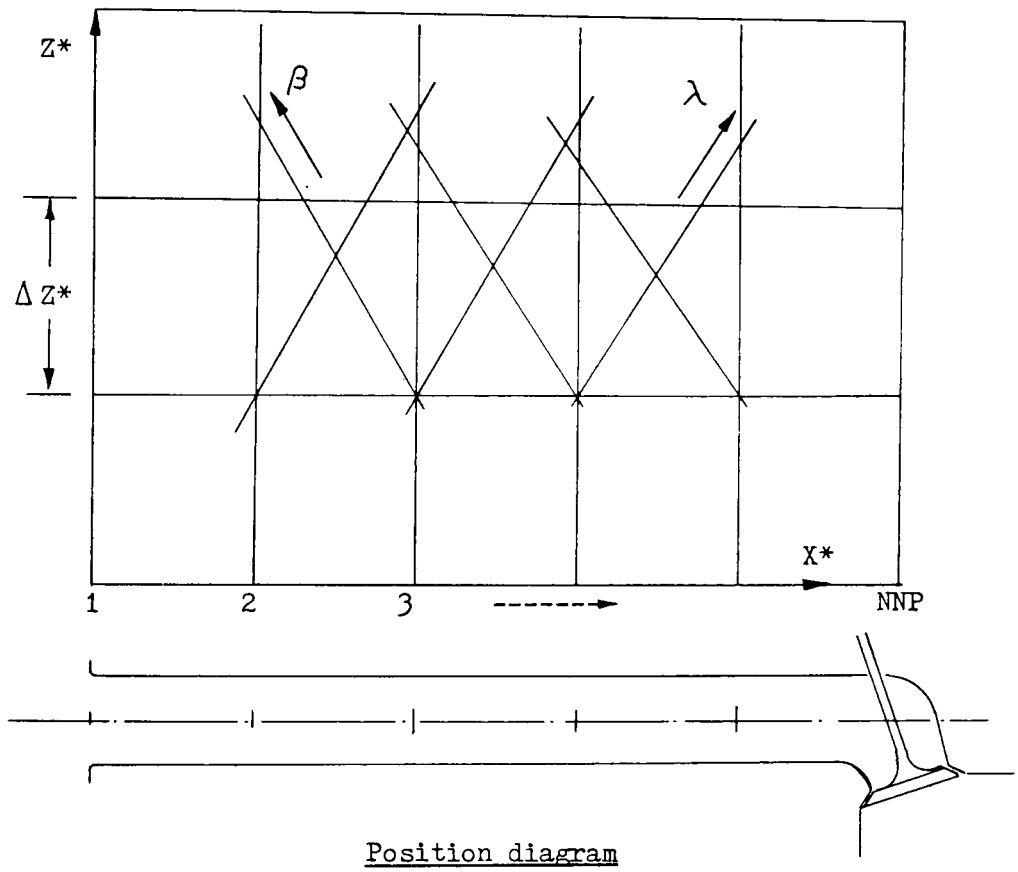

Position diagram

At this stage it is convenient to make the terms in the expressions dimensionless. If the datum acoustic velocity a_o is used, together with the pipe length L_p, the equations become:

$$\lambda = a^* + \frac{u^*}{5}$$

and $\frac{dX}{dZ} = u^* + a^*$, for waves moving in one direction and,

$$\beta = a^* - \frac{u^*}{5}$$

and, $\frac{dX}{dZ} = u^* - a^*$, for waves moving in the other direction.

Here λ and β are constants and called the pseudo Riemann variables.

$$a^* = \frac{a}{a_o} \qquad u^* = \frac{u}{a_o} \qquad X^* = \frac{x}{L_p} \text{ and } Z^* = \frac{a_o t}{L_p}$$

The physical significance of the equations for the Riemann variables is that along the characteristics on the position diagram, the values of a* and u* can only vary within the restraints of the λ and β equations. Hence, if λ and β can be determined at any instant at a particular position within the pipe, the particle velocity and fluid properties can be found.

Using the two Riemann equations gives:

$$\frac{\lambda + \beta}{2} = a^*$$

and $\frac{5}{2}(\lambda - \beta) = u^*$

Using the isentropic relationships:

$$\frac{a}{a_o} = \left(\frac{P}{P_o}\right)^{\frac{\gamma - 1}{2\gamma}} \quad \therefore \quad \left(\frac{\lambda + \beta}{2}\right)^7 = \frac{P}{P_o}$$

and $\left(\frac{\lambda + \beta}{2}\right)^2 = \frac{T}{T_o}$; $\left(\frac{\lambda + \beta}{2}\right)^5 = \frac{\rho}{\rho_o}$

In order to be able to obtain the values at a particular point in the Z* - X* field interpolation is required using the characteristics generated at the previous time. The time increment over which a successful interpolation can be achieved is limited by the stability criterion:

$$\frac{\Delta Z^*}{\Delta X^*} < \frac{1}{a^* + |u^*|}$$

$$a^* = \frac{\lambda + \beta}{2} \quad \text{and} \quad u^* = 2.5\,(\lambda - \beta)$$

$$\therefore \quad \frac{\Delta Z^*}{\Delta X^*} \quad \frac{1}{0.5\,(\lambda + \beta) + |2.5(\lambda - \beta)|}$$

Considering the mesh shown below, if a value of Z* is found that satisfies the above stability criterion, linear interpolation can be carried out as follows:

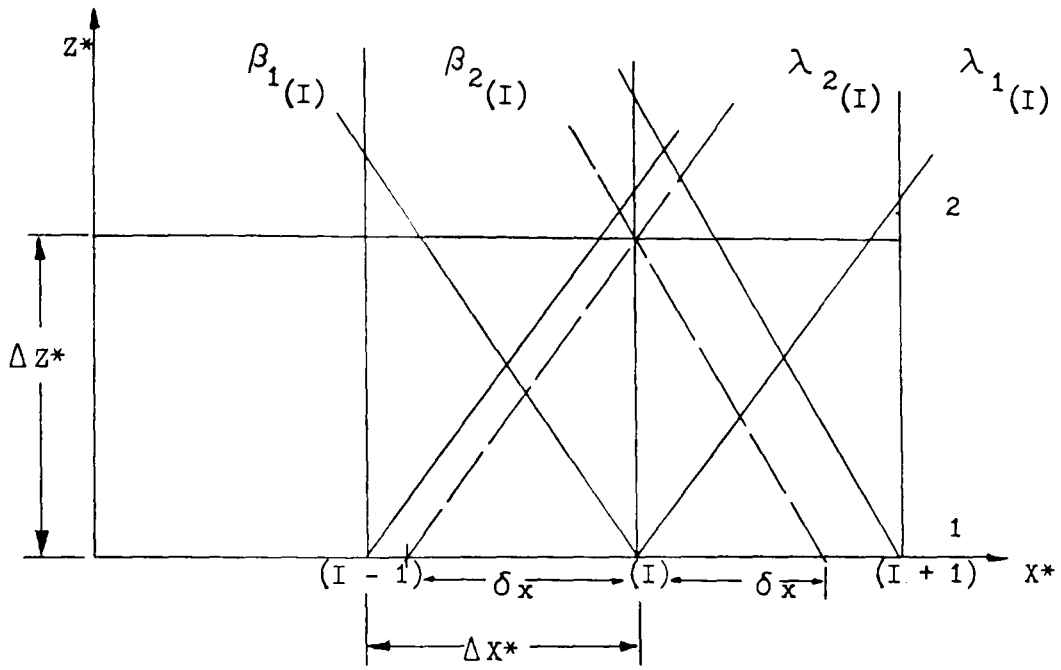

For rightward moving waves, λ characteristics

$$\frac{\delta x}{\Delta Z^*} = u^* + a^* = 3\lambda - 2\beta$$

$$\therefore \quad \delta x = \Delta Z^* \left(3\lambda_{1_{(I)}} - 2\beta_{1_{(I)}}\right)$$

$$\therefore \quad \lambda_{2_{(I)}} = \lambda_{1_{(I)}} + \frac{\Delta Z^*}{\Delta X^*} \left(3\lambda_{1_{(I)}} - 2\beta_{1_{(I)}}\right) \times \left(\lambda_{1_{(I-1)}} - \lambda_{1_{(I)}}\right)$$

and for leftward moving waves, β characteristics

$$\delta x = \Delta Z^* \left(3\beta_{1_{(I)}} - 2\lambda_{1_{(I)}}\right)$$

$$\therefore \quad \beta_{2_{(I)}} = \beta_{1_{(I)}} + \frac{\Delta Z^*}{\Delta X^*} \left(3\beta_{1_{(I)}} - 2\lambda_{1_{(I)}}\right) \times \left(\beta_{1_{(I+1)}} - \beta_{1_{(I)}}\right)$$

The initial value of ΔZ^* is determined from the crank angle interval chosen for the programme calculations.

$$\Delta_t = \frac{\Delta\theta}{6N} \quad ; \quad \Delta Z^* = \frac{a_o \Delta t}{L_p}$$

A check is now made along all the mesh points using the current values of λ and β to determine the minimum value of ΔZ^* that will satisfy the stability criterion.

If this value is less than the initial value, the interpolation procedure is carried out using 0.95 of this value.

The procedure is now repeated using a new initial value consisting of the old minus the increment used. If the minimum value is greater than the initial, only one step of interpolation is necessary.

It was found that using 2^o crank angle interval, a single interpolation was necessary down to about 4000 rev/min. after which a second or third interpolation became necessary. This was with 25 mm pipe increments.

5.3.2 Boundary conditions

There are three boundary conditions that must be accounted for:

1. Open end of inlet pipe
2. Closed valve
3. Open valve

Open end

At the open end of the inlet pipe, conditions are atmospheric and $a = a_o \quad \therefore a^* = 1$

$$\therefore \quad \frac{\lambda + \beta}{2} = 1$$

$$\therefore \quad \lambda_{2_{(1)}} = 2 - \beta_{2_{(1)}}$$

Closed valve

At the closed valve the particle velocity must be zero, i.e. $u^* = 0 \quad \therefore \frac{5}{2}(\lambda - \beta) = 0$

$$\therefore \quad \beta_{2_{(NNP)}} = \lambda_{2_{(NNP)}}$$

Open valve

Determination of the away β characteristics, when the valve is open, is not as simple as the other two boundary conditions.

The conditions at the valve during this phase must satisfy two conditions. (i) They must be compatible with the steady flow energy equation, and, (ii) they must relate to the dynamics of the induction pipe as indicated by the incoming λ characteristic.

Using the constant pressure model applied to the pipe and valve throat, the energy equation gives:

$$\frac{u_t^2 - u_p^2}{2} = \frac{1}{\gamma - 1}\left[a_p^2 - a_{R_o}^2\right]$$

$$= \frac{\gamma}{\gamma - 1}\left[\frac{P_p}{\rho_p} - \frac{P_R}{\rho_R}\right]$$

Using the continuity equation $U_p A_p \rho_p = C_d A_t U_t \rho_t$

and rearranging gives:

$$\left[\frac{P_p}{P_o}\right]^{\frac{\gamma-1}{\gamma}} - \left[\frac{P_R}{P_o}\right]^{\frac{\gamma-1}{\gamma}} = \left(\frac{\gamma-1}{2}\right)\frac{U_p^2}{a_o^2} \times$$

$$\left(\left[\frac{P_p}{P_o}\right]^{2/\gamma}\left[\frac{P_o}{P_R}\right]^{2/\gamma}\left[\frac{A_p}{C_d A_t}\right]^2 - 1\right)$$

The characteristic relationships at the valve are:

$$\frac{\lambda_{1_{(NNP)}} + \beta_{1_{(NNP)}}}{2} = \frac{a_p}{a_o}$$

and $$\lambda_{1_{(NNP)}} - \beta_{1_{(NNP)}} = \frac{U_p}{a_o}(\gamma - 1)$$

eliminating gives:

$$\frac{U_p}{a_o} = \left[\lambda_{1_{(NNP)}} - \frac{a_p}{a_o}\right]\frac{2}{\gamma-1}$$

incorporating these into the energy equation results in:

$$\left[\frac{C_d A_t}{A_p}\right]^2\left(\left[\frac{P_p}{P_o}\right]^{2/7} - \left[\frac{P_R}{P_o}\right]^{2/7}\right) = \frac{2}{\gamma-1}\left(\lambda_{1_{(NNP)}} - \left[\frac{P_p}{P_o}\right]^{1/7}\right)^2 \times$$

$$\left(\left[\frac{P_p}{P_o}\right]^{10/7} - \left[\frac{A_t C_d}{A_p}\right]^2\right)$$

using this equation with the known incoming λ characteristic and cylinder pressure P_R and

discharge coefficient C_d, a new pipe pressure adjacent to the valve can be determined.

5.4 Modelling the flow through the engine cycle

The basic construction of the model used to predict the flow conditions through the engine was similar to that suggested by Wolgemuth and Olsen (Ref. 37).

The equations are derived by applying the first law of thermodyamics to a control volume consisting of the engine working volume Fig. 5.4/1 with the usual assumptions of homogenaity.

The first law equation can be written as:

$$\dot{Q} - \dot{W} = \dot{m}_o \left(h + K_E + P_E\right)_o - \dot{m}_i \left(h + K_E + P_E\right)_i + \dot{E}_v$$

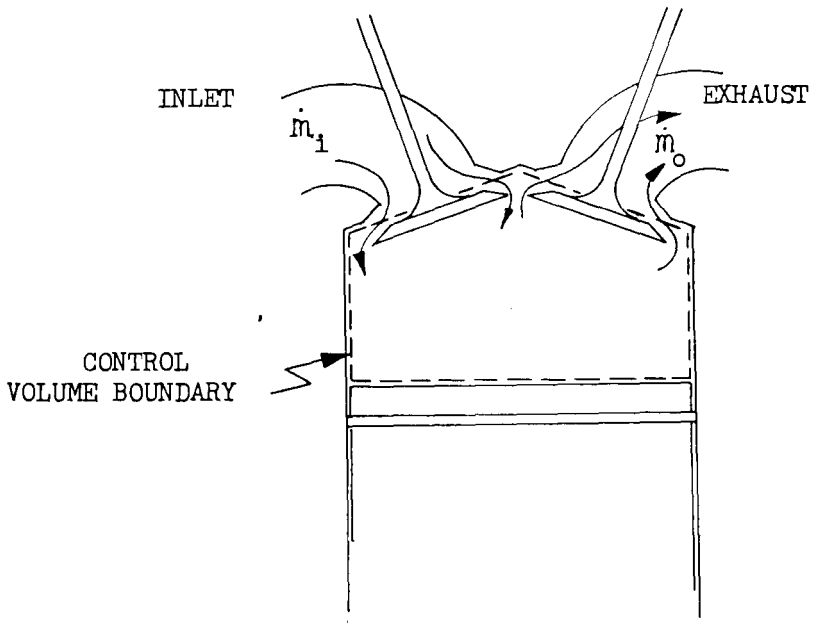

Fig. 5.4/1

If it is assumed that the kinetic and potential energy terms can be neglected, and that the energy within the control volume is purely internal energy, then:

$E_v = M\,e$ where M is the mass within the control volume and e is the specific internal energy. If the charge can be treated as a perfect gas,

$$e = C_v T \quad \text{and} \quad T = \frac{PV}{MR}$$

$$\therefore \quad Me = C_v \frac{PV}{MR} .M = C_v \frac{PV}{R}$$

$$\therefore \quad \dot{E}_V = \frac{C_v}{R}\left(\dot{P}V + \dot{V}P\right)$$

also $\dot{W} = P\dot{V}$

$\therefore$ the equation becomes

$$\dot{Q} - P\dot{V} = \dot{m}_o (h_o) - \dot{m}_i (h_i) + \frac{C_v}{R}\left(\dot{P}V + \dot{V}P\right)$$

$$\therefore \quad \dot{P} = \frac{R\dot{Q}}{VC_v} - \frac{P\dot{V}R}{VC_v} - \frac{\dot{m}_o h_o R}{VC_v} + \frac{\dot{m}_i h_i R}{VC_v} - \frac{P\dot{V}}{V}$$

$$\dot{P} = \frac{R\dot{Q}}{VC_v} - \frac{P\dot{V}}{V}\left(\gamma - 1\right) - (\dot{m}T)_o \frac{R\gamma}{V} + (\dot{m}T)_i \frac{R\gamma}{V} - \frac{P\dot{V}}{V}$$

$$\text{or} \quad \dot{P} = \frac{R\dot{Q}}{VC_v} - \frac{P\dot{V}\gamma}{V} - (\dot{m}T)_o \frac{R\gamma}{V} + (\dot{m}T)_i \frac{R\gamma}{V}$$

If flow is to be considered through both valves at the same time, the equation can be rewritten as:

$$\dot{P} = \frac{P\dot{Q}}{VC_v} - \frac{P\dot{V}\gamma}{V} - \left(E_o + I_o\right) + \left(E_i + I_i\right)$$

where $E_o = \frac{X_o TR\gamma}{V}$ outward flow through exhaust

X_o = mass flow rate

$$I_o = \frac{N_o \, TR\gamma}{V}$$

outward flow through inlet

N_o = mass flow rate

$$E_i = \frac{X_i \, T_E R\gamma}{}$$

Inlet flow through exhaust

X_i = mass flow rate

$$I_i = \frac{N_i \, T_i R\gamma}{V}$$

Inlet flow through inlet

N_i = mass flow rate

The mass flow rates required in the above equations can be determined using the flow rate equation derived in Chapter 3, Section 3.2.

$$A_E = \frac{\frac{\dot{M}\sqrt{T_{10}}}{P_{10}} \sqrt{\frac{(\gamma - 1)R}{2\gamma}}}{\left[\frac{P_T}{P_{10}}\right]^{1/\gamma} \sqrt{1 - \left[\frac{P_T}{P_{10}}\right]^{\frac{\gamma-1}{\gamma}}}}$$

Discharge coefficient $C_d = \frac{A_E}{A_R}$

Reference area $A_R = \left(n \times \frac{\pi \, D_T^2}{4}\right)$

where n = 2 for twin inlet valves.

Substituting gives:

$$\dot{M} = \frac{C_d A_R}{\sqrt{\frac{(\gamma - 1)R}{2\gamma}}} \left[\frac{\sqrt{\left[\frac{P_T}{P_{10}}\right]^{2/\gamma} - \left[\frac{P_T}{P_{10}}\right]^{\frac{\gamma+1}{\gamma}}}}{\sqrt{\frac{T_{10}}{P_{10}}}} \right]$$

which reduces to:

$$\dot{M} = C_d A_R \rho_{10} \sqrt{2 C_p T_{10} \left[\left[\frac{P_T}{P_{10}} \right]^{2/\gamma} - \left[\frac{P_T}{P_{10}} \right]^{\frac{\gamma+1}{\gamma}} \right]}$$

In the programme the term $\sqrt{\left[\frac{P_T}{P_{10}} \right]^{2/\gamma} - \left[\frac{P_T}{P_{10}} \right]^{\frac{\gamma+1}{\gamma}}}$

is in the form of a function statement (FCTN), so the mass flow equation becomes:

$$\dot{M} = C_d A_R \rho_{10} \sqrt{2C_p T_{10}} \quad \text{FCTN} \left[\frac{P_T}{P_{10}} \right]$$

This equation must be applied to the particular flow situations encountered.

a) Flow out of exhaust valve (Normal flow)

In this case the upstream condition is the cylinder condition and downstream the exhaust pipe condition, hence the equation becomes:

$$X_o = C_{DE} A_{TE} \sqrt{2C_p \frac{P_R M}{RV}} \quad \text{FCTN} \left[\frac{P_E}{P_R} \right]$$

where C_{DE} = exhaust valve discharge coefficient at the correct valve lift.

A_{TE} = exhaust valve throat area

P_R = cylinder pressure

M = Mass in cylinder

P_E = Exhaust pressure

b) Flow in the exhaust valve (Reverse flow)

Here the upstream condition is the exhaust pipe condition and the downstream the cylinder condition. The equation for X_i becomes:

$$X_i = C_{DE} A_{TE} P_E \sqrt{\frac{2C_p}{R^2 T_E}} \quad FCTN \left[\frac{P_R}{P_E}\right]$$

The exhaust pipe condition is set in the programme to a fixed state in the absence of dynamic considerations.

c) Flow through the inlet valves

There are two inlet normal flow conditions that should be allowed for (i) flow of fresh charge, and (ii) flow of products that have, in previous steps, exited through the inlet valves.

In the programme provision is made for these conditions.

Flow out of inlet valves (Reverse flow)

Upstream conditions are cylinder conditions and downstream the inlet pipe conditions adjacent to the valve. The expression for N_o becomes:

$$N_o = C_{DI} A_{TI} \sqrt{2C_p \frac{P_R M}{RV}} \quad FCTN \left[\frac{P_p}{P_R}\right]$$

Flow into inlet valves (Normal flow)

(i) Fresh charge.

Upstream conditions are inlet pipe conditions adjacent to the valve and downstream the cylinder pressure. Here the expression for N_i becomes:

$$N_i(MIX) = C_{DI}\, A_{TI}\, P_p \sqrt{\frac{2C_p}{R^2 T_p}}\ FCTN\left[\frac{P_R}{P_p}\right]$$

(ii) Products

$$N_i(PROD) = C_{DI}\, A_{TI}\, P_p \sqrt{\frac{2C_p}{R^2 T_{EM}}}\ FCTN\left[\frac{P_R}{P_p}\right]$$

Where T_{EM} is an integrated mean derived from previous incremental flows out of inlet valve.

The E and I valves can now be determined from:

$$E_o = X_o\, A1\, T_R$$

$$E_i = X_i\, A1\, T_E \left[\frac{P_E}{P_o}\right]^{\frac{\gamma - 1}{\gamma}}$$

$$I_o = N_o\, A1\, T_R$$

$$I_i = N_i\, A1\, T_p \left[\frac{P_p}{P_o}\right]^{\frac{\gamma - 1}{\gamma}}$$

or $$I_i = N_i\, A1\, T_{EM} \left[\frac{P_p}{P_o}\right]^{\frac{\gamma - 1}{\gamma}}$$

where $$A1 = \frac{R\gamma}{V}$$

5.4.1 Determination of valve lift and associated discharge coefficient

By taking the reference area used in the discharge coefficient definition as constant at the throat area, all that is required to determine the mass

flow rates, in addition to the pressure and temperature data, is the discharge coefficient at the particular valve lift.

The valve lift is determined using the polynomial

$$y = y_m + C_p x^p + C_q x^q + C_r x^r + C_s x^s + C_t x^t$$

as stated in Chapter 4.

Here x is the ratio of the valve opening angle to the lift period, measured from maximum lift, i.e. at $x = o$ $y = y_m$.

In the programme, no dwell in the valve opening period has been allowed for and x is derived from the crank angle and valve timing data.

The discharge coefficient is then found from the C_d against L/D curve fit polynomial, where D is the valve head diameter.

5.4.2 Determination of the cylinder volume and rate of change of volume

The cylinder volume at any crank angle is determined from the expression for the slide crank mechanism.

$$V = \frac{\pi B^2}{4}\left[\frac{2RC}{C-1} - R(1-\cos\theta) + L - L\sqrt{1-\left[\frac{R}{L}\right]^2 \sin\theta}\right]$$

where B = bore diameter

R = crank throw

L = connecting rod length

θ = crank angle measured from b.d.c

C = compression ratio

Differentiating with respect to time gives:

$$\dot{V} = \frac{\pi^2 B^2 NR}{2}\left[\frac{R \sin 2\theta}{2L}\sqrt{1-\left[\frac{R}{L}\right]^2 \sin^2\theta} - \sin\theta\right]$$

where N is the crankshaft speed in rev/sec.

With the rate of heat transfer determined, using the Eichelburg expression for heat transfer coefficient (Ref. 60), the rate of pressure rise can now be determined using the 4th order Rung-Kutta method of numerical integration.

5.5 Effects of engine geometry on inlet pipe pressure, flow and engine volumetric efficiency

5.5.1 Introduction

The processes involved in the inlet tract and cylinder, during and leading up to the induction period, are complex. Many attempts (Ref. 2, 3, 12, 13, 14, 38) have been made to present relatively simple expressions, as an aid to engine design and the determination of operating parameters beneficial to inertia and pulsation effects in the induction manifold gas.

All of these attempts must, however, be based on simplifications and assumptions and must be used with discretion.

Some attempts contain the results of a great deal of experimental work and provide a good indication as to the probable effects of design changes on the induction performance.

Of the above mentioned references, two were considered to present data relevant to the high speed engine configuration under consideration.

The series of articles by D. Broome (Ref. 14) presents two interrelated parameters intended to indicate favourable conditions for wave effect and inertia ramming.

The first is the 'wave ram parameter' which is, in effect, the half period of the intake pipe expressed in terms of crankshaft degrees.

$$\theta_t = \frac{12NL}{a} = \frac{P}{2}$$

where N = engine speed (rev/min)

L = effective induction pipe length (m)

a = velocity of sound (m/s)

Favourable conditions for wave ram are said to occur when θ_t is related to θ_d, the duration of the depression pulse within the induction period and one complete engine cycle (720°).

The two expressions are:

$$720^\circ > \theta_t > \theta_d$$

$$2n\,\theta_t \simeq 720^\circ$$

and $\theta_t < \theta_d$

$$(2n - 1)\theta_t + \theta_d \simeq 720^\circ$$

The value of θ_d quoted is 110° to 150°, giving favourable resonance at values of θ_t, as shown in Table 5.1.

The second parameter is the 'inertia ram parameter' which is derived by considering pressure rise

available due to the inertia of the gas in the induction pipe. Several assumptions are made and when inlet timing is neglected the expression becomes:

$$\phi_t = \theta_t^2 \left[\frac{V_{cyl}}{V_{pi}}\right]$$

This parameter is not very successful as shown by the graphs of the results of Taylor, Livengood and Tsai (Ref. 39) which show large differences in ram effect at a constant ϕ_t due to changes in the inlet valve closing angle.

An attempt is made to include the effects of friction losses in the induction pipe and a non-dimensional friction factor is produced. It is then concluded that the mean gas speed is a good guide to the maximum performance of the induction system as it relates both wave effect and inertia effect:

$$\phi_t = 12\,\theta_t \left[\frac{u}{a}\right]$$

where u = mean speed in induction pipe (m/s)

Optimum and limiting ranges of the ram parameter are given for various inlet valve timings (Table 5.2)

The results given in Tables 5.1 and 5.2 are displayed graphically and enable optimum values of θ_t and ϕ_t to be selected at the desired timing.

The pipe length is then determined from θ_t and then the pipe bore is derived from the ratio of V_{cyl}/V_{pi}.

An alternative approach is given by Yagi et al (Ref. 13) in their paper on small displacement high speed engines.

The characteristic peaks and troughs on the volumetric efficiency curves are said to be due to synchronising the induction pressure pulsation produced at inlet valve closure with t.d.c. in the succeeding induction period. A pressure pulse at t.d.c. producing a peak and a depression producing a trough.

A term q_s called the pressure pulsation order is defined as the ratio of period between I.V.C. and t.d.c.(θ^*) and the periodic time of the natural frequency of the intake pipe;

$$\text{or} \quad q_s = \frac{t}{\tau}$$

$$\text{where} \quad t = \frac{\theta^*}{360} \cdot \frac{60}{N}$$

$$\tau = \frac{4L}{a}$$

$$\therefore \quad q_s = \frac{\theta^* a}{24NL}$$

or the ratio of θ^* to the pipe period in degrees.

If this is rearranged, a new term is defined as the pulsation matching index K_s, where

$$K_s = NL = \frac{\theta^* a}{24 q_s}$$

A plot of K_s against q_s is given and a comparison made with test results which indicate good agreement, with peaks occurring for values of q_s equal to 2.0,

3.0, 4.0 and troughs at 1.5, 2.5 and 3.5.

The amplitude of the pulsations is said to be controlled by:

(i) the effective inlet valve opening angle θ_{ecs} b.t.d.c,

(ii) the effective inlet pipe length L,

(iii) the pressure pulsation order q_s,

(iv) the mean flow coefficient of the inlet valve C_m.

The effective inlet valve opening angle θ_{ecs} is the angle at which the valve curtain area is 0.5 cm^2. The effect of θ_{ecs} on the pulsation amplitude is stated as 'a reduction in amplitude occurs when $0 > \theta_{ecs} > 30$ b.t.d.c'.

Large values of L will increase the pulsation amplitude provided excessive losses can be avoided with very long pipes.

With a single induction pipe the lower orders of q_s - 2, 3, 4 - will produce the maximum amplitude.

A high value of C_m will be beneficial to pulsation amplitude, whereas a C_m below 0.25 will damp out any effective pulsations.

The possible inertia effects in the induction pipe are indicated by the use of 'the inertia supercharging index' Z^*, which is modified to incorporate the mean discharge coefficient C_m to give:

$$Z^*(\theta_{ecs}) = \frac{\pi}{30} \frac{N}{a} \sqrt{\frac{V_{cyl}\, L}{A_v\, C_m}}$$

if A_v is replaced by the throat area A_T, which is the reference area related to C_m in the current work.

$$Z^* = \frac{\pi}{30} \frac{N}{a} \sqrt{\frac{V_{cyl}\, L}{A_T\, C_m}}$$

This can be rearranged to give:

$$Z^{*2} = \frac{\pi^2}{30^2} \frac{N^2 L^2}{a^2} \left[\frac{V_{cyl}}{V_{pi}}\right] \left[\frac{A_p}{A_T}\right] \frac{1}{C_m}$$

but relating this to Broome's ϕ_t gives:

$$Z^{*2} = \frac{\pi^2}{12^2 \times 30^2}\, \phi_t \left[\frac{A_p}{A_T}\right] \frac{1}{C_m}$$

$$\text{or} \quad Z^* = \frac{\sqrt{\phi_t}}{114.6\sqrt{C_m}} \sqrt{\frac{A_p}{A_T}}$$

For comparison purposes, if A_p/A_T is taken as unity and $C_m \simeq 0.4$:

$$Z^* = \frac{\sqrt{\phi_t}}{72.5}$$

From Fig. 5.5.1/1 which is replotted from Ref. 13, a θ_{ecs} of 30° gives $\phi_t = 4743$ and a θ_{ecs} of 60° gives $\phi_t = 8883$, whilst not being in the optimum range quoted by Broome, is within the limiting range.

The expression Z^* can also be rearranged to give

$$Z^* = \frac{\pi}{30}\sqrt{\left[\frac{B}{D_T}\right]^2 \frac{V_p}{C_m a}\ 30\frac{N}{a} L}$$

where V_p is the mean piston speed.

But $\left[\frac{B}{D_T}\right]^2 \frac{V_p}{2\,C_m a} = Z$ the gulp factor or mean inlet mach index,

and $\frac{NL}{a} = 24p$ where p is the inlet pipe period.

Therefore $Z^* = 0.117\sqrt{Zp}$

Hence an engine designed for a known gulp factor at maximum torque and a known inlet valve timing can, from the plot of Z^* against θ_{ecs}, have selected an inlet pipe period and hence length, to achieve maximum inertia and pulsation effect at the designed speed.

Plotted on Fig. 5.5.1/1 are lines of constant Z value at various values of q_s the pressure pulsation order.

Table 5.3 shows values of p, the pipe period, and associated effective inlet valve closing angle θ_{ecs} for optimum Z^* for various gulp factors.

Other attempts to relate engine geometry and volumetric efficiency are rather limited, as restrictions are placed that do not apply in practice.

King (Ref. 2) produces many relationships based

on his inertia theory, but they refer to the effect of changing one parameter, which in practice is not usually the case.

Taylor (Ref. 1) presents data on the effects of changes in engine geometry, but the work mainly relates to conditions of small overlap and no inertia or pulsation effects.

5.5.2 Theoretical prediction of induction performance

The effects of engine geometry changes on the volumetric efficiency of an engine are extremely difficult to quantify to any degree of accuracy, due to the large number of interrelated parameters and the processes involved.

In order to obtain some information as to the trends involved and compare the variations with those expected from previous work, it was decided to look at three areas:

(i) Variation of engine swept volume with constant compression ratio and bore/stroke ratio.

(ii) Variation of bore/stroke ratio with constant swept volume and constant compression ratio.

(iii) Variation of inlet valve closing angle with constant bore/stroke ratio, constant swept volume and constant compression ratio.

5.5.2/1 Variation of volumetric efficiency with swept volume

Three swept volumes were considered as in Section 2 500cc, 375cc and 250cc.

The compression ratio was maintained at 11.26:1 as this represented the basic design of the Weslake WR 275 engine. The bore/stroke ratio was maintained at 1 and the basic details of engine geometry are given in Table 5.4.

The results of the programme predictions are shown in Fig. 5.5.2/1. The basic shapes of all the graphs are similar, showing the jagged nature due to pulsation effects and the peak in the average volumetric efficiency due to gas inertia.

(Note: The calculated points at 500 rev/min intervals were connected by straight lines in the absence of intermediate data.)

Looking at the 500cc results on Fig. 5.5.2/1 in detail shows that peaks occur at 7500, 6000, 5000 and 3500 rev/min. The induction pipe length was 300 mm giving pipe periods of 164.2°, 131.4°, 109.5° and 76.6°. Half these periods agree with those quoted by Broome, representing values of n of 4, 5 and 6 (Table 5.1).

(Note: θ_d was found to be approximately 105°.)

Comparison with the pulsation order q_s (Ref. 13) is less accurate due to the definition of q_s as $\frac{\theta^*}{p}$;

this is derived on the basis of a pressure pulse arriving at t.d.c. presuming that the pressure pulsations are initiated at inlet valve closure,

i.e. $\theta^* = 540 - \theta_{cs}$

Detailed plots of cylinder pressure and inlet pipe pressure Fig. 5.5.2/3 show that at 7500 rev/min the peak pressure is not synchronised with t.d.c. In fact peak pressure occurs at 20° b.t.d.c., and the pressure which is decreasing at t.d.c. assists the suction in the cylinder, Prosser (Ref. 17). Also the pressure pulsations are not initiated at inlet valve closure, the peak occurring 54° before inlet valve closure.

If the effective inlet valve angle at valve closure θ_{ecs} is taken (10% valve lift point), the peaks in the volumetric efficiency curve occur at values of of q_s of 3.1, 3.87, 4.64 which compare with 3, 4 and 5 quoted.

However, prediction of the point of maximum inertia effect using the 'inertia supercharging index' Z^* is more successful.

Effective inlet valve closing angle is 48° a.b.d.c.

giving $Z^* = 1.14$.

Valve throat area $= 1.271 \times 10^3$ mm^2

Mean discharge coefficient $= 0.4159$

$$\therefore \quad 1.14 = \frac{\pi}{30}\frac{N}{342}\sqrt{\frac{500 \times 0.312}{10^6 \times 1.271 \times 10^3 \times 0.4159}}$$

$$N = 6853 \text{ rev/min.}$$

The possible effect of changes in swept volume can be determined using a constant value for Z^* with fixed inlet valve timing. The expression can be derived as:

$$N_2 = N_1 \sqrt{\left[\frac{V_1}{V_2}\right]^{1.33} \left[\frac{D_{T_2}}{D_{T_1}}\right]^2}$$

which gives engine speeds of 7473 and 8435 rev/min for 375 cc and 250 cc respectively. This compares favourably with the graph Fig. 5.5.2/1 and with the statement by Taylor (Ref. 1) that "engines running with the same mean piston speed, same inlet and exhaust arrangements will have the same volumetric efficiency". If this is the case, the curves should be moved to the right by the ratio $\sqrt[3]{\frac{V_1}{V_2}}$ leading to peaks at 7542 and 8634 rev/min. This relationship is also true for the peaks, due to pulsation effects. As for the same pipe periods N x L must be constant, or, as L is related by the cube root of the volume change, the same expression is true for the peaks. This can be seen from the graph.

5.5.2/2 Variation of volumetric efficiency with bore/stroke ratio

Three bore/stroke ratios were considered 0.8, 1.0 and 1.2. The compression ratio was maintained by

changing the valve included angle, but the valve lift/diameter ratio was maintained at 0.2912 so keeping the mean discharge coefficient constant. Geometry details are given in Table 5.5, cylinder capacity was maintained at 500 cc. The results are shown on Fig. 5.5.2/4.

Two points are immediately obvious, (i) the improvement in volumetric efficiency at high engine speed as the bore/stroke ratio is increased and (ii) the shift in the position of peak volumetric efficiency to a lower engine speed as the bore/stroke ratio is reduced.

The changes in peak volumetric efficiency due to the bore/stroke ratio variations are difficult to relate simply. King (Ref. 2) states that according to his theory the maximum b.m.e.p. (which is directly related to volumetric efficiency) should change as the sixth root of the bore/stroke ratio, provided the ratio of the fourth root of the intake area/bore area remains constant. This last ratio does remain constant at 0.684 and so the improvement in volumetric efficiency expected, when changing from 0.8 to 1.2 bore/stroke ratio, should be 3%. The actual improvement is in the order of 12%.

The major factor influencing the relative breathing

efficiency is the effective inlet area

$$C_m \times 2 \times \pi \times \frac{D_{T_I}^2}{4} .$$

As C_m is constant, the area ratio is the ratio of the throat diameter squared. However, changing from 0.8 to 1.2 bore/stroke ratio produces an area ratio of 1.295, far in excess of the improvement of volumetric efficiency.

However, the peak points of volumetric efficiency occur at differing mean piston speeds, increasing from 18.49 m/s for a bore/stroke ratio of 1.2 to 21.29 m/s at 0.8. Taylor (Ref. 1) argues that, for an engine of fixed valve geometry, the "volumetric efficiency is a unique function of piston speed". Therefore, in a model with variable bore and stroke but fixed capacity, it is reasonable to assume that the changes in volumetric efficiency will be related to the product of the inlet effective area and the mean piston speed, at peak volumetric efficiency.

If this product is determined for the three cases considered, the results are 1, 1.058, 1.124 relative to 0.8 bore/stroke ratio. The peak volumetric efficiency ratios are 1, 1.033, 1.118.

The relative positions of the peak volumetric efficiency points can be determined using the Inertia supercharge index Z^*.

If the inlet effective closing angle is maintained constant, Z^* will be constant and the relationship becomes:

$$\frac{N_1}{a}\sqrt{\frac{V_1 L_{P_1}}{A_{mes_1}}} = \frac{N_2}{a}\sqrt{\frac{V_2 L_{P_2}}{A_{mes_2}}}$$

Now $L_{P_1} = L_{P_2}$ and $C_{m_1} = C_{m_2}$

$$\therefore \quad N_2 = \left[\frac{D_{TI_2}}{D_{TI_1}}\right] N_1$$

or the relative speeds of peak volumetric efficency are directly related to the throat diameter ratio. For a bore/stroke ratio of 0.8 the expression for Z^* reduces to:

$$Z^* = 1.782 \times 10^{-4} N$$

Now $Z^* = 1.14$ at effective I.V.C. of 48° abdc

$\therefore \quad N = 6397$ rev/min.

Using the throat diameters gives peaks at 6853 and 7283 rev/min for bore/stroke ratios of 1.0 and 1.2 respectively. These are plotted on Fig. 5.5.2/4 and give good agreement.

5.5.2.3 Variation of volumetric efficiency with inlet valve closing angle

The effect of a change in the inlet valve closing angle can be determined by considering the effect on the inertia supercharge index Z^*:

$$Z^* = \frac{\pi}{30} \frac{N}{a} \sqrt{\frac{V_{cyl}\, L}{A_T\, C_m}}$$

If the engine geometry is maintained constant, Z^* will be related directly to N; or the engine speed at which maximum volumetric efficiency occurs will be determined by Z^*.

Reducing the inlet valve closing angle in 10° increments from 260° to 250° and 240° gives effective inlet closure angles (10% lift) of 48°, 39.3° and 30.6° which represent values of Z^* of 1.12, 1.02 and 0.96.

The engine speeds at which maximum volumetric efficiency occur are then determined by the ratio

$\frac{N_2}{N_1} = \frac{Z_2^*}{Z_1^*}$ giving peak speeds at 6583, 5993 and 5642 rev/min which are plotted on Fig. 5.5.2/5 and agree quite well with the mean line drawn through the pulsation effects.

Use of the inertia ram parameter derived by Broome also indicates the relative change of engine speed at which maximum inertia effect is achieved due to a change in inlet valve timing. Table5·2 indicates that a reduction of inlet valve timing from 90° a.b.d.c. to 30° a.b.d.c. is equivalent to a change in ϕ_t from approximately 6000 to 4250. As the cylinder volume and pipe volume remain constant, the ratio

of the ϕ_t values is equal to the square of the θ_t values. This gives the engine speed ratio as $\sqrt{\frac{4250}{6000}} = 0.842$ which compares favourably with that shown.

If Fig. 5.5.2/5 is compared with Fig. 6.3.3/3, which is for an engine with no induction effects, the similarity is obvious. The optimum angle for inlet valve closing to achieve best volumetric efficiency has been shown to be a function of the gulp factor. This can be seen from the carpet graph Fig. 5.5.2/6, which indicates that an inlet valve timing of 80° a.b.d.c. is optimum for an engine speed of approximately 7000 rev/min ($Z = 0.645$). If peak volumetric efficiency were required at lower engine speed, for example 6000 rev/min ($Z = 0.553$) an inlet valve closure at approximately 62° a.b.d.c. would be required. The peak or fold in the carpet graph gives the optimum timing value as a function of gulp factor.

The above conclusions assume that the change in the valve closure point can be achieved with a constant lift and a reduced period. Whether this is possible will depend on the valve gear design constraints. By reducing the cam half period from 83° to 80° and 78° equivalent to I.V.C. at 80° a.b.d.c., 68° a.b.d.c and 60° a.b.d.c., the maximum cam nose acceleration increases from -0.00426 mm/deg^2 to -0.004597 mm/deg^2

and -0.00484 mm/deg^2. This may or may not allow the valve lift to be maintained at 9.525 mm in this case.

Conclusions:

1. Use of the 'inertia supercharge index' as defined in Ref. 13 will give a good indication as to the probable effects of changes in engine geometry on the position of the peak volumetric efficiency in the engine speed range.
Pulsation peaks can be determined using the inlet pipe period, peaks occurring at values of 245, 164, 130, 109, etc., crankshaft degrees.

2. With fixed geometry, a reduction in swept volume will increase the speed at which peak volumetric efficiency occurs but the peak efficiency will remain essentially constant.

3. Changes to the bore/stroke ratio at a constant swept volume will cause a two-fold effect on the peak volumetric efficiency - (i) its position in the speed range will depend on the relative change in throat diameter, and (ii) its magnitude will change in relation to the change in product of the mean piston speed at the peak and the inlet throat area.

4. The optimum inlet valve closing point is a function of engine speed or, in the case of fixed geometry, the gulp factor.

Movement of the position of peak volumetric efficiency due to a change in valve timing can be found directly from the effect on the 'inertia supercharge index' Z^*.

The magnitude of the change in volumetric efficiency due to changes in inlet valve timing is not easily determined. In the case considered, it was small at 0.225% per degree. It is likely that this could not be maintained below a gulp factor of 0.5, where little improvement could be expected.

5. If inertia effects are considered 0.5 does not constitute a limit on gulp factor beyond which improvements in volumetric efficiency are not possible. This is confirmed by this analysis and reference to the experimental results presented in Ref. 13. Here peak volumetric efficiencies for a 4-valve single cylinder engine occur at a Z value of 0.594.

It is possible that for engines with large valve overlap and delayed inlet valve closing, a modified gulp factor could be used which incorporates the valve timing similar to that proposed in Ref.3. The limits taken from this paper are plotted on Fig. 5.5.2/5.

The 'mean inlet mach index' Mim is not a useful design tool, as it incorporates the dependent quantity the volumetric efficiency.

6. The theoretical analysis carried out is in agreement with the predictions derived from experimentally proven relationships.

5.6 Motoring tests on the Weslake WR 275 Engine

5.6.1 Introduction:

It was decided to carry out motoring tests on the Weslake WR 275 engine which has cylinder head geometry as described in Section 2.

This validated the model used in the predictions of geometric effects on the engine volumetric efficiency. As dynamics in the induction pipe have been considered, measurements of induction pipe pressure were taken as well as the overall volumetric efficiency. This enabled a comparison to be made with the predicted values.

Various problems were encountered in attempting to motor this engine due to its high compression ratio and large bore area. Sudden torque reversals in the drive chain to the engine were produced at the start of motoring. The engine has no external flywheels, the main inertia being in the crankshaft webs.

To overcome the damaging effects of the torque reversals on the variable speed drive, the engine was started with the combustion space vented. When sufficient crankshaft speed had been obtained, the valve was closed and the engine speed could be increased to the desired value.

WESLAKE WR 275

Engine specification

Configuration: Single cylinder air-cooled 4-stroke

Capacity: 500 cm^2

Bore x stroke: 86.03 x 86.03 mm

Crank radius/con rod length: 0.25

Compression ratio: 11.26 : 1

Lubrication: Total loss

Inlet valve:

Number	2
Diameter	33.5 mm
Max. lift	9.525 mm
Opens at	72 deg b.t.c.
Closes at	100 deg b.t.c.

Exhaust valve:

Number	2
Diameter	31.75 mm
Max. lift	9.525 mm
Opens at	84 deg a.t.c.
Closes at	56 deg a.t.c.

5.6.2 Motoring test rig

A general arrangement of the test rig is shown in Fig. 5.6.2/1. The essential elements are the 2 H.P. 3 phase A.C. motor driving through the variable speed unit (Allspeeds Ltd.) to the engine via the DPX 2 Froude dynamometer.

The Allspeeds unit provides up to a 3 : 1 speed ratio and is rated at 1.5 h.p. The unit relies on the tilting of the axes of several large steel ball elements and the drive on a subsequent wedging action. It is not therefore very efficient at transmitting drive when the load shaft suffers sudden torque

reversals at low speed.

The motor runs at 1420 rev/min, giving a theoretical maximum output speed of 4260 rev/min at the engine within the limitation of 2 h.p.

The units in the drive line are mounted on two channel section girders supported on vibration isolating units

The engine is connected to the dynamometer through a very rigid rubber flanged coupling. The flange adjacent to the engine is drilled at t.d.c. and at 10, 20 and 30° intervals either side of t.d.c. The set screws are inserted to provide a crank angle marker trace via an inductive pick-up and marker amplifier.

The other flange is scalloped around the six retaining bolts and this is used to give a pulse output from an inductive pick-up to a counter timer. This displays the engine speed.

The heavily finned cylinder is cooled during prolonged running by an electrically driven centrifugal fan.

During the tests the exhaust was open to the atmosphere as no exhaust dynamics are at present incorporated in the computer model.

On the engine intake side a short cast alloy manifold converts the dual intake ports into a single circular opening for subsequent attachment of the

carburrettor in practice or, in this case, the intake pipe.

A rectangular receiver of 60 times the engine swept volume is attached to the upstream side of the intake pipe, this being fitted with a U tube manometer.

Flow through the engine was initially monitored using a 1 m^3 receiver, fitted with a 0.75 in BS 1042 orifice. This was later replaced by a Ricardo Alcock viscous flow meter, Type 1003H, which has a maximum flow capacity of 100 x $10^{-3} m^3/s$. With the 500 cc engine, 4000 r.p.m. would represent an air consumption in the order of 16 x 10^{-3} m^3/s, hence the meter is operating at the lower end of its capacity but has adequate linearity to prevent any problems at the expected flow rates.

The pressure drop across the viscous element is registered by a multi-range manometer.

During the tests, three induction pipe lengths were used, a pipe of 1.785 m, used with the $1m^3$ receiver, and two pipes of 0.516 m and 0.3 m length. The latter represented the length of the induction tract when fitted with the standard carburettor.

The pressure fluctuations in the pipe were monitored by a pressure transducer fitted in the pipe at a suitable nodal position. Details of the pressure measuring and other instrumentation is given in Section 5.6.3.

5.6.3 Instrumentation

The main instrumentation can be split into two areas, (i) pipe pressure measurement and (ii) flow measurement.

(i) Pipe pressure measurement

The pressure transducer used in the intake pipe was an RDP P5/10 121 transducer operating as an LVDT. Details of its specification are given in Table 5.6.

The transducer was connected to a Sangamo Weston Type C56 transducer meter and the system was statically calibrated using a Barnet Industrial deadweight tester, which had a range of 0.1 to 700 bar.

The system output was displayed on a Hewlett-Packard 3465 A Multimeter. An acceptable calibration was achieved using a gauge factor setting of 2.38 on range 10 of the C56. Linearity and repeatability were good, despite operating at the lowest range of the dead weight tester. The calibration is shown in Fig.5.6.3/1.

Two methods were used to display and record the pressure fluctuations; (i) by passing the signal from the C56 to a Bryans tungsten light recorder via a Tektronix storage oscilloscope, and (ii) by the use of a Gould Type OS4000 digital storage oscilloscope and an Advance

HR2000 X-Y Plotter. Details of all these instruments are given in Table 5.6.

(ii) Flow measurement

Two methods of flow measurement were used during the tests, as explained in Section 5.6.2.

The 1 m^3 receiver was a mobile unit that could be fitted with a range of BS.1042 orifices according to the flow range required. A 0.75 in diameter orifice was used for the tests, which at 3000 rev/min produced a pressure drop across the orifice of 20 mm of water.

The receiver was replaced by an Alcock viscous flow air meter Type 1003H, having a range up to 100 x 10^{-3} m^3/s.

The pressure drop across the viscous element is measured using a multislope manometer and high accuracy can be obtained.

The meter is calibrated for volumetric flow at 20°C and the volume of air leaving the meter can be determined directly by use of this calibration, the manometer reading and a scale multiplier related to the manometer slope.

The free air entering the meter can be determined by correcting for the pressure drop across the unit, which was measured using a manometer.

The mass flow rate was calibrated by converting

to normal temperature and pressure of 0°C and 760 mm Hg, and converting this volumetric rate to a mass flow rate. Little trouble was experienced with this unit, the main problem being air bubbles in the multislope manometer.

5.6.4 Experimental method

Operation of the rig was as described in the introduction, the motor ran at constant speed and the engine speed was controlled by the Allspeeds unit. In practice it was found that a maximum achievable speed of 3000 rev/min limited the range of results. The tungsten light recorder was used when a suitable trace had been obtained on the oscilloscope. The maximum paper speed available was 1000 mm/s, which gave 20 mm per cycle at 3000 rev/min, which with the rapid fluctuations in the short inlet pipe presented some difficulties in analysis. However repeatability of the trace was good and some useful results were obtained.

The change to the digital storage oscilloscope and the X-Y plotter enabled a better display and recording of the pipe pressure to be obtained.

The Gould OS4000 oscilloscope has the facility of a roll mode in which the stored signal is continually being updated at a selected rate. This gives the appearance of the trace moving across the screen and the trace can then be positioned before storing without a defined trigger point. Triggering can be initiated at a set level on a positive

or negative slope. Once stored, the trace can be outputted to the X-Y plotter via the 4002 output unit.

The output rate is preset and the X-Y plotter can be set to reproduce the screen scale as the unit produces 100mV per cm of screen height.

The oscilloscope has two channels and these were used for the pressure trace and the crank angle marker trace.

Ambient pressure was obtained on the plot by storing the line when the engine was stationary. Adjustments to the plot can then be made allowing for the fact that the transducer records were relative to the mean engine intake pressure and not ambient pressure. Theoretical results are relative to an input mean pipe pressure.

Operation of the viscous flow meter was very easy - requiring only a record of manometer readings, ambient temperature and pressure.

Frequent checks were made to ensure that the multi-slope manometer zeroed correctly and remained level.

5.6.5 Experimental results and discussion

Experimental runs were carried out up to 3000 rev/min where it was found that no further increase in speed could be obtained with the 2 h.p. motor used.

At low speeds below 1000 rev/min, the conditions were unstable and fluctuations occurred on the flow meter manometer. This was because the engine runs

with a large valve overlap of 128° and considerable reverse flow takes place through the inlet valve at low speed before inertia effects become significant.

The results of induction pipe pressure recordings are shown in Fig. 5.6.5/1 and /2. These results were at 1500 rev/min and conditions were steady. The first figure was obtained using the tungsten light recorder and the second with the digital storage oscilloscope and they show good agreement. Both traces were at node 7 of a 0.516 m long induction pipe, there being 13 nodal points in the theoretical analysis, numbered from the open end of the intake pipe.

The intake pipe length is taken as the distance from the free end to the valve seat.

Comparison with the theoretical prediction, using the method of characteristics, is shown in Fig. 5.6.5/3 and two features are evident -

(i) an apparent phase lag of the experimental trace over the theoretical, and (ii) an amplitude attenuation in the initial period of oscillation in the pipe as the inlet valve closes. The comparison however shows good agreement with the general disposition of the trace compared with the theoretical prediction. Good agreement is shown in pressure wave amplitude when approaching the inlet

valve opening period where the inlet pipe dynamics will affect the induction performance.

The inlet pipe period determined from the expression in Section 5.1 is 54.3° for the 0.516 m pipe. This compares well with the periods from the two traces during the inlet valve closure period of 52.5° from the tungsten light produced trace and 55.4° from the digital oscilloscope trace.

The average phase lag in Fig. 5.6.5/1 is 34.4° and that in Fig. 5.6.5/2 is 27.6°. This is measured relative to the crank angle marker trace. The blips on the trace from the inductive pick-up are caused by set screws in the coupling flange passing the inductive head. These screws have 4 mm heads, which represent 3° of arc on the flange so only a slight error is likely from this source.

The accuracy of positioning the crank angle markers has been checked relative to the piston t.d.c. and is accurate within the limits of angular measurement possible on the coupling flange. An error of 0.5 mm on positioning t.d.c. at the piston is equivalent to 6° crankshaft rotation.

The other source of a phase lag is within the instrumentation. When the inlet valve is closed the pipe period is 54.3° which represents a frequency of 165.7 Hz. The R.D.P. transducer, which is a 1st order system, has a frequency response of 500 Hz and is hence

operating at a normalised frequency of 0.331. Referring to the Bode plots taken from Ref. 40; Figs. 5.6.5/4-5, an attenuation of - 0.2 dB and a phase lag of 18^{o} is indicated. This represents an amplitude ratio of 0.977.

The Sangamo transducer meter is a second order system , with a damping factor of 1.4 and a corner frequency of 500 Hz. Operating at 0.331 normalised frequency produces zero attenuation, but approximately 30^{o} phase lag.

When using the tungsten light recorder, which has a frequency response of 700 Hz, an additional lag of 20^{o} might be expected. The digital storage oscilloscope has a frequency response of 1 MHz and will produce no significant distortion. This leads to the conclusion that the tungsten light trace could suffer an amplitude ratio reduction of 0.977 and a phase lag of 10.3 crank angle degrees, whereas the digital oscilloscope trace could have the same amplitude reduction but a smaller phase lag of 7.2 crank angle degrees. These figures are based on a single frequency sinusoidal input which is not the case in practice.

If the engine speed is increased, the results change quite considerably - Fig. 5.6.5/6, which is for an engine speed of 2000 rev/min. There is also a very much better comparison between the

experimental and theoretical graphs. The experimental amplitude is now greater than the theoretical amplitude but is of the same order. The phase lag has now been reduced to 12.8° of crank angle.

As the normalised frequency remains at 0.331, the amplitude ratio and phase lag previously determined from the instrument characteristics is the same at 0.977 and 48° of cycle. This translates to 0.977 at 9.6° crank angle degrees lag, which compares favourably with the results shown in Fig. 5.6.5/6. If the speed is increased further, it can be expected that the comparison will become even more favourable as inertia effects become significant during the valve overlap period.

An indication of the adverse effects of large valve overlap at low speed can be gained by an examination of the theoretical inlet valve flow during one engine cycle. At 1500 rev/min the net inlet valve flow was 4.916×10^{-4}kg. However, the gross inlet flow was 7.529×10^{-4}kg, accompanied by an outflow of 2.613×10^{-4} kg, or the outflow was 53% of the net.

At 2000 rev/min this outflow is reduced to 23% of the net flow of 5.137×10^{-4}kg. This gives an indication of the oscillatory nature of the inlet flow at low engine speeds. It is this that is thought to be

the main contributory factor to the discrepancies shown in Fig. 5.6.5/3 and /6.

Predicted and experimental results for the 300 mm 516 mm induction pipes are given in Figs. 5.6.5/7-8. Good agreement is shown above a value of n = 5 for the wave index as used by Broome (Ref. 14). After this the engine seems insensitive to pulsations of this order. This is thought to be due to the progressive reduction of engine speed intervals at which peak pulsation effects occur. This is combined with the imperfections in the induction tract away from the theoretically defined pipe, smearing the volumetric efficiency over this low range of engine speed. This, combined with a certain instability in the wave action calculations at the large valve overlap and long time interval, produces the deviation of theoretical and experimental results. This is also illustrated by the wave pressure results.

At higher engine speeds, agreement between experiment and theory is good and the model used produces a good description of the engine breathing potential.

TABLE 5.1

POINTS OF RESONANCE AS DEFINED BY THE WAVE RAM PARAMETER θ_t. from Ref.14.

n	3	4	5	6	7	8
θ_t degrees	114-120	82-87	63-68	52-55	44-47	38-41

TABLE 5.2

OPTIMUM AND LIMITING RANGES OF THE RAM PARAMETER FOR VARIOUS INLET VALVE TIMINGS. Ref. 14.

Effective inlet valve closing point Degrees a.b.d.c. at 10% lift	Inertia ram parameter $\phi/_t$		Mean gas velocity m/s	
	Optimum range *	Limiting range *	Optimum range	Limiting range
30	2500 - 3500	1000 - 6000	15 - 60	90
60	3500 - 5000	1000 - 9000	15 - 60	90
90	5000 - 7000	1000 - 14000	15 - 60	90

* Applies to cases where wave effects are entirely absent.

TABLE 5.3

PIPE PERIOD AND ASSOCIATED EFFECTIVE INLET VALVE CLOSING ANGLE FOR OPTIMUM Z* FOR VARIOUS GULP FACTORS

Z Gulp factor	p Inlet pipe period $/\theta_{ecs}$ effective inlet valve closing angle			
	$q_s = 1$	$q_s = 2$	$q_s = 3$	$q_s = 4$
0.3	$474/63$	$249/38$	$177/2$	
0.4		$245/51$	$169/32$	$133/2$
0.5		$240/59$	$167/43$	$128/28$

TABLE 5.4

DETAILS OF ENGINE GEOMETRIES USED IN EXAMINING THE EFFECT OF SWEPT VOLUME ON VOLUMETRIC EFFICIENCY

Swept volume cc	Bore mm	Valve included angle	Inlet valve dia.mm	Inlet throat dia.mm	Mean discharge coeff.	Inlet valve lift mm
500	86.02	40°	32.70	28.45	0.4159	9.53 *
375	78.16	40°	29.64	25.61	0.4159	8.63 *
250	68.27	40°	25.80	22.06	0.4159	7.51 *

TABLE 5.5

DETAILS OF ENGINE GEOMETRIES USED IN EXAMINING THE EFFECT OF BORE/STROKE RATIO ON VOLUMETRIC EFFICIENCY

Bore/stroke ratio	Valve included angle	Bore mm	Inlet valve dia.mm	Inlet throat dia.mm	Mean discharge coeff.	Inlet valve lift mm
0.8	59°	79.86	30.66	26.56	0.4159	8.93 *
1.0	40°	86.02	32.70	28.45	0.4159	9.53 *
1.2	28°	91.42	34.62	30.24	0.4159	10.08 *

* The $\frac{L}{D}$ ratio was maintained at 0.291.

TABLE 5.6

INSTRUMENT	SPECIFICATION	OPERATING CONDITION
PRESSURE TRANSDUCER R.D.P. P5/10 121 L.V.D.T	$\pm$ 10 psia ($\pm$ 0.689 bar) OVER PRESSURE 4X RATED. SENSITIVITY at 5V @ 5 kHz ENERGISING SUPPLY 18 mv/psi (0.261v/bar) FREQUENCY RESPONSE 500 Hz @ 5 kHz ENERGISING SUPPLY. TEMPERATURE COEFFICIENT $\pm$ 0.05% FSD/^{o}C TEMPERATURE RANGE -20^{o}C - +100^{o}C	$\pm$ 2 psi ($\pm$ 0.138 bar) ENERGISING SUPPLY 5V @ 5 kHz up to 300 Hz AMBIENT TEMPERATURE
TRANSDUCER METER SANGAMO WESTON CONTROL Type C56	5Vrms @ 5 kHz OSCILLATOR STABILITY over 24 hr. $\pm$ .1% FSD TEMPERATURE COEFFICIENT OF SPAN $\pm$ 0.1%/^{o}C ACCURACY OF GAIN better than 3% MAXIMUM GAIN 0.4mVrms INPUT, 5V d.c OUTPUT ACCEPTABLE GAUGE FACTOR OF LVDT 0.5mV/V/unit MINIMUM 20 mV/V/unit MAXIMUM INPUT IMPEDANCE @ 5kHz 50k OUTPUT VOLTAGE $\pm$ 5V OUTPUT-INPUT FREQUENCY RESPONSE CHARACTERISTIC 2nd ORDER, LOW PASS BUTTERWORTH RESPONSE CORNER FREQUENCY 500 Hz DAMPING FACTOR 1.4 ATTENUATION ABOVE 500 Hz-40dB/decade ATTENUATION AT 500 Hz 3 dB	 3.6 mV/V/unit Up to 300 Hz

INSTRUMENT	SPECIFICATION	OPERATING CONDITION
TUNGSTEN OSCILLOGRAPH BRYANS SOUTHERN INSTRUMENTS LTD. SERIES 10-650	SENSITIVITY 20 - 0.1 V/cm GAIN X10 MAXIMUM INPUT VOLTAGE 200V INPUT RESISTANCE 1 M FREQUENCY RANGE D.C. TO 700 Hz FLAT TO WITHIN $\pm$5% TYPE OF GALVANOMETER SMI OPEN FRAME 1.1 kHz NATURAL FREQUENCY FLUID DAMPED PAPER SPEEDS 3 to 1000 mm/s OPERATING TEMPERATURE 0 - 45°C	 Up to 300 Hz AMBIENT TEMPERATURE
DIGITAL STORAGE OSCILLOSCOPE GOULD ADVANCE TYPE OS4000	DISPLAY 8 x 10cm. CRT VERTICAL DEFLECTION TWO CHANNELS BANDWIDTH DC - 10 MHz IN NORMAL MODE SENSITIVITY 5mV/cm to 20V/cm ACCURACY $\pm$3% HORIZONTAL DEFLECTION TIME BASE 1 us/cm to 20sec/cm ACCURACY $\pm$3% X EXPANSION CONTINUOUSLY VARIABLE FROM X1 to X10 DISPLAY VIA STORE VERTICAL RESOLUTION 25 STEPS/cm HORIZONTAL RESOLUTION DOUBLE TRACE 50 SAMPLES/cm	 Up to 300 Hz INPUT $\pm$2.75V MAX.

INSTRUMENT	SPECIFICATION	OPERATING CONDITION
OUTPUT UNIT GOULD ADVANCE TYPE 4002	ANALOGUE OUTPUT CHANNELS 1 and 2 AMPLITUDE 100mV/cm SCREEN HEIGHT with OV CORRESPONDING TO MIDDLE OF SCREEN. ACCURACY ±3% OF DISPLAY READ-OUT RATE RANGE 20s/cm - 200us/cm BY SWITCH 50s/cm - 1s/cm PRESET READ-OUT BANDWIDTH DC = 16kHz (-3dB)	
ALCOCK VISCOUS AIR FLOW METER	CALIBRATED RANGE	
G. CUSSONS TYPE No.1003H	0 - 100 x 10^{-3} $m^3/_s$	16 x 10^{-3} $m^3/_s$ MAX.
MULTI-RANGE MANOMETER RICARDO ALCOCK	5 POSITION MANOMETER CALIBRATED WHEN FILLED WITH BLENDED OIL RD 0.784 at 20°C	

FIG 5.5.1/1.

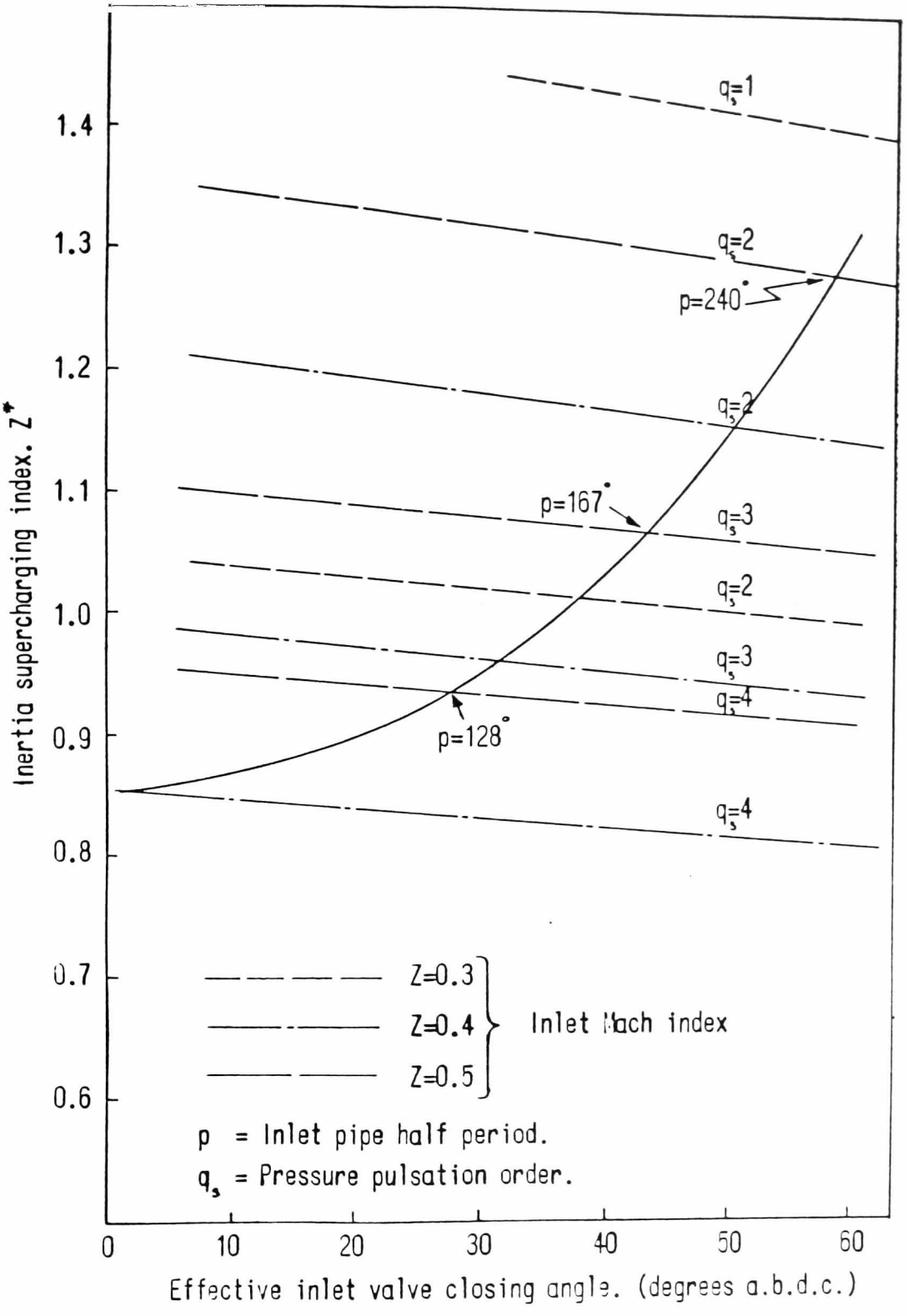

(FIG 5.5.1/1) REPLOT FROM REF(13) OF INERTIA SUPERCHARGING INDEX Z AGAINST EFFECTIVE INLET VALVE CLOSING ANGLE θ_{ecs}

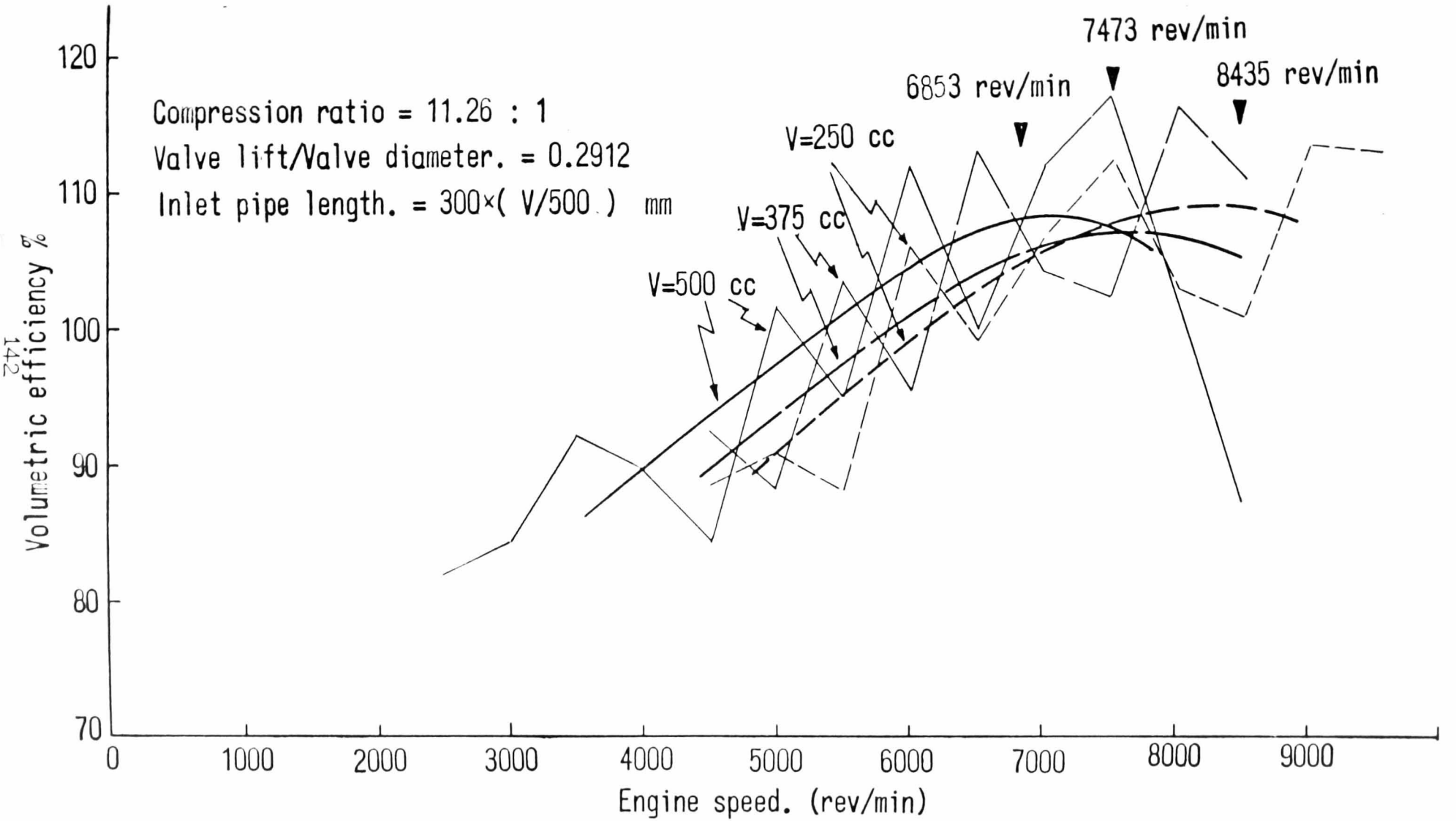

(FIG 5.5.2/1.) Effect of swept volume on volumetric efficiency.

FIG 5.5.2/1.

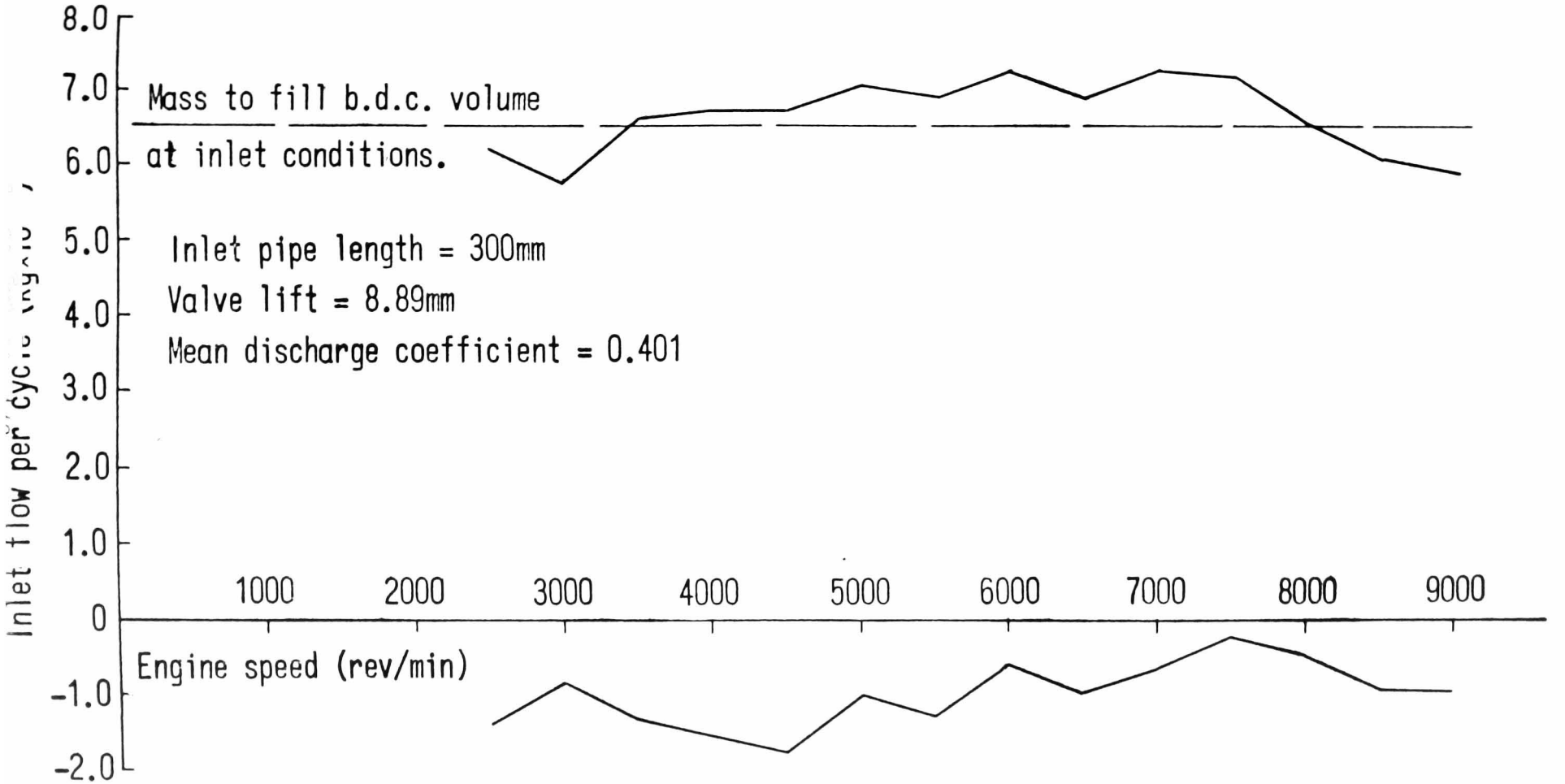

(FIG 5.5.2/2) Inlet flow per cycle against engine speed for the Weslake WRP 275 engine geometry.

FIG 5.5.2/2.

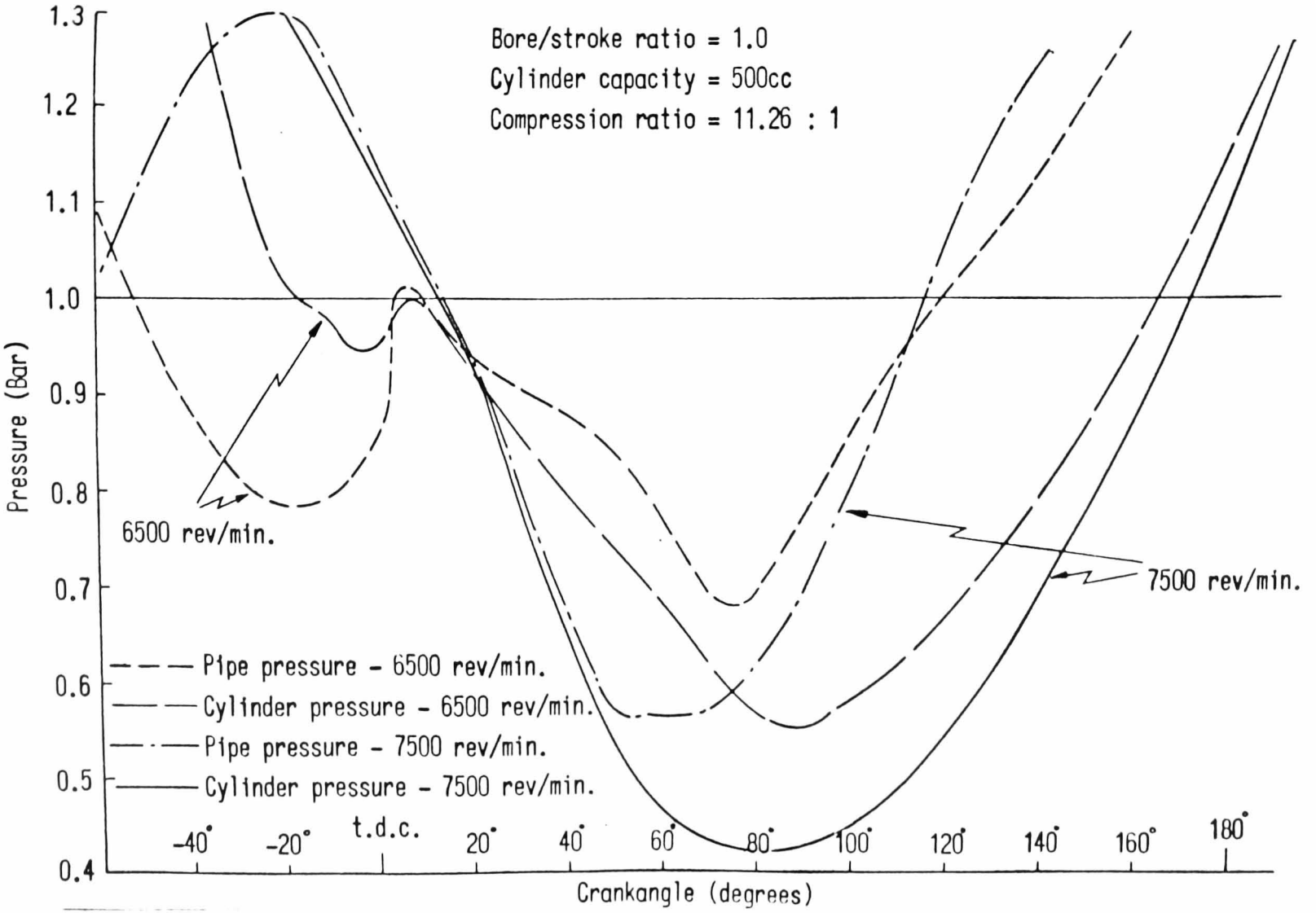

(FIG 5.5.2/3) Cylinder pressure and pipe pressure adjacent to the valve.

FIG 5.5.2/3.

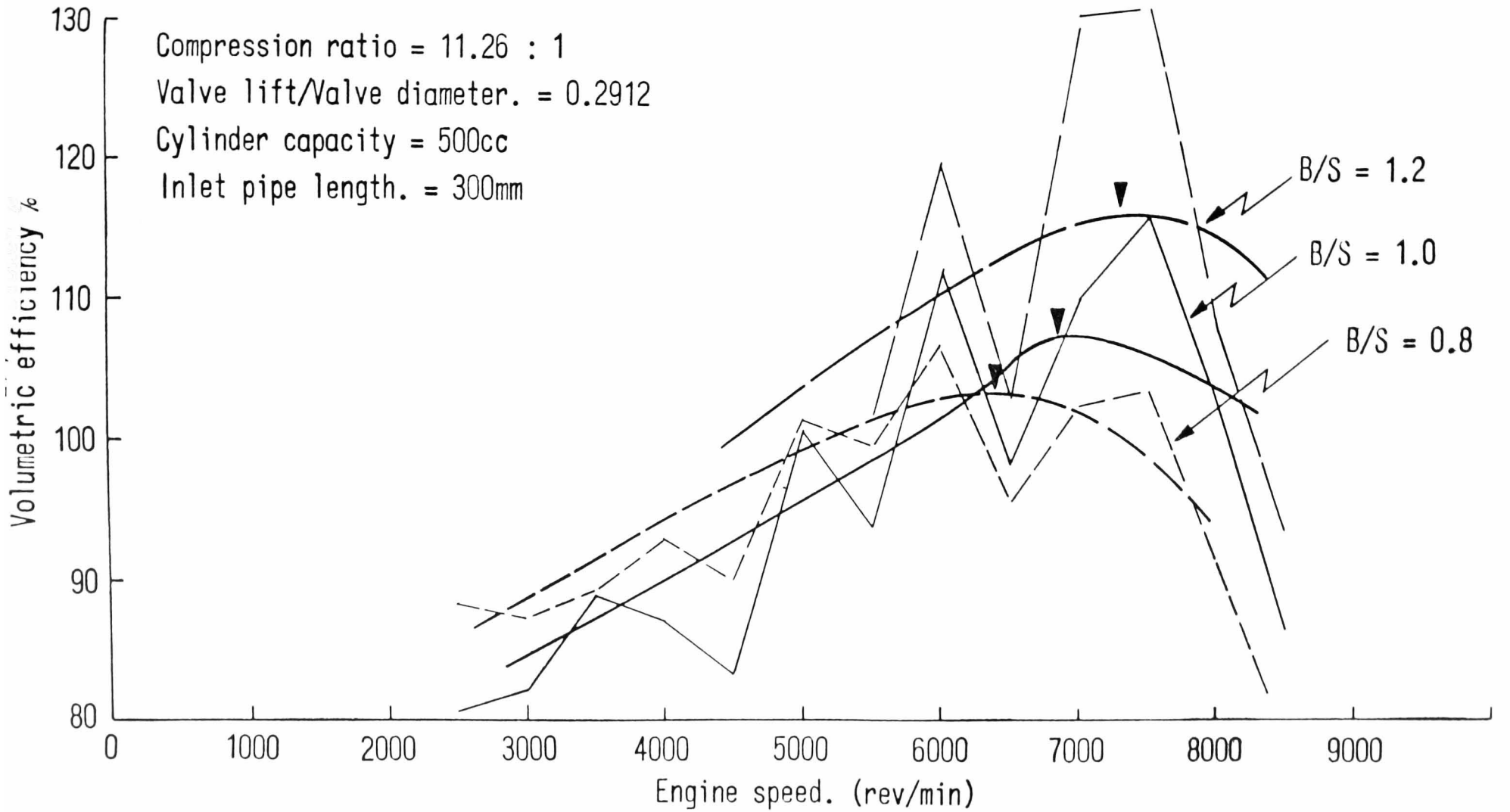

(FIG 5.5.2/4) Effect of Bore/Stroke ratio on volumetric efficiency.

FIG 5.5.2/4.

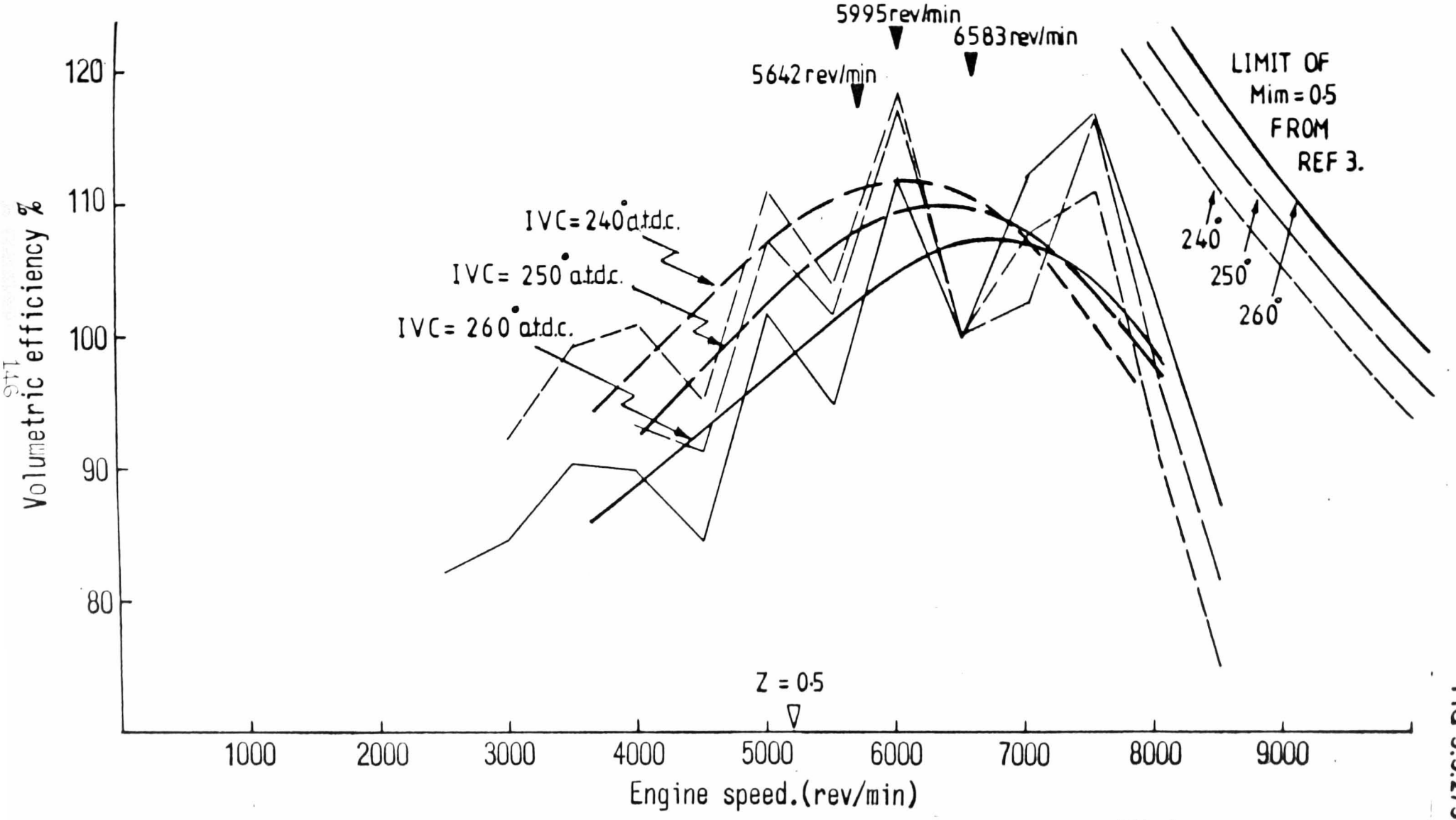

(FIG 5.5.2/5) Effect of inlet valve closing angle on volumetric efficiency.

FIG 5.5.2/5.

FIG 5.5.2/6.

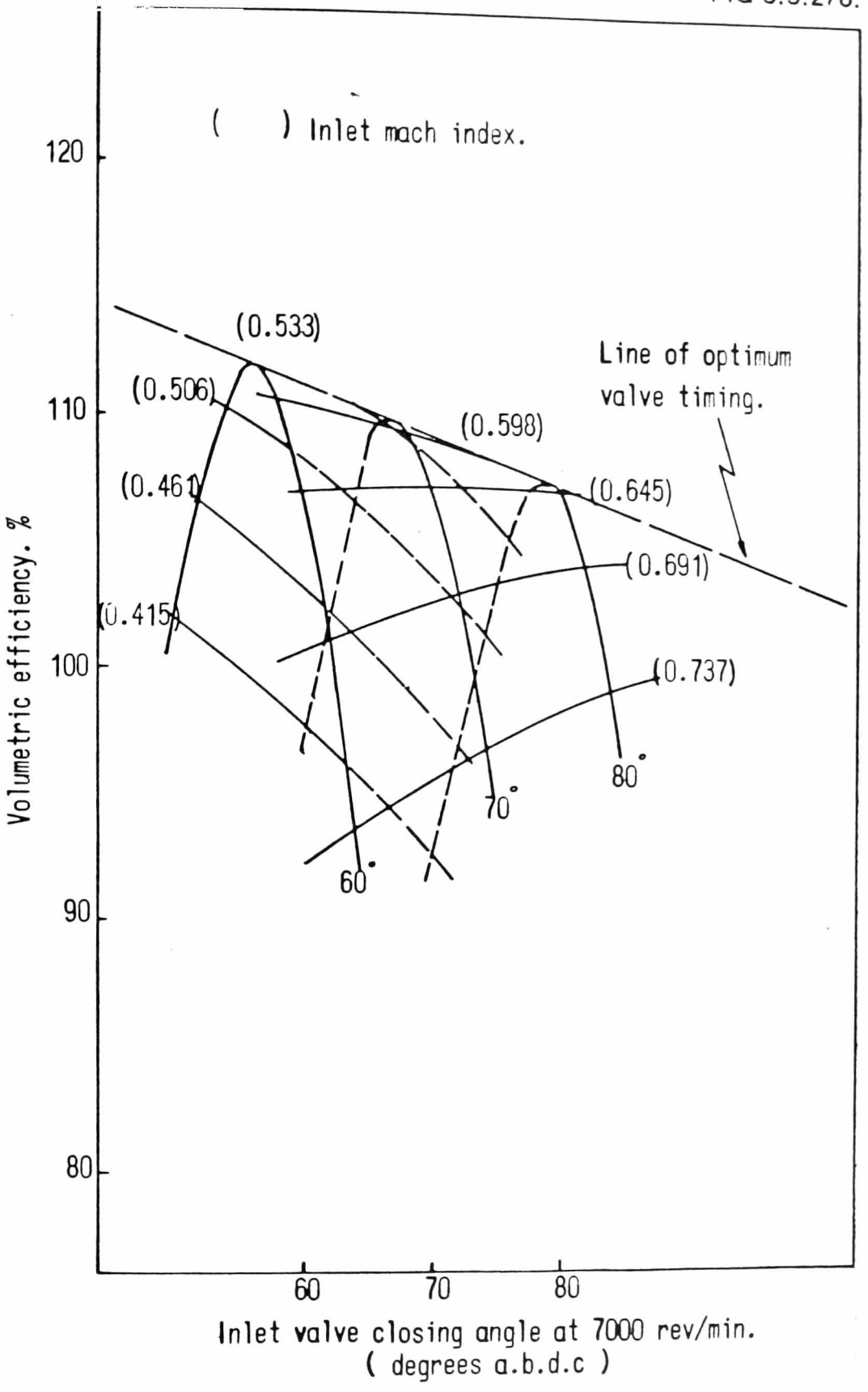

(FIG 5.5.2/6) VOLUMETRIC EFFICIENCY AGAINST INLET VALVE CLOSING ANGLE FOR VARIOUS VALUES OF INLET MACH INDEX.

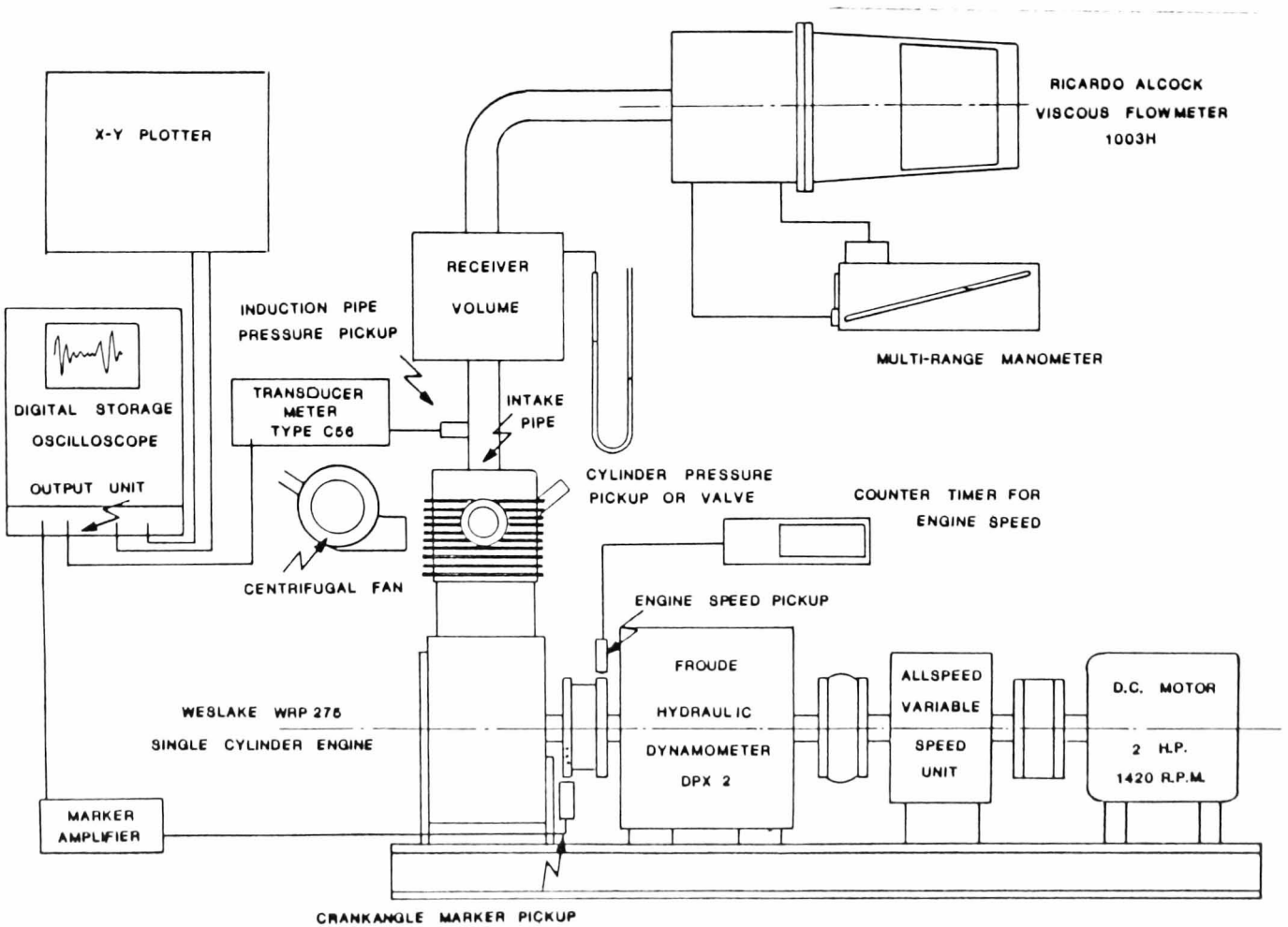

(FIG 5.6.2/1) General arrangement of motoring test rig.

FIG 5.6.3/1.

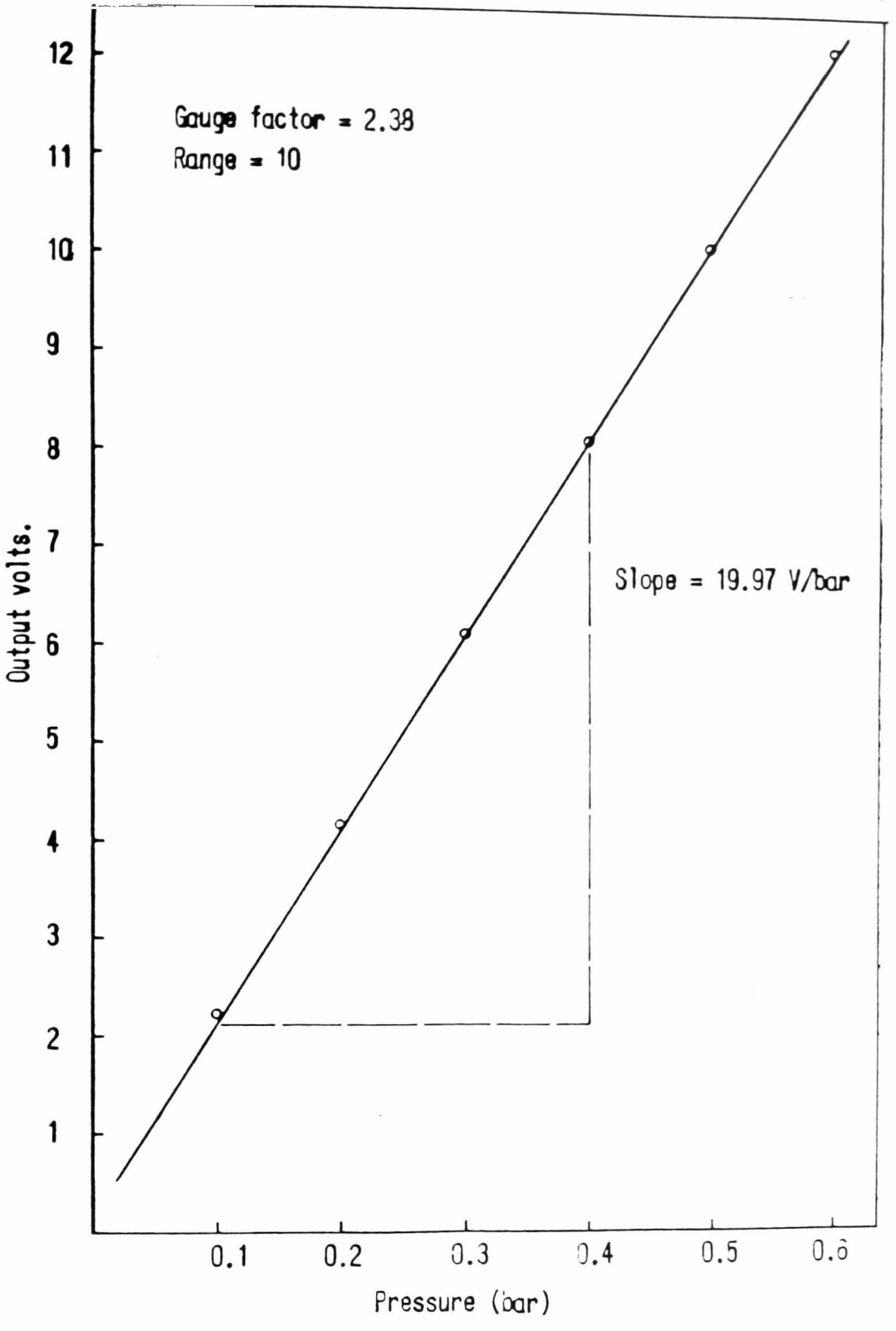

(FIG 5.6.3/1) CALIBRATION OF R.D.P. PRESSURE TRANSDUCER AND SANGAMO C56 UNIT.

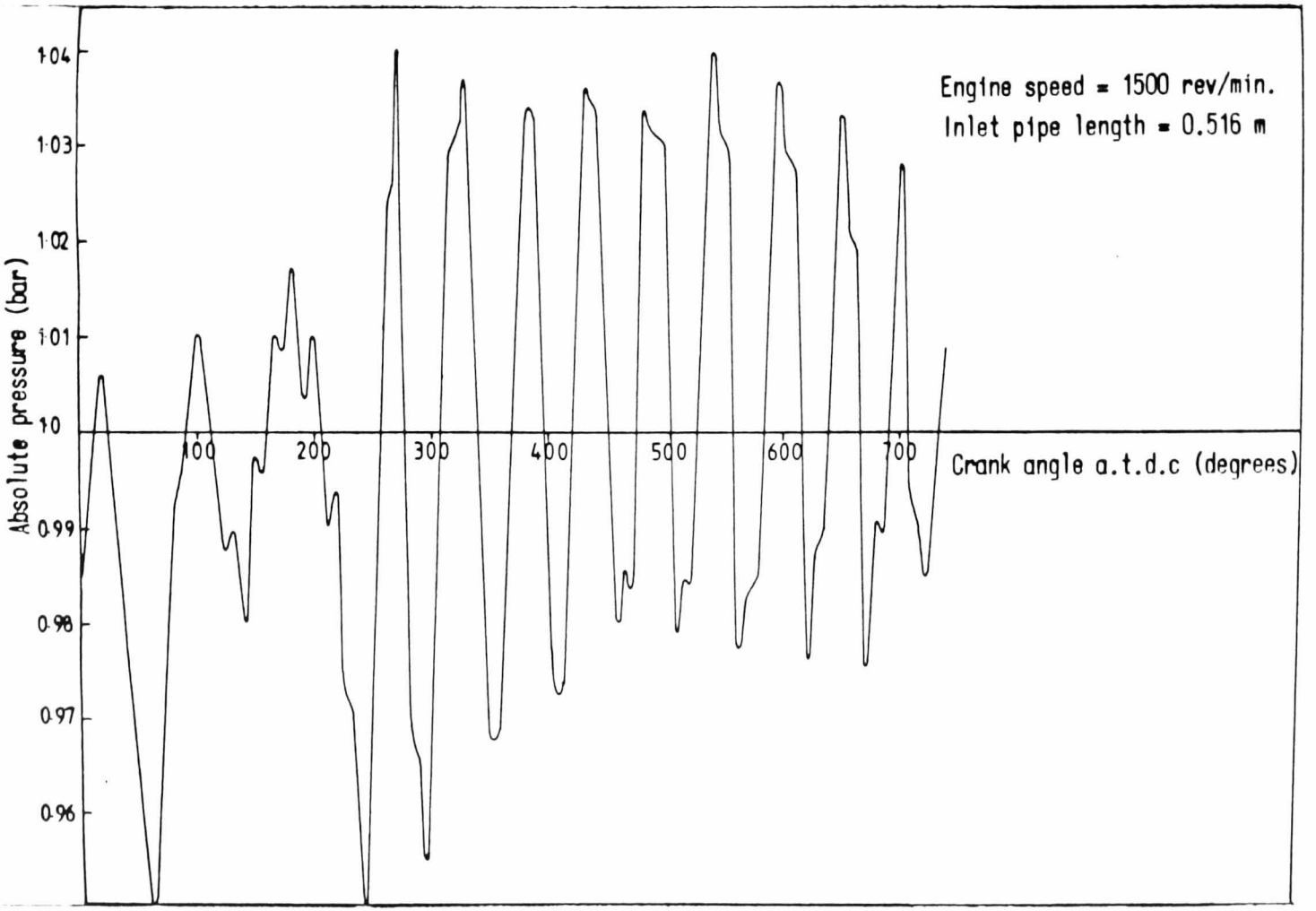

(FIG 5.6.5/1) Experimental results of inlet pipe pressure at node 7 using the tungsten light recorder.

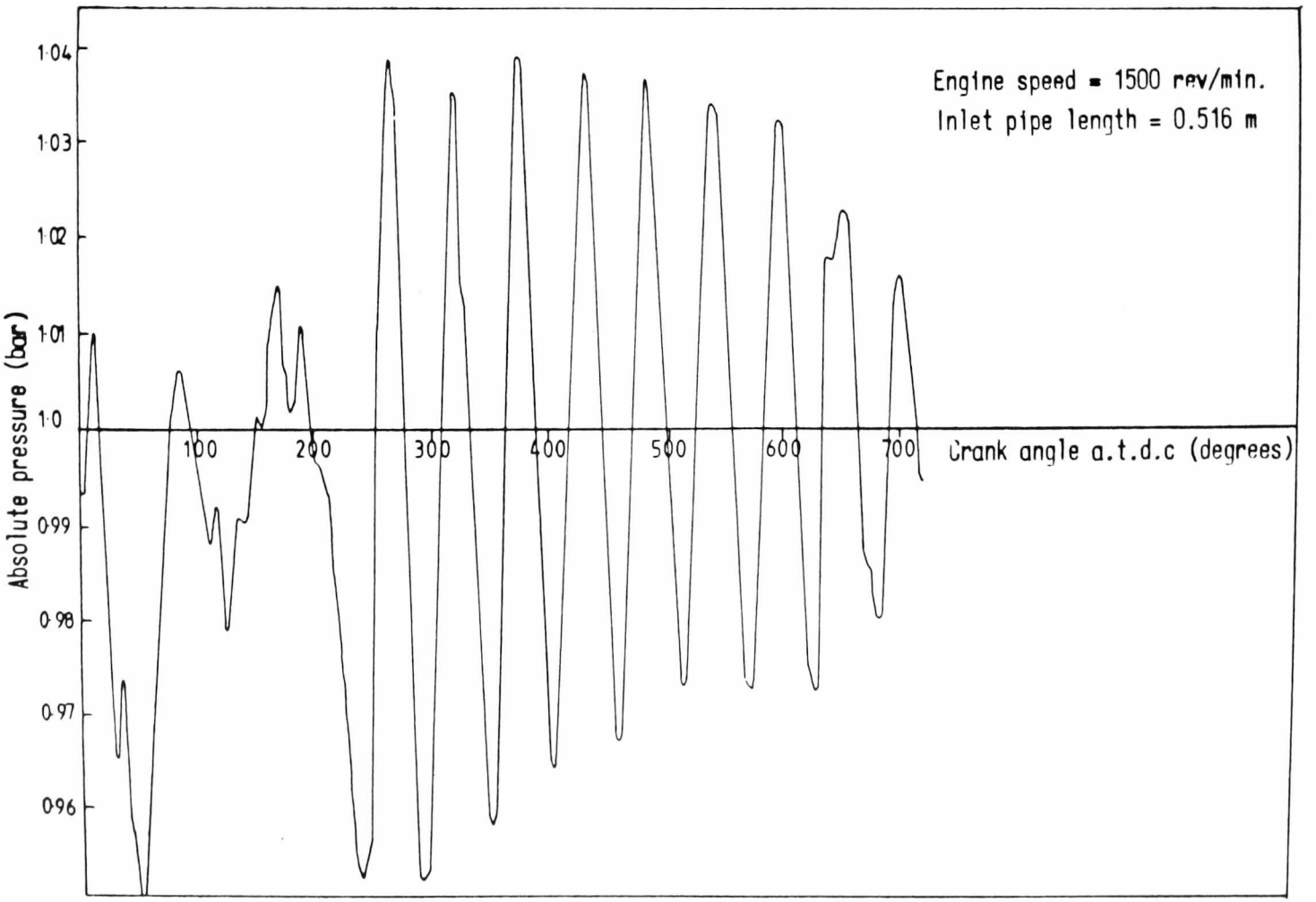

(FIG 5.6.5/2) Experimental results of inlet pipe pressure at node 7 using the digital storage oscilloscope.

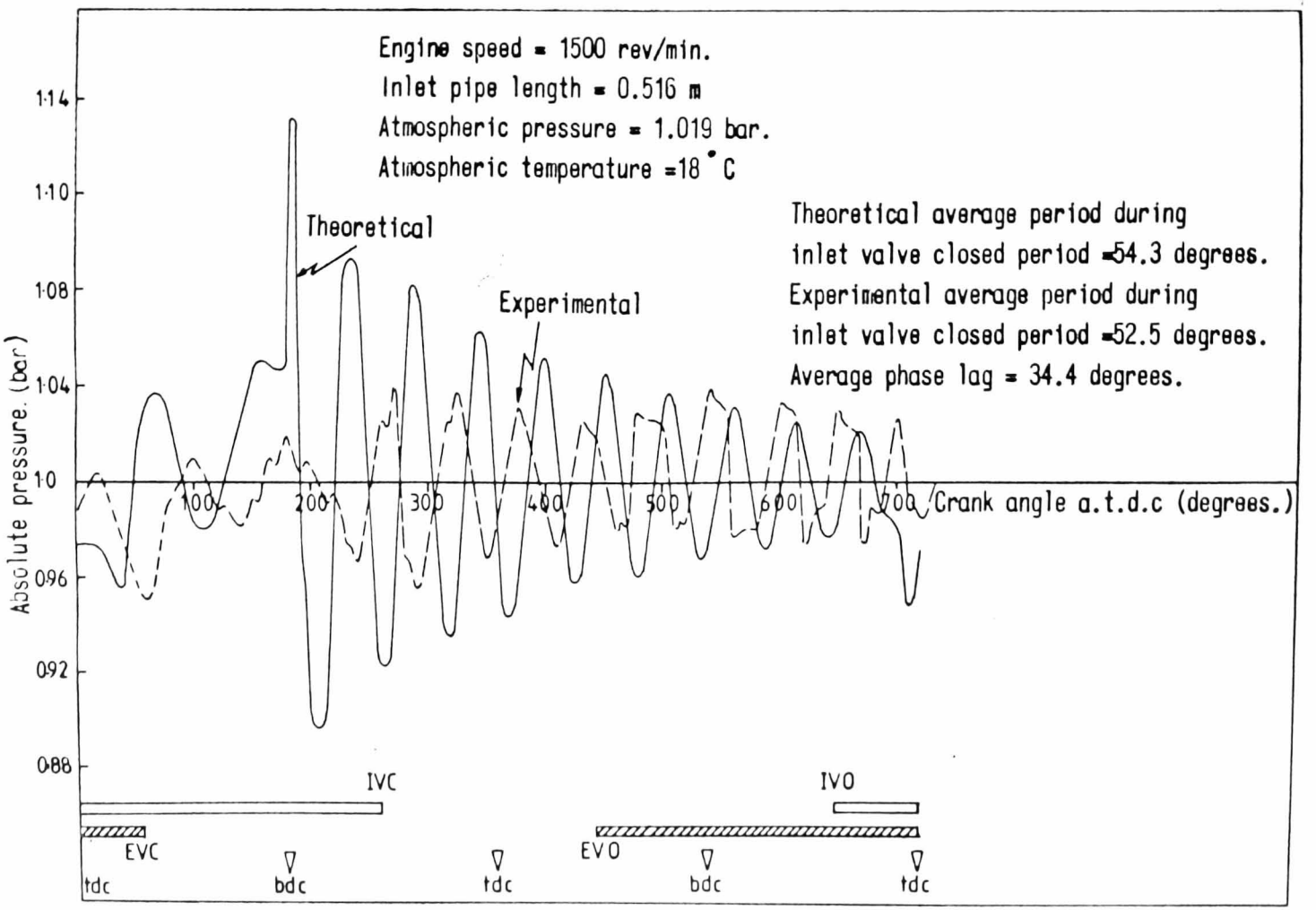

(FIG 5.6.5/3) Comparison of experimental and theoretical results for pipe pressure at node 7. (1500 rev/min.)

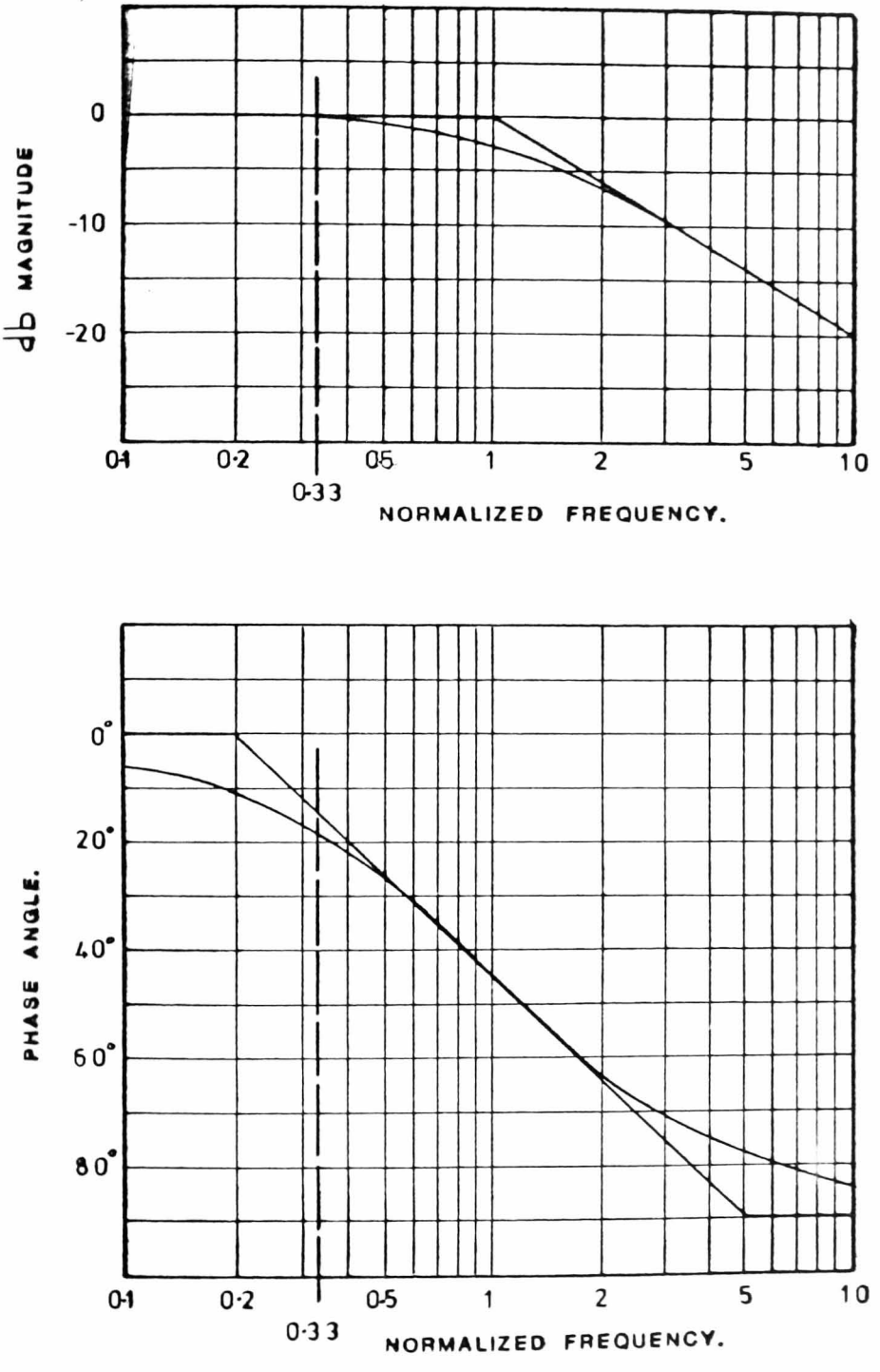

(FIG 5.6.5/4) BODE PLOT FOR A FIRST ORDER SYSTEM TAKEN FROM REF 40.

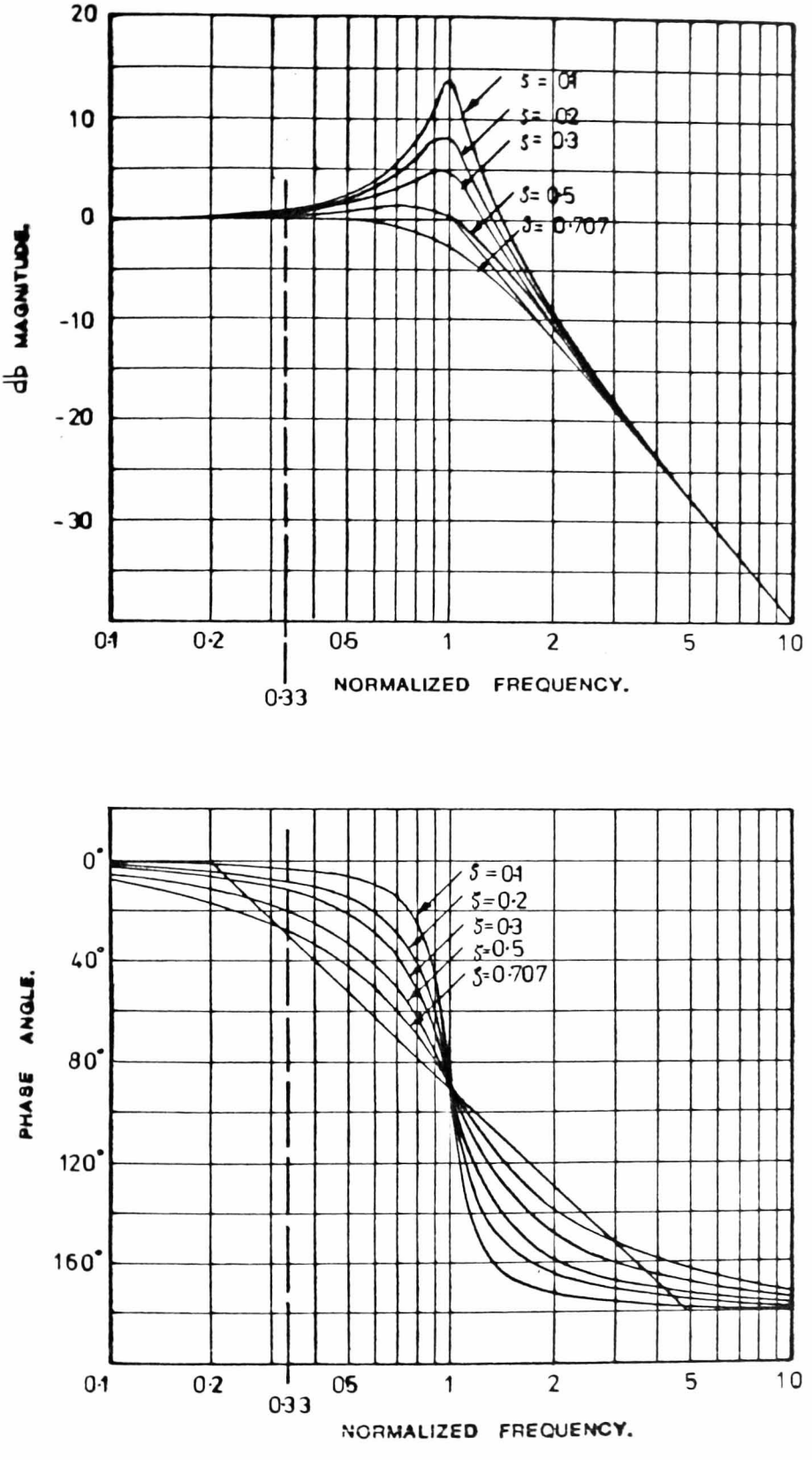

(FIG 5.6.5/5) BODE PLOT FOR A SECOND ORDER SYSTEM TAKEN FROM REF 40.

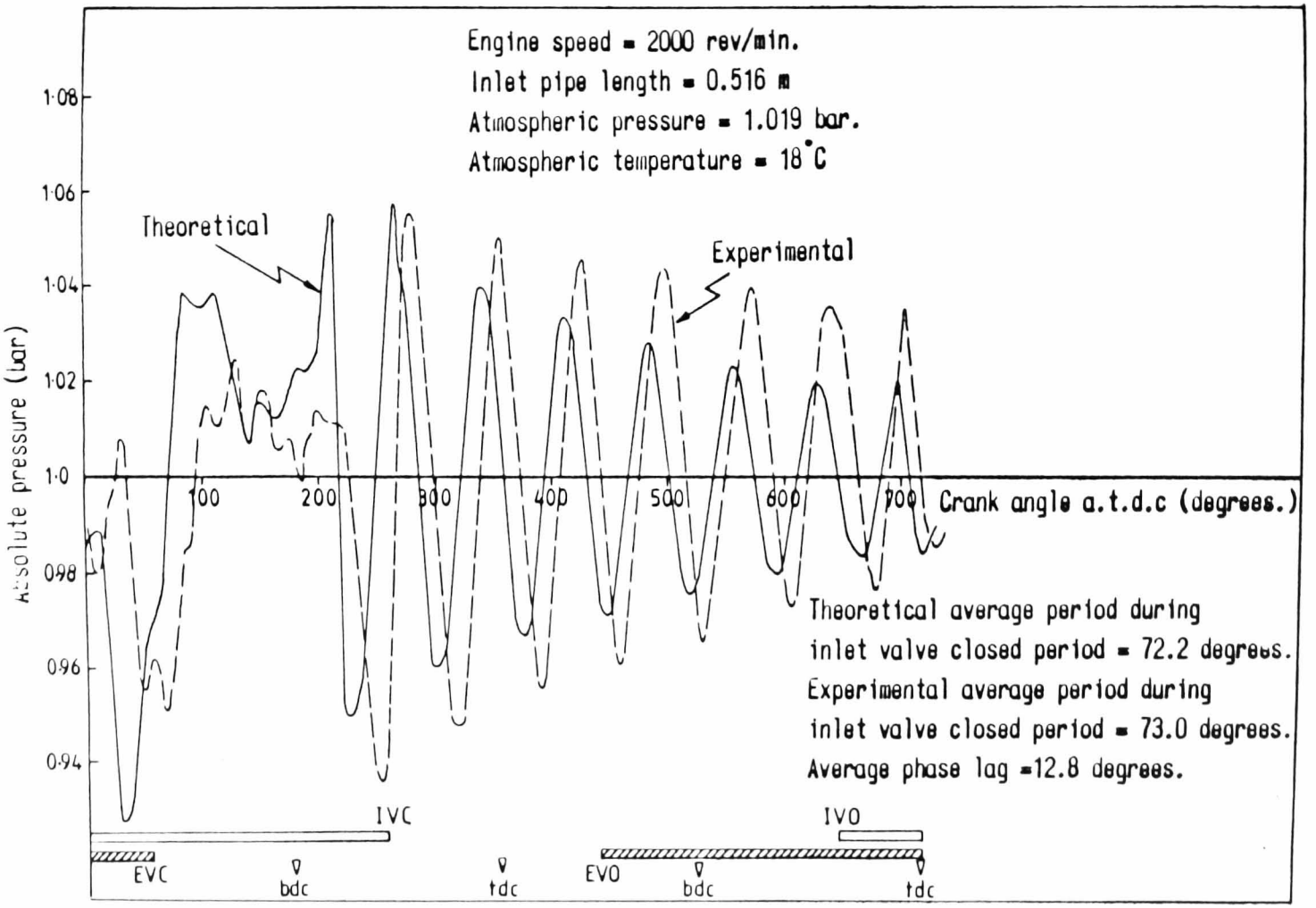

(FIG 5.6.5/6) Comparison of experimental and theoretical results for pipe pressure at node 7. (2000 rev/min.)

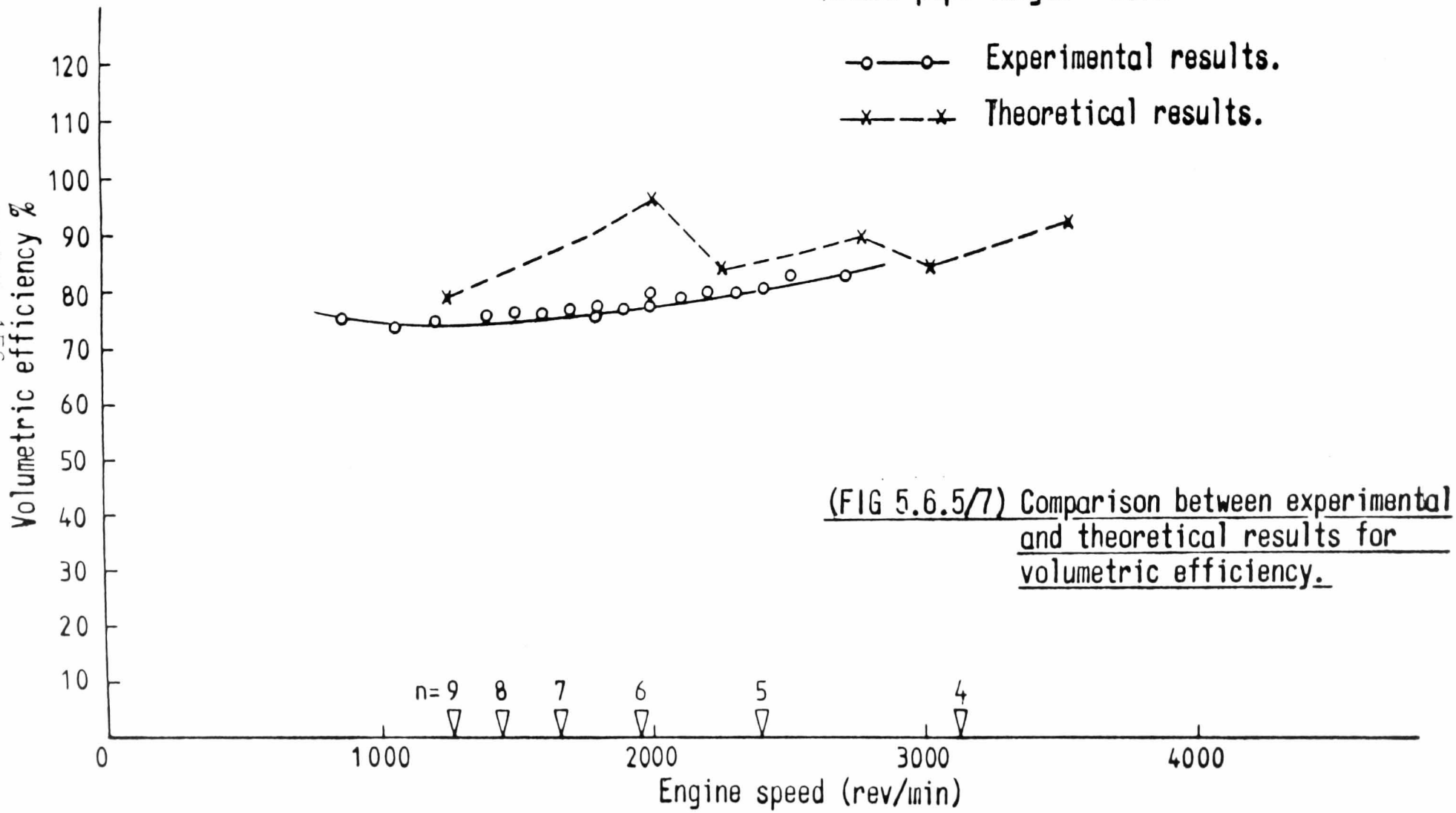

(FIG 5.6.5/7) Comparison between experimental and theoretical results for volumetric efficiency.

FIG 5.8.5/7.

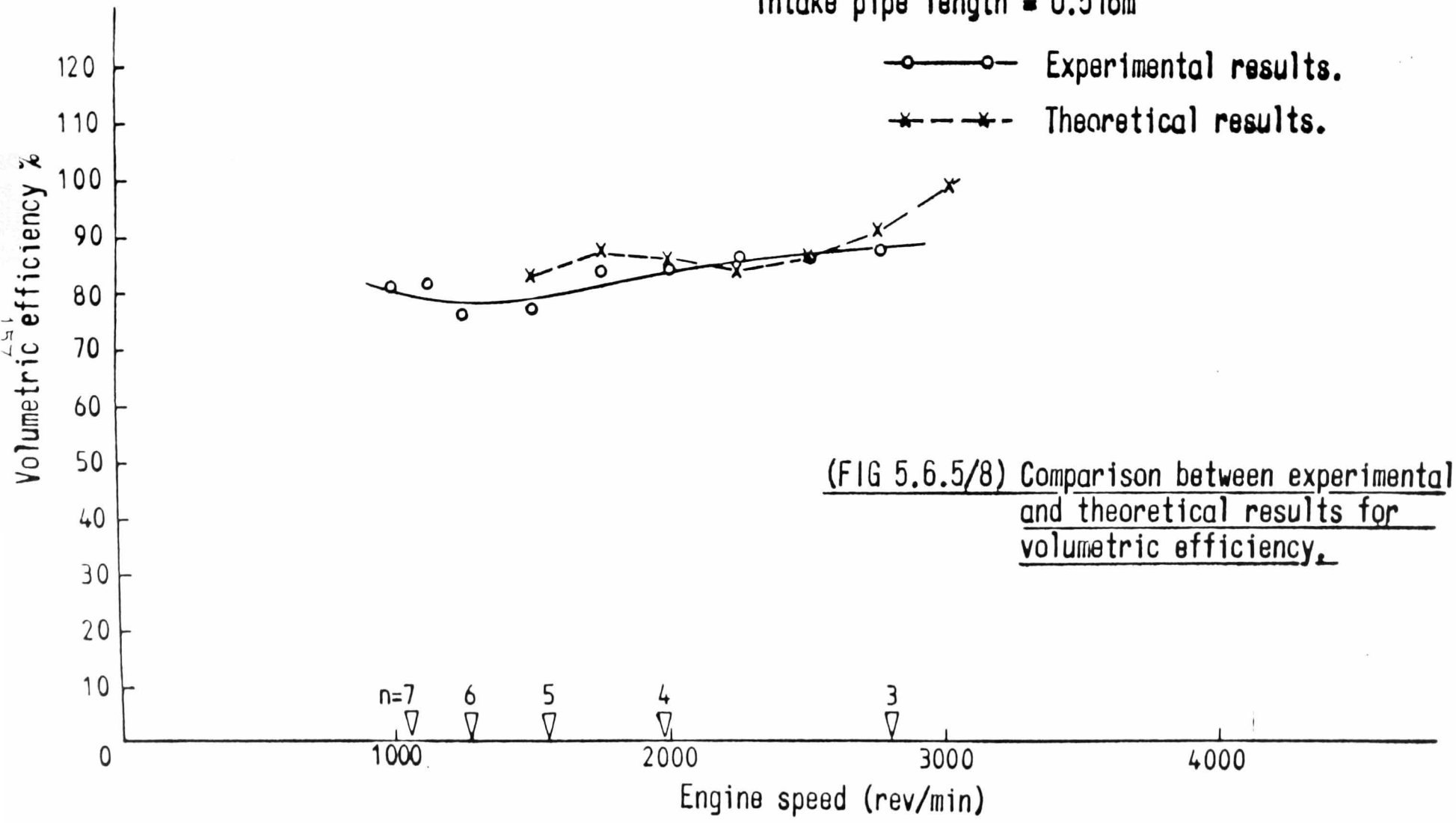

(FIG 5.6.5/8) Comparison between experimental and theoretical results for volumetric efficiency.

FIG 5.6.5/8.

CHAPTER 6 : COMBUSTION MODELLING AND EFFECTS OF MIXTURE MOTION ON FLAME PROPAGATION

CHAPTER 6 - COMBUSTION MODELLING AND EFFECTS OF MIXTURE MOTION ON FLAME PROPAGATION

6.1 Introduction

An introduction to combustion modelling was given in Section 1.4. In this, two approaches were described to deal with the heat release rate. Firstly, the entrainment of a mass of unburnt charge by an advancing flame front at a turbulent burning velocity U_T. This is related to the laminar burning velocity U_L by a constant related to engine speed.

$$\frac{U_T}{U_L} = K$$

The mass entrained is then burnt during the increment of time before the flame advances further.

The constant K is determined experimentally for a particular engine and is usually expressed as $K = 1 + AN$, where A is constant and N is the engine speed. The value of A is usually about 0.002.

The more complex method is to attempt to define the turbulence structure and then analyse the combustion in two stages, (i) engulfment of the individual eddies at a rate governed by the flame front area, and the sum of the laminar flame speed U_L and the turbulent intensity u', (ii) burning of the engulfed eddies at a rate determined by the characteristic eddy burn-up time.

In the first method, turbulence effects on the burn rate are directly rated to engine speed, an external operating

parameter, whereas in the second, burn rate is related to internal turbulence parameters.

In the following chapter, an attempt has been made to relate the burn rate to external operating parameters and geometric configuration through the development of an expression for the flame speed ratio U_T/U_L of the form $1 + AN$, where A is controlled by the geometrical arrangement of the engine, the unburnt charge condition and the characteristics of the inlet tract.

The derivation of the relationship is not absolutely rigorous, as the understanding of turbulent combustion is far from complete. It is based on previously reported evidence on the possible relationships between turbulence structure and engine geometry, physical intuition and, to some extent, mathematical convenience.

6.2 Relevance of mixture motion on the initiation and progression of the flame in a spark ignition internal combustion engine

It is well known that one of the major factors affecting the combustion performance of a S.I. i/c engine is the mixture motion at the point of ignition and during the subsequent perod of flame travel. In order to attempt to relate mixture motion to combustion, it is necessary to produce some parameters related to the degree of turbulence. Investigations have shown that the turbulence present can, in the absence of gross swirl, be treated as homogeneous and isotropic - i.e. turbulence of which the statistical

properties do not vary with position and have no preferred directions. A measure of the degree of turbulence or random fluid motion at a point can be described by the root mean square of the fluctuating velocity about a mean. This is called the turbulent intensity $u' \quad u' = \sqrt{\overline{u^2}}$. Hence at any instant the velocity at the point is the mean velocity $\overline{U}$ plus the fluctuating component u.

As mentioned previously, Section 1.4, physical scale of turbulence can be described in terms of a macro integral scale l_e and a Taylor micro-scale λ. If the turbulence is to be related to engine geometry, certain design parameters must be considered:

(i) Bore and stroke and bore/stroke ratio

(ii) Geometric compression ratio

(iii) Valve geometry (lift, valve diameter, disposition)

(iv) Inlet tract design

(v) Combustion chamber shape.

When considering a particular type of engine configuration such as the 4-valve pent-roof combustion chamber with a flat topped piston, certain factors are preset. Valve disposition, inlet tract design and basic combustion chamber shape are all to a large extent limited in scope for variation. Another factor which plays a large part in combustion performance is the spark plug position, which being central is already in the most advantageous position. (Ref. 41).

Two commonly used methods of producing mixture motion within an engine are swirl and squish. The first relates

to solid body motion within the cylinder, usually produced by valve masking, be it by the proximity of the valve to the chamber wall or by shrouded valves. The latter relates to the motion produced by the movement of the piston as it approaches t.d.c. when there are areas of very small clearance.

Recent work by Lucas et al (Ref.42) has indicated that any burn time reduction with a high squish chamber is more likely to be a result of the improved chamber compactness rather than the mixture motion. There is some indication that reverse squish when the piston descends may be beneficial to reduced burn time. All of the initial motion of the mixture is induced by the piston movement, be it squish directly or swirl and turbulence from the inlet tract. During combustion however, the turbulence levels can be enhanced by the movement of the flame front and the change in properties of the unburnt charge.

For purposes of analysis it is advantageous to divide the combustion process into four phases:

(i) Development of the flame kernel

(ii) Transition from flame development to a fully developed turbulent flame front

(iii) The fully developed turbulent flame combustion period

(iv) Retardation and extinguishing of the flame.

It is convenient for modelling purposes to put together the first two phases and term them the delay period.

The second two phases will be treated as one with a fully developed turbulent flame. Retardation can be accounted for by a reduction in laminar flame speed as the surface/volume ratio increases in the end gas region.

Consideration of these two phases of combustion will lead to a better understanding as to how the turbulence levels and hence engine design parameters may affect the combustion duration.

6.2.1 Development of the flame kernel and transition to a fully developed turbulent flame

The development of the flame from the point of ignition has been studied by many researchers. Whilst studying the effect of turbulence on cyclic dispersion, Windsor and Patterson (Ref. 43), introduced the concept of a critical distance d_c that was related to the total distance from the point of ignition to the chamber wall D, the mean burn time $\overline{t_b}$, the standard deviation of the burn time $S(t_b)$, the mean velocity $\overline{U}$ and the standard deviation of the velocity $S(u)$, by:

$$d_c = D \frac{S(t_b)}{t_b} \frac{\left[1 + \left[S(u)/\overline{u}\right]^2\right]}{\frac{S(u)}{\overline{U}}}$$

(Note: $S(u)$ is the turbulent intensity u')

This critical radius was calculated to be about 10 mm in this engine. The engine was a C.F.R. engine with a cylindrical combustion chamber, for which the minimum dimension was 15 mm.

The model used in this work defines the critical distance d_c as the distance within which all of the disturbances leading to cyclic combustion take place. "Before this period the flame will be wholly contained in one or two eddies and consequently will propagate at a slow rate, nearly that of a laminar flame. After this critical period the flame will be much larger than the eddies. Therefore each eddy will only locally disturb the flame front and the flame will average these local disturbances. The average flame speed after the critical period will be the higher turbulent flame speed which will depend on the average turbulent velocity in the mixture." No measurement of eddy size was made but an assessment of 2.5 mm for the eddy diameter was given.

Work was also done on a C.F.R. engine by Lancaster et al (Ref. 44). He considers flame speed ratios, FSR's at various stages of the flame propagation. Development of the flame from ignition up to what is termed a fully developed turbulent flame is divided into two regions. 'Ignition and kernel growth' is shown to occupy a very small region up to a radius of about 5 mm. From there on 'flame development' continues to fully developed turbulent flame at about 30 mm.

However, the figures show a plateau of flame speed

from about 0.5 - 0.75 cm to 1.5 - 1.9 cm.

The flame speed ratio is approximately 3 for the shrouded valve test and 2 for the non-shrouded valve test. This effect is attributed to the interaction between the flame and the piston crown. It is interesting to note the rapid acceleration of the flame before this interaction or quenching takes place. It might be concluded that a pent roof chamber would allow greater flame development to take place before this retardation of flame acceleration. A higher rate of pressure rise may be exhibited which will perhaps be less sensitive to variations of mixture motion during this period.

The mechanism of flame development offered here is as follows:-

Acceleration of the flame is assumed to be due to wrinkling of the flame front by eddies.

Initially only small (micro scale) eddies can affect the development of the kernel and give an effective flame speed greater than the laminar flame speed. Large eddies at this stage only move the kernel bodily. As the enflamed area grows, larger eddies are engulfed and produce a greater flame front area and hence a more rapid apparent flame speed. However a stage is reached when the flame reaches a maximum FSR dependant upon the turbulent intensity of the mixture.

Flame speed ratio during the flame development period from these results has been described by an equation relating the flame speed ratio to the maximum flame speed ratio at the fully developed turbulent flame at radius r_{max} by the following expression:

$$\frac{FSR_{(r)}}{FSR_{(max)}} = \left[\frac{r}{r_{max}}\right]^{\frac{m-1}{2}} \quad \text{for this engine}$$

$$FSR_{(r)} = FSR_{(max)}\left(\frac{r}{3}\right)^{\frac{1}{2}}$$

The importance of an effective model for the initiation and development of the flame is illustrated by Lancaster's results.

In the standard condition with unshrouded valves the flame development period, up to fully developed turbulent flame, occupied approximately 35% of the burn time whilst accounting for only 7 to 8% of the mass fraction burnt. This is relevent to the definition used in Section 6.5 for delay period.

In addition to the scale of turbulence affecting the development of the flame kernel, it is necessary to attempt to assess the effect of magnitude and direction of the mean velocity present during the flame initiation.

Work done by Curry (Ref. 28) which supports the use of a spherical flame form as used in the majority

of computer simulations, also indicates the distortion due to swirl from shrouded valves.

Flame maps for the CFR engine with shrouded and non-shrouded inlet valves show considerable movement of the end gas region, as well as flame propagation rates. Another factor is the apparent slow burning at high compression ratios. This appears to be due to quenching during the last third of the flame travel as there is a considerable increase in flame speed during the first third.

Data on the effect of the magnitude of the mean velocity at the spark-ignition point are provided in work by Bolt and Harrington (Ref. 45) on lean limits, using a combustion bomb with paddle wheel induced swirl. Their Fig. 8 shows the very significant effect that mixture velocity has in this context on the rate of pressure rise after the spark.

Their conclusion as to the effects of mixture motion on combustion are summarised as follows:

(i) Mixture velocity has a greater effect on the ignition and combustion characteristics of lean mixtures than on stoichiometric mixtures.

(ii) For rapid combustion and minimum heat loss, it is preferable to have a high swirl velocity, especially at very lean mixture ratios.

(iii) For minimum variation in rates of pressure rise, peak pressures, and burning times, it is desirable to minimise the variations in swirl velocity or, if this cannot be done, to use the highest nominal swirl velocity and avoid very lean mixtures.

(iv) To ignite a very lean mixture it is advisable to have the velocity of the mixture at the spark gap as low as possible.

Thus there is a need for high swirl velocities and minimum velocity at the spark plug for ignition and combustion of lean mixtures.

It must be noted that the conditions in the bomb experiments differ quite considerably from those in an actual engine. There is, however, some correlation with the results of Lancaster regarding the basic development of the flame kernel and its growth through micro and macro scale turbulence to a flame speed dependent on the overall turbulence field or turbulent intensity. There is also the restraint that account must be taken of the influence of a local mean velocity on the rate of development of the flame kernel.

Attempting to categorise induction and piston induced motion into specific effects is extremely difficult. An attempt to study the effects of various ways of introducing mixture motion on the

combustion rate in a spark ignition engine was made by Mayo (Ref. 41). Here the addition of squish, swirl and high port velocities was studied using modified production engines. The difficulties in evaluating the contribution of any one type of motion is illustrated here by the wide variation in combustion duration or burn time with the differing combinations.

As far as delay period or flame development is concerned the following tentative conclusions can be made:

(i) Squish was not advantageous to flame development. In four chambers it resulted in an increase in delay time and in three others only a slight decrease. It was only in the central gap chamber that any appreciable decrease was noted:- an 18.5% reduction.

(ii) Increased charge velocity, similarly, did not present a conclusive result. In five chambers, an increase in delay time occured, in two a medium reduction in delay time was indicated, but in the open chamber central gap chamber a reduction of 27.0% was observed.

(iii) The effect of swirl on the other hand was more clearly defined. All chambers, except the open, central gap chamber with high velocity, benefited from the addition

of swirl. The open chamber, in particular, showed a considerable reduction in delay period, 33.2% for the standard open chamber and 25.8% for the central gap open chamber. The delay time is defined as the time between ignition and when 10% of the charge is burnt.

6.2.2 Conclusions on effects of mixture motion on kernel growth and flame development

The initial ignition of the mixture by the spark will be related to two main features of the charge dynamic conditions, (i) the prevalence and size of small scale turbulence, (ii) the bodily movement of this small scale turbulence past the point of ignition.

Development of the flame front will be influenced by the large scale turbulence and its relationship to the physical constraints of the combustion chamber. From the original definitions of micro and macro scale, the methods of inducing mixture motion can perhaps be related to the type of turbulence produced.

As the induction process is a transient feature, the mixture motion produced by the induction is likely to have, by the time of ignition, a large fraction of the turbulence spectrum in the small scale (or high wave number) region due to decay. Hence port velocity and swirl are likely to

contribute greatly to the initial flame development. On the other hand, squish being late in the cycle is more likely to produce large scale motion. Produced by the squeezing action of the piston and displacement of the roll up vortex (Ref. 46) created during the upward stroke. With a combination of squish and swirl, a situation can arise where the motion produced by the squish disorganises and reduces the residual motion from the swirl, leading to an increase in burn time.

6.2.3 Fully developed turbulent flame front

At the end of the flame development period, the flame is said to be fully turbulent and its speed relative to the unburnt mixture is termed the turbulent flame speed U_T. The relationship between this and the equivalent laminer flame speed U_L has been studied by many researchers and the results are far more conclusive than for the previous section.

The work by Lancaster et al (Ref. 44) gives detailed analysis of FSR across the chamber. Relating fully developed FSR to the motored turbulent intensity u' produced a linear relationship.

It is suggested that the intercept at zero u' should be 1, i.e. the turbulent flame speed equals the laminar flame speed. It is, however, approximately 1.25 and thus assumed to be due to experimental error. It could alternatively have been a mean velocity effect. This linear relationship appears to be independent of most parameters for this engine.

A further plot that is of interest is his Fig. 17, which relates FSR to relative volumetric flow (corrected for manifold density changes)

The results are very interesting as they show a linear dependence of FSR on volumetric flow for a particular inlet geometry.

It is suggested that a characteristic velocity could be assigned to the flow taking into account reductions in flow area due to the valve shrouding. This would produce a single line for both tests. These conclusions should be regarded with caution as the engine does not have squish, or any appreciable swirl, but it is certainly a step in relating flame development to externally measured engine parameters.

6.3 The relationship between the turbulent and laminar burning velocities as dictated by engine operating and design parameters

6.3.1 Introduction and definition of terms

The description of the movement of the flame front in the combustion chamber must be related to a datum. Two such data exist, (i) the chamber wall and (ii) the unburnt charge.

The chamber wall provides a suitable reference from which the progression of the flame front can be studied. Usually by means of ionization probes or optically. The flame front movement relative to the chamber wall can be termed the flame propagation velocity V_T. (The suffix indicating that the propagation is influenced by the turbulence structure within the engine). A suitable reference for V_T is often quoted as V_L the laminar propagation velocity. Here the chamber contents are assumed quiescent.

If the unburnt charge is taken as the datum, the velocity of the flame front is termed the burning velocity or entrainment velocity. Again this velocity can be influenced by turbulence giving a turbulent burning velocity U_T or in a quiescent mixture a laminar burning velocity U_L. The effect of turbulence can usefully be illustrated using the ratio of U_T/U_L, the flame speed ratio (F.S.R).

The difference between the flame propagation velocity and the turbulent burning velocity is due to the compression of the unburnt charge. Hence the propagation velocity will usually be greater than the burning velocity. In order to arrive at an empirical relationship for F.S.R. it is often quoted that it can be assumed that for a constant volume process:

$$\frac{V_T}{V_L} = \frac{U_T}{U_L}$$

In a changing volume situation, as in an engine due to the lower value of U_L compared to U_T, the value of V_T will be influenced considerably by the piston motion. This is true especially at high engine speeds where the F.S.R. is large, or in cases where the duration of combustion is prolonged, due possibly to lean mixture operation, Fig. 6.3.1/1

6.3.2 Development of an expression for flame speed ratio for use in diagnostic model

The prediction of a turbulent burning velocity for use in combustion models has been the subject of extensive work. One of the most effective relationships has been a linear dependence on engine speed. This has been used by many researchers using differing engines with remarkably similar results as shown in Table 6.1. These results, however, relate to engines running at 1000 rev/min to

3000 rev/min which gives a flame speed ratio of about 5.

At the other end of the scale the work done by Nakamura (Ref. 4) on high speed petrol engines indicates that the propagation velocity during the latter part of the combustion increases exponentially whilst the initial region shows a linear relationship. This difference is further emphasised by the fact that, whilst the initial period of combustion occupies about 42° of crank angle and is independent of speed, the latter part actually decreases, reducing from about 11° at 8000 rev/min to about 4° at 16000 rev/min. These results are said to also apply to engines running up to 23000 rev/min illustrating the extent to which the flame speed can be influenced by turbulence.

The use of the engine rotational speed to reflect the mixture turbulence is an over-simplification of the situation albeit a very useful simplification. An alternative to the engine speed is an actual description of the turbulence in the form of the turbulent intensity u'.

Many expressions have been formulated using a wrinkled laminar flame model which assumes that the significant effect of the turbulence is to make available a larger flame surface area for molecular transport. These expressions are summarised by Andrews et al (Ref. 24).

One such relationship is that by Shelkin (Ref. 62) used in the work on intake valve throttling by Stivender (Ref. 48).

$$U_T = u' + \left[\left(\frac{\sigma - 1}{3} \right) \left(1 - \left[\frac{U_L}{U_T} \right]^2 \right)^{\frac{1}{2}} + 1 \right] U_L$$

where σ is the ratio of the enflamed volume to total chamber volume, and is an attempt to introduce combustion generated turbulence. For high turbulent situations this reduces to $U_T \simeq u'$.

Lancaster (Ref. 44) also quotes Shelkin's relationship in the same form as quoted in Ref. 24,

$$\frac{U_T}{U_L} = \left(1 + B \left[\frac{u'}{U_L} \right]^2 \right)^{\frac{1}{2}}$$

A comparison of Lancaster's motoring tests and results using Shelkin's expression is shown in Fig. 6.3.2/1. It was suggested that the constant B should be selected to suit the engine geometry.

One conclusion made in this work was that -

"The F.S.R. for the fully developed turbulent flame is a linear function of turbulent intensity. There is no indication that turbulent scale affects this correlation".

The statement about the non-effect of turbulent scale is not consistent with the analysis by Andrews et al (Ref. 24) who concluded that -

"The microscale Reynolds number R_λ is an important parameter in turbulent combustion".

This conclusion was arrived at by an analysis of various workers' results, using a wide range of mixtures, and a plot of U_T/U_L against R_λ showed an almost linear relationship. The microscale Reynolds number can be shown to be the ratio of the integral scale ℓ_e to the Taylor microscale λ so a relationship of the form $\frac{U_T}{U_L} = 1 + C\left[\frac{\ell_e}{\lambda}\right]$ could be proposed.

The inclusion of the integral scale in the F.S.R. expression was also suggested by Sanematsu (Ref. 50), who produced the expression:

$$\frac{U_T}{U_L} = C + D\left[\frac{u'}{U_L}\right]\left[\frac{\ell_e}{b}\right]$$

Where C and D are constants (said to be dependent on equivalence ratio), and b is a characteristic length (the grid size used for producing turbulence in this case).

It has been shown that u' is a strong linear function of the engine speed and if C = 1 to give $U_T = U_L$ at zero turbulent intensity, a relationship of the form below could be proposed:

$$\frac{U_T}{U_L} = 1 + F\left[\ell_e, b, U_L\right] N$$

where b is a characteristic dimension related to engine geometry.

A further relationship for the F.S.R. is quoted by Hire et al (Ref. 26) when developing their turbulent combustion model:

$$\frac{U_T}{U_L} = C_s \left[\frac{u'}{U_L}\right]^{\frac{1}{3}} \left[\frac{\rho_i}{\rho_u}\right]^{\frac{1}{9}} \left[\frac{u' L_i}{\nu}\right]^{\frac{1}{3}}$$

$$\text{or} \quad \frac{U_T}{U_L} = C_s \left(u'^{\frac{2}{3}} \; U_L^{-\frac{1}{3}} \; L_i^{\frac{1}{3}} \left[\frac{\rho_i}{\rho_u}\right]^{\frac{1}{9}} \right)$$

where L_i is a characteristic eddy size and is equivalent to ℓ_e.

The ratio ρ_i/ρ_u, the ignition density over the unburnt charge density is intended to take account of variations in spark advance and equivalence ratio effects not allowed for in the use of U_L.

If the strong function of u' with N is maintained, together with the characteristic dimension b, an expression of the form below is suggested:

$$\frac{U_T}{U_L} = 1 + K \left(\ell_e^{\frac{1}{3}} \; d^2 \; b^{-1} \; U_L^{-\frac{1}{3}} \left[\frac{\rho_i}{\rho_u}\right]^{\frac{1}{9}} \right) N$$

where d is introduced for dimensional correctness and is associated with u' and N. This seems reasonable as it reduces the dependence on scale.

In order to relate F.S.R. to engine geometry, use is made of relationships proposed by Blizard and Keck and McCuiston (Ref. 21, 23).

Here an attempt has been made to describe the characteristic eddy size in terms of the valve lift and the piston position at ignition; the argument being that on decay the characteristic turbulent scale approached the minimum chamber dimension. As a disc type combustion chamber was used in this work, the minimum chamber dimension was the chamber height, this agrees with the statement made by Andrews et al (Ref.24).

The expressions used were:

$$L_i = 0.17 \left[\frac{h_s}{h_i}\right] L_v$$

by Blizard and Keck (Ref. 21), and:

$$L_i = 0.5 \left[\frac{h_s}{h_i}\right] L_v$$

by McCuiston et al (Ref. 23).

where h_{s/h_i} is the ratio of piston clearance at spark to the clearance at b.d.c.

$$\therefore \frac{U_T}{U_L} = 1 + K\left(\left[\frac{h_s}{h_i}\right]^{\frac{1}{3}} L_v^{\frac{1}{3}} \frac{d^2}{b} U_L^{-\frac{1}{3}} \left[\frac{\rho_i}{\rho_u}\right]^{\frac{1}{9}}\right) N$$

It is now required to determine which characteristic dimension to use as b and how this and the valve lift L_v can be related to the inlet port flow conditions.

One possibility is that b should be the inlet throat diameter D_T, which is related to the flow aperture at maximum lift.

$$\therefore \quad \frac{U_T}{U_L} = 1 + K\left(\left[\frac{h_s}{h_i}\right]^{\frac{1}{3}} \frac{L_v^{\frac{1}{3}}}{D_T} \frac{d^2}{U_L^{\frac{1}{3}}} \left[\frac{\rho_i}{\rho_u}\right]^{\frac{1}{9}}\right) N$$

If D_T is squared and the top multiplied by the stroke S times the stroke/bore ratio Q, the expression becomes:

$$\frac{U_T}{U_L} = 1 + K\left(\left[\frac{h_s}{h_i}\right]^{\frac{1}{3}} \frac{L_v^{\frac{1}{3}} \; S \, d^2 \, Q}{D_T^2 \, U_L^{\frac{1}{3}}} \left[\frac{\rho_i}{\rho_u}\right]^{\frac{1}{9}}\right) N$$

This can be done as $D_T/_B$ = constant as shown in Fig. 6.3.2/2.

An obvious choice for d is the bore, B, and if D_T^2 is modified by C_m the mean inlet discharge coefficient to give an effective area, then:

$$\frac{U_T}{U_L} = 1 + K\left(\left[\frac{h_s}{h_i}\right]^{\frac{1}{3}} \frac{L_v^{\frac{1}{3}}}{U_L^{\frac{1}{3}}} \left[\frac{B}{D_T}\right]^2 \frac{S \, N \, Q}{C_m} \left[\frac{\rho_i}{\rho_u}\right]^{\frac{1}{9}}\right)$$

But, $\left[\frac{B}{D_T}\right]^2 \frac{2 \, S \, N}{C_m} = Za$, where Z is the Gulp factor or inlet mach index and `a' is the inlet sonic velocity.

$$\therefore \quad \frac{U_T}{U_L} = 1 + K\left(\left[\frac{h_s}{h_i}\right]^{\frac{1}{3}} \frac{L_v^{\frac{1}{3}}}{U_L^{\frac{1}{3}}} \left[\frac{\rho_i}{\rho_u}\right]^{\frac{1}{9}} Z \, a \, Q\right)$$

This is the relationship used in the analysis of engine geometry effects on combustion.

The relationship between U_T/U_L and Z is supported by Hires et al (Ref. 26), who used the mean piston speed to relate to u' rather than the engine speed. It is suggested that this is a better correlation when dealing with variable engine geometry.

6.3.3 Evaluation of the constant in the flame speed ratio equation

Data for a cylindrical combustion chamber on the C.F.R. engine (Ref. 49) are applicable.

Engine data:

Bore	=	82.55 mm
Stroke	=	114.2 mm
Compression ratio	=	8.72 : 1
Inlet valve closing	=	210 a.t.d.c
Inlet valve lift	=	6.8 mm
Ignition	=	30° b.t.d.c

Inlet mach index at 2,000 rev/min:

$$Z = \frac{2000}{60} \times \frac{2 \times 114.3}{1000} \times \pi \times \frac{82.55^2}{4} \times$$

$$\frac{1}{341 \times \quad \times 0.485 \times 82.55 \times 6.8 \times 0.4}$$

$$= 0.349$$

(Note: this assumes Inlet valve dia. = 0.485 x bore and a mean flow coefficient of 0.4.)

At 30° b.t.d.c timing of ignition $\left[h_s/h_i\right]^{\frac{1}{3}} = 0.575.$

$$\therefore \quad \frac{U_T}{U_L} = 1 + K\left(\frac{0.575}{U_L^{\frac{1}{3}}} \frac{(6.8)^{\frac{1}{3}}}{10} \times 0.349 \times 0.722 \times 0.857\right)$$

$$= 1 + K\left(\frac{2.35227 \times 10^{-2}}{U_L^{\frac{1}{3}}}\right)$$

(assuming sonic velocity is incorporated in K)

(Note: this assumes:

$$\frac{\rho_i}{\rho_u} = 0.857 \text{ or,}$$

$$\left[T_u/T_i\right]^{\frac{1}{9}} = \left[\frac{600}{2400}\right]^{\frac{1}{9}} = 0.857, \text{ as,}$$

$$P_u/\rho_u = R\,T_u \text{ and } P_i/\rho_i = R/T_i \;)$$

From Lancaster for fully developed turbulent flame:

$U_T = 16.24$ m/s $\quad U_L = 3.85$ m/s

$$\therefore \quad 4.218 = 1 + K\left(\frac{2.35227 \times 10^{-2}}{1.5673}\right)$$

$$K = 214.419$$

$$\therefore \quad \frac{U_T}{U_L} = 1 + 214.419\left(\left[\frac{h_s}{h_i}\right]^{\frac{1}{3}} \frac{L_V^{\frac{1}{3}}}{U_L^{\frac{1}{3}}} Z\,Q \left[\frac{\rho_i}{\rho_u}\right]^{\frac{1}{9}}\right)$$

where L_V is in mm $\quad U_L$ is in m/s

Note: for Lancaster's data this reduces to:

$$\frac{U_T}{U_L} = 1 + 0.001609\,N$$

6.3.4 Effects of changes in engine geometry on flame speed ratio

6.3.4-1 Compression ratio

If the compression ratio of an engine of fixed swept volume and geometry is raised, this entails a change in value of $\left[h_s/h_i\right]^{\frac{1}{3}}$ in the expression for F.S.R. Raising the compression ratio by 4 points from 6 : 1 to 10 : 1 would change this factor from 0.62 to 0.56 (Fig.6.3.3/1) i.e. a reduction of 9.6%. This would produce a reduction of F.S.R. of about 7.4%.

Lancaster (Ref. 44) shows a small consistent drop in F.S.R. with increasing compression ratio. From his Fig. 12, a drop of about 5-6% seems to be indicated for a 4 point raising of C.R.

6.3.4-2 Bore/stroke ratio

Changing the bore/stroke ratio with a fixed swept volume has three effects on F.S.R.

(i) It changes the Gulp factor by its effect on the valve flow area.

(ii) It could change the valve lift.

(iii) It has a direct effect on the equation.

Taking the Lancaster results as a datum.

Increasing the B/S ratio to square i.e. 1.

The cylinder capacity is 611.7 cc.

$\therefore$ New bore = 92.0 mm

$\therefore$ New valve lift = 11.16 mm

$$\therefore \quad Z = \frac{2000}{60} \times \frac{2 \times 92.0}{1000} \times \frac{\pi \times 92^2}{4} \times \frac{1}{341 \times \pi \times 0.485 \times 92 \times 11.16 \times .4}$$

$$= 0.191$$

$\therefore$ Total effect on F.S.R:

$$\frac{U_T}{U_L} = 1 + 0.001609 \times \frac{0.191}{0.349} \times \left[\frac{11.16}{6.8}\right]^{\frac{1}{3}} \times \frac{1}{0.722} N$$

$$= 1 + 0.001439 \, N$$

This assumes that the valve lift is $\frac{1}{4}$ of the inlet valve diameter.

The reduction in the flame speed ratio illustrates that a compromise must be reached between a large bore, large valved engine with good breathing and low turbulence levels and a small bore, small valved engine with poor volumetric efficiency, but improved turbulence and hence higher F.S.R.

6.3.4-3 Reduction in valve lift

Here two effects occur:

(i) Reduction of $L_v^{\frac{1}{3}}$

(ii) Increase of Z.

Assume a 20% reduction of L_v.

$L_v^{\frac{1}{3}}$ reduces by 0.9655.

Reducing $L/_D$ will reduce the mean valve flow

coefficient by 0.785 (Fig. 6.3.3/2) and the valve area by 0.9. The Gulp factor Z will hence increase by a factor of 1.415.

∴ The overall effect will be to increase the F.S.R. equation to:

$$\frac{U_T}{U_L} = 1 + 0.0022\ N$$

i.e. an increase of F.S.R. by 28%.

However the volumetric efficiency is probably reduced by 0.948 (Fig. 6.3.3/3) and Z is very close to 0.5. This indicates the possibilities of inlet valve throttling.

6.3.4-4 Engine speed

Changes in engine speed directly affect the F.S.R due to its relationship to piston speed in Z.

6.3.4-5 Changes in combustion chamber geometry

Some effects of combustion chamber geometry have already been considered as related to the compression ratio. The other term in the expression requiring investigation is the $\left[\rho_i/\rho_u\right]^{\frac{1}{9}}$ term. This will be determined by factors related to the movement of the flame front across the chamber.

The two major quantities related to the advancement of the flame front are:

(i) the enflamed volume as a function of the radius from the spark plug

(ii) flame front area and the total burnt region area as a function of radius.

The use of radius here is an attempt to describe the flame front progression as a spherical progression as observed by Curry and supported by other workers.

Plots of V_f/V against r/R are shown in Fig. 6.3.3/4-7. Fig. 6.3.3/4-5 are for a cylindrical combustion chamber with a central spark, Fig. 6.3.3/6-7 are as used by Blizard and Keck for a cylindrical combustion chamber with an offset spark.

The actual effect of these geometry changes can only be determined by a combustion calculation. However, perhaps an attempt to evaluate their potential can be obtained by plotting an equivalent spherical diameter against chamber radius where the equivalent diameter is defined as $3V/A$ which will give a sphere of the same surface to volume ratio of the burnt region. This technique has still to be investigated but it has possibilities as far as comparing geometrically different chambers and also accounting for swirl and mean velocities within the chamber.

6.4 Description of combustion model used

6.4.1 Introduction

The combustion simulation used is a thermodynamic model on conventional lines, but uses expressions for ignition delay period and flame speed ratio developed from turbulent entrainment models.

The philosophy behind the simulation is to combine the simplicity of the thermodynamic model with the specifity of the turbulent combustion model in order to be able to undertake a parametric survey of the effects of changes in engine geometry.

6.4.2 Basic assumptions

(i) The engine cylinder volume is treated as a variable volume plenum in which the pressure is uniform throughout.

(ii) The charge is assumed homogeneous during compression.

During combustion two zones exist; a burnt zone and an adiabatic unburnt zone. Each zone is assumed uniform in temperature and composition.

(iii) Heat loss is determined using the Eichelberg (Ref. 60), heat transfer coefficient.

(iv) After ignition a delay period occurs in which 10% of the charge is burnt. This delay period is determined using an expression developed by Hires et al (Ref. 26).

During this delay period the mass fraction

burnt is determined using a Wiebe function (Ref. 56).

(v) After the delay period the flame progresses through the unburnt mixture at a rate determined from the expression for flame speed ratio and the calculated laminar flame speed based on the unburnt charge conditions.

(vi) The flame front is assumed to be that of a sphere radiating from the spark plug intersected by the cylinder walls and piston surface.

(vii) The relationship between cylinder gas internal energy and temperature as suggested by Picken (Ref. 51) and as used by Soliman (Ref. 52) was used to determine the mean charge temperature and hence the burnt temperature.

The unburnt zone was treated as subject to an adiabatic process.

6.5 Details of the calculation procedure

Two versions of the combustion model were used; one written in BASIC and used on the PET mini-computer, the other written in FORTRAN and used in conjunction with the complete cycle analysis on the Burroughs main frame computer.

The BASIC version, AppendixA8, was used to carry out a parametric study on a cylindrical combustion chamber geometry and is initiated at 90^{o} b.t.d.c. with a fixed

charge, and terminated at 90° a.t.d.c. It is this version that will be described here.

6.5.1 Compression and expansion procedure

The mass within the cylinder at 90° b.t.d.c. is calculated from the volume at b.d.c. and an assumed pressure of 1 bar and a temperature of 300 K.
This is then multiplied by (1 - F) where F is the residual fraction.
The Eichelberg (Ref.60) heat transfer coefficient is determined from:

$$h = 2.265 (V_p)^{\frac{1}{3}} \quad P/T \quad kJ/m^2/°C$$

and the heat transferred calculated based on a mean wall temperature of 500 K, the charge temperature and the total chamber surface area. The specific internal energy of the charge is calculated from the polynomial previously referred to in Section 6.4.
Work done is determined from the volume change during the crank angle interval considered.
The new internal energy is calculated from the first law, and the mean temperature calculated by solving the polynomial. By applying the perfect gas law, the new pressure is determined and taken as the new initial value.

6.5.2 Initiation of combustion and calculation of the delay period

The concept of an ignition delay period stems from an examination of a pressure crank angle trace for

a firing engine compared with that of a motored engine.

The ignition delay period can be defined as the interval between the time of the spark and the point at which the pressure trace deviates significantly from the motored trace. This delay period can be interpreted as the interval required to initiate the flame kernel and establish a turbulent flame.

In previous thermodynamic models, several attempts have been made to include the delay period. Soliman (Ref. 52) assumes a flame kernel consuming 0.001 of the total mass of the charge, after which the flame progresses with a turbulent burning velocity. Lucus and James (Ref. 18) take a spark energy of 20 mJ which is released in the chemical reaction that begins the combustion process. Phillips and Orman (Ref. 19) also take 0.001 of the total mass but indicate that ignition delay effects can be accounted for by initiating the calculation procedure at a different point to the spark. This allows for a match to be made between experimental and calculated values for the mass fraction burnt. A different interpretation on the delay period is used by Heywood et al. (Ref. 53) in their cycle simulation. (Appendix A9.)

The delay period quoted here, $\Delta\theta_{id}$, can be

interpreted as development of the flame kernel and $(\Delta\theta^{*}_{id} - \Delta\theta_{id})$ as the period to establish a fully turbulent flame. So the definition of 'delay period' as the 0-10% mass fraction burnt period can be related to the discussion in section 6.2 and this is the definition that will be used in this work. Determination of the 0-10% delay period and its relationship to engine design parameters, requires reference to the turbulent entrainment models.

An expression derived by Hires et al. (Ref. 26) is based on the assumption that the delay period (here stated as 0-1%) is proportional to the time to burn a turbulent eddy:

$$\Delta t_{ig} = C_1 \tau_b$$

This is developed to produce an expression for the delay period in terms of degrees of crank angle.

$$\Delta\theta_{ig} = C_{ig} (V_p)^{\frac{1}{3}} (h/U_L)$$

where V_p = mean piston speed

ν = kinematic viscosity

h = instantaneous chamber height

U_L = Laminar flame speed

C_{ig} = constant

The assumptions made in this derivation can be found in the paper, the two most significant being that the turbulent intensity u' at t.d.c. is assumed proportional

to the mean piston speed and that the characteristic eddy size is proportional to the chamber height. It is stated in the paper by Hires (Ref. 26), regarding the 0-1% definition of ignition delay period, that, "Although this definition of the end of the ignition interval is somewhat arbitrary, it represents a convenient reference state near which significant energy release begins and a fully developed turbulent flame front has been established". With reference to the discussion in Section 6.2, it is considered that the definition of 0-10% mass fraction burnt is justified and that as this period will be related to the turbulent conditions in the chamber during this period, the use of the Hires equation will give an adequate representation of the delay period as related to the engine geometry.

6.5.3 Heat release during the delay period

Heat release during the ignition delay period was determined using a Wiebe function for the mass fraction burnt. (Ref. 56)

This can be written as:

$$x = 1 - e^{-A\left[\frac{\theta - \theta_o}{\Delta\theta_c}\right]^{(m+1)}}$$

In order for this expression to match with the definition of delay period, x must equal 0.1 when

$$(\theta - \theta_o)/\Delta\theta_c = \Delta\theta_{ig}/\Delta\theta_c$$

The value of m can be determined from:

$$0.1 = 1 - e^{-A\left[\Delta\theta_{ig}/\Delta\theta_c\right]^{(m+1)}}$$

$$m = \frac{(-2.25037 - \ell_n(A))}{\ell_n\left[\Delta\theta_{ig}/\Delta\theta_c\right]} - 1$$

The correct burn rate at x = 0.1 will depend on the value of A. By differentiating to find $\dot{x}$ and equating to the burn rate expressed in terms of the turbulent flame speed and a spherical flame front will give an expression for determining A.

$$\frac{dV_F}{d_t}\frac{M}{V} = A\, e^{-A\left[\frac{\Delta\theta_{ig}}{\Delta\theta_c}\right]^{(m+1)}} (m+1)\left[\frac{\Delta\theta_{ig}}{\Delta\theta_c}\right]^{(m+1)}$$

where $\frac{dV_F}{d_t}$ = Rate of entrainment of charge

M = Total mass of charge

V = Total volume

but $\frac{dV_F}{d_t} = U_T A_F = U_L.FSR.A_F$

By substitution of the expressions for FSR and A_F a quadratic in A can be found and solved. A value of A = 1 was found to be satisfactory in all cases.

6.5.4 Heat transfer

Allowance for heat transfer has been made using Eichelberg's (Ref. 60) equation, which has produced

satisfactory results in previously reported work. The two zones, burnt and unburnt, have separate heat transfer areas, Appendix A5 and the heat loss has been determined according to the expression:

$$Q_i = E_n\left[A_B T_B + A_U T_U - A_T T_W\right]$$

where E_n = Eichelberg's heat transfer coefficient

A_B = Surface area of burnt zone

A_U = Surface area of unburnt zone

$A_T = (A_U + A_B)$

6.5.5 Calculation of flame speed ratio and the turbulent flame speed

The turbulent to laminar flame speed ratio has been determined at each 2° crank angle intervals as the combustion progresses across the chamber (See Section 6.4).

$$FSR = \frac{U_T}{U_L} = 1 + K\left(\left[\frac{h_s}{h_i}\right]^{\frac{1}{3}} \frac{L_v^{\frac{1}{3}}}{U_L^{\frac{1}{3}}} Z Q \left[\frac{\rho_i}{\rho_u}\right]^{\frac{1}{9}}\right)$$

The laminar flame speed U_L was determined from the expression used by Annand (Ref. 54) and modified by Soliman, Fig. 6.5.5/1

$$U_L = 57.0\, R\, \mu\, T_u^{1.647}\, f(\phi)$$

where $f(\phi) = 4.69 - 8.72(1.1 - \phi)^2$

ϕ = equivalence ratio

$$= \frac{\text{Stochiometric air/fuel ratio}}{\text{actual air/fuel ratio}}$$

R = gas constant

μ = viscosity of unburnt charge

T_u = temperature of unburnt charge

6.5.6 Procedure during the step of the combustion process

The calculation procedure during the combustion period is slightly different between the delay period and afterwards. During the delay period the mass fraction burnt (M_B) is determined from the Wiebe function. This is then used to obtain the increment of volume burnt (V_B) using the relationship.

$$V_B = V \frac{M_B}{M}$$

where M = total charge mass

V = chamber volume

The new inflamed volume is found and a flame radius determined by a loop routine in the enflamed volume sub-routine (Appendix A5).
In the fully turbulent region, a new flame radius is determined from the turbulent flame speed and the time increment for 2^o crank angle rotation. This radius is now used to find the new enflamed volume and hence the volume burnt. The mass burnt is found using the previous expression for V_B arranged to give M_B.

Heat release is now found from the mass burnt, the equivalence ratio, the stochiometric fuel/air ratio (F_A), the residual fraction (F) and the heating value of the fuel (C_h):

$$Q_B = M_B \, C_h \, \emptyset \, F_A \, (1 - F)$$

Using the first law, at constant volume with no heat transfer and the expression for internal energy, enables a new mean pressure and temperature to be determined.

The charge is now expanded to the new volume at the end of the 2^o interval with allowance for heat transfer. A new mean temperature and pressure are determined. If the process occurs during the delay period, no attempt is made to determine burnt and unburnt temperatures, and the calculation proceeds to the next interval.

When the delay period has passed, the unburnt temperature is determined using the expression:

$$T_{U_2} = T_{U_1} \left[\frac{P_{U_2}}{P_{U_1}} \right] \frac{\gamma - 1}{\gamma}$$

The subscripts refer to the initial and final states.

The internal energy (E_u) is determined using T_{U_2} and the burnt zone internal energy found from:

$$E_B = \left[M E - M_U E_U \right] / M_B$$

This enables a burnt gas temperature T_B to be determined.

The new unburnt zone volume is calculated from:

$$V_{U_2} = V_{U_1} \left[\frac{P_{U_1}}{P_{U_2}} \right]^{1/\gamma}$$

and hence the new enflamed volume.

This enables the new flame radius to be found.

The flame propagation velocity is determined from this new radius and the radius at the end of the previous step.

During the calculations the characteristic gas constant R has been given a fixed value of 0.287 kJ/kgK, but the ratio of the specific heats γ has been determined using the following expressions taken from Ref. 52 by Soliman.

$$C_1 = -23.787 + 1.085T + 6.933 \times 10^{-5} T^2$$

$$C_2 = -23.787 + 0.7925T + 6.933 \times 10^{-5} T^2$$

$$\gamma = C_1/C_2$$

T = Absolute gas temperature (K)

6.6 Observations on results of combustion model

Results of the output from the combustion model as applied to the geometry of the cylindrical form combustion chamber as quoted in Section 6.6 are shown in Figs. 6.5.7/1-7. The graph of temperature and pressure against crank angle shows fairly typical values for this engine configuration and running condition. The graph of the burnt zone temperature should start at the ignition temperature of approximately 900K, the rise from the unburnt temperature being due to the use of the concept of a mean temperature.

The blending of the Wiebe function for the mass fraction burnt during the delay period and the values calculated using the flame speed is shown in Fig. 6.5.7/1, giving an acceptable graph of mass fraction burnt.
Also shown in this figure is the instantaneous flame radius against crankangle. The convex region is during the delay period and is in the region where the enflamed volume is hemispherical and increasing with the cube of the radius. Subsequently after intersection with the piston crown, the rate of change of volume with respect to time or crank angle becomes nearly constant and the slope of the radius curve is dependant on FSR and the flame surface area. With FSR constant, the radius curve will be proportional to the inverse of the flame front area. Hence the gradual steepening of the curve as the flame front area decreases with increasing radius.

The effect of piston motion on the enflamed volume and flame front surface area is shown in Fig. 6.5.7/3, which is plotted for a 10mm offset of the spark plug. The only significant effect of the piston motion in this case is due to the change in the position of the intersection point with the piston crown. This is significant when considering Lancaster's comments regarding the step in his graphs of FSR against radius.

It is beneficial to ensure that full turbulent flame development has occurred before intersection with the piston crown, so as to prevent this delay in the development of the FSR. This is perhaps most significant in the case of high compression lean burn engines with an extended delay period and is conceivably one reason for the success of the high compression lean burn engine with a recess under the exhaust or inlet valve, as used by May (Ref.55).

The 4-valve pent-roof chamber with a flat-topped piston also has this advantage.

The flame velocities of propagation and burning are shown in Figs. 6.5.7/4-6, together with the FSR's. Determination of the velocities and FSR during the ignition delay period using the present model is unlikely to be of significance due to the assumptions made regarding the heat release rate.

The graphs show very large propagation velocities and burning velocities during this period, and this is directly related to the plot of flame radius against

crank angle, Fig. 6.5.7/2. The convex region, as mentioned previously, being the reason for the high velocity values shown.

Subsequent to the delay period, the predicted values of propagation velocity, burning velocity and FSR are in good agreement with the trends and values given in Lancaster's paper (Ref. 49). The values shown in Table 6.2 are for the CFR engine run in the datum condition as stated in the paper.

One point that does result from these plots is the value of V_T. The propagation velocity V_T is the combination of the burning velocity and the component of the expansion of the burnt volume into the unburnt charge.

If the rate of compression of the total charge is sufficiently high at a time when the burning velocity is low, it is conceivable that, due to the reduction of the burnt and unburnt volumes, the propagation velocity could be less than the burning velocity.

That the piston motion greatly influences the flame propagation can be seen from Fig. 6.5.7/4-6. With reference to the combustion of the mixture V_T has little relevance and it can be seen that $\frac{U_T}{U_L} \neq \frac{V_T}{V_L}$

where V_L is the propagating velocity when FSR = 1

The effect of ignition timing on the burn rate, Fig. 6.5.7/7, is as expected and can be compared with Fig. 6.5.7/8, which is taken from the paper by Hires (Ref. 26)

6.7 Application of the combustion model to the geometry of the cylindrical combustion chamber

The geometry of the combustion chamber will have considerable effects on the progression of the combustion phase. These effects will be the result of two main factors:

(i) Influence on the FSR due to variations in the factors in the FSR expression, notably h_s/h_i, L_V, Z and ρ_i/ρ_u.

(ii) A direct effect due to the shape of the volume against radius characteristic, the slope of this, dV_F/d_R being most significant.

The chamber compactness will considerably affect the heat loss during the combustion phase.

The spark plug position is the controlling factor when determining the enflamed volume characteristics and as stated in section 6.2 will greatly influence the duration of combustion. The other main parameters that can be varied are the bore/stroke ratio and the compression ratio.

The comparisons made in the following sections are based on a datum case with the following parameters:

Capacity	:	250 cc
Bore/stroke ratio	:	1
Bore	:	68.28 mm
Stroke	:	68.28 mm
Connecting rod length	:	112 mm

Compression ratio : 8:1

Engine speed : 6000 r.p.m.

Inlet valve diameter : 0.43 x bore = 29.36 mm

(Single inlet and exhaust valve)

Inlet valve lift : 0.25 x inlet valve dia

= 7.34 mm

Mean inlet valve flow coefficient = 0.357

Ignition advance : 30°

Height of chamber at T.D.C. : 9.75 mm

Height of chamber at ignition : 15.63 mm

A parametric survey was carried out initially for the central spark plug geometry and gave the following results: Holding the bore/stroke ratio at 1 and varying the compression ratio from 6 to 12 indicated little if any effect on the combustion duration. This was in spite of (i) a reduction of 26% in the delay period at the higher compression ratio, Fig. 6.6/1., and (ii) the decrease in FSR caused by the reduced chamber height affecting the turbulent scale. This reduction outweighed the improvement in laminar flame speed due to the higher temperature at the initiation of combustion.

The conclusion that compression ratio does not significantly affect the burn duration is confirmed by Mayo (Ref. 41), and a comparison with his Figure 9 is shown on Fig.6.6/2. One factor that will have a significant effect on the combustion duration is the equivalence ratio. This is mainly due to the change in the laminar flame speed U_L

as shown in Fig. 6.6/3. However, with fixed timing, the point of 50% mass burnt occurs at significantly different piston positions which affects the FSR. The comments of Lancaster et al (Ref. 44) regarding this point agree even though his points of 50% mass fraction burnt were much closer together, Fig. 6.6/4. It is not therefore correct to assume that the FSR is indendent of equivalence ratio.

The bore/stroke ratio parameter influences the FSR in several ways as stated in Section 6.3. It also changes the enflamed volume characteristic, the chamber surface to volume ratio and hence the heat loss, Fig. 6.6/5-7. However the major effect on burn duration is caused by reducing the delay period with increased bore/stroke ratio. This is due to the reduced chamber height which decreases the characteristic eddy burn time.

The combination of the two effects, which indicates a slight reduction of combustion duration with increasing bore/stroke ratio is shown in Fig. 6.6/8-9.

Engine speed, or more significantly, mean piston speed has a direct effect on both the delay period and the FSR. The delay period is proportional to $(\text{piston speed})^{\frac{1}{3}}$, and hence shows a decreasing dependence on engine speed as the piston speed increases.

The FSR contains the piston speed in the Gulp Factor directly. However, due to the fact that the FSR = 1 at zero engine speed and the expression for FSR takes the form:

$$FSR = 1 + K_1 V_p$$

the ratio will become more directly dependent on V_p as $FSR \gg 1$.

This leads to the combustion duration approaching a nearly constant value at high engine speeds, Fig.6.6/10

[Note: This presumes that the Gulp Factor remains below 0.5 and hence the volumetric efficiency is not adversely affected.]

Two other engine geometry parameters have to be considered:

(i) the effect of inlet valve and port geometry, as represented by the inlet valve size and mean discharge coefficient, and,

(ii) the cylinder swept volume.

Including the mean discharge coefficient in the expression for FSR is a means of reflecting the 'effective' inlet tract dimensions as related to the actual throat diameter D_T.

This concept enables a term directly related to inlet flow quality to be represented in the FSR expression. A more detailed explanation is included in Chapter 3.

The effect of variations of C_m are shown in Fig. 6.6/11 where a 20% reduction of the discharge coefficient produces a 21% increase in FSR and a 16% reduction in 10-90% burnt region, the ignition delay period remaining constant.

By comparison, Mayo in Ref. 41 reports that the high velocity port gave 24% reduction in burn time in the

open standard chamber and a 25% reduction in the open chamber with a central spark plug. These results were obtained using a port with reduced area, with flow characteristics as shown in his Fig. 4. This figure indicates a reduction of mean discharge coefficient of about 18% with the high velocity port.

Reduction of inlet valve diameter whilst maintaining the mean discharge coefficient means a reduction in valve lift. Both the valve diameter (or throat diameter) and the valve lift appear in the FSR expression and a reduction of either will increase the FSR. Therefore the burn time is more sensitive to this parameter than the discharge coefficient. The effect is shown in Fig. 6.6/12 where a 20% reduction in valve diameter and lift produced an increase of F.S.R. of 39.8% and a reduction of the 10-90% burn time of 32.9%.

Changes in engine cylinder size, whilst maintaining the same geometry, will change three parameters used in determination of delay period and FSR. The major influence on the FSR will be due to changes in mean piston speed, as contained in the Gulp Factor. Secondary effects will be due to the reduction in valve lift, reflecting the reduction in turbulent scale. These two effects combined give a 24% reduction in FSR between 500 cc and 250 cc swept volume. This reduction in volume of 50% results in a reduction in dimensions of 21% and therefore the 10-90% burn time increases slightly.

However the reduced piston speed and chamber height will cause the delay period to decrease by 21% and hence the 0-90% burn time decreases slightly.

The results are shown in Fig. 6.6/13.

Finally the total flame travel path and enflamed volume characteristic can be altered by the offset of the spark plug. The result of offsetting the plug on the enflamed volume characteristic for a fixed chamber volume is shown in Fig. 6.6/14.

TABLE 6.1

REFERENCE	EXPRESSION	ENGINE
PHILLIPS & ORMAN (Ref.19)	$\frac{U_T}{U_L} = 1 + 0.002N$	RICARDO E6
HOGETTS (Ref.47)	$\frac{U_T}{U_L} = 1 + 0.0017N$	FORD ZODIAC
LUCUS & JAMES (Ref.18)	$\frac{U_T}{U_L} = 1 + 0.00197N$	RENAULT
GURGIS & TIDMARSH (Ref20)	$\frac{U_T}{U_L} = 1 + 0.0016N$ TO $1 + 0.0013N$	CHRYSLER AVENGER

TABLE 6.2

COMPARISON WITH VALUES FROM Ref. 49*

	ϕ	U_T m/s	V_T m/s	FSR
COMBUSTION MODEL	0.8	7.49	12.41	3.2
LANCASTER UNSHROUDED VALVE	0.8	9.2	12.9	2.9
SHROUDED VALVE	0.8	16.0	21.7	4.2

* ALL VALUES AT 50% MASS FRACTION BURNT

Data for this run was as stated in the paper.

Bore = 82.55 mm
Stroke = 114.3 mm
Con. rod length = 254 mm
Comp. ratio = 8.72
Speed = 1500 r.p.m.
Vol eff. = 50%

FIG 6.3.1/1.

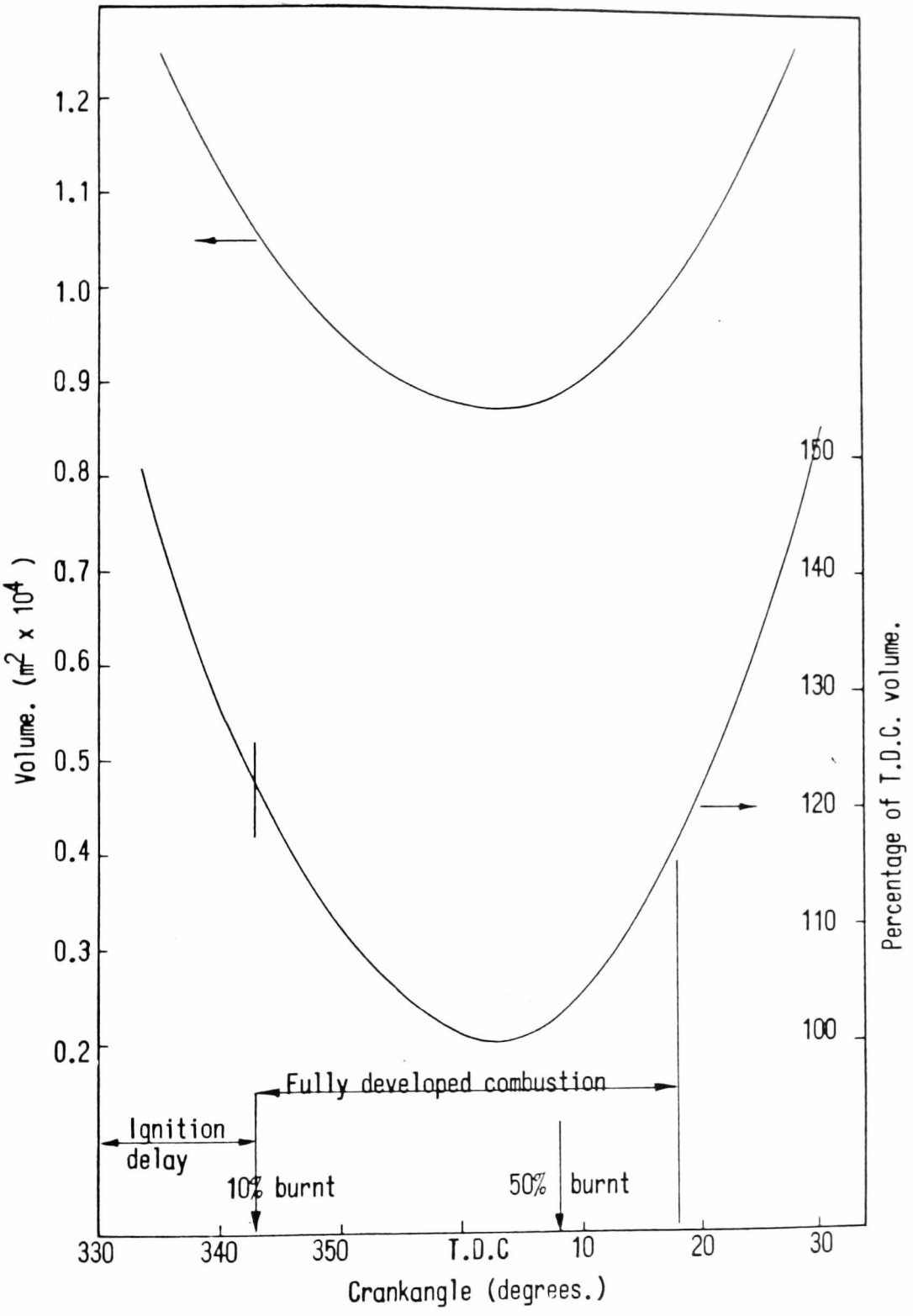

(FIG 6.3.1/1) GRAPH SHOWING CHANGE IN CYLINDER VOLUME DURING COMBUSTION PERIOD.

FIG 6.3.2/1.

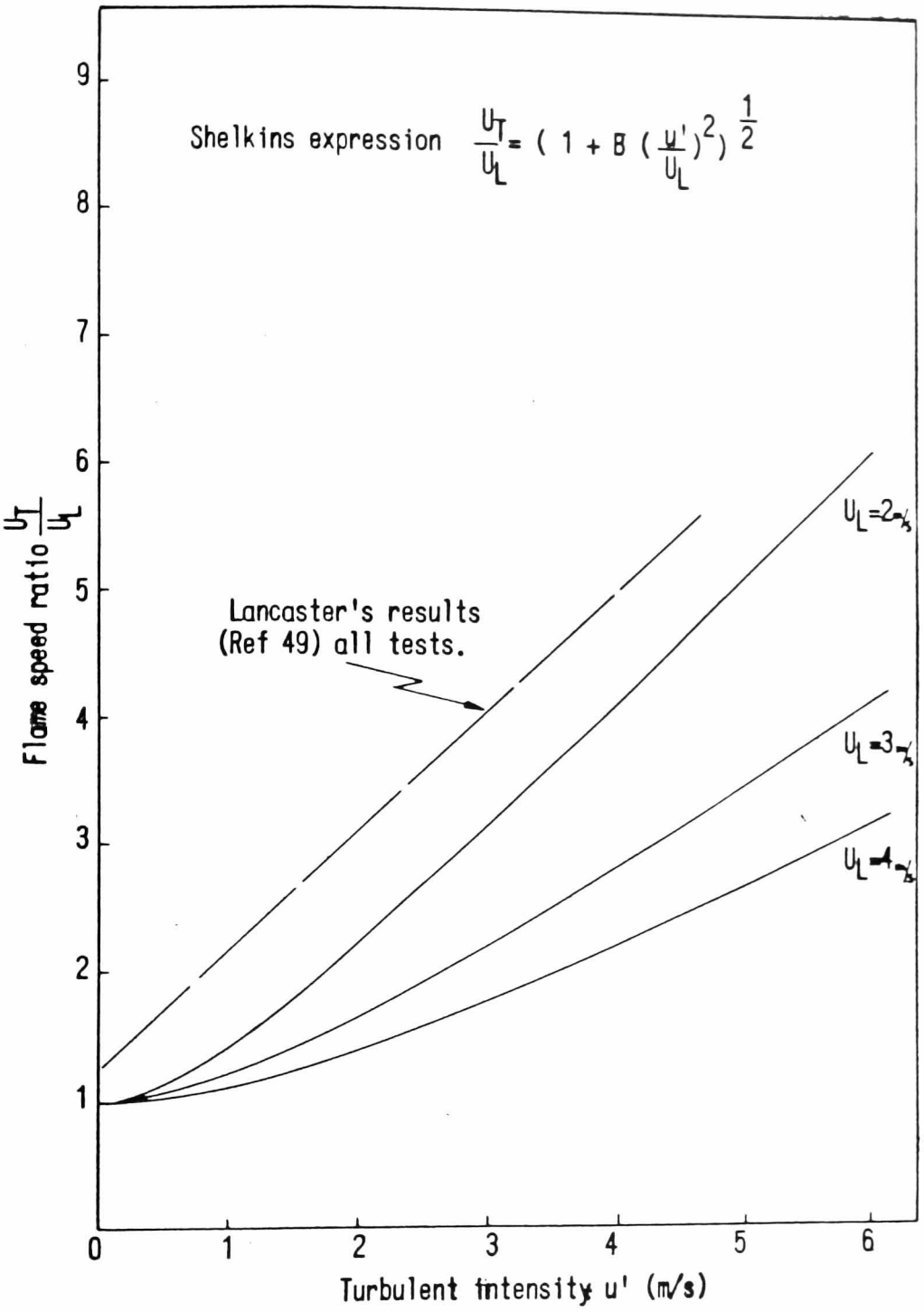

(FIG 6.3.2/1) FLAME SPEED RATIO AGAINST TURBULENT INTENSITY. A COMPARISON OF LANCASTERS RESULTS REF 49 WITH SHELKINS EXPRESSION FOR F.S.R.

FIG 6.3.2/2.

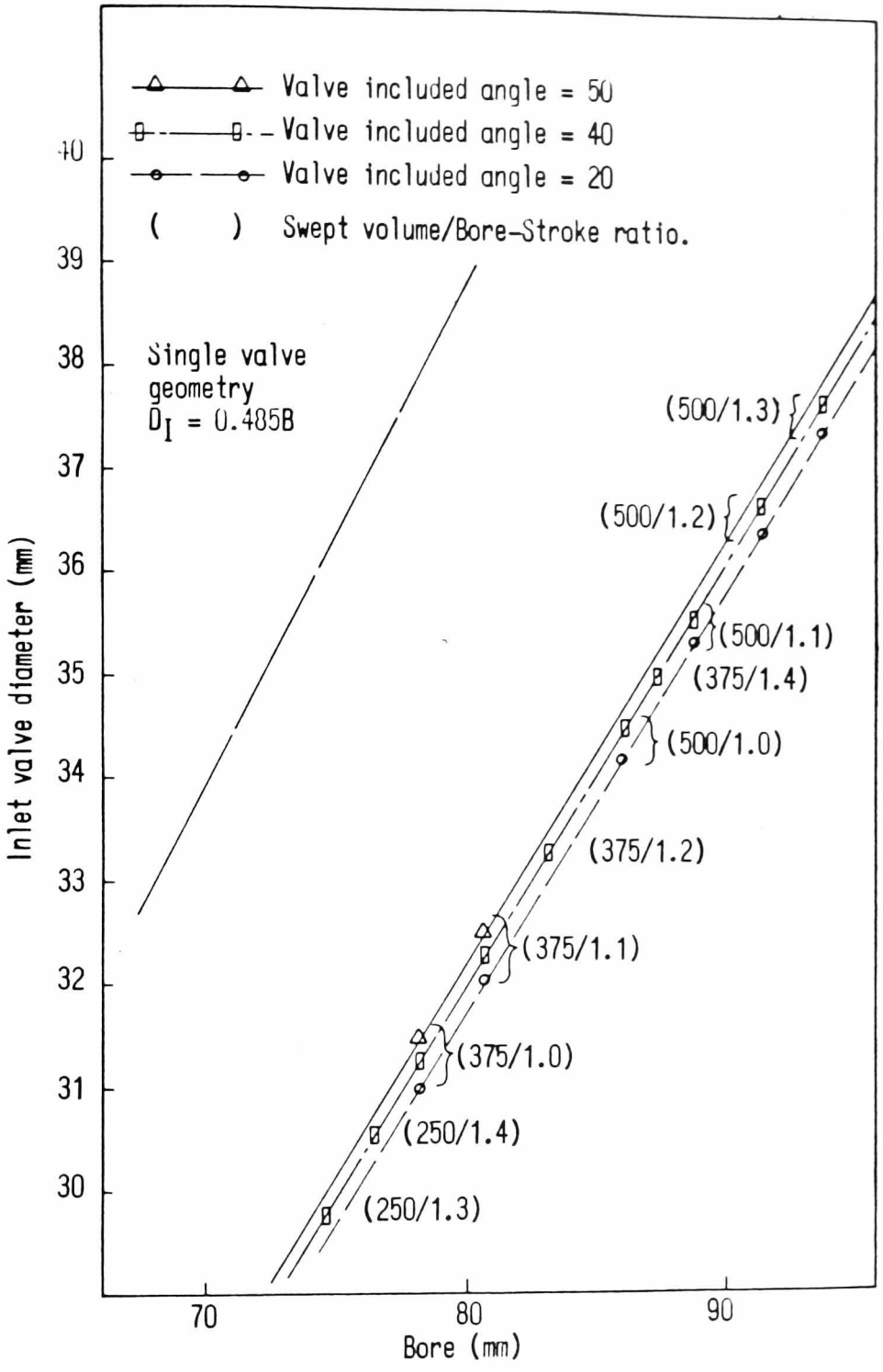

(FIG 6.3.2/2) INLET VALVE DIAMETER AGAINST BORE FOR VARIOUS CYLINDER CAPACITIES AND BORE/STROKE RATIOS FOR 4 VALVE GEOMETRY.

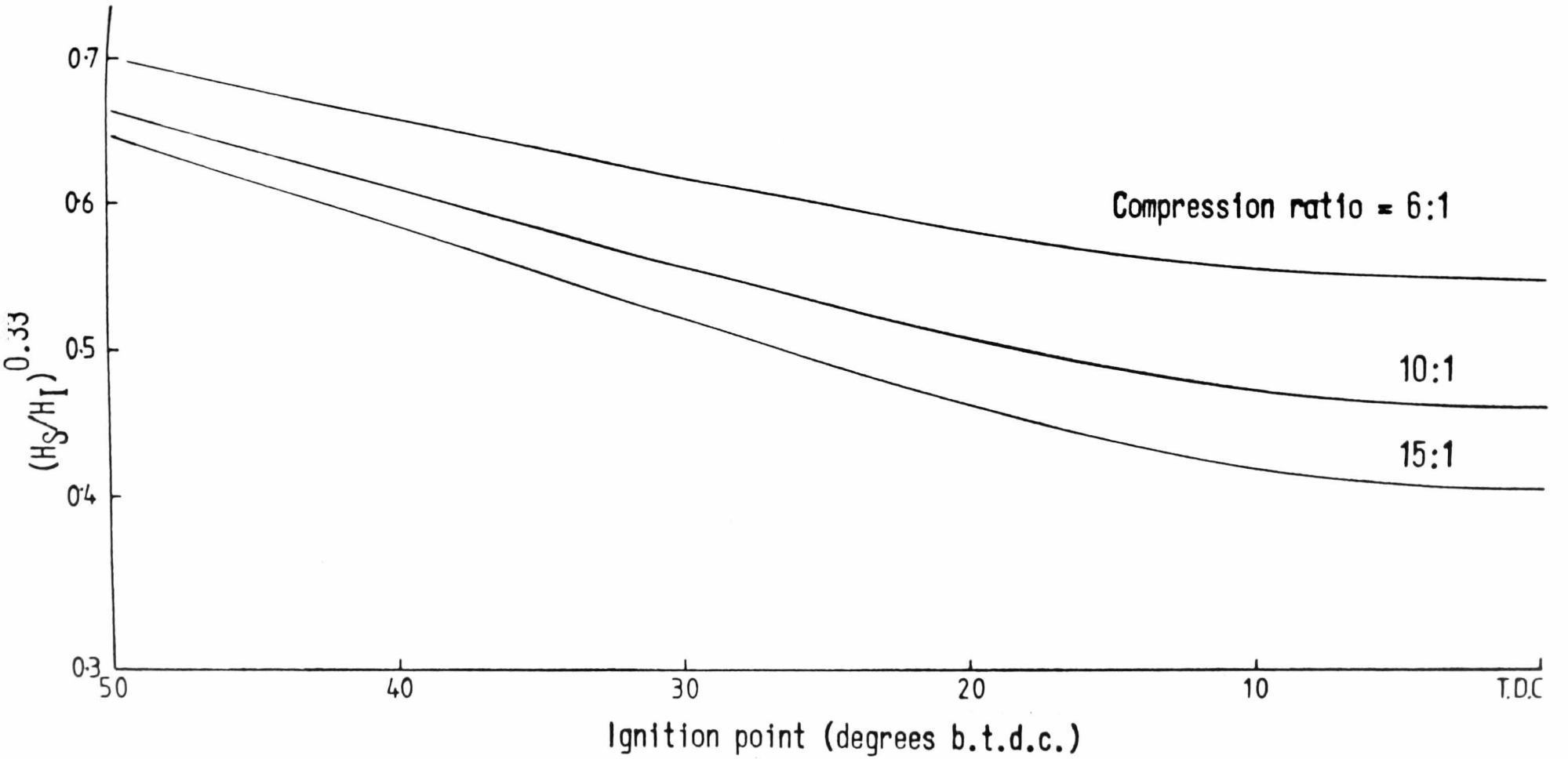

(FIG 6.3.3/1) Graph of $(H_S/H_I)^{0.33}$ against ignition point for a cylindrical combustion chamber-(Independant of cylinder volume and Bore/Stroke ratio)

FIG 6.3.3/1.

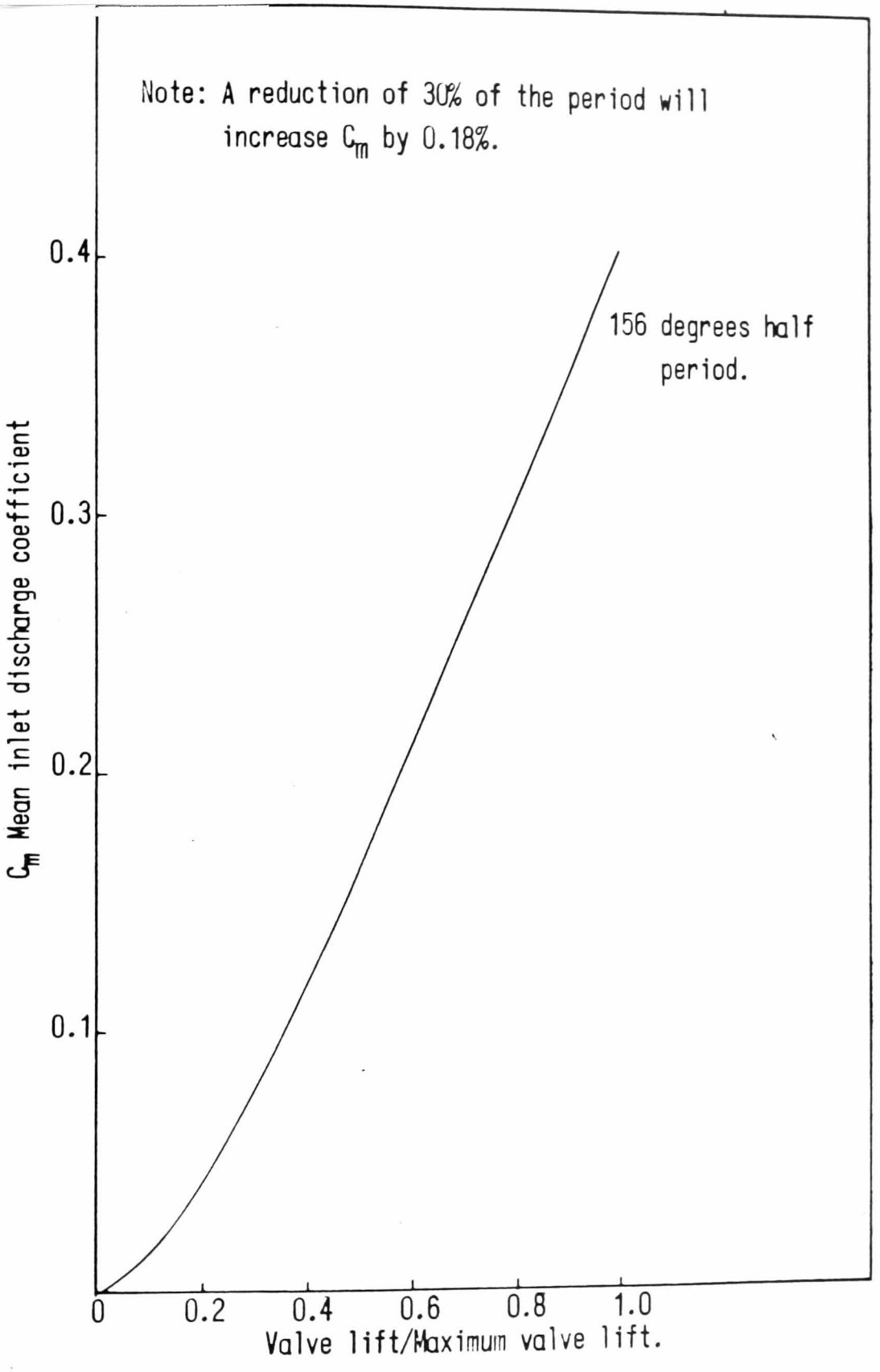

(FIG 6.3.3/2) MEAN DISCHARGE COEFFICIENT AGAINST FRACTION OF MAXIMUM VALVE LIFT FOR WESLAKE 4 VALVE ENGINE.

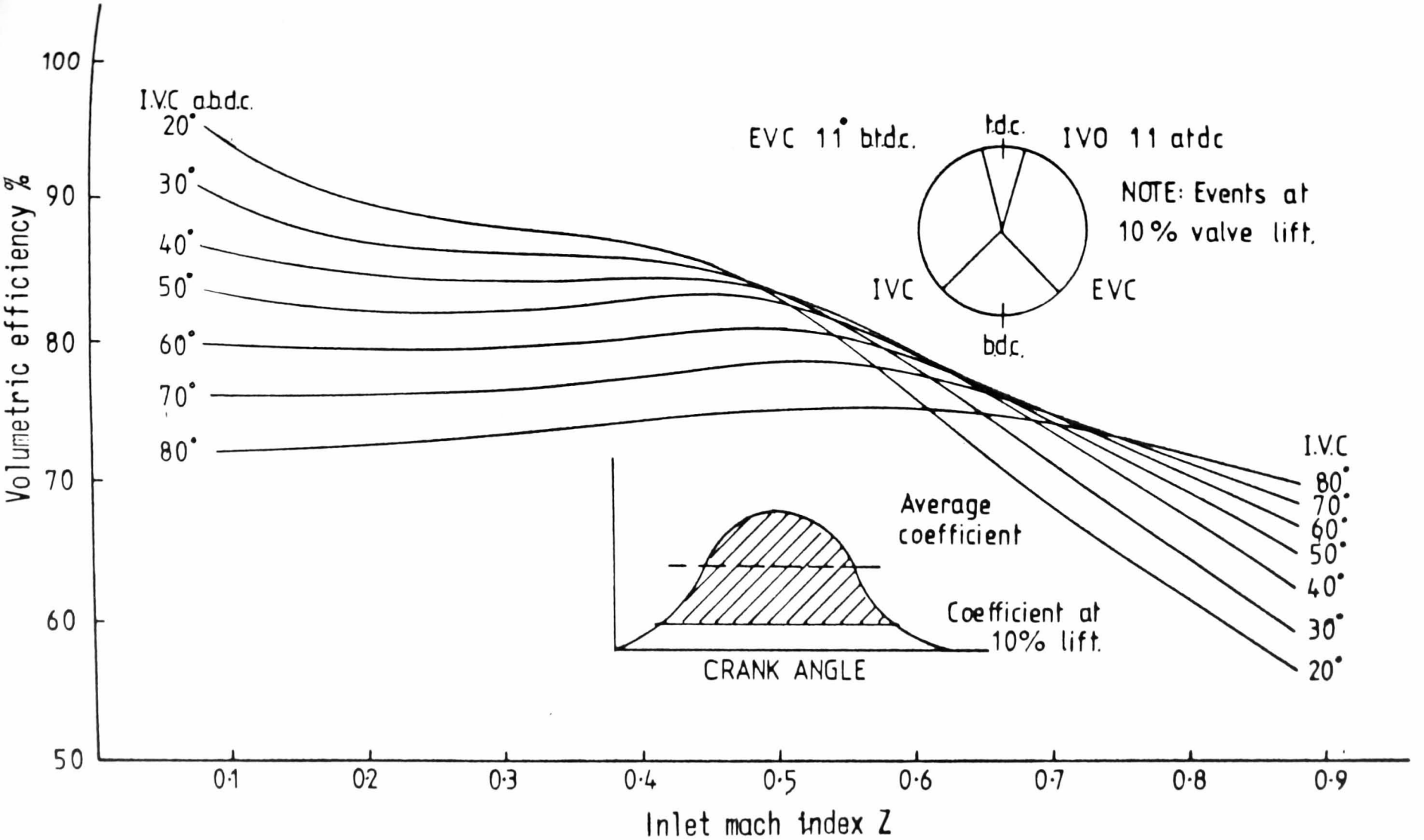

(FIG 6.3.3/3) Graph of volumetric efficiency against inlet mach index
(From NASA tech note No 1366 replotted by Texaco–from Ref61)

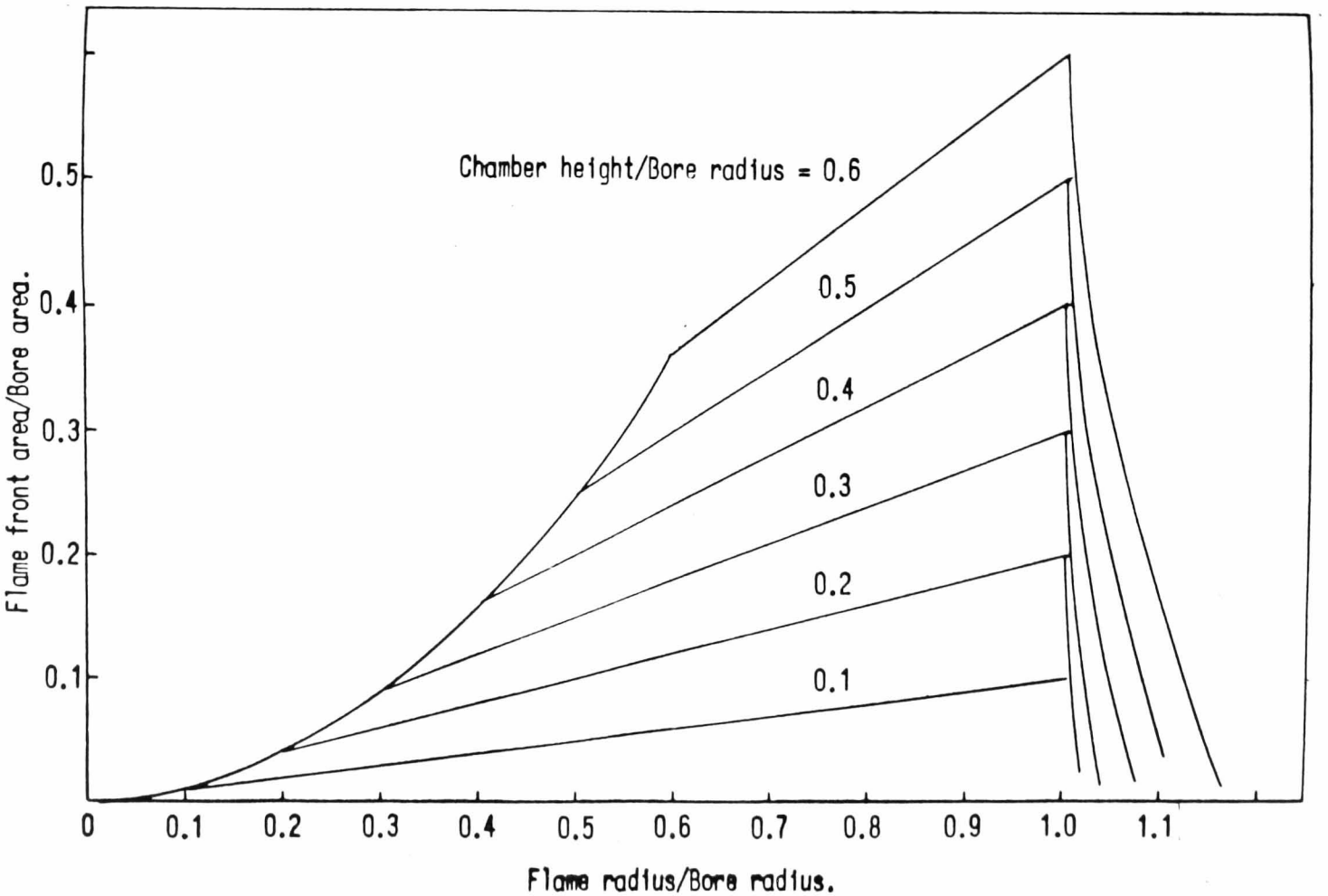

(FIG 6.3.3/4) Flame front area ratio against non-dimensional flame radius for a cylindrical combustion chamber with a central plug.

FIG 6.3.3/4.

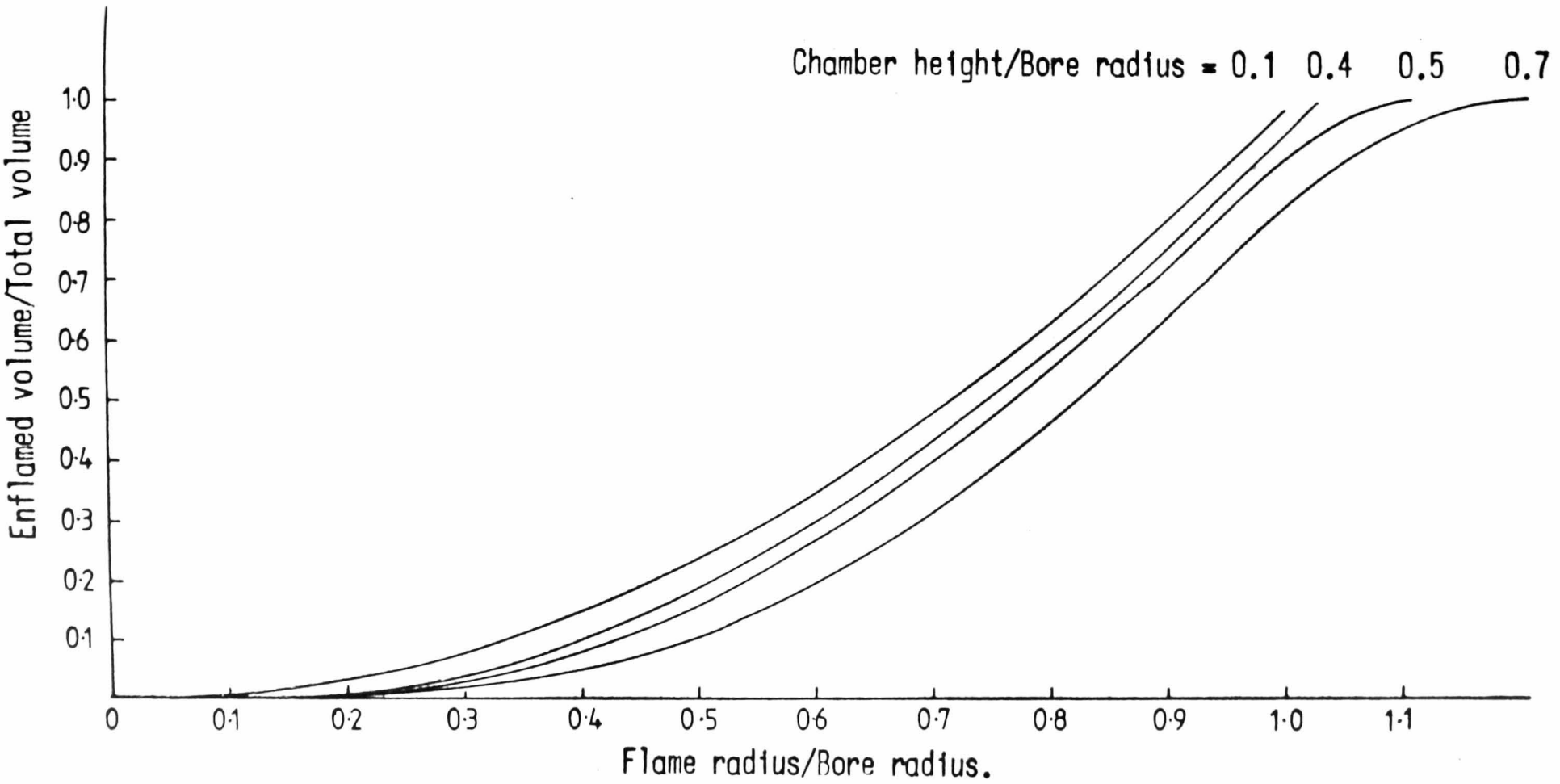

(FIG 6.3.3/5) Enflamed volume/Total volume against Flame radius/Bore radius for cylindrical combustion chamber with a central sparking plug.

FIG 6.3.3/5.

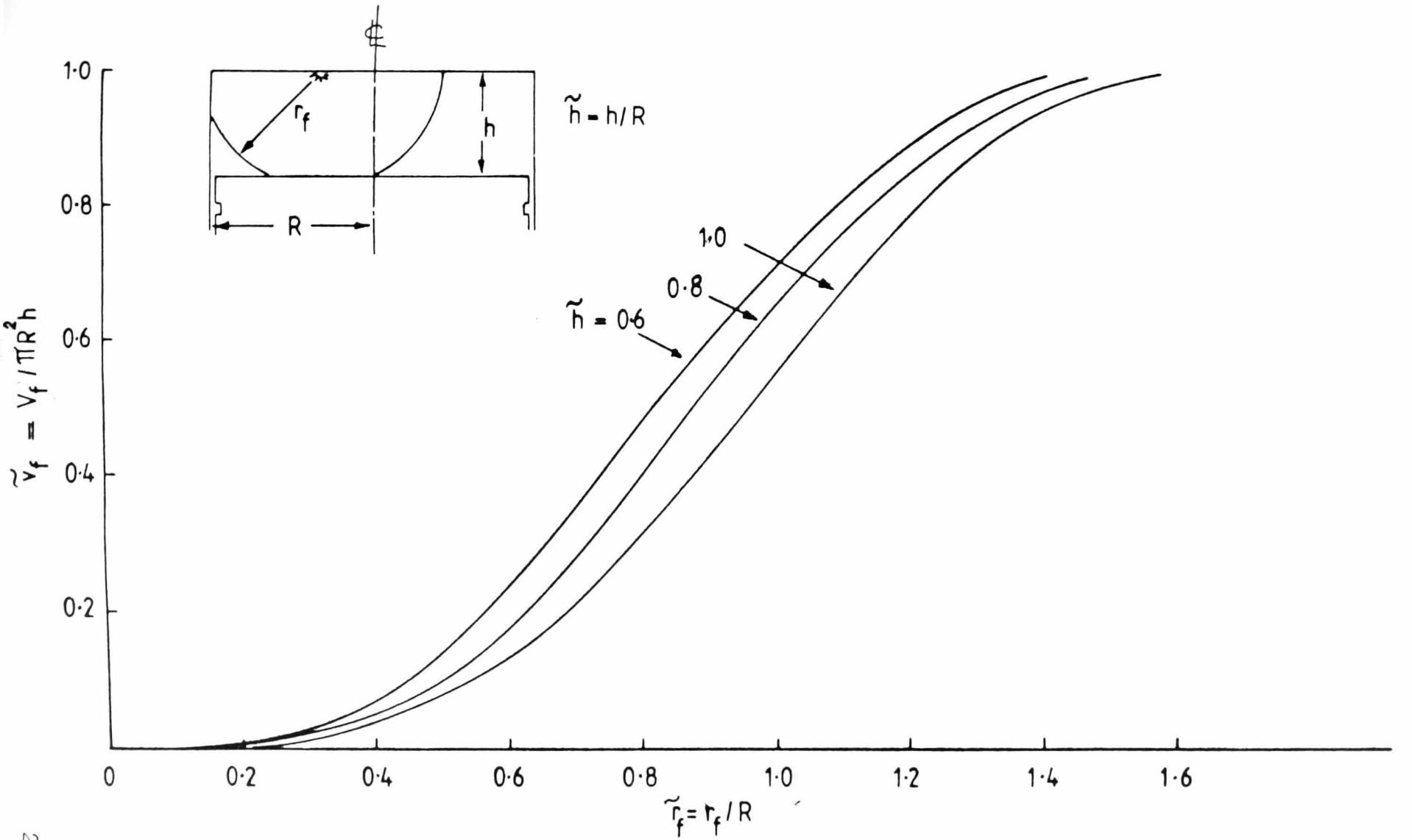

(FIG 6.3.3/6) Graph of non-dimensional enflamed volume against non-dimensional flame radius as used in Ref 21.

FIG 6.3.3/6.

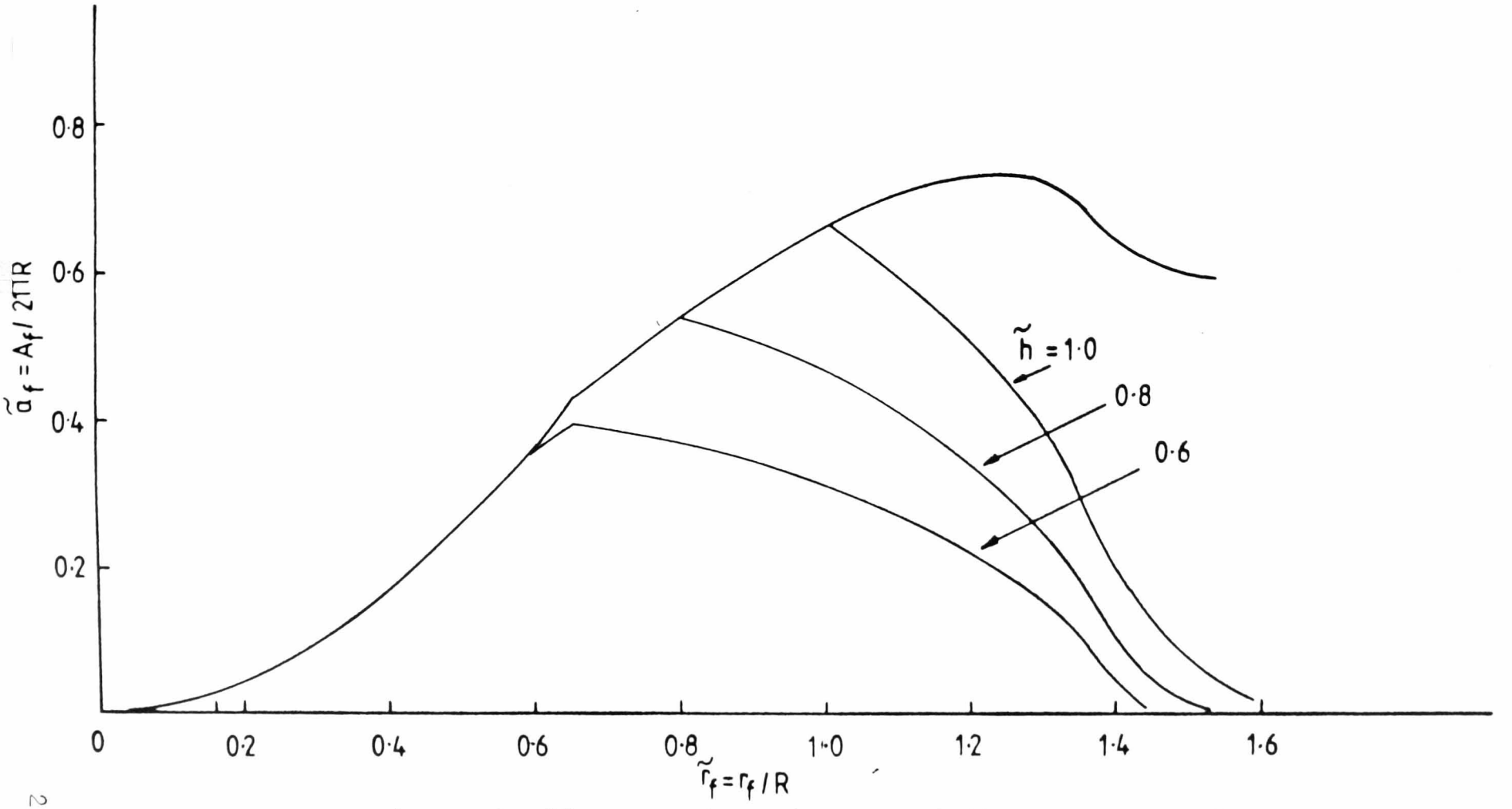

(FIG 6.3.3/7) Graph of non-dimensional flame area against non-dimensional flame radius as used in Ref 21.

FIG 6.3.3/7.

FIG 6.5.5/1.

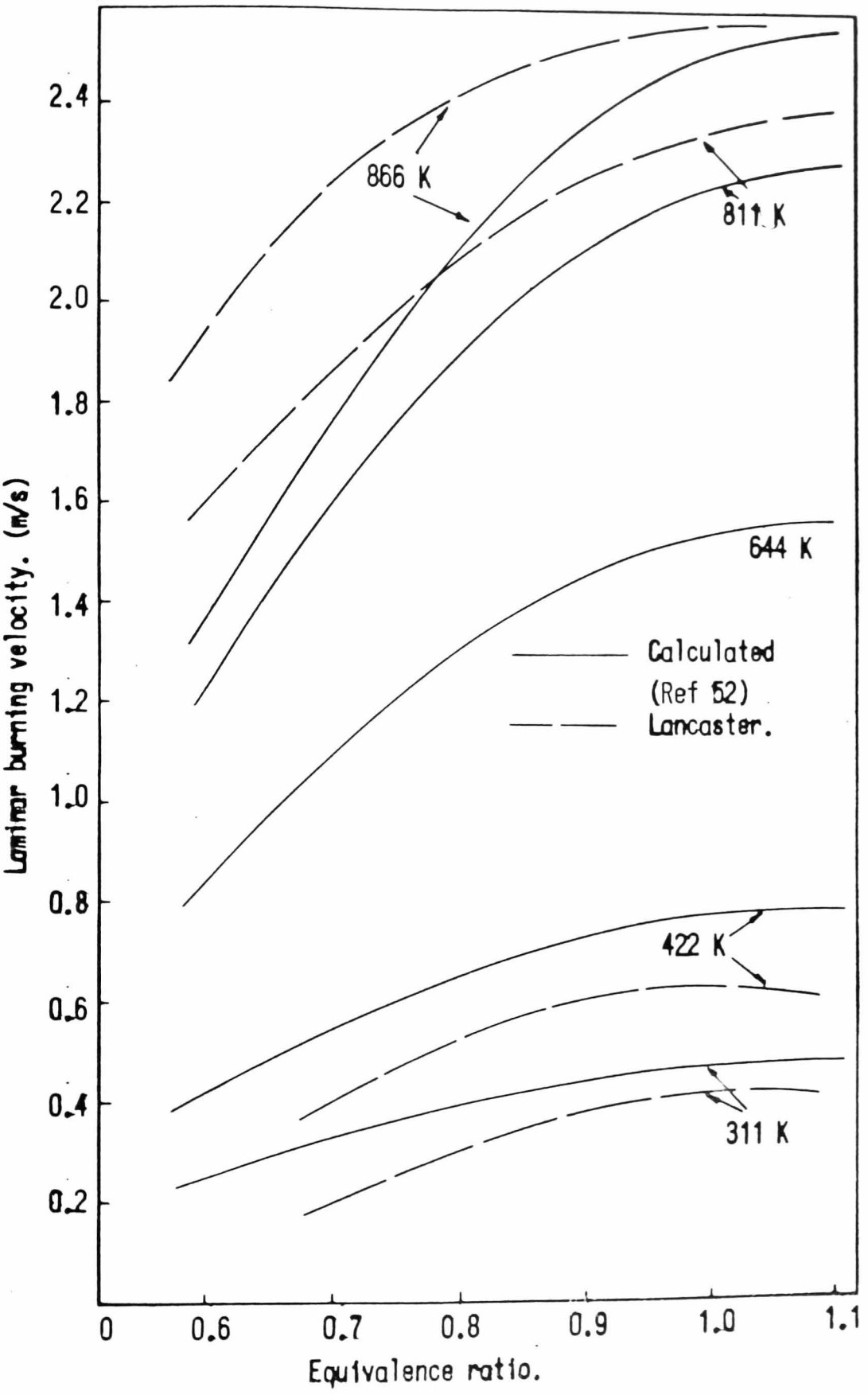

(FIG 6.5.5/1) LAMINAR FLAME SPEED AGAINST EQIVALENCE RATIO. A COMPARISON BETWEEN THAT USED REF 52 AND THAT REPORTED BY LANCASTER REF 49.

FIG 6.5.7/1.

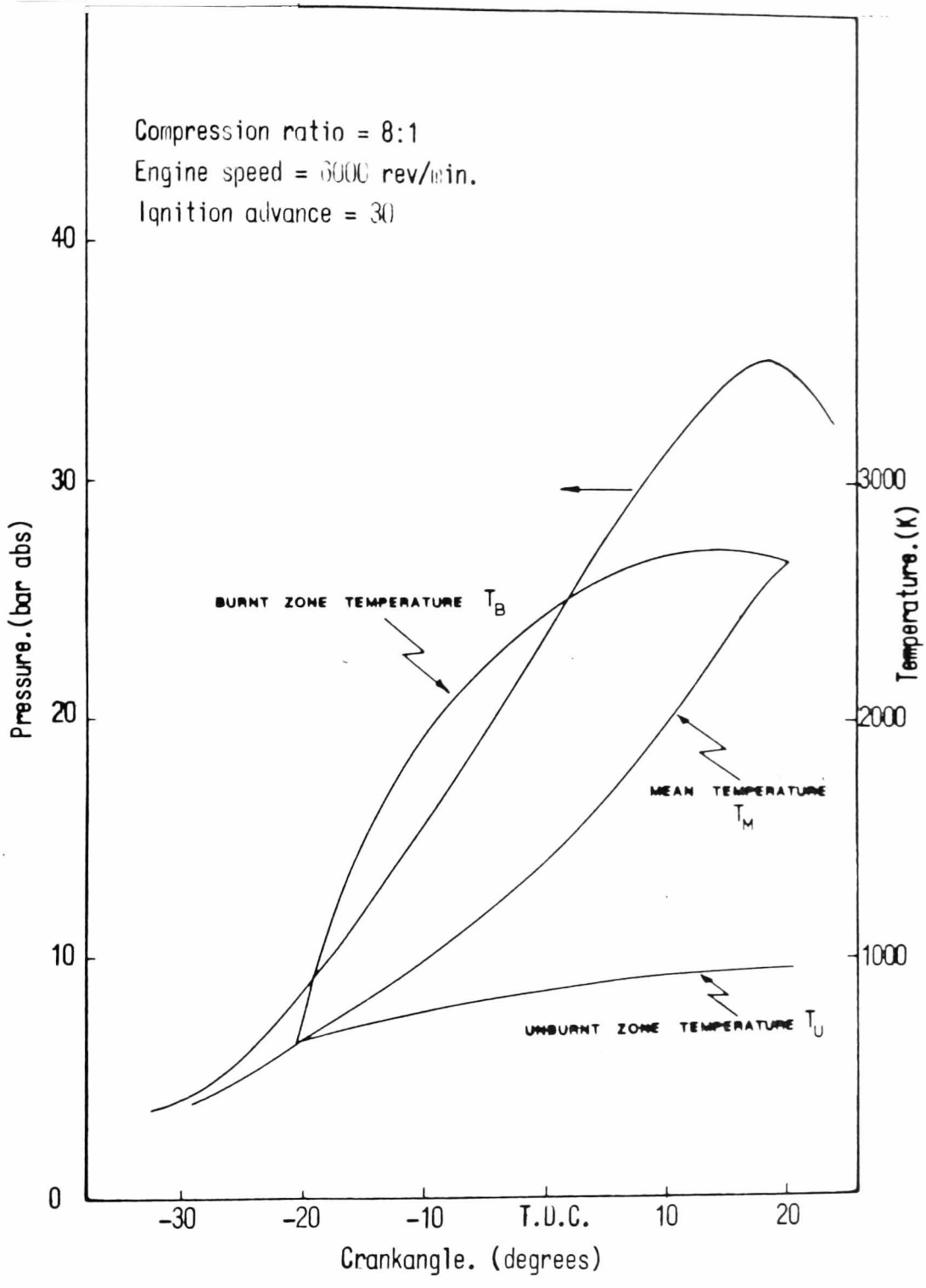

(FIG 6.5.7/1) TEMPERATURES AND PRESSURE FROM A TYPICAL RUN OF THE COMBUSTION PROGRAM.

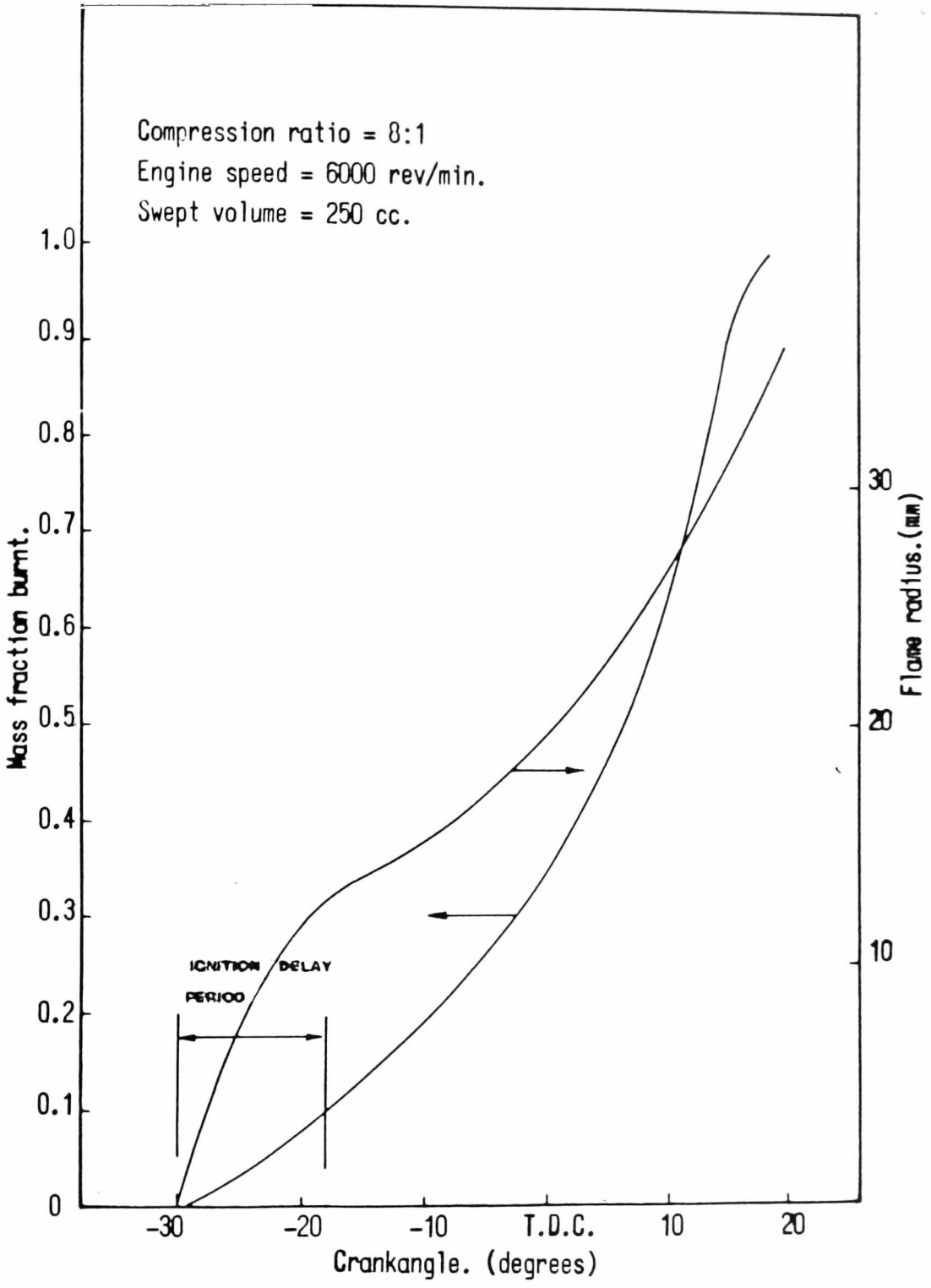

(FIG 6.5.7/2) MASS FRACTION BURNT AND FLAME RADIUS AGAINST CRANKANGLE FOR A CYLINDRICAL COMBUSTION CHAMBER.

FIG 6.5.7/3.

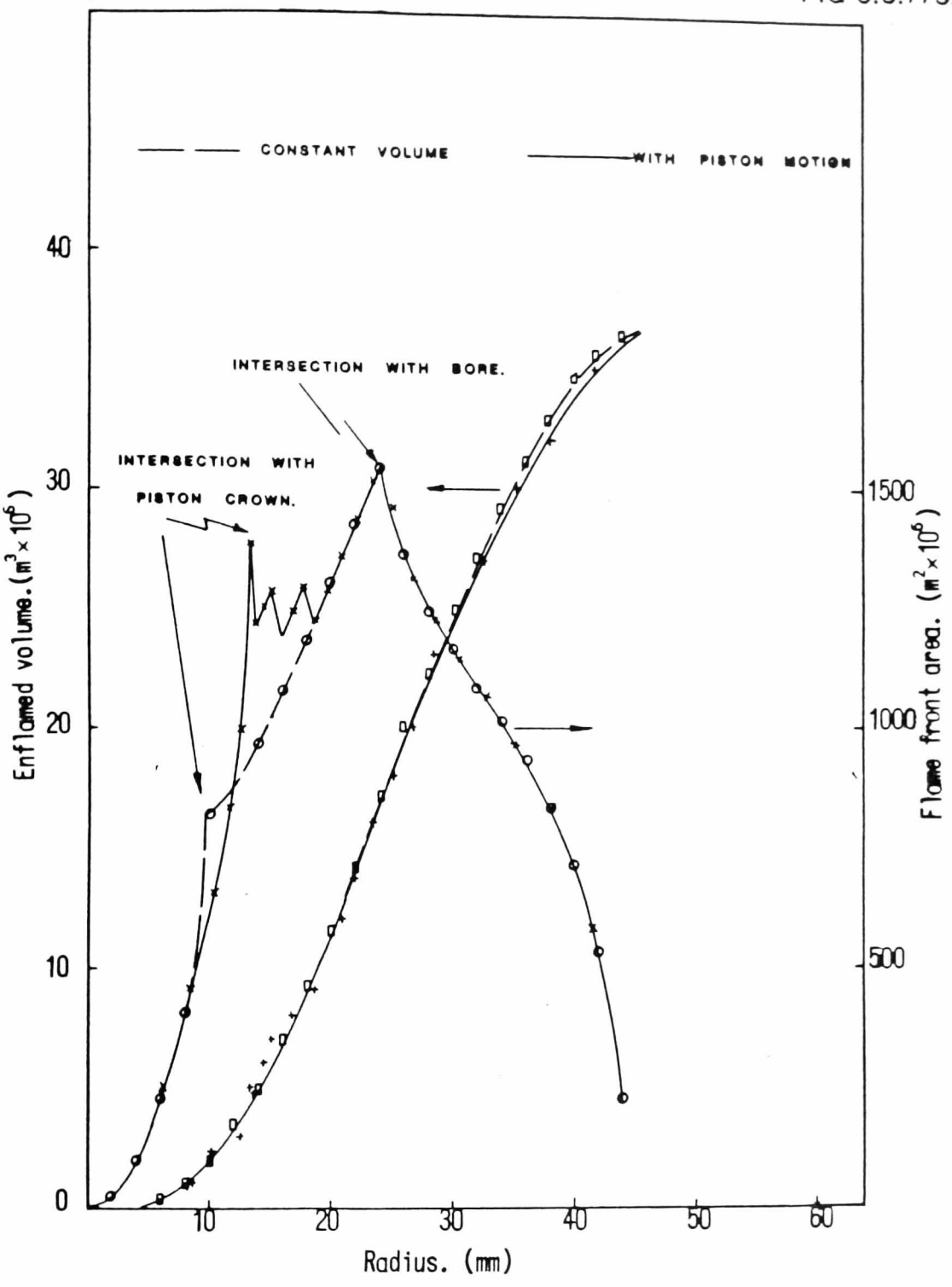

(FIG 6.5.7/3) COMPARISON OF ENFLAMED VOLUME AND FLAME FRONT AREA WITH AND WITHOUT PISTON MOTION.

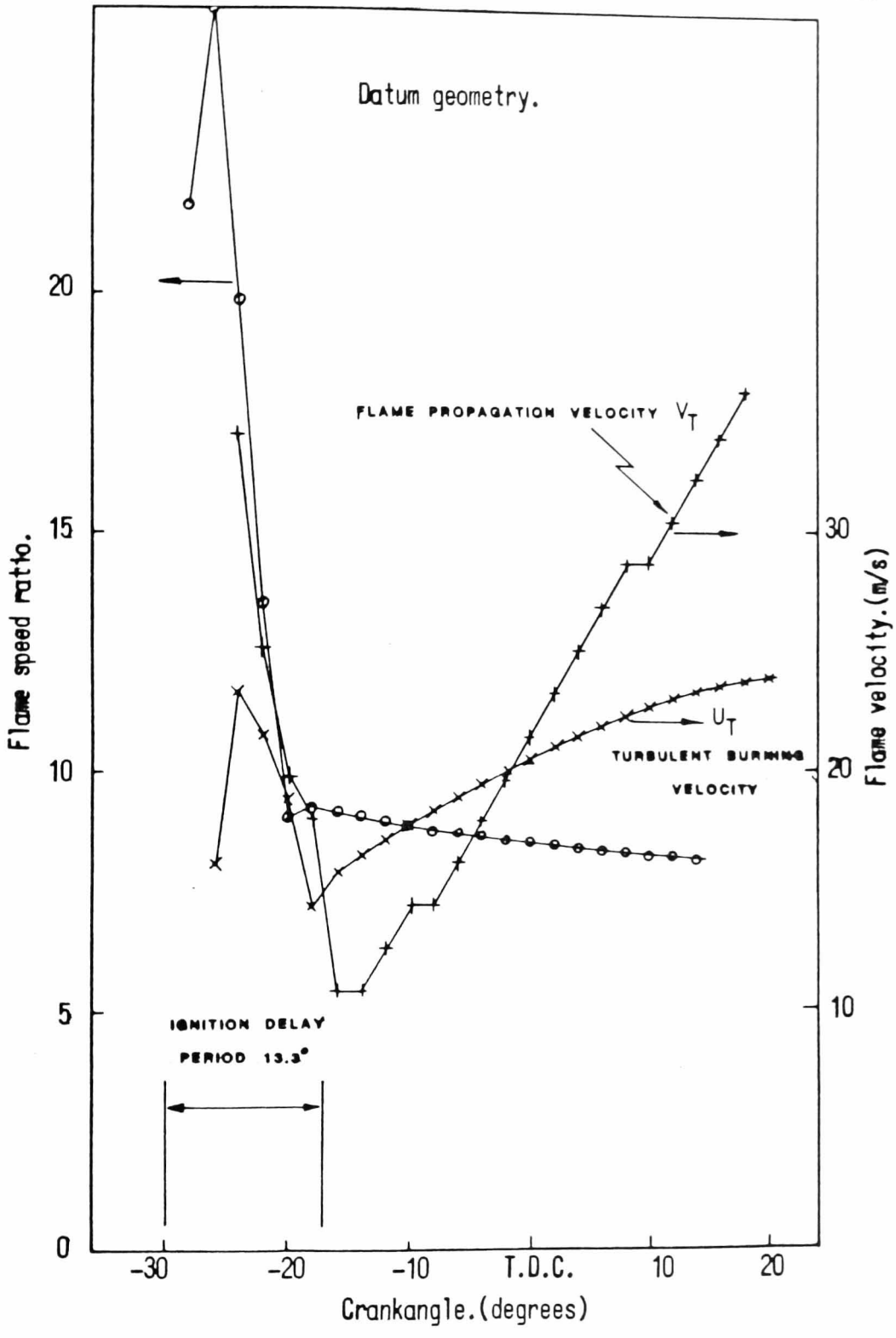

(FIG 6.5.7/4) FLAME SPEED RATIO AND FLAME VELOCITIES AGAINST CRANKANGLE.

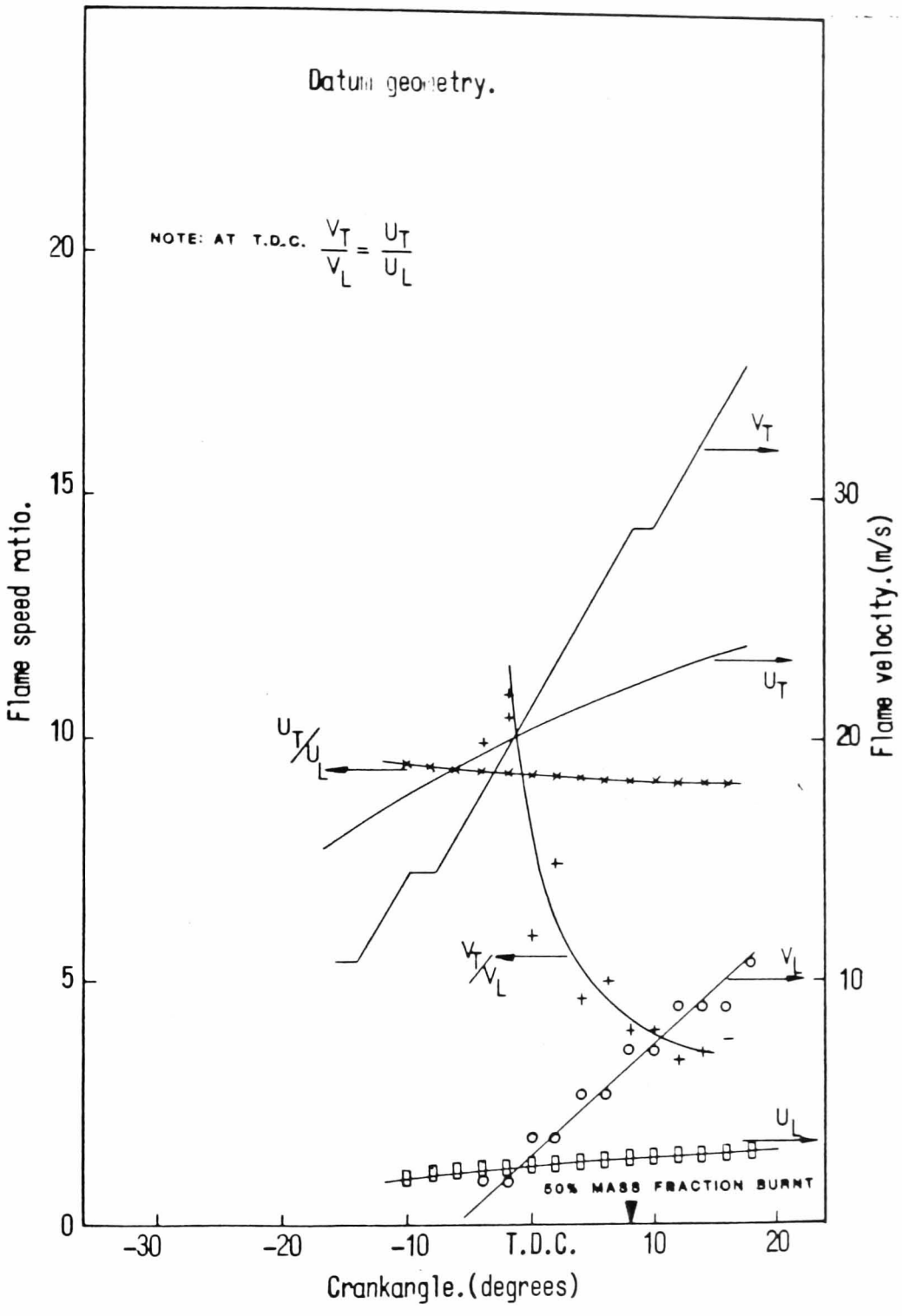

(FIG 6.5.7/5) COMPARISON BETWEEN TURBULENT AND LAMINAR BURNING AND PROPAGATING VEOCITIES

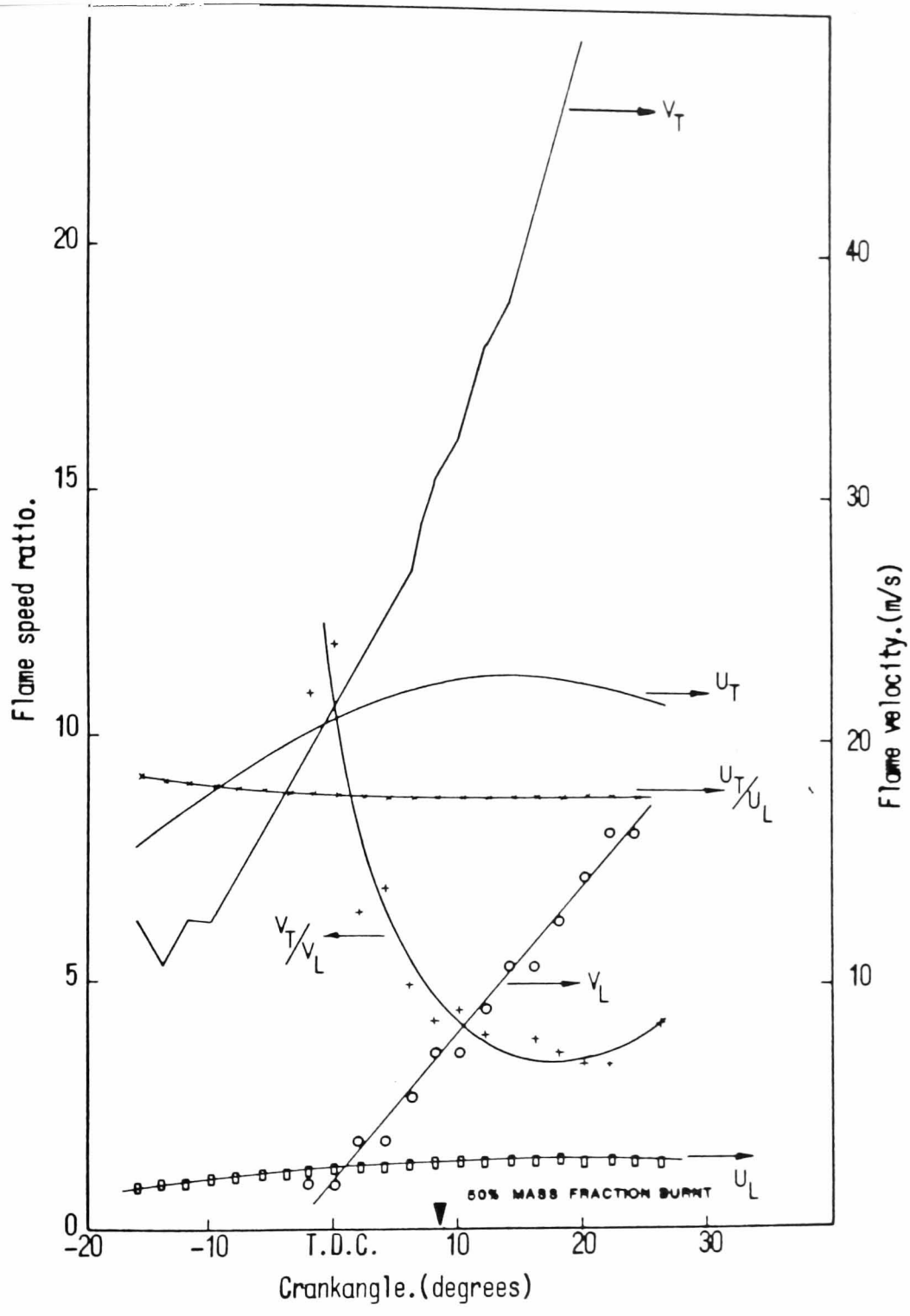

(FIG 6.5.7/6) COMPARISON BETWEEN TURBULENT AND LAMINAR BURNING AND PROPAGATION VELOCITIES WITH A 20mm OFFSET PLUG.

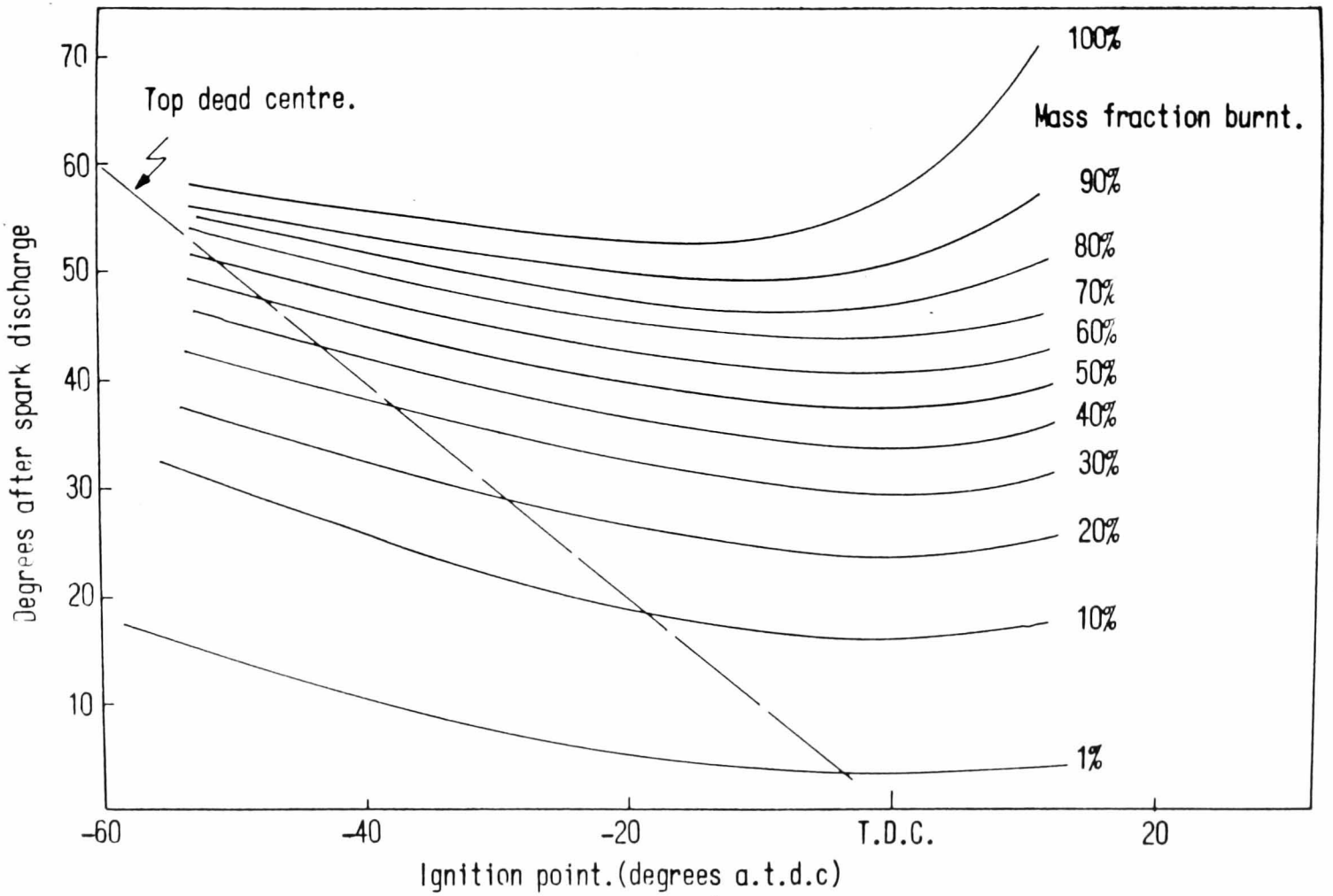

(FIG 6.5.7/7) Effect of ignition timing on burn duration and ignition delay.

FIG 6.6/1.

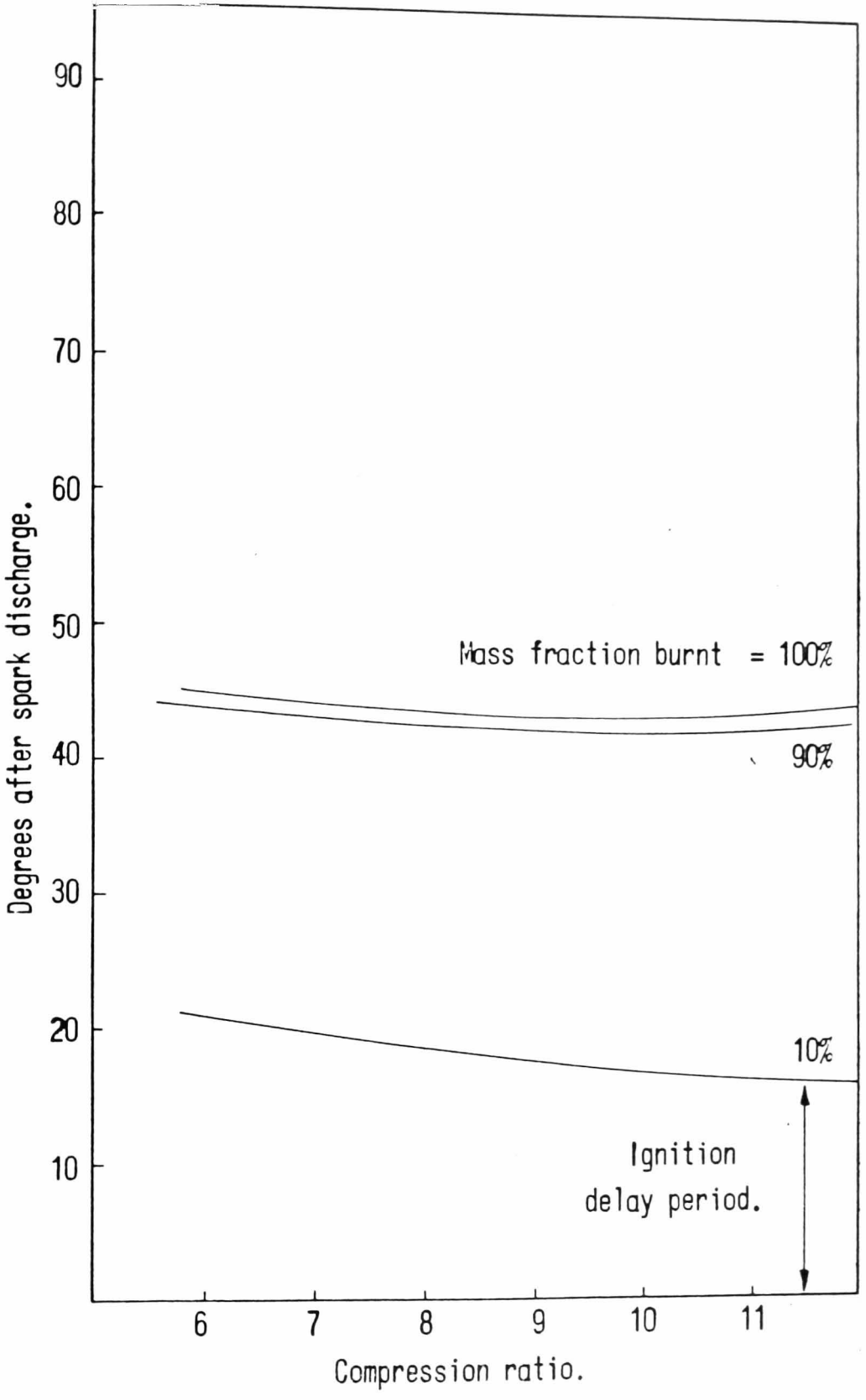

(FIG 6.6/1) COMBUSTION DURATION AGAINST COMPRESSION RATIO. (IGNITION TIMING FOR PEAK PRESSURE AT 14° a.t.d.c)

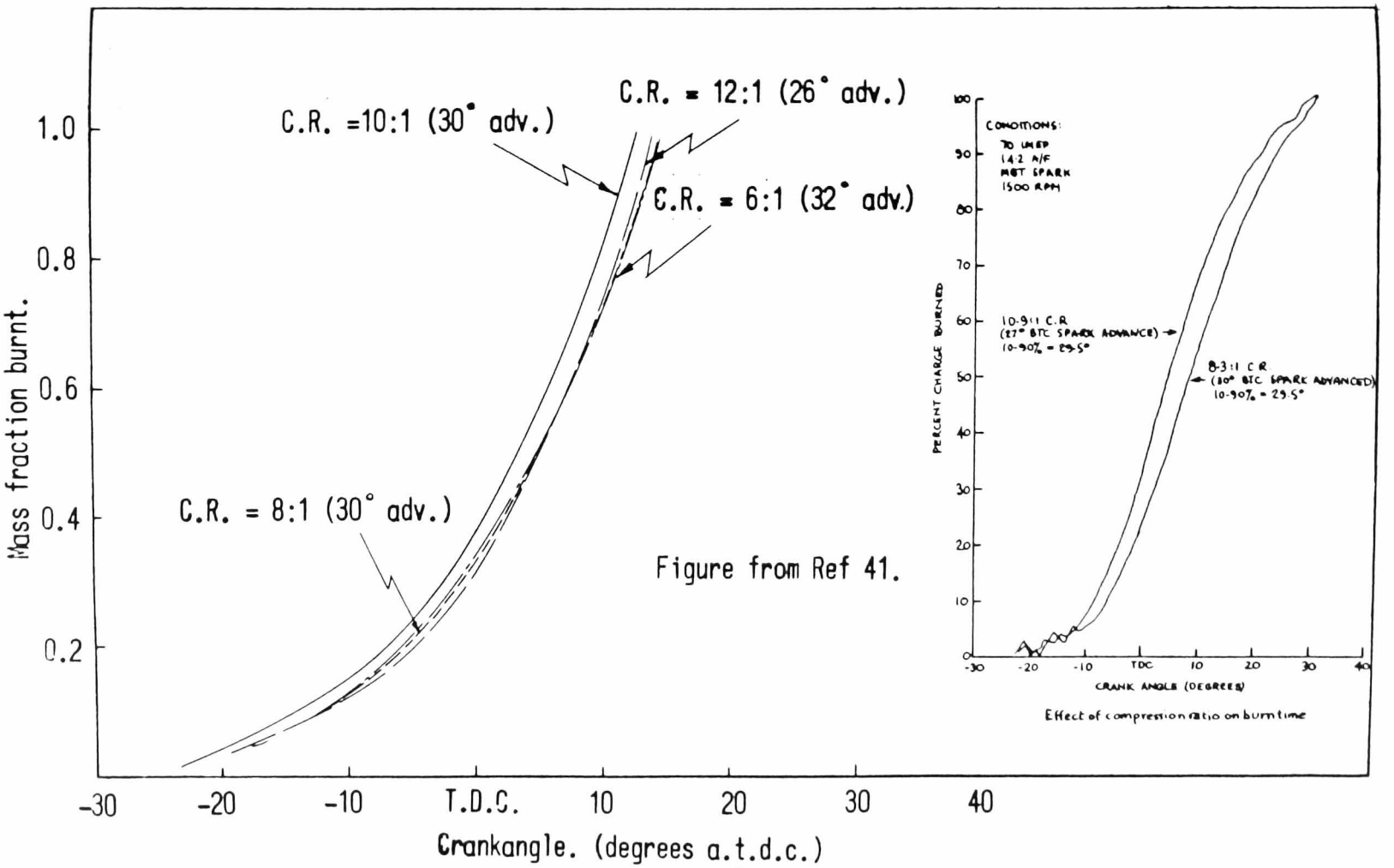

(FIG 6.6/2) Mass fraction burnt against crankangle for various compression ratios.

FIG 6.6/2.

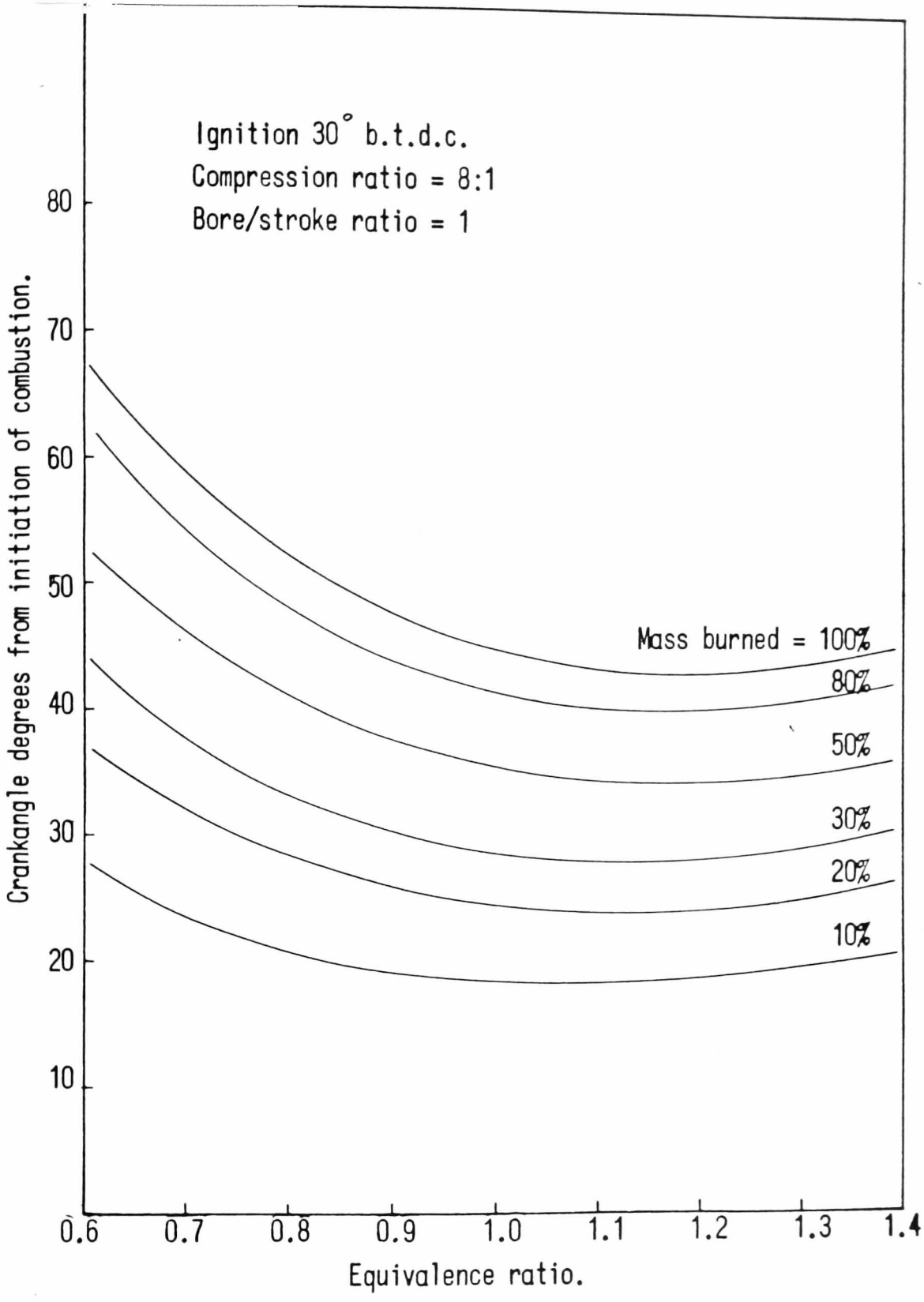

(FIG 6.6/3) BURN DURATION AGAINST EQUIVALENCE RATIO.

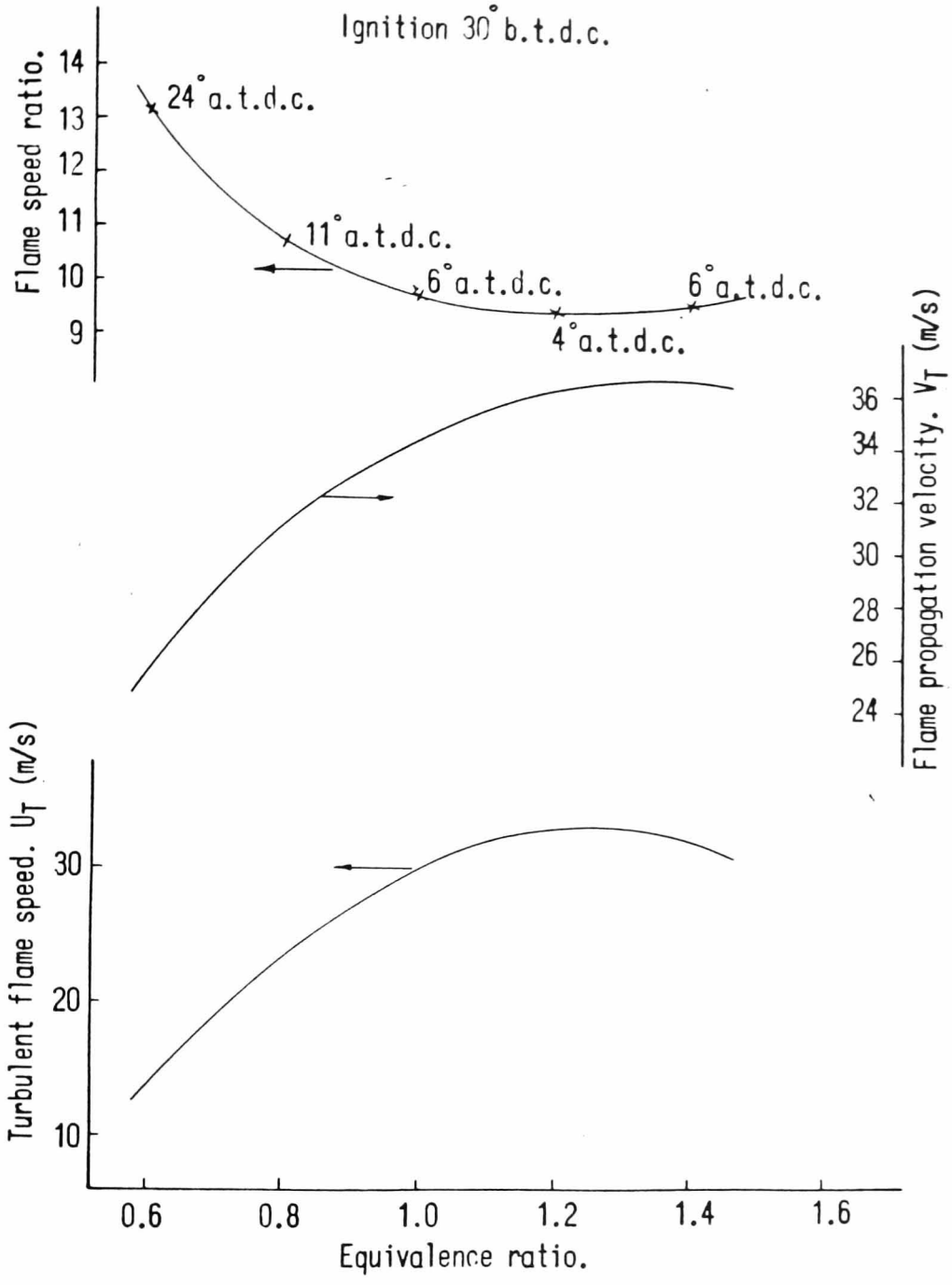

(FIG 6.6/4) EFFECT OF EQUIVALENCE RATIO ON FLAME SPEED, FLAME PROPAGATION VELOCITY AND FLAME SPEED RATIO AT 50% MASS BURNT.

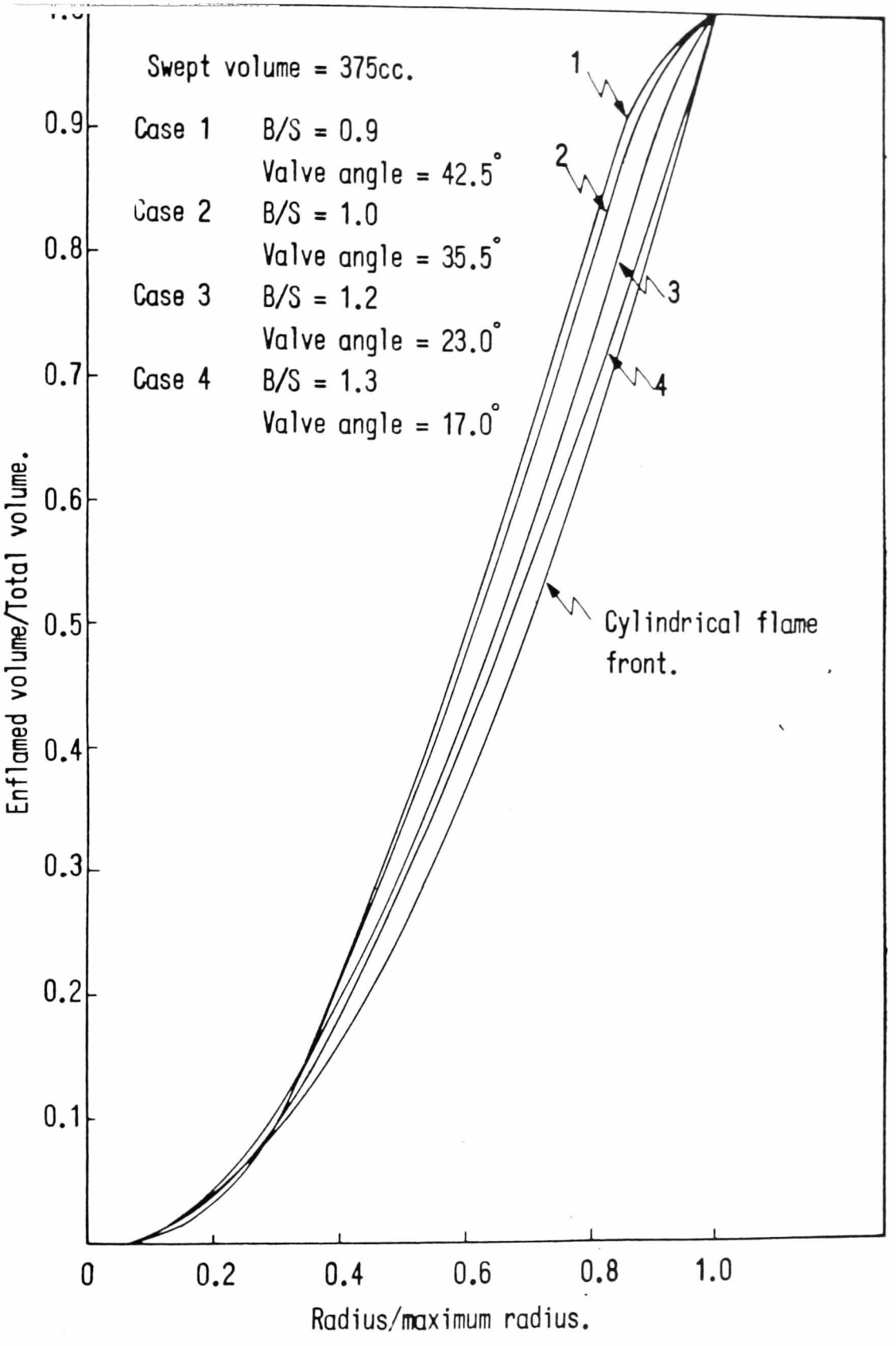

(FIG 6.6/5) COMPARISON OF ENFLAMED/TOTAL VOLUME AGAINST RADIUS/MAX RADIUS FOR FOUR CASES.

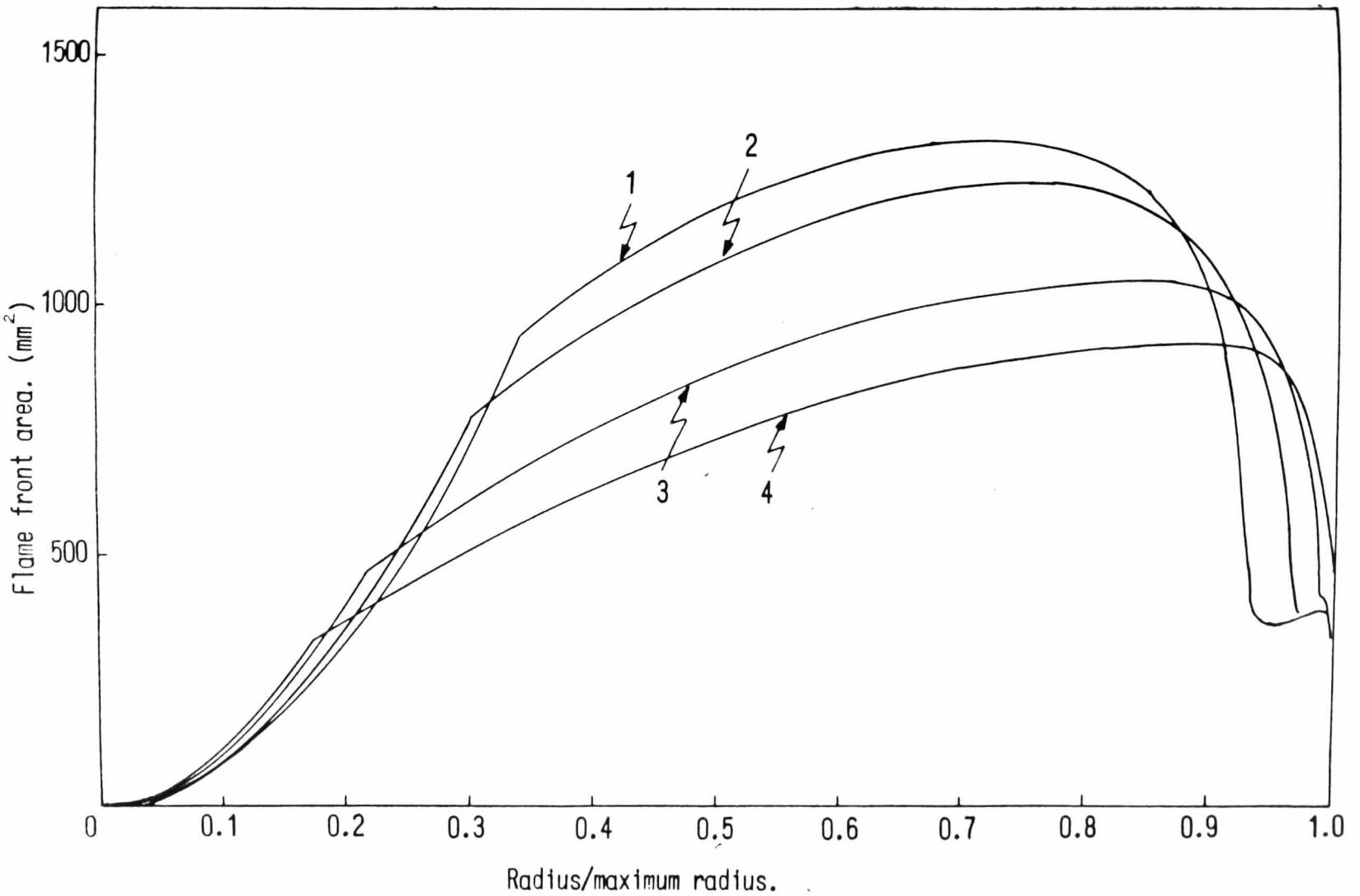

(FIG 6.6/6) Flame front area against radius/maximum radius for four cases at a 12:1 compression ratio and 375cc swept volume.

FIG 6.6/6.

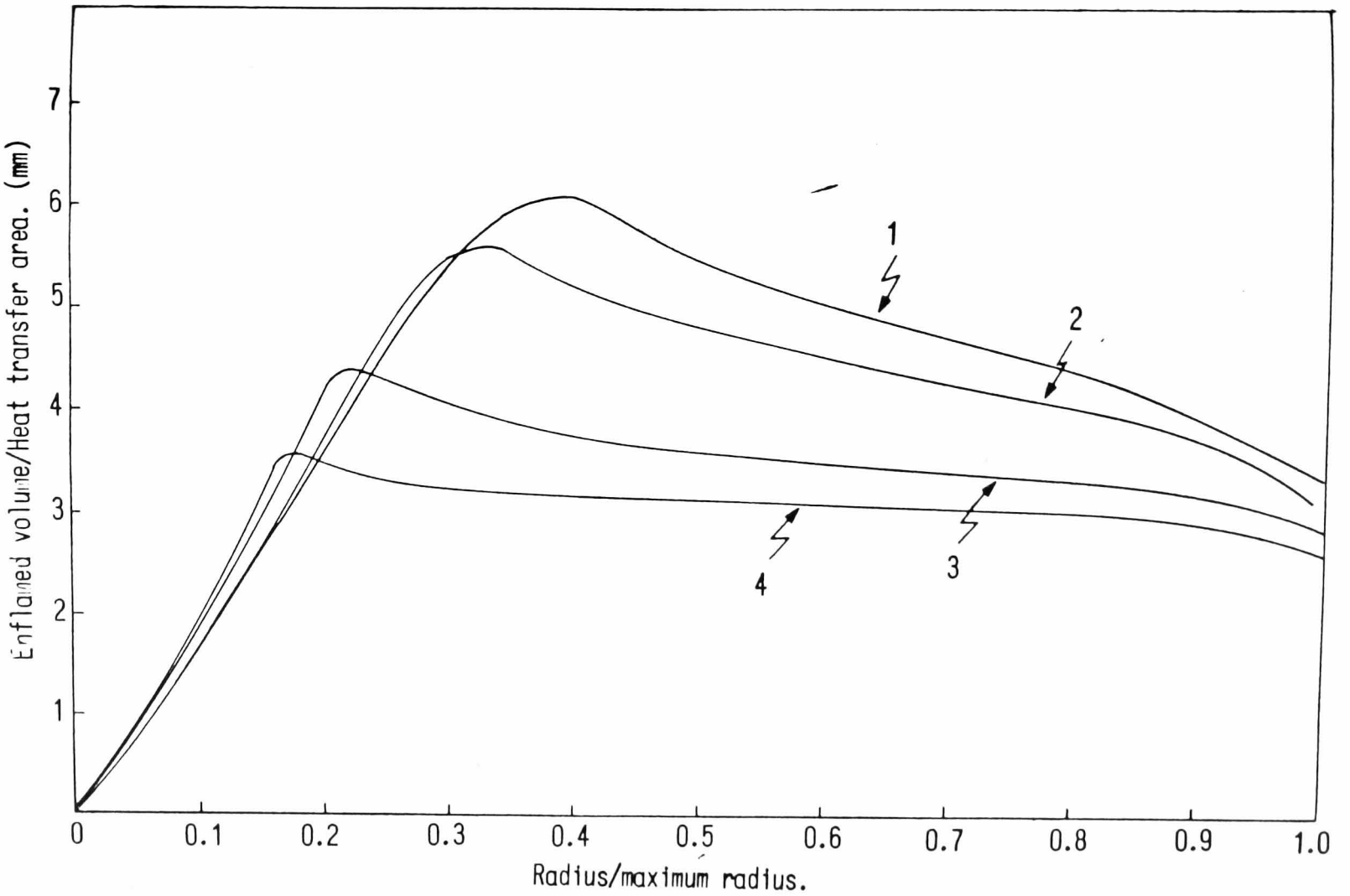

(FIG 6.6/7) Enflamed volume/heat transfer area against radius/maximum radius for four cases at a 12:1 compression ratio and 375cc swept volume.

FIG 6.6/7.

FIG 6.6/8.

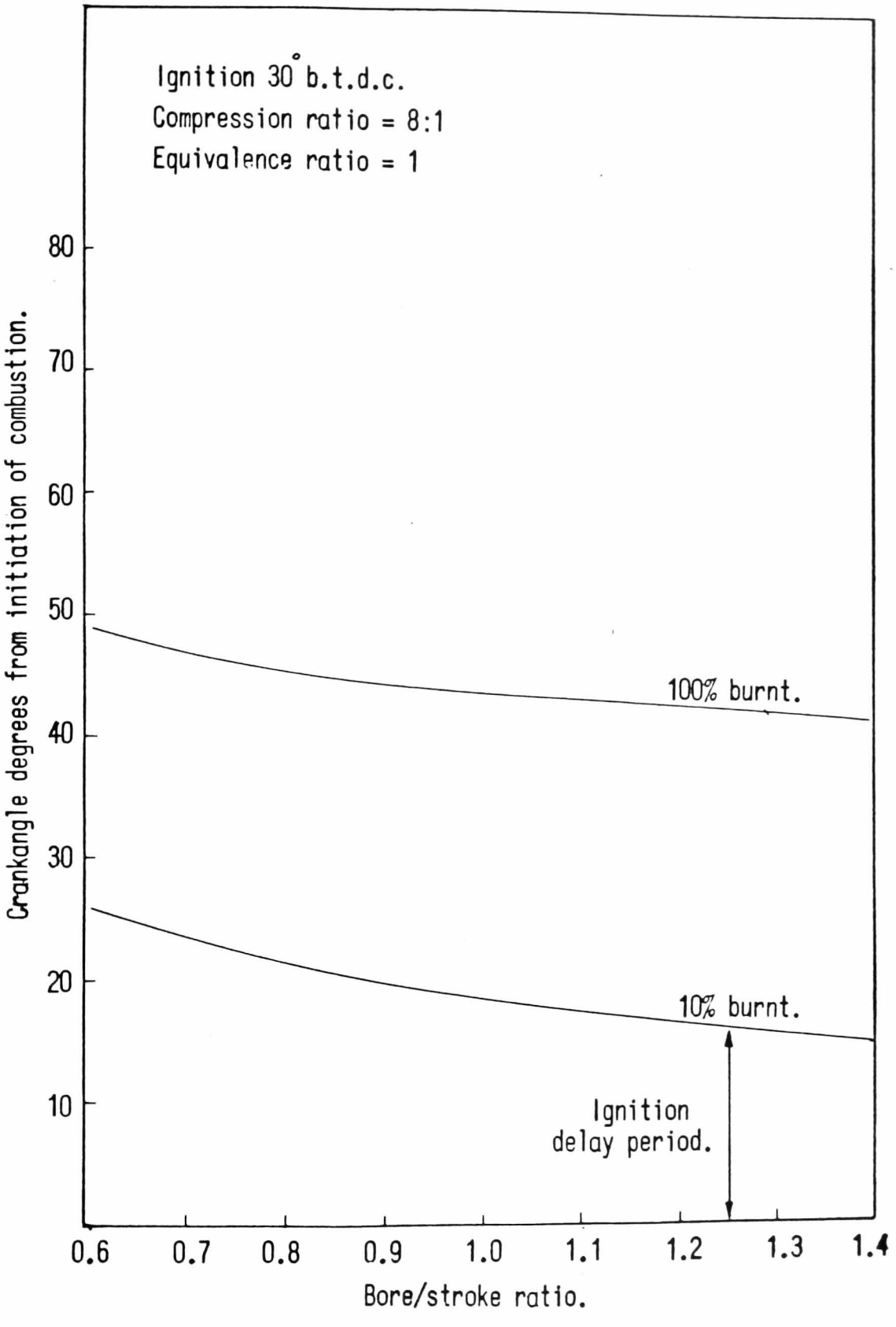

(FIG 6.6/8) COMBUSTION DURATION AGAINST BORE/STROKE RATIO.

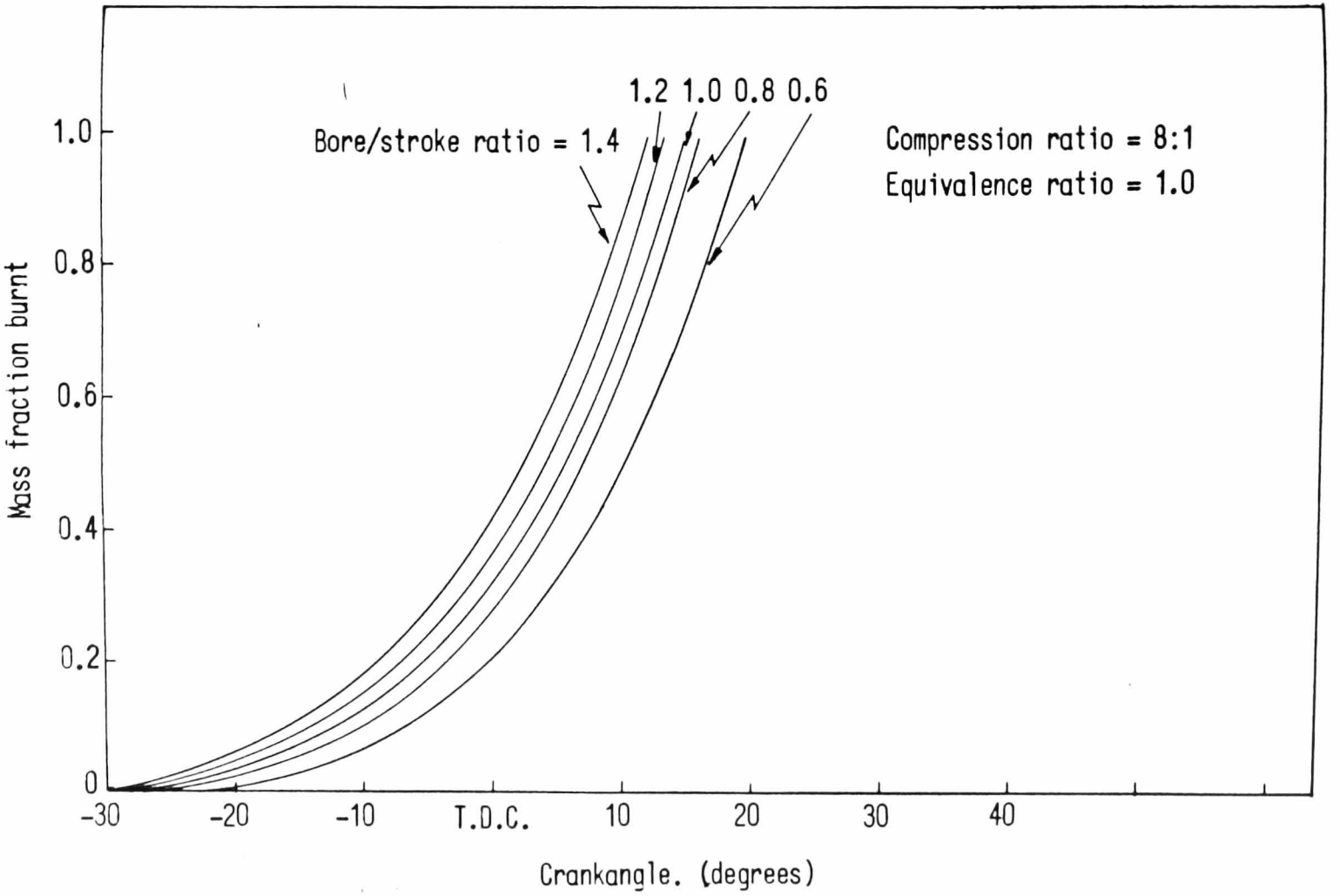

(FIG 6.6/9) Mass fraction burnt against crankangle for various bore/stroke ratios.

FIG 6.6/9.

FIG 6.6/10.

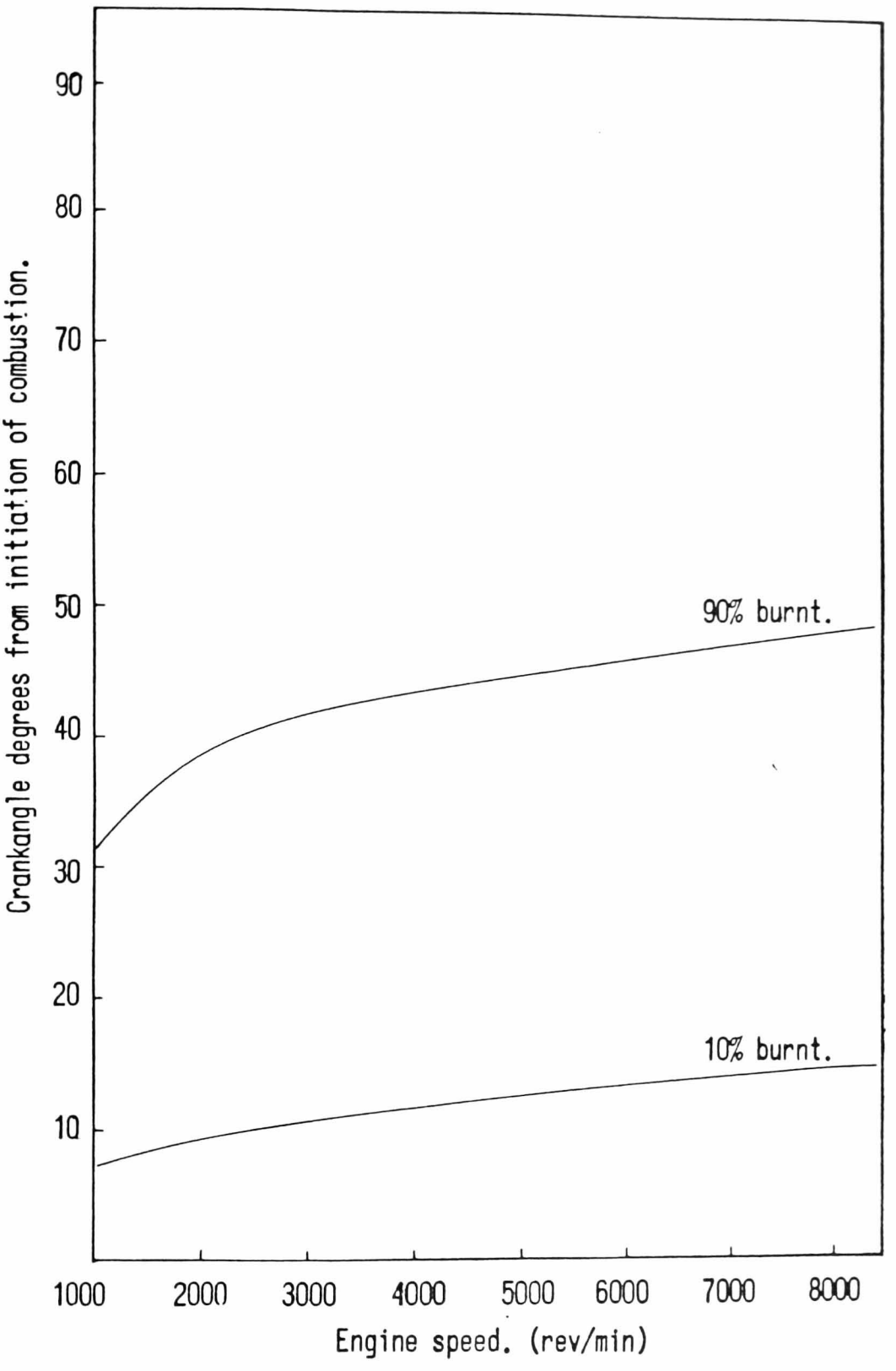

(FIG 6.6/10) COMBUSTION AGAINST ENGINE SPEED FOR DATUM CASE.

FIG 6.6/11.

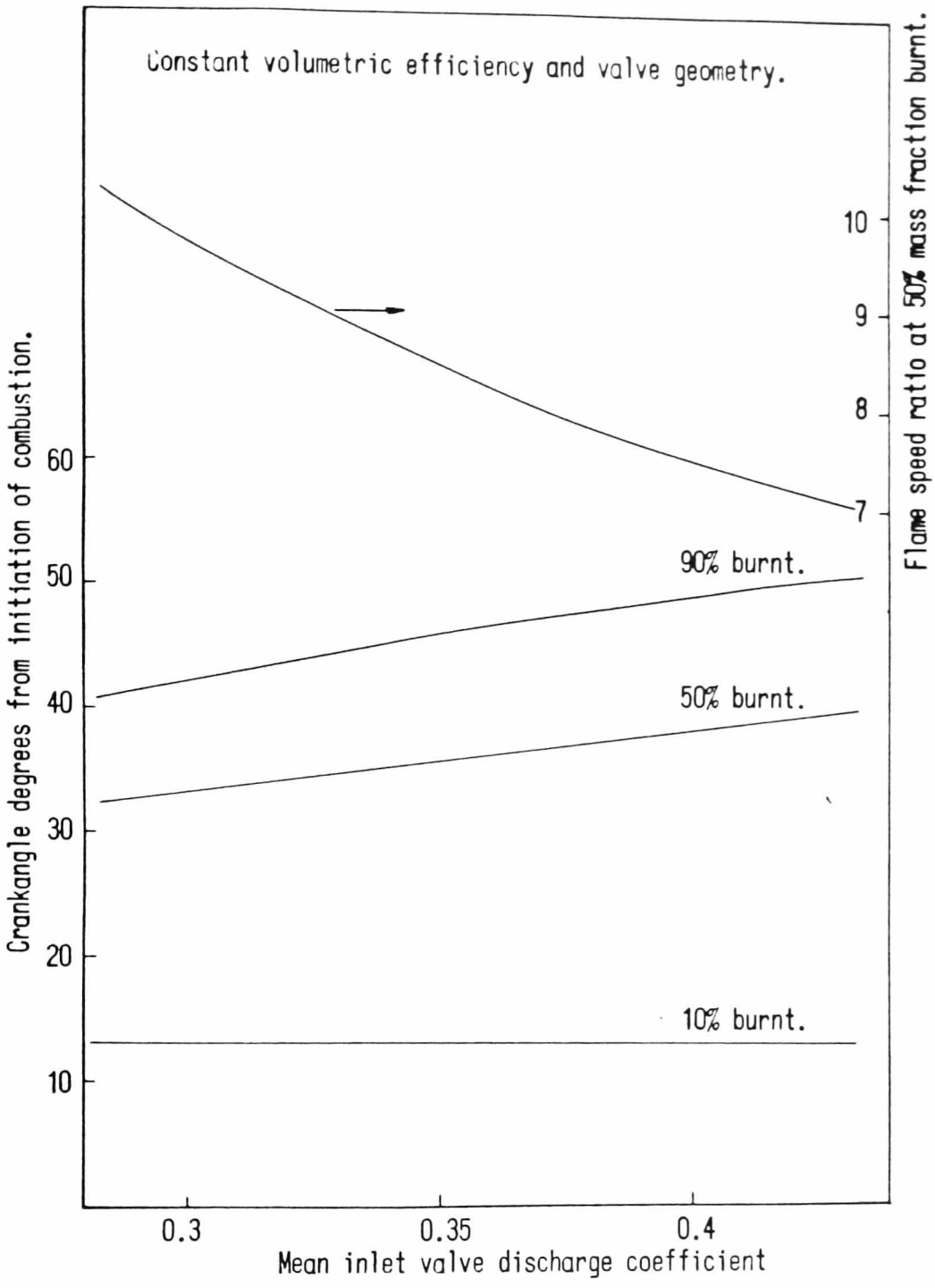

(FIG 6.6/11) COMBUSTION DURATION AND FLAME SPEED RATIO AGAINST MEAN INLET VALVE DISCHARGE COEFFICIENT.

FIG 6.6/12.

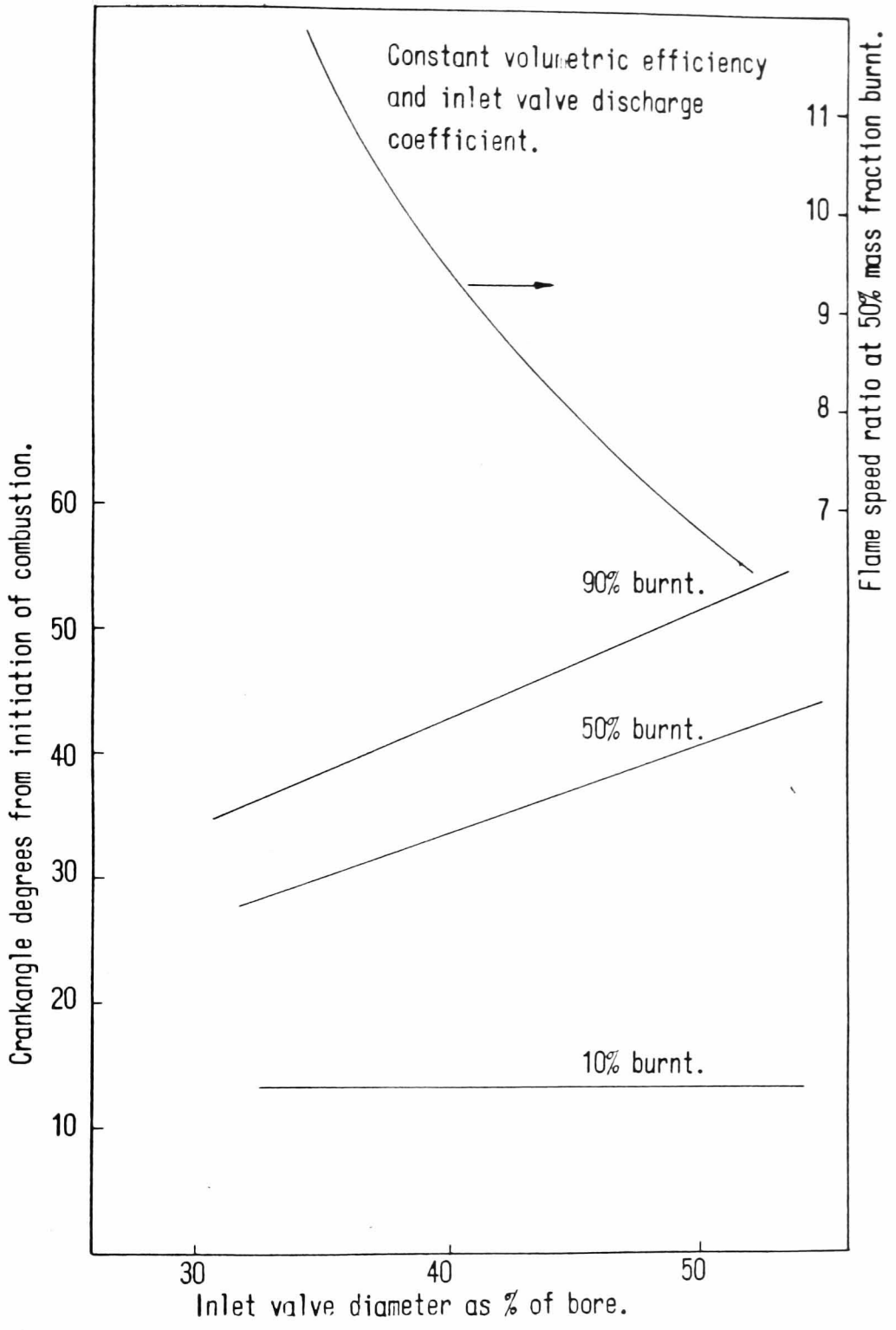

(FIG 6.6/12) COMBUSTION DURATION AND FLAME SPEED RATIO AGAINST INLET VALVE DIAMETER.

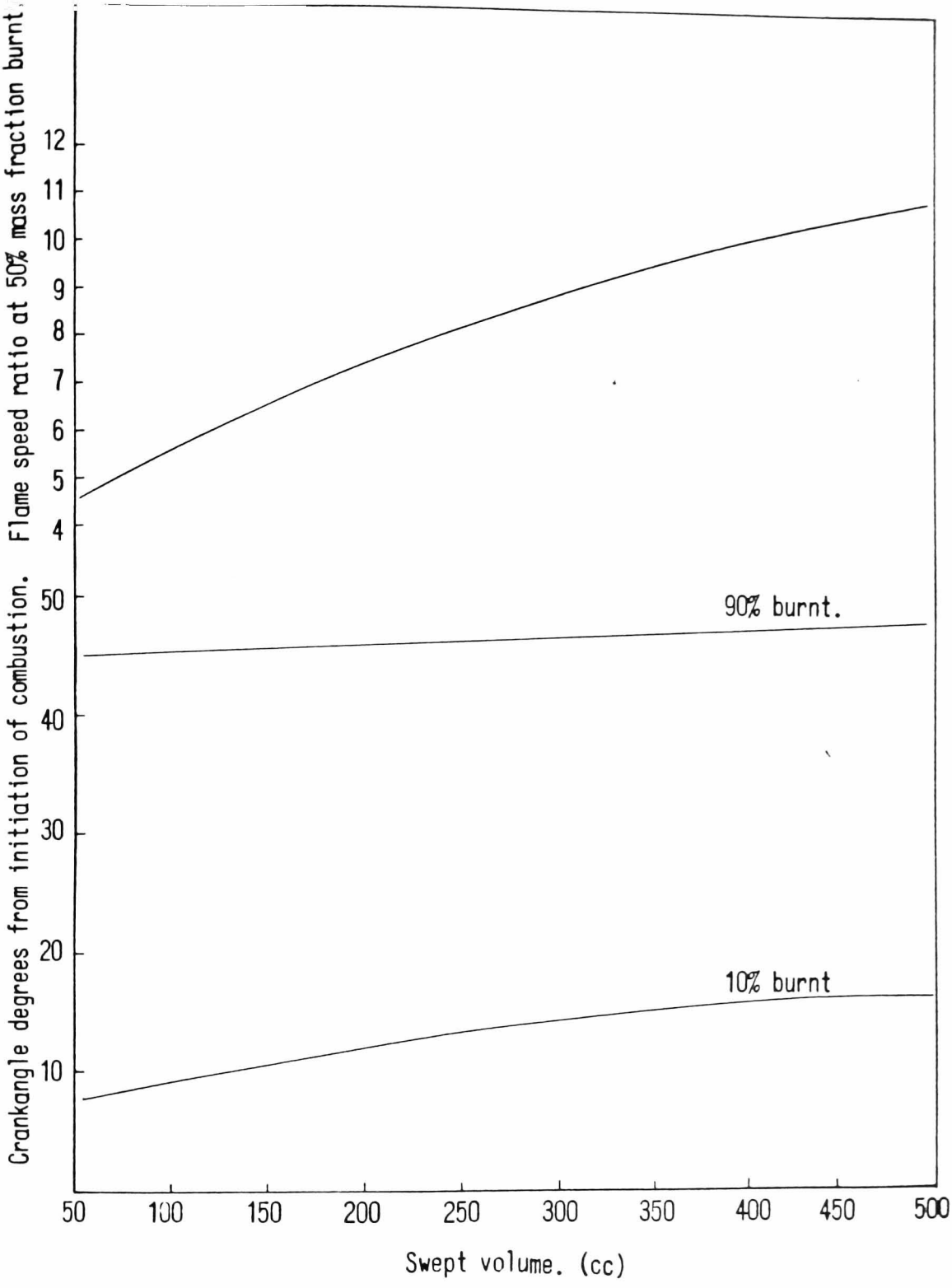

(FIG 6.6/13) COMBUSTION DURATION AND FLAME SPEED RATIO AGAINST ENGINE SWEPT VOLUME.

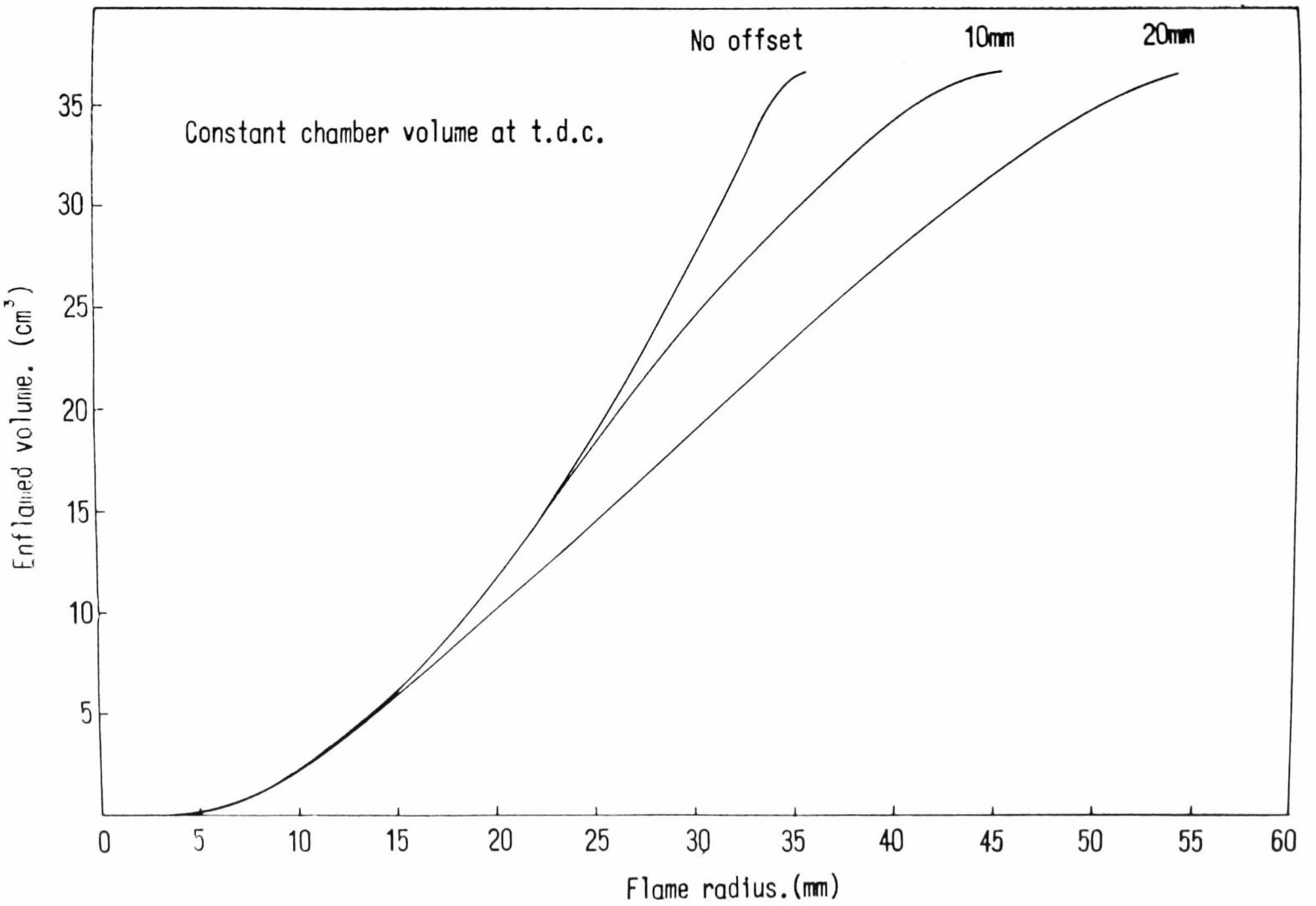

(FIG 6.6/14) Graph of enflamed volume against flame radius for datum geometry with various spark plug offsets.

CHAPTER 7 - CONCLUSIONS AND SUGGESTIONS FOR FOR FURTHER WORK

7.1 Summary of conclusions

		Discussion
(i)	A cylinder head of the 4-valve configuration as used in current manufacture has been mathematically modelled to give accurate detailed dimensional data	Section 2.3
	This modelling technique can be applied to any cylinder head whose geometry can be mathematically described.	
	Information has been gained from the geometrical analysis on the probable design limitations on breathing performance and mechanical limitations.	Section 2.3
	This enables a wide range of design options to be readily assessed without resorting to detailed layouts.	
(ii)	The 4-valve configuration has been shown to be able to provide a high compression compact combustion chamber with an acceptable surface to volume ratio without detrimental effects on volumetric efficiency.	Section 2.3
(iii)	A method has been developed whereby the spherical flame front plot for any 4-valve, pent-roof, configuration can readily be produced in order to study the probable burn rate influences.	Section 2.3

(iv) It has been shown that the 2-inlet valve configuration exhibits a high inlet valve flow coefficient that is insensitive to valve inclination. Section 3.4

(v) The effects of changes of engine geometry on volumetric efficiency can be rapidly determined using the 'Inertia supercharge index' as defined in Reference 13, and fixed induction pipe periods. Section 5.5

(vi) If inertia effects are considered, the value 0.5 does not constitute a limit on inlet mach index beyond which improvements in volumetric efficiency are possible. Section 5.5

(vii) The method of characteristics for homentropic flow has been shown to provide a usable method of analysis for the dynamic effects in the induction system, but it has problems with stability at low engine speeds and with large valve overlap.

(viii) An expression for the flame speed ratio in the fully developed turbulent burning region has been related to engine geometry and gives a good indication as to the probable effects of changing geometry. Section 6.6

Discussion

(ix) The results indicate that the 4-valve configuration could be the basis of a lean-burn engine, if designed in a high compression ratio, low surface-to-volume configuration, with reduced valve lift. This will still maintain an adequate breathing performance.

Section 2·3·1 p32

Section 6·6 p200

Section 6·7 p205-6

7.2 Suggestions for further work

(i) Extension of the geometric analysis to provide graphical output of the combustion chamber geometry.

(ii) The addition of exhaust pipe dynamics to the engine cycle simulation and further experimental verification at higher engine speeds.

(iii) Conversion of engine to run on gasoline by the addition of a strengthened piston and reduced compression ratio. (It is designed to run on methanol.)

(iv) Experimental determination of flame speed and relationship to inlet duct conditions.

(v) Build engine to a configuration suggested by the analysis to give satisfactory operation at lean mixture conditions, whilst maintaining adequate volumetric efficiency, and verify experimentally.

REFERENCES

1. C.F. Taylor. "The internal combustion engine in theory and practice: Vol.1: Thermodynamics, fluid flow and performance". The M.I.T. Press.

2. F.R.B. King. "The inertia theory of engine breathing": Parts 1, 2 and 3, Automobile Engineer, March, April & May 1968.

3. I. Fukutani & E. Watanabe. "An analysis of the volumetric efficiency characteristics of 4-stroke cycle engines using the mean inlet Mach index". S.A.E. 790480 1979.

4. Y. Nakamura. "Small high speed, high performance gasoline engine". S.A.E. meeting, San Francisco, Aug 1964.

5. C.F. Taylor. "The internal combustion engine in theory and practice: Vol.2: Combustion, fuels, materials & design". The M.I.T. Press.

6. R. Siewert. "Engine combustion at large bore to stroke ratios". S.A.E. 780968 1978.

7. C. Scheffler. "Combustion chamber surface area, a key to exhaust hydrocarbons". S.A.E. 660111.

8. L. Kastner, T. Williams & J. White. "Poppet inlet valve characteristics and their influence on the induction process". Proc. Inst.Mech.Engrs. 1963-64, 178 (Pt.1, No. 36), 955.

9. W. Woods. "Steady flow tests on twin poppet valves". Proc.Inst.Mech.Engrs. 1967-68, 182 (Pt. 3D).

10. W. Annand, G. Roe. "Gas flow in the internal combustion engine: Power performance, emission control and silencing". G.T. Foulis & Co.Ltd.

11. W. Woods & S. Khan. "An experimental study of flow through poppet valves". Inst.Mech.Engrs. and Adv. Sch.Auto.Eng.Symp. on diesel engine breathing and combustion, Cranfield 1966.

12. P. Vorum. "Short pipe manifold design for four-stroke engines", Parts 1 & 2. A.S.M.E. Papers Nos. 76-WA/DGP-4 & 80-DGP-6 1980.

13. S. Yagi, A. Ishizuya & I. Fujii. "Research and development of high-speed, high performance, small displacement Honda engines". S.A.E. 700122 1970.

14. D. Broome. "Induction ram". Parts 1, 2 and 3, Automobile Engineer, April, May & June 1969.

15. R. Benson, R. Garg & D. Woolatt. "A numerical solution of unsteady flow problems". Inst.J.Mech.Sci. 6p 117, 1964.

16. G. Blair & J. Goulburn. "An unsteady flow analysis of exhaust systems for multicylinder automobile engines". S.A.E. 690469 1969.

17. T.G. Prosser. "Induction ramming a motored high-speed four-stroke reciprocating engine - influence of inlet port pressure waves on volumetric efficiency". Proc.Inst.Mech. Engrs. 188, 49/74.

18. G. Lucuc & E. James. "A computer simulation of a spark ignition engine". S.A.E. 730053 1973.

19. R. Phillipps & P. Orman. "Simulation of combustion in a gasoline engine using a digital computer". 4th Annual Symp. Adv.Sch.Auto.Eng. on combustion pressures in the spark ignition engine. Cranfield 1965.

20. N. Gurgis & D. Tidmarsh. "Modelling the effect of combustion chamber configuration on engine performance". Inst.Mech.Engrs. Conf. on Fuel economy and emissions of lean burn engines Paper C114/79.

21. N. Blizard & J. Keck. "Experimental and theoretical investigation of turbulent burning model for internal combustion engines". S.A.E. 740191 1974.

22. R. Tabaczynski, C. Ferguson & K. Radhakrishnan. "A turbulent entrainment model for spark ignition combustion". S.A.E. 770647 1977.

23. F. McCuiston, G. Lavoie & C. Kauffman. "Validation of a turbulent flame propagation model for a spark ignition engine". S.A.E. 770045 1977.

24. G. Andrews, D. Bradley & S. Lwakabamba. "Turbulence and turbulent flame propagation - a critical appraisal". Combustion and Flame. 24, 285-304 1975.

25. R. Tabaczynski, F. Trinker & B. Shannon. "Further refinement and validation of a turbulent flame propagation model for spark ignition engines". Combustion and Flame. 39: 111-121 1980.

26. S. Hines, R. Tabaczynski & J. Novak. "The prediction of ignition delay and combustion intervals for a homogeneous charge, spark ignition engine". S.A.E. 780232 1978.

27. H. Barnes-Moss, "A Designer's viewpoint". Inst.Mech.Engrs. Conf. Passenger car engines 1973, paper C343.

28. S. Curry. "A three-dimensional study of flame propagation in a spark ignition engine". S.A.E. Trans. Vol.71. 1963.

29. M. Rashidi. "Measurement of flame velocity and entrained velocity from high-speed photographs in the SI engine". Proc.Inst.Mech.Engrs. 194, 1980.

30. S. Kumagai & Y.Kudo. "Flame studies by means of ionization gap in a high-speed spark ignition engine". Ninth(Int) Symp. on Combustion. Academic Press, New York. 1963.

31. G. Harrow & P. Orman. "A study of flame propagation and cyclic dispersion in a spark ignition engine". Advances in Automobile Engineering (Part IV) New York Pergamon Press 1966.

32. G. Fawcett & J. Fawcett. "Comparison of polydyne and non-polydyne cams". Cams and cam mechanisms - J. Rees-Jones. Mech.Eng.Pub.Ltd. 1978.

33. W. Dudley. "New methods in valve cam design". S.A.E. Trans. Vol.2 (1948) p.19.

34. T. Thoren, H. Engemann & D. Stoddart. "Cam design as related to valve train dynamics". S.A.E. Quarterly Trans. Vol.6, No.1. Jan. 1952.

35. J. Nourse, R. Dennis & W. Wood. "Recent developments in cam design". S.A.E. Technical progress series Vol.5. Applications of computers in valve gear design. 1963.

36. H. Watson & E. Milkins. "The design of camshafts for racing engines". Cams and cam mechanisms, edited by J. Rees-Jones. Mech.Eng.Pub.Ltd. 1978.

37. C. Wolgemuth & D. Olson. "A study of engine breathing characteristics". S.A.E. 650448, 1965.

38. T. Williams. "Industion ramming of reciprocating engines". Engineering March 20, 1959.

39. C. Taylor, J. Livengood & D. Tsai. "Dynamics in the inlet system of a four-stroke single cylinder engine". Trans.Am. Soc.Mech.Engrs. 1955, 77 p.1133-1145.

40. Di Stefano, Stubberud & Williams. "Schaum's outline series, theory and problems of feedback and control systems." McGraw-Hill Book Co.Ltd., p.279-282.

41. J. Mayo. "The effect of engine design parameters on combustion rate in spark ignited engines". S.A.E. 750355 1975.

42. G. Lucus, M. Brunt & R. Anton. "The effect of squish on charge turbulence and flame propagation in an S.I. engine Auto.Div.Inst.Mech.Engrs. Conf. on Fuel economy and emissions of lean burn engines. paper C87/79. June 1979.

43. R. Winsor & D. Patterson. "Mixture turbulence - a key to cyclic combustion variation". S.A.E. 730086.

44. D. Lancaster, R. Krieger, S. Sorenson & W. Hull. " Effects of turbulence on spark ignition engine combustion". S.A.E. 760160, 1976.

45. Bolt & Harrington. "The effects of mixture motion upon the lean limit and combustion of spark-ignited mixtures". S.A.E. 670467, 1967.

46. A. Oppenheim et al. "A cinematographic study of combustion in an enclosure fitted with a reciprocating piston". Auto.Div.Inst.Mech.Engrs. Conf. on Stratified charge engines. Paper C256/76. Nov. 1976.

47. D. Hoggetts. Discussion of R. Philips & P. Orman paper. Ref. 19.

48. D. Stivender. "Intake valve throttling (I.V.T); A sonic throttling intake valve engine". S.A.E. 680399, 1968.

49. D. Lancaster. "Effects of engine variables on turbulence in a spark ignition engine". S.A.E. 760159, 1976.

50. H. Sanematsu. "Turbulent flame propagation in a homogeneous gas mixture". Combustion and Flame, Feb. 1969.

51. D. Picken. "The effects of liquefied petroleum gas as a secondary fuel in a compression ignition engine". Ph.D. Thesis., Dept.Mech.Eng., Lanchester Polytechnic, 1970.

52. H. Soliman. "The effects of methane/kerosene mixtures as spark ignition engine fuels". Ph.D. Thesis., Dept.Mech.Eng., Leicester Polytechnic, 1978.

53. J. Heywood, J. Higgins, P. Watts & R. Tabaczynski. "Development and use of a cycle simulation to predict S.I. engine efficiency and NO_x emissions". S.A.E. 790291, 1979.

54. G. Annand. "A new computation model of combustion in the spark ignition engine". Proc.Inst.Mech.Engrs. Vol.185 (11/71) 1970/71.

55. M. May. "The high compression lean burn spark ignited 4-stroke engine". Auto.Div.Inst.Mech.Engrs. Conf. on "Fuel economy and emissions of lean burn engines". Paper C97/79, June 1979.

56. R. Tabaczynski & E. Klomp. "Calculated nitric oxide emissions of an unthrottled spark ignited, stratified charge internal combustion engine". Research Report FD-19, General Motors Research Laboratories, 1973.

57. W. Daniel. "Flame quenching at the wall of an internal combustion engine". Sixth Symp.(International) on Combustion. Yale University, New Haven, Connecticutt, Reinhold Pub.Corp. 1956.

58. W. Daniel. "Engine variable effects on exhaust hydrocarbon composition; (A single cylinder engine study with propane as the fuel)". S.A.E. 670124, 1967.

59. British Standard 1042, Part 1, 1964. "Methods for the measurement of fluid flow in pipes, Part 1, Orifice plates, nozzles and venturi tubes".

60. G. Eichelburg. "Some new investigations of old internal engine problems". Engineering, 148, pp 463-466, pp 547-550, pp 603-605: and No.149, pp 297-299. 1939.

61. Leydorf, Minty & Fingeroot. "Design refinements of induction and exhaust systems using steady flow bench techniques". S.A.E. 720214.

62. K.I. Schelkin, Ya. K. Troshin. "Gasodinamika goreniya". Izdatel stvo Akademii Nauk S.S.S.R., Moscow, 1963. ("Gas dynamics of Combustion", NASA TT F-231, Oct. 1964.)

APPENDIX A1

Historical development of the 2-inlet/2-exhaust valve, pent-roof configuration combustion chamber

The pent-roof combustion chamber having 2 inlet valves on one inclined plane and 2 exhaust valves situated on a similar plane, with the planes intersecting on the engine axis, dates back to 1912.

The first of this design to use the central spark plug position, as used in this investigation, was the 7.76 litre 4-cylinder engine of the 1912 Grand Prix Peugeot racing car. This design was the work of Swiss Engineer, Ernest Henry, possibly resulting from ideas from two Peugeot drivers at the time, Zuccarelli and Georges Boillot.

The design was immediately successful and as such was soon copied, in some cases in detail. In 1914, Sunbeam, Humber and Vauxhall all produced versions of this design to race in the Tourist Trophy of that year. The design became popular in America after the importation of Sunbeam and Peugeot cars in 1915, and was adopted by Chevrolet. The design is also evident in the engines of Harry Miller and subsequently his plant manager, Offenhauser, whose engines are still used for racing in America.

The development of the current engine is evident from Table A1.

Another noteworthy design was that of Dr. H. Ricardo (later Sir Harry Ricardo), who in 1922 produced a 3-litre design for Vauxhall Motors Ltd. The bore/stroke ratio at 0.64 was an increase on the value of 0.53/0.59 current at the time and enabled him to run this 4-cylinder engine at crankshaft speeds similar to an

8-cylinder engine with a mean piston speed of 3,900 ft/min.
The valve included angle of 90° enabled large valves to be used and was possible with an acceptable piston crown at the compression ratio of 5.8:1 used.

Development of the 4-valve/cylinder design in the racing car engine was to a great extent terminated by the introduction, in 1923, of the 2-litre limit of swept volume, and later the development of supercharging, which did not require the benefits of volumetric efficiency made available by the use of multiple inlet valves.

Use of the pent-roof type combustion chamber continued in the field of sports cars and motor cycles, some notable examples being the Sunbeam, single O.H. camshaft 3-litre engine of 1922, and the Rudge motor cycle engines built from 1924 up to 1939. Some of the later Rudge engines did diverge from the classic pent-roof design, having the exhaust port arranged radially in the part spherical chamber.

Current use of the configuration is also found in racing, both car and motor cycle; the most successful racing engine being the Cosworth DFV V8, which employs a flat piston crown and a valve included angle of 32°. This enables a compression ratio of 11.75:1 to be achieved with a bore/stroke ratio of 1.32.

It is interesting to note that with the advent of turbo-charging, the advantages of high volumetric efficiency with the multiple valve layout is not quite so necessary. However, the use of multiple valves has other advantages, particularly in the field of valve dynamics and thermal loading.

The predominant engine used in speedway racing is the Weslake WR 275 engine produced by Westlake and Co.Ltd., which is manufactured in push-rod, single and double overhead camshaft form, all with central spark plug position.

The field of production vehicles presents several examples of this type of combustion chamber, Lotus and British Leyland (Triumph Dolomite Sprint) producing engines for cars, and Yamaha and Honda, engines for motor cycles.

Details of some historic and current engines employing the 4-valve pent-roof chamber are given in Table A1.

TABLE A1

DETAILS OF SOME HISTORIC AND CURRENT 4-VALVE/CYLINDER DESIGNS

YEAR	MAKER	DESIGNER	V Lt	N_{cyls}	B mm	S mm	B/S	VALVES/CYL		θ_{VLV}	N_{CAMS}	BHP @ N_{REV}	BHP/V	M.P.S ft/min
								IN.	EX.					
1912	PEUGEOT	E.HENRY	7.60	4	110	200	0.55	2	2	45	2	130 @ 2200	17.1	2,890
1913	PEUGEOT	E.HENRY	2.98	4	78	156	0.5	2	2	60	2	90 @ 2900	31,2	2,970
1913	PEUGEOT	E.HENRY	5.60	4	100	180	0.55	2	2	60	2			
1914	PEUGEOT	E.HENRY	2.47	4	75	140	0.54	2	2	60	2	80 @ 3000	32.4	2,760
1914	PEUGEOT	E.HENRY	4.49	4	92	169	0.54	2	2	60	2	112	24.9	
1914	SUNBEAM	L.COATALEN	3.30	4	81	160	0.51	2	2	60	2	99 @ 3000	33.0	3,150
1914	SUNBEAM	L.COATALEN	4.40	4	94	160	0.59	2	2	60	2			
1914	HUMBER	T.BURGESS	3.30	4	82	156	0.53	2	2		2	100 @ 3200	30.3	3,270
1914	MERCEDES	P.DAIMLER & WALLINGER	4.48	4	93	165	0.56	2	2	60	1	115 @ 2800	25.7	3,030
1915	STUTZ		4.88	4	97	165	0.59	2	2		1	130	26.6	
1919	BALLOT	E.HENRY	4.82	8	74	140	0.53	2	2	60	2	140	29.0	
1920	BALLOT	E.HENRY	2.96	8	65	112	0.58	2	2	60	2	108 @ 4000	36.4	2,790
1920	FRONTENAC	L.CHEVROLET	2.98	4	79	152	0.52	2	2	60	2	98	32.9	2,940

YEAR	MAKER	DESIGNER	V Lt	N_{cyls}	B mm	S mm	$B/_S$	VALVES/CYL		θ_{VLV}	N_{CAMS}	BHP @ N_{REV}	$BHP/_V$	M.P.S ft/min	
								IN.	EX.						
1912	SUNBEAM	L.COATALEN-TALBOT-DARRACQ	2.98	8	65	112	0.58	2	2	60	2	108 @ 4000	36.4	2,940	
1922	VAUXHALL	H.RICARDO	3.00	4	85	132	0.64	2	2	90	2	129 @ 4500	43.0	3,900	
1966	MEYER-DRAKE	OFFENHAUSER	4.11	4	109	110	0.99	2	2	70	2	402 @ 6000	97.8	4,375	
1967	COSWORTH	K.DUCKWORTH	3.0	8	86	65	1.32	2	2	32	2	410 @ 9000	137.0	3,838	
1968	FORD	K.DUCKWORTH	1.6	4	86	69	1.25	2	2	40	2	222 @ 9000	139.0	4,074	
1972	WESLAKE		3.0	12	75	56	1.22	2	2	22	2	495 @ 11250	165.0	4,170	
1974	TRIUMPH		2.0	4	90	78	1.15	2	2	35	1	127 @ 5700	63.5	2,917	*
1974	LOTUS		2.0	4	95	69	1.38	2	2	40	2	140 @ 6500	70.0	2,942	*

* PRODUCTION ENGINES

APPENDIX A2

Derivation of equations used in determining cylinder head and valve pocket volumes and surface areas

Basic geometry

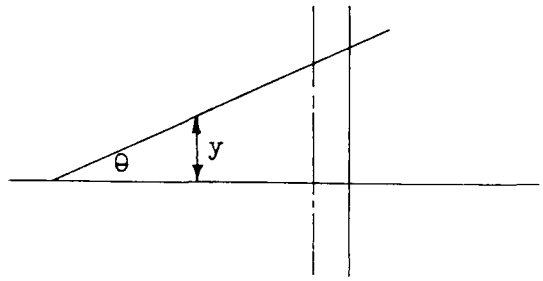

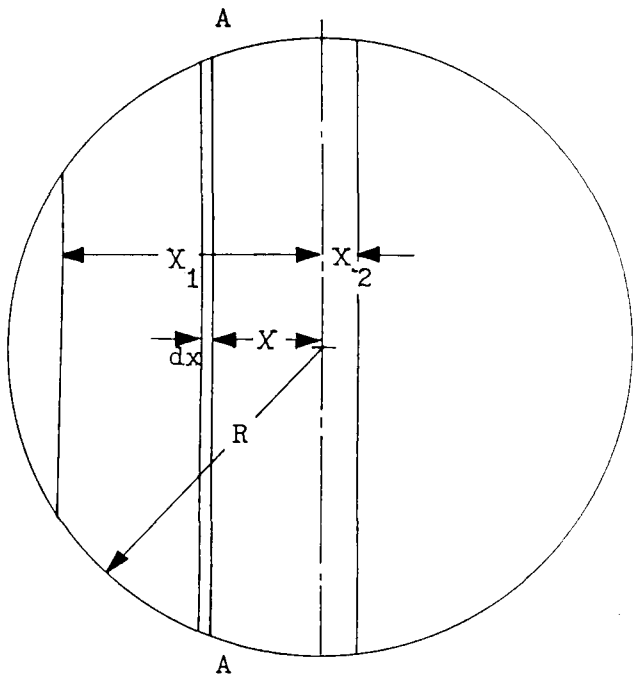

A2.1 Calculation of cylinder head volume

Volume of element $dV = 2\sqrt{R^2 - X^2}\, ydx$

But $y = (X_1 - X) \tan \theta$

$\therefore$ Volume $dV = 2\sqrt{R^2 - X^2} \tan \theta (X_1 - X)$

$\therefore$ Total volume between limits of X_1 and X_2

$$V = 2 \tan \theta \left[X_1 \frac{1}{2}\left(X\sqrt{R^2 - X^2} + R^2 \sin^{-1}\left[\frac{X}{R}\right]\right) + \frac{1}{3}\sqrt{\left(R^2 - X^2\right)^3}\right]_{X_2}^{X_1}$$

With radiused edges

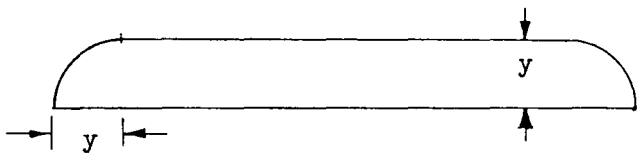

Section AA

$$V_1 = \int_{X_2}^{X_1} \left[\left(2\sqrt{R^2 - X^2} - 2y\right) y + \frac{\pi y^2}{2}\right] dx$$

$$= \int_{X_2}^{X_1} 2y\sqrt{R^2 - X^2}\, dx - \left[\frac{4-\pi}{2}\right]\int_{X_2}^{X_1} y^2 dx$$

$$V_1 = V - \left[\frac{4-\pi}{2}\right]\int_{X_2}^{X_1} y^2 dx$$

$$V_1 = V - \left[\frac{4-\pi}{2}\right]\frac{\tan^2\theta}{3}\left[X_1 - X_2\right]^3$$

$$V_1 = V - 0.1431 \tan^2\theta \left[X_1 - X_2\right]^3$$

A2.2 Calculation of the surface area of the cylinder head

Area of sloping face

$$A_1 = \int_{X_2}^{X_1} 2\sqrt{\frac{R^2 - X^2}{\text{Cos }\theta}}\, dx$$

$$= \frac{1}{\text{Cos }\theta}\left[X\sqrt{R^2 - X^2} + R^2 \sin^{-1}\frac{X}{R}\right]_{X_2}^{X_1}$$

With radiused edges

$$A_2 = \int_{X_2}^{X_1} \left[2\sqrt{R^2 - X^2} - 2y\right] \frac{dx}{\text{Cos }\theta} + \pi y \frac{dx}{\text{Cos }\theta}$$

NOTE: The last term is an approximation that underestimates at one limit and overestimates at the other.

$$A_2 = \frac{1}{\text{Cos }\theta}\int_{X_2}^{X_1} \left[2\sqrt{R^2 - X^2} + y\left(\pi - 2\right)\right] dx$$

$$A_2 = A_1 + \left(\frac{\pi - 2}{2}\right)\frac{\sin\theta}{\cos^2\theta}\left(X_1 - X_2\right)^2$$

$$= A_1 + 0.5708\,\frac{\sin\theta}{\cos^2\theta}\left(X_1 - X_2\right)^2$$

PIN = CODI/tan θ

X_8 = ID/2 - PIN

X_7 = ID/2

ABCOI = area of base of inlet cut-out

$$\text{ABCOI} = \int_{X_7}^{X_8} 2\sqrt{\left(ID/2\right)^2 - X^2}\, dx$$

$$= \left[X\sqrt{\left(ID/2\right)^2 - X^2} + \left(\frac{ID}{2}\right)^2 \sin^{-1}\frac{2X}{ID} \right]_{X_7}^{X_8}$$

This is a function in the program termed HCAL.

$\therefore$ ABCOI = HCAL (X_8, ID) - HCAL (X_7, ID)

Calculation of the side area

$$y = (X - X_8)\tan\theta_1 \qquad \phi = \cos^{-1}\left(2X_8/ID\right)$$

ASCOI = area of side of inlet valve cut-out

$$\text{ASCOI} = \int_0^{\phi_1} ID \tan\theta_1 (X - X_8)\, d\phi$$

$$= ID \tan\theta_1 \left[\sqrt{\left(\frac{ID}{2}\right)^2 - X_8^2} - 8\cos^{-1}\left(2X_8/ID\right) \right]$$

A2.3 Valve pocket geometry

Inlet side:

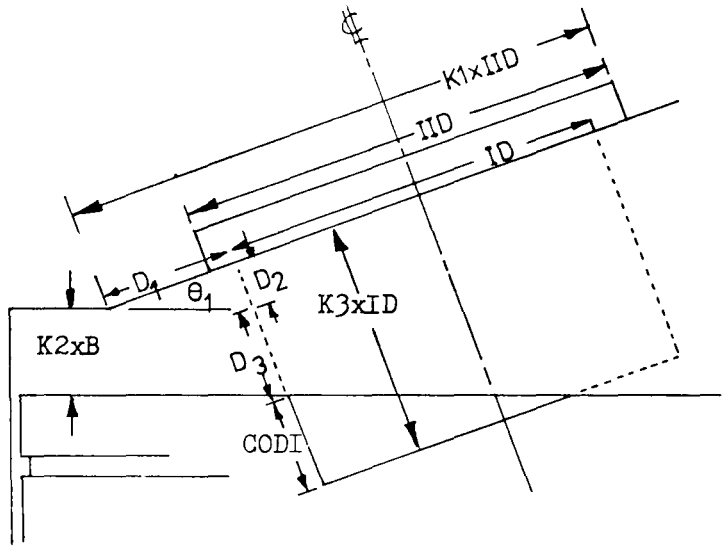

IID = inlet insert diameter

ID = inlet valve diameter

B = cylinder bore

D_1 = IID(K1 - 0.5) - ID/2.0

D_2 = $D_1 \tan \theta_1$

D_3 = $K_2 B / \cos \theta$

$\therefore$ CODI = $K_3 ID - (D_2 + D_3)$ (maximum depth of pocket)

A2.3.1 Partial cut-outs
PIN<ID

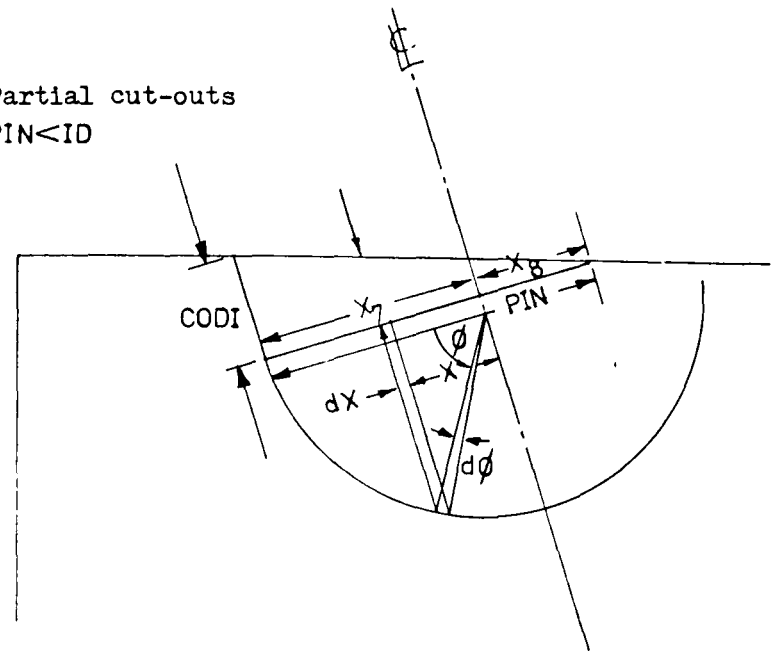

Volume of partial valve pocket

VICO = Volume of inlet valve cut-out

$$VICO = \int_{X_7}^{X_8} 2\sqrt{\left(\frac{ID}{2}\right)^2 - X^2}\, y\, dx$$

but $y = \tan\theta_1 (X - X_8)$

$$VICO = 2\tan\theta_1 \int_{X_7}^{X_8} \sqrt{\left(ID/2\right)^2 - X^2}\, (X - X_8)\, dx$$

$$= -\frac{2}{3}\tan\theta_1 \left[\left[\left(\frac{ID}{2}\right)^2 - X^2\right]^{3/2} \right]_{X_7}^{X_8} - X_8 \tan\theta_1 \, ABCOI$$

which is in the form of a function in the programme:

VICO = VCO (X7, ABCOI, ID, X8, THETA 1)

A2.3.2 Full cut-out

PIN > ID

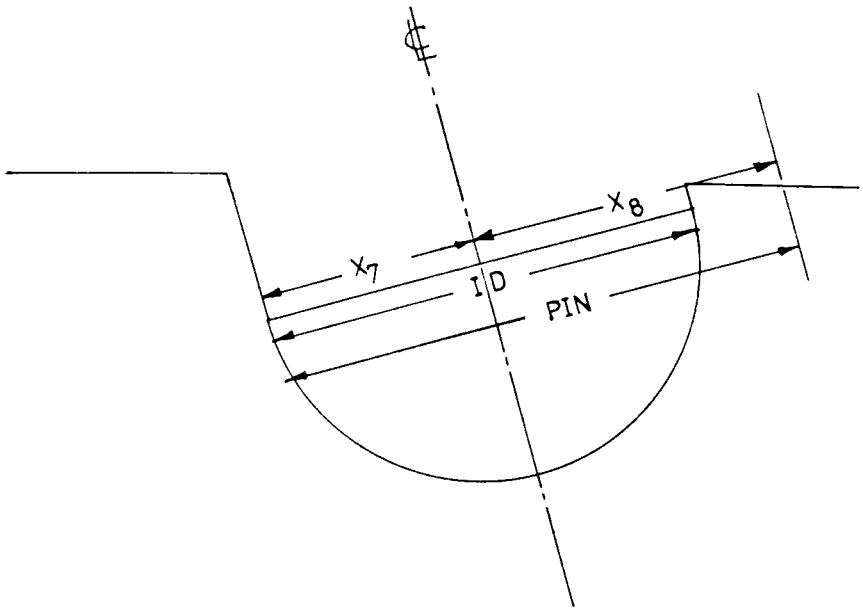

$$ABCOI = \pi\, ID^2/4$$

$$ASCOI = \int_0^{\pi} ID \tan\theta_1 \,(X - X_8)\, d\phi$$

$$= -\pi\, X_8\, ID \tan\theta_1$$

$$VICO = -\pi\, X_8 \left(ID/2\right)^2 \tan\theta_1$$

APPENDIX A3

Derivation of equations used for determining spherical flame front area and enflamed volume

A3.1 Flame front area excluding valve pockets

From AppendixA1 the limits on the radii are given by:

$R1 = K1 \times IID \sin \theta_1 + BB \times B \times \tan \theta_{1/2} + K22 \times BB$

$R2 = BB/_2 - K1 \times IID \sin \theta_1$

$R3 = AB \cos (\phi/_2)/2$

K22 includes the effect of piston motion and is calculated from:

$K22 = K2 + K21$

where K2 is a constant and :

$$K21 = \left[\left[SS/_2\right] (1 - \cos \psi) + L - L\sqrt{1 - \left(SS/_{2L}\right)^2 \sin^2 \psi} \right]$$

where SS = stroke

L = connecting rod length

ψ = crank angle measured from b.d.c.

The flame front area is calculated from a basic area which is that of the sphere radiating from the point of ignition intersected by the two valve planes. This is then modified at each limit on the radii.

The basic area is:

$$A = 2R^2 (\pi - \phi)$$

where ϕ is the included valve angle.

If $R > R1$ intersection with the piston crown occurs:

Reduction in area = $2R(R - R1)R$.

If $R > R2$ account must be taken of the effect of the curvature of the sides. In this case , expressions were derived using the lengths of bore wall intersected by the curved areas.
Certain assumptions were made in order to simplify the calculations, but these introduce very little error.
The three area reductions for this region are given by:

$$DR1 = H1\left[1 - \sqrt{1 - \left(\frac{R - R2}{H1}\right)^2}\right]^2$$

$$AA1 = ARCI \times DR1$$

$$AA2 = ARCE \times DR1$$

$$AA3 = 2 \times BB \times B \times DR1$$

where ARCI = Arc length of curved intersection on inlet side

ARCE = Arc length of curved intersection on exhaust side

AA1 = Reduction of area inlet side

AA2 = Reduction of area on exhaust side

AA3 = Reduction of area on centre strip

If $R > R3$ the flame has progressed into the region under the squish areas. In this case, an additional area must be added to compensate for the fact that the valve planes do not project this far.

$$\text{Additional area} = 4(R - R3)R \sin\left(\frac{\phi}{2}\right) \sin^{-1}\left[\sqrt{1 - \left(\frac{AB}{2R \cos(\phi/2)}\right)^2}\right]$$

All that is now required is an allowance for the valve pockets. This is given in the next section.

A3.2 Contribution of valve pockets to flame front area

A3.2.1 Partial valve pockets: PIN < ID

$$Y1 = \sqrt{PIN \times ID - PIN^2}$$

$$R5 = \sqrt{Y1^2 + GAPI^2}$$

$$R6 = \sqrt{\left(\left(GAPI + PIN\right)/\cos\theta_1\right)^2 + \left(\left(ID + C \times BB\right)/2\right)^2}$$

$$E = (RC - GAPI)/\cos\theta_1 - (PIN - ID/2)$$

$$Y = \sqrt{(ID/2)^2 - E^2}$$

$$\alpha = \sin^{-1}\left[\left[\left(ID/2 + \frac{C \times BB}{2}\right) - Y\right]/RC\right]$$

$$\beta = \sin^{-1}(GAPI/RC)$$

Arc length $ARL = RC\left(\pi/2 - \alpha - \beta\right)$

$$H3 = (RC - GAPI)\ CODI \cos\theta_1 / PIN$$

$$Area = H3 \times ARL/2$$

A3.2.2 Full pockets: PIN > ID

$$RR = (ID/2)^2 + (K3 \times ID - CODI\ (2\ PIN/ID - 1.0))^2$$

$$DC = \sqrt{RR - H1^2}$$

$$R5 = \sqrt{DC^2 + ((C \times BB + ID)/2)^2} - ID/2$$

R6 calculated as before.

$$PS = \tan^{-1}\left[\left(\left(ID + C \times BB\right)/2\right)/\left(ID/2 \cos\theta_1 + GAPI\right)\right]$$

$$AR = 2\ RC(PS - \alpha)$$

The rest of the calculation is the same as for partial cut-out.

APPENDIX A4

Derivation of equations used for determining the heat transfer areas

AREA 1 = πR^2

If R > R1 intersection with piston:

AP = $\pi (R^2 - R1^2)$

(NOTE: Valve pocket surface taken as plan area)

If R > R2 intersection with curved sides:

This region is dealt with with a summation routine:

AR1 = ARCI + B x $BB/_2$

AR2 = ARCE + B x $BB/_2$

AREA 2 = $(AR1 \times DR1 / (H1 - DR1) + DR1 \times \sqrt{(1 + (AR1/_{H1})^2)}) \times DR$

AREA 3 = $(AR2 \times DR1/(H1 - DR1) + DR1 \times \sqrt{(1 + (AR2/_{H_1})^2)}) \times DR$

AREA 4 = AREA 4 + AREA 2

AREA 5 = AREA 5 + AREA 3

ADA = 2(AREA 4 + AREA 5)

(Burnt area) BAREA = AREA 1 + 2 x R x B x BB + ADA + AP

UBAREA = SURFA - BAREA

APPENDIX A5

Enflamed volume and heat transfer area subroutine for cylindrical combustion chamber.

In order to investigate the effect of combustion chamber geometry on the combustion process, it was decided to use the cylindrical combustion chamber with provision for spark plug offset, as the simplest to analyse.

The output from the subroutine that is required in the programme is as follows:

(i) At any flame radius:

The enflamed volume

The burnt region heat transfer surface area

The unburnt region heat transfer surface area.

(ii) At any enflamed volume:

The radius of the flame.

The geometry using an offset spark plug in a cylindrical combustion chamber is shown below and is as shown in the paper by Blizard & Keck (Ref. 21).

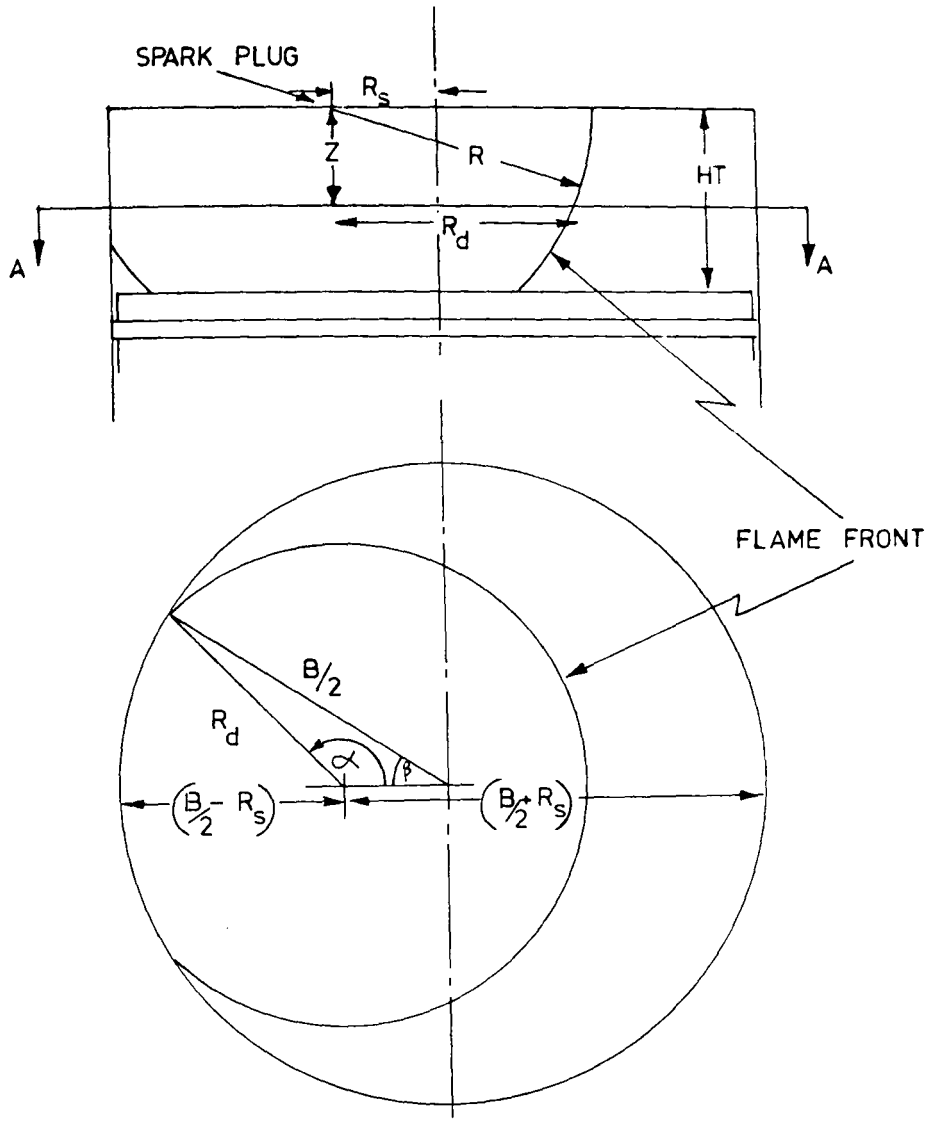

SECTION AA

The plan area across any section AA is determined from:

$$\text{Area} = \frac{B^2\beta}{4} + \alpha R_d^2 - R_s \frac{B}{4} \sin\beta \qquad \text{——————} \quad 1$$

Hence the volume can be found by integration. When the cross-section is circular the same expression can be used by putting

$\beta = 0 \quad \alpha = \pi$

The burnt region heat transfer area can be found from

$$dA_b = B\beta\, dz \qquad \text{——————} \quad 2$$

for the bore area and the area from equation 1 at z = 0 and z = HT.

The heat transfer area of the unburnt region is determined by subtracting the burnt region area from the total chamber area.
These areas and volumes are calculated at every crank angle interval, having first determined the chamber height HT.

Non-dimensional graphs for this geometry are shown in Figs. 6.3.3/4-7.

APPENDIX A6

Computer program used in determination of valve flow coefficients

```
5 DIM DAT(16)
6 REM**THIS PROGRAM CALCULATES THE PORT FLOW COEFFICIENT,VOLUMETRIC FLOW RATE,
7 REM**LIFT/DIA RATIO AND EFFECTIVE AREA OF A PAIR OF VALVES AND PORT AT A
8 REM**SERIES OF VALVE LIFTS.
9 REM**FLOW THROUGH THE VALVES IS ASSUMED TO HAVE BEEN MEASURED USING A 1.25IN
10 REM**DIAMETER ORIFICE IN A 4IN LINE WITH D&D/2 TAPPINGS ACCORDING TO BS1042
11 REM**THE BASIC AREA IS TAKEN AS TWICE THE THROAT AREA OF A SINGLE VALVE.
12 REM**THE EFFECTIVE AREA IS CALCULATED USING THE CONSTANT PRESSURE MODEL
13 REM**ASSUMING SUBSONIC FLOW AT THE THROAT.
20 PRINT"****FLOW COMFFICIENT PROGRAM****"
25 PRINT"INPUT THE FOLLOWING DATA SEPARATED BY COMMAS"
26 PRINT"THROAT DIA (MM)?"
27 PRINT"AMBIENT PRESSURE (MM HG)?"
28 PRINT"AMBIENT TEMPERATURE (DEG C)?"
30 INPUTD,PAM,TAM
40 AR=D^2*1.571E-6
55 PRINT"INPUT RUN DATA IN THE SAME FORMAT"
56 PRINT"VALVE LIFT (MM)?"
57 PRINT"ORIFCE HEAD (CM WATER)?"
58 PRINT"DOWNSTREAM PRESSURE (CM WATER)?"
59 PRINT"DOWNSTREAM TEMP (DEG C)?"
60 INPUTVL,H,P,T
70 IFVL<0THEN
80 TAM=TAM+273
90 TAB=T+273
100 PAB=PAM*1.36-P
110 RHO=0.34169*PAB/TAB
120 EPS=1-0.018714*H/P
130 Z1=1
140 ZR=Z1
150 W=23.9818*ZR*EPS*SQR(H*RHO)
160 MU=(0.429*TAB+56)*1.0E-7
170 RD=0.0111395*W/MU
180 Z1=1.0077-RD*7.4026E-8
190 IFABS((Z1-ZR)/ZR)>0.01THEN140
200 Q=W/RHO
210 X1=PAB/(PAM*1.36)
220 X2=X1^0.714*SQR(1-X1^0.2857)
230 X3=(W*SQR(TAB)/PAB)*1.8131E-5
240 AT=X3/X2
250 VFC=AT/AR
260 XL=VL/D
261 A$="MM"
262 B$="CUB M/SEC"
263 C$="SQ M"
270 PRINT"VALVE LIFT=";VL;A$
271 PRINT"FLOW COEFF=";VFC
272 PRINT"LIFT/DIA RATIO=";XL
273 PRINT"VOLUMETRIC FLOW RATE=";Q;B$
274 PRINT"EFFECTIVE AREA=";AT;C$
275 GOTO60
276 END
```

APPENDIX A7

The Polydyne cam design method

Various methods are available for determining a desired cam profile for a defined valve motion. The Polydyne method was thought most suitable in this case as it progresses from a selected valve motion back to the cam via the valve train. This would take into account the valve dimensions and hence mass, as derived in the geometric analysis, and so provide another link in the design chain.

It has also been shown by Fawcett (Ref. 32) the polydyne cam should give better motion than a polynomial cam where the Follower motion is described by a polynomial, at all speeds above $W_1/\sqrt{2}$ where W_1 is the polydyne cam design speed. This is the most important part of the speed range as large vibrations would not normally occur at low speed.

With regard to cam excited vibrations in the Follower system, the polydyne cam is only theoretically superior when the design speed W_1 is some way from the valve crash speed. It has been shown, however, that by the use of dual valves and a multiplicity of cylinders, the valve bounce speed can be as high as 25000 r.p.m. (Ref. 13).

The valve bounce speed can be determined from:

$$N_e = 2C\sqrt{\frac{F\,K}{W(-\ddot{y})}}$$

where N_e = engine speed (r.p.m)

F = Valve spring force at maximum lift (kgf)

$K = g\left[\frac{30}{\pi}\right]^2$ $\quad (g = 9.81 \times 10^3\ mm/s^2)$

W = Equivalent inertia weight of valve train (kgf)

$\ddot{y}$ = maximum negative acceleration (mm/rad^2)

C = Constant - the value of C is 0.85 for valve jumping or 1.0 for valve bounce.

The Polydyne method of designing a suitable cam profile to produce a polynomial valve motion, was originally suggested by Dudley (Ref.33) and later refined by Thoren, Engemann and Stoddart (Ref. 34). Further work, using computer techniques, was done by Nourse et al (Ref. 35) and it was this work that formed the basis of the current programme.

For a push-rod design, the valve train is idealised into the single degree of freedom shown below.

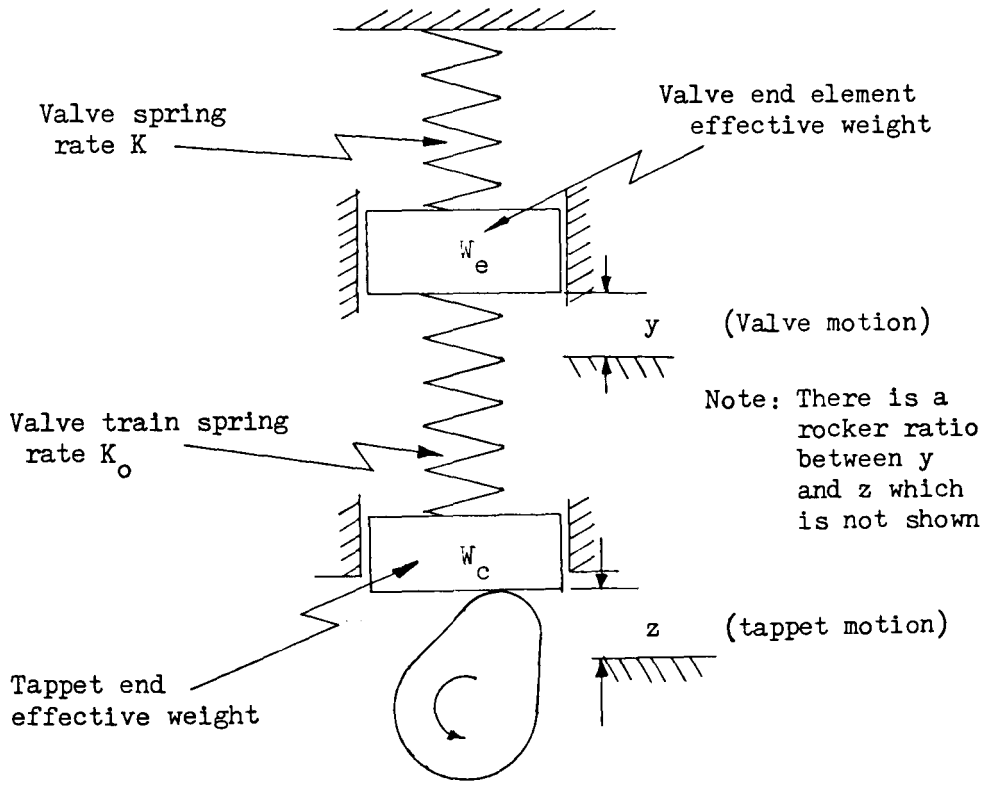

Fig. A7.1

Basic equations:

The valve motion is described by a 5th order polynomial:

$$y = y_m + C_p p^p + C_q q^q + C_r r^r + C_s s^s + C_t t^t$$

The constant coefficients C_p, C_q, C_r, C_s and C_t are determined from the boundary conditions:

$$C_p = \frac{-qrst.y_m - (q + r + s + t - 6)V + AA}{(q - p)(r - p)(s - p)(t - p)}$$

$$C_q = \frac{-prst.y_m - (p + r + s + t - 6)V + AA}{(p - q)(r - q)(s - q)(t - q)}$$

$$C_r = \frac{-pqst.y_m - (p + q + s + t - 6)V + AA}{(p - r)(q - r)(s - r)(t - r)}$$

$$C_s = \frac{-pqrt.y_m - (p + q + r + t - 6)V + AA}{(p - s)(q - s)(r - s)(t - s)}$$

$$C_t = \frac{-pqrs.y_m - (p + q + r + s - 6)V + AA}{(p - t)(q - t)(r - t)(s - t)}$$

$$V = \frac{XR^3.VR}{\phi}$$

$$AA = \frac{AR.XR^4}{\phi}$$

where XR = Cam lift period (deg)

VR = Velocity at end of ramp ($^{in}/_{deg}$)

AR = Acceleration at end of ramp ($^{in}/_{deg^2}$)

ϕ = Dynamic deflection coefficient

The equivalent cam motion, neglecting the rocker ratio (RR) is given by:

$$y_o = y_r + \rho y + \phi \ddot{y}$$

Tappet motion $Z_o = y_o/RR$

Velocities and accelerations can be determined from the differentials of these expressions:

ρ = static deflection coefficient

$$= \frac{K_o + K_1}{K_o}$$

and $\phi = 0.093 \frac{W N^2}{K_o}$

where W = Effective weight $(W_{EP} + W_{ER} + W_{EV})$

$W_{EP} = {}^{WP}/_{RR^2}$ Pushrod weight/rocker ratio^2

$W_{ER} = {}^{WR \times RR}/_{5}$ Rocker weight x rocker ratio/5

$W_{EV} = WV + {}^{WS}/_{3}$ Valve weight + $\frac{1}{3}$ spring weight

Using this method and selecting suitable polynomial powers and ramp exit valves, a suitable cam design can be produced.

The ramp used in this particular programme was a constant velocity ramp; details of the ramp calculations are shown in the programme print-out.

```
      FILE    3(KIND=PRINTER)
      FILE    2=KEEP/DATA,UNIT=D,SK
              COMMON FA(100),FL(100),RA(100),RL(100),A1,A2,A3,B1,B2,B3
              COMMON ITYPE,N,I
              DIMENSION Z(100),Z1(100),Y(100),Y1(100)
              DIMENSION DAT(16)
              REAL N,KO,K1,KF,LC,LV
            1 WRITE(3,101)
          101 FORMAT(1H ,20H CAM DESIGN PROGRAM )
           10 DO 20 I = 1,100
              FA(I) = 0.0
              FL(I) = 0.0
              RA(I) = 0.0
              RL(I) = 0.0
              Z1(I) = 0.0
              Z(I) = 0.0
              Y1(I) = 0.0
              Y(I) = 0.0
           20 CONTINUE
           30 READ(5,/)ITYPE
              IF (ITYPE.EQ.2.) GOTO 109
              IF (ITYPE.EQ.9.) CALL EXIT
              IF(ITYPE.EQ.1.) GOTO 60
              WRITE(3,50) ITYPE
           50 FORMAT(20H INVALID TYPE NO. = ,I1)
              GOTO 30
           41 FORMAT(I10,2F10.0)
           60 READ(2,/)N1,ROLLER,BASE
              IF(N1.LE.100)GOTO 80
              READ(2,/)(P,Q,I=1,N1)
              GOTO 30
           80 READ(2,/)(FA(I),FL(I),I=1,N1)
           90 FORMAT (3F10.4)
              WRITE(3,95) (FA(I),FL(I),I=1,N1)
           95 FORMAT (14H1INPUT DATA       /19H   ANGLE       LIFT       /
             *(1X,2F11.6))
              R=ROLLER+BASE
              NN=N1-1
              DO 100 I = 2,NN
              A1 = FL(I)
              A2 = FL(I-1)
              A3 = FL(I+1)
              B1 = FA(I)
              B2 = FA(I-1)
              B3 = FA(I+1)
              CALL CALC (Z(I))
          100 CONTINUE
              NN = NN - 1
              DO 110 I = 2,NN
              A1 = Z(I)
              A2 = Z(I-1)
              A3 = Z(I+1)
              B1 = FA(I)
              B2 = FA(I-1)
              B3 = FA(I+1)
              CALL CALC (Z1(I+1))
          110 CONTINUE
              NN=N1-1
              DO 120 I = 2,NN
              TANA = ATAN2(-57.23*Z(I-1),R+FL(I-1))
              TANB = ATAN2(-57.23*Z(I),R+FL(I))
```

```
      TANC = ATAN2(-57.28*Z(I+1),R+FL(I+1))
      A1= (R+FL(I))*COS(TANB)-ROLLER
      A2= (R+FL(I-1))*COS(TANA)-ROLLER
      A3= (R+FL(I+1))*COS(TANC)-ROLLER
      RA(I) = TANB * 57.29 + FA(I)
      RA(I-1) = TANA * 57.28 + FA(I-1)
      RA(I+1) = TANC * 57.28 + FA(I+1)
      B1 = RA(I)
      B2 = RA(I-1)
      B3 = RA(I+1)
      RL(I) = A1
      RL(I-1) = A2
      RL(I+1) = A3
      CALL CALC (Y(I))
  120 CONTINUE
      NN = NN - 1
      DO 130 I = 2,NN
      A1 = Y(I)
      A2 = Y(I-1)
      A3 = Y(I+1)
      B1 = RA(I)
      B2 = RA(I-1)
      B3 = RA(I+1)
      CALL CALC (Y1(I+1))
  130 CONTINUE
      WRITE(3,140) ROLLER,BASE
  140 FORMAT (1H1,20X,15H RESULTS FOR          /
     *15H ROLLER RAD. =  ,F 15.6/13H BASE RAD. =  ,F 15.6)
      WRITE(3,150)
  150 FORMAT (47H1    ANGLE       LIFT     VELOCITY     ACCELERATION
      WRITE(3,160) (FA(I),FL(I),Z(I),Z1(I),I=1,N)
  160 FORMAT (4F11.6)
      WRITE(3,150)
      WRITE (3,160) (RA(I),RL(I),Y(I),Y1(I),I=1,N)
      GOTO 10
  100 WRITE(6,201)
  201 FORMAT(1H ,13H INPUT IPRNT )
  640 READ(5,210) IPRNT
  210 FORMAT(A2)
      IF(IPRNT.IS.2HAB)GOTO 200
      IF(IPRNT.IS.2HB ) GOTO 200
      IF(IPRNT.IS.2HA ) GOTO 200
      WRITE(3,300) IPRNT
  300 FORMAT(26H INVALID OUTPUT REQUEST = ,A2)
      GO TO 10
  200 WRITE(6,202)
  202 FORMAT(1H ,31H INPUT DATA?,YR,YM,XR,P,Q,R,S,T)
      N=4906.
      K0=25650.0
      K1=702.00
      WP=0.4041
      WR=0.6723
      WV=0.276396
      WS=0.141093
      RR=1.25
      RB=0.48
      RF=0.375
      PL=117.8
      KF=2020.0
      CW=0.4
      READ(5,*)ZR,YM,XR,P,Q,R,S,T
      WRITE(6,203)
  203 FORMAT(1H ,11H DATA READ )
      WRITE(3,220)N,YR,K0,K1,WP,WR,WV,WS,YM,XR,RR,RB,RF,PL,
     *KF,CW,P,Q,R,S,T
      WRITE(3,211)
```

```
12800      251 WRITE(6,211)
12900      211 FORMAT(1HO,2X,10HRAMP DATA )
13000      205 READ(5,/) XRMP,YR,VR,AR
13100          WRITE(3,212)XRMP,YR,VR,AR
13200      212 FORMAT(1HO,8H XRMP = ,F12.6/6H YR = ,F12.6/
13300         *6H VR = ,F12.6/6H  A = ,F12.6)
13400          WRITE(3,232)
13500          WRITE(6,232)
13600      232 FORMAT(1HO,14H     X     ZO    )
13700          N2=0.0
13800          X1=XR+XRMP+1.0
13900          WRITE(2,/) X1,RF,RB
14000          WRITE(2,/)N2,N2
14100      220 FORMAT(1HO,25H   DATA FOR RUN TYPE 2:- //
14200         *6H  N = ,F12.5/6H YR = ,F12.6/
14300         *6H KO = ,F12.6/6H K1 = ,F12.6/6H WP = ,F12.6/6H WR = ,F12.6/
14400         *6H WV = ,F12.6/6H WS = ,F12.6/6H YM = ,F12.6/6H XR = ,F12.6/
14500         *6H RR = ,F12.6/
14600         *6H RB = ,F12.6/6H RF = ,F12.6/6H PL = ,F12.6/
14700         *6H KF = ,F12.6/
14800         *6H CW = ,F12.6/6H  P = ,F12.6/6H  Q = ,F12.6/
14900         *6H  R = ,F12.6/6H  S = ,F12.6/6H  T = ,F12.6)
15000      230 FORMAT(4H1  X,6X,1HY,7X,2HY1,10X,2HY3,11X,2HY4,9X,2HYO,
15100         *8X,3HYO1,7X,3HZO1,7X,3HZO2)
15200      231 FORMAT(4H1  X,6X,2HY2,7X,3HYO2,10X,2HZO,10X,2HRC,8X,1HE,
15300         *7X,2HSF,7X,2HLV,6X,2HLC,6X,2HSB,9X,2HFC)
15400          NN=XRMP+3.0
15500          WEP=WP/(RR**2)
15600          WER=WR*RR/5.0
15700          WEV=WV+WS/3.0
15800          W = WEP + WER + WEV
15900          PHI = 0.093 * W * N **2 / KO
16000          RHO = (KO + K1) / KO
16100          X=XR+XRMP+1.0
16200      237 X=X-1.0
16300          ZO2=AR
16400          ZO1=-AR*((XRMP+XR)-X)
16500          ZO=AR*((XRMP+XR)-X)**2/2.0
16600          IF(ZO1.GE.VR) GO TO 209
16700          WRITE(6,204)
16800      204 FORMAT(1H ,18HCONSTANT VELOCITY )
16900          WRITE(3,204)
17000          GO TO 209
17100      235 X=X-1.0
17200          VR=ZO1
17300          ZO=ZO-VR
17400          ZO2=0.0
17500          IF(ZO.GE.ZR)  GO TO 208
17600          IF(X.LE.XR) GO TO 207
17700          GO TO 209
17800      208 WRITE(6,205)
17900      205 FORMAT(1H ,31H RAMP HEIGHT DECISION,YES OR NO)
18000          READ(5,/) DEC
18100          IF(DEC.EQ."YES") GO TO 207
18200          GO TO 251
18300      207 YR=RR*ZO
18400          VR=VR*RR
18500          W = XR ** 3 * VR / PHI
18600          AA=(A*XR**4)/PHI
18700          P = 2.0
18800          CP=(-Q * R * S * T * YM - (Q + R + S + T - 6.0) * W + AA )/
18900         *     ((Q - P) * (R - P) * (S - P) * (T - P))
19000          CQ=(-P * R * S * T * YM - (P + R + S + T - 6.0) * W + AA )/
19100         *     ((P - Q) * (R - Q) * (S - Q) * (T - Q))
19200          CR=(-P * Q * S * T * YM - (P + Q + S + T - 6.0) * W + AA )/
19300         *     ((P - R) * (Q - R) * (S - R) * (T - R))
```

```
19400           CS=(-P * Q * R * T * YM - (P + Q + R + T - 6.0) * V + AA
19500          *     ((P - S) * (Q - S) * (R - S) * (T - S))
19600           CT=(-P * Q * R * S * YM - (P + Q + R + S - 6.0) * V + AA
19700          *     ((P - T) * (Q - T) * (R - T) * (S - T))
19800           X=XR
19900       240 XXR=X/XR
20000           YY=YM+CP*XXR**P+CQ*XXR**Q
20100          *        + CR * XXR ** R + CS * XXR ** S
20200          *        + CT * XXR ** T
20300           YY1=CP*P*XXR**(P-1.0)+CQ*Q*XXR**(Q-1.0)
20400          *    + CR * R * XXR ** (R-1.0) + CS * S * XXR ** (S-1.0)
20500          *    + CT * T * XXR ** (T-1.0)
20600           YY2=CP*P*(P-1.0)*CQ*Q*(Q-1.0)*XXR**(Q-2.0)
20700          *    + CR * R * (R-1.0) * XXR ** (R-2.0)
20800          *    + CS * S * (S-1.0) * XXR ** (S-2.0)
20900          *    + CT * T * (T-1.0) * XXR ** (T-2.0)
21000           YY3=CQ*Q*(Q-1.0)*(Q-2.0)*XXR**(Q-3.0)
21100          *    + CR * R * (R-1.0) * (R-2.0) * XXR ** (R-3.0)
21200          *    + CS * S * (S-1.0) * (S-2.0) * XXR ** (S-3.0)
21300          *    + CT * T * (T-1.0) * (T-2.0) * XXR ** (T-3.0)
21400           YY4=CQ*Q*(Q-1.0)*(Q-2.0)*(Q-3.0)*XXR**(Q-4.0)
21500          *    + CR * R * (R-1.0) * (R-2.0) * (R-3.0) * XXR ** (R-4.0
21600          *    + CS * S * (S-1.0) * (S-2.0) * (S-3.0) * XXR ** (S-4.0
21700          *    + CT * T * (T-1.0) * (T-2.0) * (T-3.0) * XXR ** (T-4.0
21800           YY1=YY1/XR
21900           YY2=YY2/XR**2
22000           YY3=YY3/XR**3
22100           YY4=YY4/XR**4
22200           YY0=(YR+RHO*YY+PHI*YY2)
22300           YY01=RHO*YY1+PHI*YY3
22400           YY02=RHO*YY2+PHI*YY4
22500           Z0=YY0/RR
22600           Z01=YY01/RR
22700           Z02=YY02/RR
22800       209 RAA=RB+RF
22900           R1=RAA+Z0
23000           RHO1=-((R1**2+(Z01*57.28)**2)**1.5)
23100           RHO2=(R1**2+2*(Z01*57.28)**2-R1*57.28**2*Z02)
23200           IF (ABS(RHO2).LT.0.00001) GO TO 2
23300           RHOK=RHO1/RHO2
23400           GO TO 3
23500         2 RHOK=100000.
23600         3 RC=RHOK+RF
23700           ALPHA=ATAN2(-57.28*Z01,R1)
23800           RG=COS(ALPHA)*(RB+RF+Z0)-RF
23900           SF=PL+K1*YY
24000           LV=0.093*W*W**2*YY02
24100           LC=RR*(LV+SF)
24200           SB=(Z0+RB+E)/57.2
24300           FC=KF*SQRT(ABS(LC/(RC+CW)))
24400           ALPHA=ATAN2(-57.28*Z01,(RF+RB+Z0))
24500           E=RF*SIN(ALPHA)
24600           IF(X.GT.XR) GO TO 233
24700           IF(X.LE.XR) GO TO 234
24800       233 WRITE(6,7)X,Z0,RG,(X+57.28*ALPHA)
24900           WRITE(3,235)X,Z0,RG,(X+57.28*ALPHA)
25000       235 FORMAT(1H ,2X,I5,2X,F12.6,2X,F12.6,2X,F12.6)
25100           IF(Z01.LE.V9) GO TO 236
25200           GO TO 237
25300       234 CONTINUE
25400           E=RG
25500           FC=(ALPHA*57.28)+X
25600           IF(IPRNT.EQ.2HB )GOTO 600
25700           WRITE(3,700)X,YY2,YY02,Z0,RC,E,SF,LV,LC,SB,FC
25800       700 FORMAT(1X,F5.1,2(1X,F9.6),1X,F12.6,1X,E10.4,1X,F8.5,1X,F8.
25900          *2(1X,F7.1),1X,F7.5,F12.6)
```

```
26000           GOTO 249
26100       600 WRITE(3,300)X,YY,YY1,YY2,YY4,YY0,YY01,Z01,Z02
26200       300 FORMAT(1X,F5.1,1X,F9.6,1X,F9.6,2(1X,F12.6),2(1X,F9.5),2(1X,F12.
26300       249 NN = NN + 1
26400           IF (NN.LE.58)GOTO 250
26500           IF(IPRNT.EQ.2HB ) WRITE(3,230)
26600           IF(IPRNT.EQ.2HA .OR.IPRNT.EQ.2HAB) WRITE(3,231)
26700           NN = 3
26800       250 X=X-1.0
26900           IF(X.GE.0.0) GO TO  240
27000     LOCK(2)
27100           VAREA = XR*(YM+CP/(P+1.0)+CQ/(Q+1.0)+CR/(R+1.0)
27200          *+CS/(S+1.0)+CT/(T+1.0))
27300           IF(IPRNT.EQ.2HAB) WRITE(3,500)VAREA
27400       500 FORMAT(9HOVAREA = ,_13.7)
27500           IF(IPRNT.NE.2HAB)GOTO 10
27600           IPRNT = 2HB
27700       108 STOP
27800           END
27900           SUBROUTINE CALC (X)
28000           COMMON DUMMY(400),A1,A2,A3,B1,B2,B3
28100           X = 0.5 *((A1-A2) / (B1-B2) + (A3-A1) / (B3-B1))
28200           RETURN
28300           END
```

APPENDIX A8

(i) Combustion program written in BASIC for use on the Commodore PET micro-computer. Used for combustion analysis.

(ii) Full geometry and cycle analysis program written in 'FORTRAN IV' for use on the Burroughs 6700.

For use in analysing the performance of a 4-valve/cylinder configuration spark ignition engine.

```
100 INPUT"HARDCOPY";A$:IFA$="N"THEN140
110 OPEN7,4,2:OPEN4,4
120 PRINT£7,"999 99.99 9999.9 99999.9 9999.9 99.99 9.999  99.9 99.9 99.9 99.9"
130 OPEN6,4,1
140 M=2.2
150 TU=300.0
160 TR=TU:TC=TU:TB=TU
170 CI=37
180 CR=8
190 DT=2
195 DP=0
200 IT=330
210 EQR=1.0
230 A=1
240 CH=44500
250 F=.00
260 FA=0.06455
270 RE=6000
280 BB=68.28
290 SS=68.28
300 L=112
305 RS=0:RS=RS/1000
310 CDI=0.357
320 DI=.43*BB
330 YM=DI/4
340 DC=60
350 CA0=347
360 N=RE/60
370 PE=DT/RE
380 TM=PE/6
390 QS=0
400 R0=0
410 R1=0:R=0
420 VY=0
425 TW=500
430 TS=900
440 PR=1:PC=PR
450 H1=SS/(CR-1)
460 RG=0.287
470 K1=0.015
480 TH=180
490 GOSUB2010
500 VI=V
505 MT=PR*VI*100/(.287*TU)
506 TH=IT
507 GOSUB2010
508 VS=V
510 TH=270
520 GOSUB2010
530 V0=V:VC=V
550 XF=0
```

```
560 GOSUB2230
570 E1=A1+A2*TR+A3*TR^2
580 E0=E1
590 NN=0
600 U2=MT
620 PS=2*SS*N/1000
630 IFTH=ITTHEN650
640 TH=TH+DT
645 IFTH=450THEN2365
650 T=TR
660 GOSUB2190
670 EI=2.265*(PS)^0.333*SQR(PR*TR)
690 HI=SS+H1
700 HSP=VS*1E+9*4/(*BB^2)
710 HT=VC*1E+9*4/(*BB^2)
711 HT=HT/1000
714 AT=(BB/2000)^2**2+*(BB/1000)*HT
715 IFTH<=ITTHEN718
716 IFMM=1THEN718
717 QL=EI*(AB*TB+AU*TU-TW*AT)*1.0E-3:GOTO730
718 QL=EI*AT*(TR-TW)*1.0E-3
730 RM=SQR(((BB/2000)+RS)^2+HT^2)
732 IFTH>=ITTHEN736
734 QB=0:PA=PC:TA=TC:GOTO1390
736 IFMM=0THEN740
738 QB=0:PA=PC:TA=TC:GOTO1390
740 HF=(HSP/HI)^0.333
750 GOSUB2080
760 UL=U
770 RI=PR*1.0E2/(RG*TS)
780 RU=PR*1.0E2/(RG*TU)
790 RHF=(RI/RU)^0.1111
800 GU=2*(BB/DI)^2*SS*N/(CDI*CA0*1000)
805 PRINTGU
810 FF=150.000*(HF*(YM/1000)^.333*GU*(BB/SS)*RHF*UL^-0.333)
820 FF=FF/(60*N)
830 FSR=1+FF*N*60
840 IFTH=ITTHEN860
850 GOTO950
860 S=100./TU
870 MU=(TU^.5/(.5528+2.811*S^13.5083*S^2+39.353086*S^3-41.419387*S^4))*10.E-7
880 IG=CI*(PS*MU/RU)^.333*(HSP/UL)^.6667
890 IFA$="N"THEN910
900 PRINT£4,"IGNITION DELAY PERIOD=";IG
910 PRINT"IGNITION DELAY PERIOD=";IG
920 IG=INT(IG/2)*2
930 TG=IG*TM/DT
940 XG=TG*UL*1000
950 IFTH=ITTHEN640
960 IFTH<=(IT+IG)THEN990
970 GOTO1140
980 IFNN=1THEN1010
990 M=(-2.25037-LOG(A))/LOG(IG/DC)-1
1000 NN=1
```

```
1010 XF=1-EXP(-A*((TH-IT)/DC)^(1+M))
1020 XI=INT(1000*XF)/1000
1030 B2=XF*MT
1040 MB=B2-B1
1050 U2=MT-B2
1060 VB=MB*VC/MT
1070 VF=VF+VB
1080 VU=VC-VF
1090 GOSUB2280
1100 U=(R-R1)/TM
1110 R1=R
1115 R0=R
1120 FSR=U/UL
1130 GOTO1290
1140 U=UL*FSR
1145 U1=U
1150 F1=SQR(1+(1.823E-8/1.30)*((BB*RU/(2000*MU))*(U1+12*PS^1.75))^1.42)
1160 UX=F1*UL
1170 IFABS(1-UX/U1)<0.01THEN1190
1175 PRINTTH,F1,UX,UL
1180 U1=UX:GOTO1150
1190 PRINTTH,F1,UX,UL
1200 DR=U*TM
1210 R=R+DR
1220 GOSUB1780
1230 VF=VE
1240 VU=VC-VF
1250 VB=VF-VY
1260 MB=MT*VB/VC
1270 B2=B2+MB
1280 U2=MT-B2
1290 QB=MB*CH*EQ*FA*(1-F)
1300 QD=QB
1310 GOSUB2230
1320 DW=0
1330 E3=(QD-DW)/MT
1340 E2=E1+E3
1350 A4=A1-E2
1360 TA=(-A2+SQR(A2^2-(4.0*A3*A4)))/(2*A3)
1370 PA=PC*TA/TC
1380 E1=E2
1390 GOSUB2010
1400 V0=V
1410 QD=TM*QL
1420 DW=FR*(V0-VC)*100
1430 E3=(QD-DW)/MT
1440 E2=E1+E3
1450 A4=A1-E2
```

```
1460 TR=(-A2+SQR(A2^2-(4.0*A3*A4)))/(2*A3)
1470 PR=PA*VC*TR/(V0*TA)
1475 IFTH<ITTHEN1600
1476 IFMM=1THEN1600
1480 IFTH>=(IT+IG)THEN1500
1490 T2=TR:T3=TR:GOTO1570
1500 T=TU:GOSUB2190
1510 T2=(PR/PC)^((GA-1)/GA)*TU
1520 EU=A1+A2*T2+A3*T2^2
1530 EB=(MT*E2-EU*U2)/B2
1540 A4=A1-EB
1550 T3=(-A2+SQR(A2^2-(4.0*A3*A4)))/(2.0*A3)
1560 XF=B2/MT
1570 VU=VU*(PA/PR)^(1/GA)
1580 VF=V0-VU:GOSUB2280
1590 IFXF>1THEN2330
1595 TU=T2
1600 W=W+DW
1610 Q=Q+QD
1615 DP=DP+PR*DT
1620 VT=(R-R0)/TM
1640 TB=T3
1650 TC=TR
1660 PC=PR
1670 VC=V0
1680 E1=E2
1690 B1=B2
1700 R0=R
1710 VY=VF
1720 R=R*1000
1730 IFA$="N"THEN1750
1740 PRINT#6,TH,PR,TR,TB,TU,U,XF,R,VT,FSR,F1
1750 PRINTTH,PR,TR,TB,TU,U,XF,R,VT,FSR,F1
1760 R=R/1000
1770 GOTO640
1780 IF(R<HT)AND(R<(BB/2000))THEN1960
1790 IF(R<HT)AND(R>(BB/2000))THEN1930
1800 IF(R>HT)AND(R<(BB/2000))THEN1900
1810 IFR>=RMTHEN2330
1820 AB=*(BB/2000)^2+*SQR(R^2-(BB/2000)^2)+*(R^2-HT^2)
1830 HH=HT
1840 H2=SQR(R^2-(BB/2000)^2)
1850 AF=*2*R*(HH-H2)
1860 V1=*(BB/2000)^2*H2
1870 V2=*(R^2*(HH-H2)-(HH^3-H2^3)/3)
1880 VE=V1+V2
1890 GOTO1990
1900 H2=0:HH=HT
```

```
1910 AB=*R^2+*(R^2-HT^2)
1920 GOTO1850
1930 HH=R:H2=SQR(R^2-(BB/2000)^2)
1940 AB=*(BB/2000)^2+*H2*BB/1000
1950 GOTO1850
1960 AF=2**R^2
1970 VE=2**R^3/3
1980 AB=*R^2
1990 AT=2**(BB/2000)^2+*BB*HT/1000
2000 AU=AT-AB
2010 TH=TH+180
2020 S2=COS(TH/57.2958)
2030 S3=SIN(TH/57.2958)
2040 V=*(BB/2)^2*(SS/(CR-1)+(SS/2)*(1+S2)+L-L*SQR(1-(SS/(2*L))^2*S3^2))
2050 V=V*1.0E-9
2060 TH=TH-180
2070 RETURN
2080 FI=4.69-8.72*(1.1-EQR)^2
2090 TL=TU
2100 U=57.0+0.287*4.83E-7*TL^1.647*FI
2110 RETURN
2120 TH=TH+180
2130 S3=SIN(TH/57.2958)
2140 S4=SIN(TH*2/57.2958)
2150 T4=(S4*SS/(4.*L))/(SQR(1-(SS/(2.*L))^2*S3^2)-S3)
2160 VD=(^2*BB^2*N*SS/4.0E+9)*T4
2170 TH=TH-180
2180 RETURN
2190 C1=-23.787+(1.085*T)+6.933E-5*T^2
2200 C2=-23.787+(.7925*T)+6.933E-5*T^2
2210 GA=C1/C2
2220 RETURN
2230 XX=140*XF*FA
2240 A1=-23.787+5.797*XX+0.8*XX^2
2250 A2=0.798-.00538*XX+.0011996*XX^2
2260 A3=(6.933+0.3283*XX+0.036*XX^2)*.00001
2270 RETURN
2280 FORR=ROTORMSTEP1E-4
2290 GOSUB1780
2300 IFVE<VFTHEN2320
2310 GOTO2360
2320 NEXTR
2330 IFA$="N"THEN2350
2340 PRINT#4,"TOTAL VOL ENFLAMED",VE,VF,V0,R,RM,VE/V0,R/RM,B2/MT:MM=1:GOTO1595
2350 PRINT,"TOTAL VOL ENFLAMED",VE,VF,V0,R,RM,VE/V0,R/RM,B2/MT:MM=1:GOTO1595
```

```
2360 VF=VE:RETURN
2365 MEP=DP/180
2366 PRINT£4,"MEP=";ME
2367 PRINT£4,"W=";W
2368 PRINT£4,"Q=";Q
2369 PRINT£4,"BB=";BB
2370 PRINT£4,"SS=";SS
2371 PRINT£4,"FF=";FF
2372 PRINT£4,"EQR=";EQR
2373 PRINT£4,"CR=";CR
2400 GOTO5390
```

```
100 $RESET FREE
200 FILE    3(KIND=PRINTER)
300 C     OPTIMIZATION PROGRAMME FOR 4-VALVE  SPARK IGNITION
400 C      ENGINE       AUTHOR  A.A.NEWLYN.    17.1.73
500         DIMENSION DAT(15),
600        •VOL(100),UT(100),DXD(100),DMF(100),BETA(2,20)
700         COMMON BB,PHR,THETA1,THETA2,IID,KK,K1,K2,K3,K22,B1,AB,
800        •ARC1,ARC2,C,CODI,CODE,PIT,PEN,ED,ID,H1,SURFA
900         REAL L,LD,N,MD,MT,MDI,MDIT,KK,K1,K2,K3,N1,THETAX,THPROD,THV
           \,THMAX,
1000        •THPRD,BB,SII,SIIT,A,K4,LF,IO,LPIP,LAM(2,20),MF(100),
1100        •KK1,KK2,KK3,KK4,K,ID,IID,K22,MU,IG,MB
1200         INTEGER TS,XTC,P,R,S,T,EVO,EVC
1300         RADCON=2.0•3.14159265/360.
1400         DO 65 I=1,2,1
1500         DO 65 J=1,20,1
1600         BETA(I,J)=1.0
1700         LAM(I,J)=1.0
1800      65 CONTINUE
1900      61 LINE=6
2600         READ(5,/)QQ,PHII,VV
3000         B1=0.066
3100         C=0.047
3200         KK=1.0496
3300         K1=1.09
3400         K2=0.0203
3500         K3=0.206
3600         WRITE(3,63)QQ,PHII,VV,B1,C,KK,K1,K2,K3
3800      63 FORMAT(15H1 INPUT DATA´-//
3900        •7H  QQ = ,F10.6/8H PHII = ,F10.6/
4000        •7H VV = ,F10.6/7H B1 = ,F10.6/
4100        •7H  C = ,F10.6/7H  KK = ,F10.6/
4200        •7H K1 = ,F10.6/7H K2 = ,F10.6/
4300        •7H K3 = ,F10.6)
4400         PHIA=PHII
4500     900 FORMAT(9E14.7/1X)
4600      64 BB=(4.0•QQ•VV/3.14159265)••0.333333•10.0
4700         SS=BB/QQ
4800         PI=3.14159265
4900         PHR=PHII•RADCON
5000         THETA1=ATAN((SIN(PHR))/(KK+COS(PHR)))
5100         THETA2=PHR-THETA1
5200         E=(COS(THETA1)•(K1-0.5)-(K1/2.0)•(COS(THETA1)
5300        •+COS(THETA2)/KK))
5400     410 E1=(BB/2.0)•(1.0-B1)
5500         E2=(BB/2.0)•(2.0•C+B1)
5600         AA1=(1.0+E•E)
5700         BB1=(2.0•E2-BB•E+2.0•E1•E)
5800         CC1=(E2•E2-BB•E1+E1•E1)
5900         IID=(-BB1+SQRT(BB1••2-4.0•AA1•CC1))/(2.0•AA1)
6000         B2=0.07•IID/BB
6100         IF(ABS(BB•(B1-B2)).LE.0.01) GOTO 400
6200         B1=B2
6300         GOTO 410
6400     400 EID=IID/KK
6500         DTI=((-1.127+SQRT(1.27+4.0•IID))/2.0)••2
6600         ATI=PI•DTI••2/(2.0E+6)
6700         ID=DTI+SQRT(0.635•DTI)
6800         DPI=0.877•DTI
6900         DTE=((-1.127+SQRT(1.27+4.0•EID))/2.0)••2
7000         ATE=PI•DTE••2/(2.0E+6)
7100         ED=DTE+SQRT(0.635•DTE)
```

```
7200        DPE=0.877*DTE
7300        AB=ID*(K1*(COS(THETA1)+COS(THETA2)/KK))+BB*B1
7400        X1=AB/2.0
7500        X2=X1-K1*ID*COS(THETA1)
7600        AIH=(HCAL(X1,BB)-HCAL(X2,BB))/COS(THETA1)
7700        X3=AB/2.0
7800        X4=X3-K1*EID*COS(THETA2)
7900        H1=K1*ID*SIN(THETA1)
8000        AEH=(HCAL(X3,BB)-HCAL(X4,BB))/COS(THETA2)
8100        ATS=2.0*BB*B1*(SQRT((BB/2.0)**2-X2**2)-H1)
8200        ARCI=(BB/2.0)*(ARCSIN(X1*2.0/BB)-ARCSIN(X2*2.0/BB))
8300        CSI=0.5707963*SIN(THETA1)*(X1-X2)**2/COS(THETA1)**2
8400        ARCE=(BB/2.0)*(ARCSIN(X3*2.0/BB)-ARCSIN(X4*2.0/BB))
8500        CSE=0.5707963*SIN(THETA2)*(X3-X4)**2/COS(THETA2)**2
8600        ASS=BB*B1*H1*1.5707963*2.0
8700        X5=BB/2.0
8800        X6=AB/2.0
8900        AFL=2.0*(BB**2*0.3927-HCAL(X5,BB))
9000        ACYLH=AFL+ASS+ATS+AIH+AEH+CSI+CSE
9100        BWA=K2*PI*BB**2
9200        ID=1.07*ID
9300        D1=ID*(K1-0.5)-ID/2.0
9400        D2=D1*TAN(THETA1)
9500        D3=K2*BB/COS(THETA1)
9600        CODI=K3*ID-(D2+D3)
9700        IF(CODI.GT.0.0) GO TO 95
9800        ABCOI=0.0
9900        ASCOI=0.0
10000         GO TO 110
10100    95 CONTINUE
10200       PIN=CODI/TAN(THETA1)
10300       X7=ID/2.0
10400       X8=X7-PIN
10500       IF(PIN.GT.ID) GOTO 100
10550 C     PARTIAL VALVE CUTOUT.
10600       ABCOI=(ID**2*0.3927-HCAL(X8,ID))
10700       ASCOI=ID*TAN(THETA1)*(SQRT((ID/2.0)**2-X8*X8)-X8*ARCOS(2.0*
10800      *X8/ID))
10900       GO TO 110
10950 C     FULL VALVE CUTOUT.
11000   100 ABCOI=PI*((ID/2.0)**2)
11100       ASCOI=-ID*TAN(THETA1)*X8*PI
11200   110 ED=1.07*ED
11300       E11=EID*(K1-0.5)-ED/2.0
11400       E22=E11*TAN(THETA2)
11500       E33=K2*BB/COS(THETA2)
11600       CODE=K3*ED-(E22+E33)
11700       IF(CODE.GT.0.0) GO TO 115
11800       ABCOE=0.0
11900       ASCOE=0.0
12000       GO TO 130
12100   115 CONTINUE
12200       PEN=CODE/TAN(THETA2)
12300       X9=ED/2.0
12400       X10=X9-PEN
12500       IF(PEN.GT.ED) GO TO 120
12550 C     PARTIAL VALVE CUTOUT.
12600       ABCOE=(ED**2*0.3927-HCAL(X10,ED))
12700       ASCOE=ED*TAN(THETA2)*(SQRT((ED/2.0)**2-X10*X10)
12800      *-X10*ARCOS(2.0*X10/ED))
12900       GO TO 130
```

```
12950 C      FUEL VALVE CUTOUT.
13000    120 ABCOE=PI*(ED/2.0)**2
13100        ASCOE=-ED*TAN(THETA2)*X10*PI
13200    130 APISCR=PI*(BB/2.0)**2+2.0*ASCOI+2.0*ASCOE
13300       *-2.0*ABCOI*(1.0/COS(THETA1)-1.0)-2.0*ABCOE*(1.0/COS(THETA2)\
           \-1.0)
13400        GAPI=K1*ID*COS(THETA1)+BB*B1/2.0-K2*BB*TAN(THETA1)-CODI/
            *SIN(THETA1)
13500        GAPE=K1*ED*COS(THETA2)+BB*B1/2.0-K2*BB*TAN(THETA2)-CODE/
            *SIN(THETA2)
13600        GAP=GAPI+GAPE
13700        SURFA=ACYLH+BWA+APISCR
13800        VCYLI=VCAL(X1,BB,THETA1)-VCAL(X2,BB,THETA1)
13900        VCYLE=VCAL(X3,BB,THETA2)-VCAL(X4,BB,THETA2)
14000        VCYLC=ATS*BB*B1
14100        VCI=0.14306*TAN(THETA1)**2*(X1-X2)**3
14200        VCE=0.14306*TAN(THETA2)**2*(X3-X4)**3
14300        VSS=H1*H1*BB*B1*1.570796
14400        VCLS=PI*(BB/2.0)**2*K2*BB
14500        VOCH=VCYLI+VCYLE+VCYLC-VCI-VCE+VSS
14600        IF(PIN.LE.ID) VICO=VCO(X7,ABCOI,ID,X8,THETA1)
14700        IF(PEN.LE.ED) VECO=VCO(X9,ABCOE,ED,X10,THETA2)
14800        IF(PIN.GT.ID) VICO=-(ID/2.0)**2*TAN(THETA1)*PI*X8
14900        IF(PEN.GT.ED) VECO=-(ED/2.0)**2*TAN(THETA2)*PI*X10
15000        CLVOL=VOCH+VCLS+2.*VICO+2.*VECO
15100        POCV=(VCI+VCE)/CLVOL
15200        SQA=4.0*AFL/(3.14159*BB**2)
15210        CHT=H1+K2*BB
15220        STVR=SURFA/CLVOL
15230        CCR=(VV*1000.+CLVOL)/CLVOL
15300        ED=ED/1.07
15400        ID=ID/1.07
15500        CLVOL=CLVOL/1000.0
15600  C     END OF GEOMETRY CALCULATIONS OUTPUT MAIN PARAMETERS.
15700        WRITE(3,41)VV,QQ,BB,SS,ID,ED,CLVOL,CCR,STVR,CHT,CODI,CODE,
            *POCV,SQA
15800     41 FORMAT(24H0BASIC GOEMETRY OUTPUT  //
15900       *19H SWEPT VOLUME     = ,F10.6,2HCC/
16000       *21H BORE/STROKE RATIO = ,F10.6/
16100       *19H  BORE            = ,F10.6,2HMM/
16110       *19H  STOKE           = ,F10.6,2HMM/
16120       *19H INLET VALVE DIA  = ,F10.6,2HMM/
16130       *19H EXH VALVE DIA    = ,F10.6,2HMM/
16140       *19H CLEARANCE VOLUME= ,F10.6,2HCC/
16200       *19H COMP RATIO       = ,F10.6/
16300       *19H SURFACE/VOL RATIO=,F10.6,2X,4H1/CM/
16400       *25H CHAMBER HEIGHT AT TDC = ,F10.6,2HMM/
16500       *29H DEPTH INLET VALVE POCKETS = ,F10.6,2HMM/
16600       *29H DEPTH EXH VALVE POCKETS   = ,F10.6,2HMM/
16610       *34H VALVE POCKET VOL/CLEARANCE VOL = ,F10.6/
16620       *25H SQUISH AREA/BORE AREA = ,F10.6)
16630        CLVOL=CLVOL*1000.0
16640        GOTO270
16650        WRITE(3,310)QQ,ID,ED,IID,THETA1,THETA2,VOCH,CLVOL,STVR,PIN,
            *PEN,GAPI,GAPE,ARCI,ARCE,VCLS,VICO,VECO,CODI,CODE
16900    310 FORMAT(1H0,F8.1/7(3X,G12.6)/4X,6(3X,G12.6)/8X,6(3X,G12.6))
16980
16984
16987
16990
```

```
17000   270 READ(9,/)N
17200       L=1.99*SS
17300       EVO=444.
17400       EVC=56.
17500       IVO=348.
17600       IVC=250.
17700       YMI=9.525
17800       YME=9.525
17900       LPIP=300.0*(VV/500.0)**0.3333
18000       NNP=20
18100       DPIP=1.4142*DTI
18300       P=2.
18400       Q=10.
18500       R=20.
18600       S=30.
18700       T=40.
18800       CP=-14.9201007
18900       CQ=9.52495484
19000       CR=-6.34995358
19100       CS=2.72140545
19200       CT=-0.50131097
19300       C1=-0.00462
19400       C2=3.72253
19500       C3=-0.91264
19600       C4=-15.49552
19700       CDM=C1*(YMI/ID)+C2*(YMI/ID)**2/2.0+C3*(YMI/ID)**3/3.0+
19800      *C4*(YMI/ID)**4/4.0
19840       CDM=CDM*ID/YMI
19850       TS=330.0
19900       TC=75.
20000       XTC=20.
20100       HV=20000.
20200       EQR=1.0
20300       FARST=0.06455
20400       DPHI=1.0
20500       PO=1.0
20600       TO=20.0
20700       TEM=TO
20800       PP=1.0
20900       PE=1.0
21000       PP2=1.0
21100       MOT=0.0
21200       TW=227.
21300       NCYLS=3
21350       WRITE(3,107)BB,SS,CCR,L,EVO,EVC,IVO,IVC,YMI,YME,DTI,DTE,
21400      *ID,ED,N,P,Q,R,S,T,
21450      *    C1,C2,C3,C4,TS,TC,XTC,HV,EQR,FARST,DPHI,PO,TO,PE,TW\
     \,NCYLS
21500   107 FORMAT(16H OPERATING DATA //7H BORE = ,F10.6,4H MM /10H\
     \ STROKE = ,
21550      *      F10.6,4H MM /14H COMP RATIO = ,F10.4/
21600      *      18H CON ROD LENGTH = ,F10.4,4H MM /
21650      *      7H EVO = ,I5,5H DEG /
21700      *      7H EVC = ,I5,5H DEG /7H IVO = ,I5,5H DEG /7H IVC = \
     \,I5,
21750      *      5H DEG /24H MAX VALVE LIFT INLET = ,F10.4,4H MM /
21800      *      26H MAX VALVE LIFT EXHAUST = ,F10.4,4H MM /
21850      *      20H INLET THROAT DIA = ,F10.4,4H MM /
21900      *      22H EXHAUST THROAT DIA = ,F10.4,4H MM /
21950      *      19H INLET VALVE DIA = ,F10.4,4H MM /
22000      *      21H EXHAUST VALVE DIA = ,F10.4,4H MM /
22050      *      16H ENGINE SPEED = ,F10.4,5H RPM /5H P = ,I5/
```

```
22100      •      5H Q = ,I5/5H R = ,I5/5H S = ,I5/5H T = ,I5/6H C1 = \
     \,F10.6
22150      •      /6H C2 = ,F10.6/6H C3 = ,F10.6/6H C4 = ,F10.6/
22200      •      13H IGN POINT = ,I5,5H DEG /17H COMB DURATION = ,I5,
22250      •      5H DEG /7H XTC = ,I5,5H DEG /25H HEATING VALUE OF\
     \ FUEL = ,
22300      •      F10.1,7H KJ/KG /21H EQUIVALENCE RATIO = ,F10.6/
22350      •      33H STOICHIOMETRIC FUEL AIR RATIO = ,F10.6/
22400      •      13H INCREMENT = ,I5,5H DEG /
22450      •      16H INLET PRESSURE = ,F10.3,5H BAR /
22500      •      21H INLET TEMPERATURE = ,F10.3,7H DEG C /
22550      •      20H EXHAUST PRESSURE = ,F10.3,5H BAR /
22600      •      13H WALL TEMP = ,F10.3,7H DEG C /
22650      •      20H NUMBER OF CYCLES = ,I5)
24000        WRITE(3,109)
24100    109 FORMAT(1HO,9X,35H PRESSURE   TEMP     VOLUME     MASS/
24200       •10X,23H   BAR     DEG K      CC,8X,2HKG)
24300        PI=3.1415)
24400        N=I/60.0
24500        PHI=0.0
24600        PR=P0
24700        TO=T0+273.0
24800        TR=T0
24900        TW=TW+273.0
25000        TE=1000.0
25100        TEM=T0
25200        TM=0.0
25300        TU=T0
25400        X0=0.0
25500        XI=0.0
25600        E0=0.0
25700        N0=0.0
25800        NI=0.0
25900        II=0.0
26000        I0=0.0
26100        MIIT=0.0
26200        MII=0.0
26300        QD=0.0
26400        QOD=0.0
26500        MD=0.0
26600        FLOI=0.0
26700        PD=0.0
26750        BAREA=0.0
26760        UBAREA=SURFA
26800        PRATIO=PP/PR
26900        K=1.4
27000        RG=0.286
27100        CV=0.718
27200        ATI=2.•PI•DTI••2/4.0E+6
27300        LPIP=LPIP/1000.0
27400        AP=PI•DPIP••2/4.0E+6
27500        DXX=1.0/(NNP-1)
27600        CA0=SQRT(K•RG•1000.0•T0)
27700        DZZ=(CA0•DPHI/(360.0•N•LPIP))
27800        XXI=(720+IVC-IVO)/2
27900        XXE=(720-EVO+EVC)/2
28000        H2=DPHI/(360.0•N)
28100        SV=VV•1000.0
28200        VT=CLVOL
28300        MT=PR•VT/(RG•T0•1.0E7)
28400        M=MT
28500        F=0.05
```

```
28520        CI=37.0
28525        AK=1.0
28530        LLL=1.0
28600        NC=0
28700        DD=0.92
28800        VP=2.0*N*SS/1000.0
28900        QULP=((BB/DTI)**2*VP)/(2*CAO*COM)
29200      1 CONTINUE
29300        V=VOM(PHI,BB,SS,CCR,L,PI)
29400        VO=VOT(PHI,PI,BB,SS,N,L)
29410        PHI=PHI+180.0
29420        PHIR=PHI*0.0174533
29430        S21=((SS/2000.0)*(1.0+COS(PHIR))+L/1000.0-
29440       *L*SQRT(1.0-(SS/(2.0*L))**2*SIN(PHIR)**2)/1000.0)
29450        K22=K2+S21*1000.0/BB
29460        BWA=K22*PI*BB**2
29470        SURFA=ACYLH+BWA+APISCR
29480        PHI=PHI-180.0
29600        A1=RG*1000.0*K/V
29700        DZT=DZZ
29800        DZA=0.0
29810        IF((PHI.GT.PS).AND.(LLL.EQ.0)) GOTO 88
29820        QHD=HTFR(PR,TR,VP,TW,SURFA)
29830        GOTO 150
29840       88 HTAREA=(BAREA*TB+UBAREA*TU-SURFA*TW)/(TW-TR)
29850        QHD=HTFR(PR,TR,VP,TW,HTAREA)
29900      150 DO 74 I=1,NNP-1,1
30000        DZ1=DXX/(0.5*(LAM(1,I)+BETA(1,I))+ABS(2.5*(LAM(1,I)-
30100       *BETA(1,I))))
30200        IF(I.EQ.1) GOTO72
30300        DIN=DZ1
30400       72 IF(DZ1-DIN)73,74,74
30500       73 DIN=DZ1
30600       74 CONTINUE
30700        IF(DIN.GT.DZT) GOTO76
30800        DZ=0.95*DIN
30900        GOTO77
31000       76 DZ=DZT
31100       77 DZDX=DZ/DXX
31200      204 CONTINUE
31300        H=DZ*LPIP/CAO
31400      105 CONTINUE
31500        IF((PHI.GE.IVC).AND.(PHI.LE.EVO)) GOTO8
31600        IF(PHI.GE.EVC)GOTO2
31700        THETA=(PHI+(XXE-EVC))/XXE
31800        GOTO32
31900        7 IF(PHI.LE.IVC) GOTO10
32000        IF(PHI.LE.IVO) GOTO 96
32100        THETA=((IVO+XXI)-PHI)/XXI
32200        GOTO 13
32300        8 IF((PHI.GE.PS).AND.(PHI.LT.(TS+TC))) GOTO50
32500        GOTO 52
32600       96 NO=0.0
32700        NI=0.0
32800        II=0.0
33000        MII=0.0
33100        MIIT=0.0
33200        MOI=0.0
33300        MOIT=0.0
33400        UU=0.0
33500        GOTO 52
```

```
33600      2 IF((PHI.GE.EVO).AND.(PHI.LE.(EVO+720))) GOTO 30
33700        XO=0.0
33800        XI=0.0
33900        EI=0.0
34000        EO=0.0
34100        GOTO 7
34200     10 IF(PHI.LE.(IVC-XXI)) GOTO12
34300        THETA=((IVC-XXI)-PHI)/XXI
34400        GOTO 13
34500     12 THETA=(PHI-(IVC-XXI))/XXI
34600     13 LF=LFT(THETA,YMI,P,Q,R,S,T,CP,CQ,CR,CS,CT)
34700        LD=LF/ID
34800        CDI=CD1(LD,C1,C2,C3,C4)
34900        IF(PR.GT.PP)GOTO20
35000 C      INFLOW THROUGH INLET VALVES
35100        FCTN=FP1P2(PR,PP)
35200        IF(TEM.EQ.T0) GOTO 14
35300 C      PRODUCTS
35400        NI=Z1(CDI,DTI,PP,TEM,FCTN)
35500        RHOP=PP*100.0/(RG*TEM)
35600        UU=NI/(RHOP*AP)
35700        II=NI*A1*TEM*(PP/P0)**((K-1.0)/K)
35800        MII=MO1+NI*H
35900        MIIT=MO1T+MII*TEM
36000        TEM=MIIT/MII
36100        IF(TEM.LT.T0) TEM=T0
36200        NO=0.0
36300        IO=0.0
36400        GOTO 50
36500 C      FRESH CHARGE,
36600     14 NI=Z1(CDI,DTI,PP,T0,FCTN)
36700        RHOP=PP*100.0/(RG*T0)
36800        UU=NI/(RHOP*AP)
36900        II=NI*A1*T0*(PP/P0)**((K-1.0)/K)
37000        TMI=TMI+H*NI
37100        NO=0.0
37200        IO=0.0
37300        GOTO 50
37400 C      OUTFLOW THROUGH INLET VALVES
37500     20 FCTN=FP1P2(PP,PR)
37600        NO=-Z(CDI,DTI,PR,M,V,FCTN)
37700        RHOP=PP*100.0/(RG*TEM)
37800        UU=NO/(RHOP*AP)
37900        IO=NO*A1*TR*(PR/P0)**((K-1.0)/K)
38000        NI=0.0
38100        II=0.0
38200        GOTO 50
38300     30 IF(PHI.LE.(EVO+XXE)) GOTO 31
38400        THETA=(PHI-(EVO+XXE))/XXE
38500        GO TO 32
38600     31 THETA=((EVO+XXE)-PHI)/XXE
38700     32 LF=LFT(THETA,YME,P,Q,R,S,T,CP,CQ,CR,CS,CT)
38800        LD=LF/ED
38900        CDE=CD1(LD,C1,C2,C3,C4)
39000        IF(PR.GT.PE) GOTO 40
39100 C      INFLOW THROUGH EXHAUST VALVES
39200        FCTN=FP1P2(PR,PE)
39300        XI=Z(CDE,DTE,PE,M,V,FCTN)
39400        EI=XI*A1*TE*(PE/P0)**((K-1.0)/K)
39500        XO=0.0
39600        EO=0.0
39700        GOTO 7
```

```
39800 C       OUTFLOW THROUGH EXHAUST VALVES
39900      40 FCTR=FP1P2(PE,PR)
40000         XK=-D(XDE,DTE,PE,TE,V,FCTR)
40100         TE=TR
40200         EQ=XK*A1*TR*(PR/PE)**((K-1.0)/K)
40300         XI=0.0
40400         EI=0.0
40500         GOTO 7
40700 C       MOTORING.
40800      50 IF(NOT.EQ.1) GOTO 52
40850         IF(PHI.EQ.TS)GOTO51
40900 C       NO COMBUSTION.
41000         IF(LLL.EQ.1) GOTO 52
41050 C       COMBUSTION MODEL.
41055      51 LLL=0.0
41100         IF(PHI.NE.TS) GOTO 87
41200 C       INITIAL SETUP.
41300         VS=VOL(PHI,BB,SS,CCR,L,PI)
41350         B11=0.0
41360         R11=0.0
41400         VC=V
41500         TU=TR
41550         PC=PR
41560         TCC=TR
41600         U2=M
41700         RU=PR*1.0E+2/(RG*TU)
41800         HSP=H1+K22*BB+(VS-CLVOL*1.0E-9)*4.0E+9/(PI*BB**2)
41900         UL=U(EQR,TU)
41910 C         IGNITION DELAY PERIOD CALCULATION.
41920         S=100./TU
41930         MU=(TU**0.5/(0.5528+2.811*S+13.5083*S**2+39.353086*S**3
41940        *-41.419387*S**4))*10.0E-7
41950         IG=CI*(VP*MU/RU)**0.3333*(HSP/UL)**0.6667
41970         XM=(-2.25037-ALOG(AK))/ALOG(IG/TC)-1.0
41973         TG=IG*H2/DPHI
41975         IG=INT(IG/2.0)*2
41980         XG=TG*UL*1000.
42000      87 CONTINUE
42050         PHI=PHI+DPHI
42100         IF(PHI.LE.(TS+IG)) GOTO 83
42150 C       COMBUSTION AFTER IGNITION DELAY.
42200         HI=SS+H1+K2*BB
42300         HSP=H1+K22*BB+(VS-CLVOL*1.0E-9)*4.0E+9/(PI*BB**2)
42400         HF=(HSP/HI)**0.3333
42500         UL=U(EQR,TU)
42600         RI=PR*1.0E+2/(RG*TI)
42700         RU=PR*1.0E+2/(RG*TU)
42800         RHF=(RI/RU)**0.1111
42900         FF=150.000*(HF*(YMI/1000.)**0.3333*GULP*QQ*RHF*
43000        *UL**(-0.3333))
43100         FF=FF/(60.0*N)
43200         FSR=1.0+FF*N*60.0
43230         WRITE(6,/)PHI,HF,YMI,GULP,QQ,RHF,FF,FSR,UL
43250         GOTO 84
44400 C       COMBUSTION DURING IGNITION DELAY.
44450      83 IF(PHI.EQ.(TS+IG)) TI=PHI
44800         XF=1.0-EXP(-AK*((PHI-TS)/TC)**(1.0+XM))
44900         XI=INT(1000.*XF)/1000
45000         B22=XF*M
45100         MB=B22-B11
45200         U2=M-B22
```

```
45400          VF=VF+VB
45500          VU=VC-VF
45600          CALL FLFRNT(2.0,0.0,VF,RDS,BAREA,UBAREA)
45700          RD=RDS
45800          UF=(RD-R11)/(H2*1000.0)
45900          R11=RD
46000          RD=RD
46100          FSR=UF/UL
46200          GOTO 85
46300      84  UF=UL*FSR
46350          DR=UF*H2*1000.0
46400          RD=RD+DR
46430          VY=VF
46500          CALL FLFRNT(1.0,RD,0.0,RDS,BAREA,UBAREA)
46550          VU=VC-VF
46600          VB=VF-VY
46700          MB=M*VB/VC
46800          B22=B22+MB
46900          U2=M-B22
46950 C          HEAT RELEASE AT CONSTANT VOLUME.
47000      85  QB=MB*HV*EQR*FARST*(1.0-F)
47100          QD=QB
47200          CALL INTE(XF,EQR,AA1,AA2,AA3)
47300          DW=0.0
47400          E3=(QD-DW)/M
47500          E2=E1+E3
47600          AA4=AA1-E2
47700          TA=(-AA2+SQRT(AA2**2-(4.0*AA3*AA4)))/(2.0*AA3)
47800          PA=PC*TA/TCC
47850          QHD=HTFR(PA,TA,VP,TW,SURFA)
47900          E1=E2
47950 C          HEAT TRANSFER WITH VOLUME CHANGE.
48000          VO=VOM(PHI,BB,SS,CCR,L,PI)
48100          QD=TH*QHD
48200          DW=PR*(VO-VC)*100.
48250          E3=(QD-DW)/M
48300          E2=E1+E3
48400          AA4=AA1-E2
48500          TR=(-AA2+SQRT(AA2**2-(4.0*AA3*AA4)))/(2.0*AA3)
48600          PR=PA*VC*TR/(VO*TA)
48610          IF(PHI.LE.(TS+IG)) GOTO 333
48630          IF(PHI.GE.(TS+IG)) GOTO334
48640          T2=TR
48650          T3=TR
48660          GOTO 335
48700      334 K=GA(TU)
48800          T2=(PR/PC)**((K-1.0)/K)*TU
48900          EU=AA1+AA2*T2+AA3*T2**2
49000          EB=(M*E2-EU*U2)/B22
49100          AA4=AA1-EB
49140          WRITE(6,/)PR,PC,TU,M,E2,U2,B22
49150          WRITE(6,/)K,AA1,AA2,AA3,AA4,T2,EU,EB
49200          T3=(-AA2+SQRT(AA2**2-(4.0*AA3*AA4)))/(2.0*AA3)
49300          XF=B22/M
49400      335 VU=VU*(PA/PR)**(1.0/K)
49500          VF=VO-VU
49600          CALL FLFRNT(2.0,0.0,VF,RDS,BAREA,UBAREA)
49700          RD=RDS
49800          IF(XF.GE.1.0) GOTO 86
49900          TU=T2
50000      333 VT=(RD-RO)/(H2*1000.0)
```

```
50100          TB=T3
50200          TCC=TR
50300          PC=PR
50400          VC=V0
50500          E1=E2
50600          B11=B22
50700          R0=RD
50810          GOTO 104
50820 C        END OF COMBUSTION.
50830     86   TC=PHI-TS
50840          LLL=1
50850          GOTO 104
51000 C        RUNGE KUTTA SOLUTION
51100     52   CONTINUE
51200          IF(NN.EQ.4)GOTO104
51300          IF(NN.EQ.3)GOTO103
51400          IF(NN.EQ.2)GOTO102
51500          IF(NN.EQ.1)GOTO101
51600          P01=PR
51700          KK1=H*FXY(RG,QHD,V,CV,P01,VD,K,E0,I0,E1,I1)
51800          P02=P01+KK1/(2.0E5)
51900          PHI=PHI+DPHI/2.0
52000          QHD=HTFR(P02,TR,VP,TW,SURFA)
52100          VD=VDT(PHI,PI,BB,SS,N,L)
52200          V=VOM(PHI,BB,SS,CCR,L,PI)
52300          PR=P02
52400          NN=1
52500          GOTO105
52600    101   KK2=H*FXY(RG,QHD,V,CV,P02,VD,K,E0,I0,E1,I1)
52700          P03=P01+KK2/(2.0E5)
52800          QHD=HTFR(P03,TR,VP,TW,SURFA)
52900          PR=P03
53000          NN=2
53100          GOTO105
53200    102   KK3=H*FXY(RG,QHD,V,CV,P03,VD,K,E0,I0,E1,I1)
53300          P04=P01+KK3/1.0E5
53400          PHI=PHI+DPHI/2.0
53500          VD=VDT(PHI,PI,BB,SS,N,L)
53600          V=VOM(PHI,BB,SS,CCR,L,PI)
53700          QHD=HTFR(P04,TR,VP,TW,SURFA)
53800          PR=P04
53900          NN=3
54000          GOTO105
54100    103   KK4=H*FXY(RG,QHD,V,CV,P04,VD,K,E0,I0,E1,I1)
54200          P1=P01+(KK1+2.0*KK2+2.0*KK3+KK4)/(6.0E5)
54300          DELP=P1-P01
54400          PR=P1
54500          QHD=HTFR(P04,TR,VP,TW,SURFA)
54600          NN=4
55000          GOTO105
55100    104   CONTINUE
55200          NN=0
55300          IF(PHI.LE.648.0)GOTO89
55400     89   CONTINUE
```

```
55500 C      WAVE ACTION IN INLET PIPE
55600 C      BY METHOD OF CHARACTERISTICS
55700 C      NO HEAT TRANSFER NO FRICTION.
55800        IF(TEM.LT.TO) GO TO 21
55900        CA1=SQRT(K*RG*1000.0*TO)
56000        GO TO 22
56100     21 CA1=SQRT(K*RG*1000.0*TEM)
56200     22 CAR=SQRT(K*RG*1000.0*TR)
56300        CDA=CA1/CAO
56400        CARD=CAR/CAO
56500        UDA=UU/CAO
56600        LAM(2,NNP)=LAM(1,NNP)+DZDX*(3.0*LAM(1,NNP)-2.0*BETA(1,NNP))
56700       **(LAM(1,NNP-1)-LAM(1,NNP))
56800        IF(PHI.LT.IVC) GOTO 26
56900        IF((PHI.GE.IVO).AND.(PHI.LT.(IVC+720)))GOTO 26
57000 C      REFLECTION FROM CLOSED VALVE.
57100        BETA(2,NNP)=LAM(2,NNP)
57200        PP=P0*((BETA(2,NNP)+LAM(2,NNP))/2.0)**7
57300        GOTO 58
57400 C      REFLECTION AT OPEN VALVE.
57500     26 IF(PHI.LT.640) GOTO 112
57600    112 BX=PR**0.143/P0
57700        CX=(CDI*ATI/AP)**2
57800        BX1=BX**10
57900        GX=5.0/BX1
58000        GX1=10.0*LAM(2,NNP)/BX1
58100        GX2=5.0*LAM(2,NNP)**2/BX1
58200        DD=DD-0.01
58300        IF(DD.LT.0.92) GOTO 122
58400        GOTO 44
58500    122 DD=0.92
58600     44 DD=DD+0.002
58700        IF(PHI.LT.IVO) GOTO 222
58800    222 CONTINUE
58900        DX1=DD**10
59000        DX2=GX*DX1*DD*DD-GX1*DX1*DD+GX2*DX1-
59100       *6.0*CX*DD*DD+10.0*LAM(2,NNP)*CX*DD-
59200       *5.0*LAM(2,NNP)**2*CX+BX**2*CX
59300        IF(DX2) 25,92,803
59400    803 DAX=DD
59500        DX4=DX2
59600        IF(DD.GT.1.20) GOTO 93
59700        GOTO 44
59800     93 DD=LAM(2,NNP)
59900        GOTO 92
60000     25 DD=DAX+DX4*(DD-DAX)/(DX4-DX2)
60100     92 BETA(2,NNP)=2.0*DD-LAM(2,NNP)
60200        CARD=0.5*(LAM(2,NNP)+BETA(2,NNP))
60300        UDA=-2.5*(BETA(2,NNP)-LAM(2,NNP))
60400        PP=P0*CARD**7
60500     58 CONTINUE
60600        DO 23 I=2,NNP,1
60700        LAM(2,I)=LAM(1,I)+DZDX*(LAM(1,I-1)-LAM(1,I))*
60800       *(3.0*LAM(1,I)-2.0*BETA(1,I))
60900     23 CONTINUE
61000        DO 24 J=1,(NNP-1),1
61100        BETA(2,J)=BETA(1,J)+DZDX*(BETA(1,J+1)-BETA(1,J))*
61200       *(3.0*BETA(1,J)-2.0*LAM(1,J))
61300        IF(BETA(2,J).LT.1.5) GOTO444
61400        BETA(2,J)=1.5
```

```
51500  444 IF(J.NE.1) GOTO24
51600      LAM(2,1)=2.0-BETA(2,1)
51700   24 CONTINUE
51800      DO 27 I=1,NP,1
51900      LAM(1,I)=LAM(2,I)
52000      BETA(1,I)=BETA(2,I)
52100   27 CONTINUE
52200      XD=XI+XI+XO+XO
52300      FLOO=FLOO-XO*H
52400      FLOI=FLOI+XI*H
52450      FLEO=FLEO-XO*H
52460      FLEI=FLEI+XI*H
52500      M=M+MD*H
52600      DZA=DZA+DZ
52700      IF(DZA-DZZ)71,28,28
52800   71 DZT=DZZ-DZA
52900      PHI=PHI-DPHI
53000      XI=0.0
53100      NI=0.0
53200      XO=0.0
53300      MO=0.0
53400      EI=0.0
53500      EO=0.0
53600      II=0.0
53700      IO=0.0
53800      GOTO150
53900   28 CONTINUE
54000      P7=PO*(0.5*(LAM(2,7)+BETA(2,7)))**7
54100      DW=PR*VO*100.0*H2
54200      W=W+DW
54300      IF(PHI.EQ.720.0) GOTO 111
54400    4 IF(PHI.NE.IVC) GO TO 6
54500      F=(M-(FLOI-FLOO))/M
54600      MOI=0.0
54700      MOIT=0.0
54800      TMI=0.0
54900    6 TR=PR*1.0E2*V/(M*RG)
55000      V=V*1.0E+6
55050      PVEL=CAO*UDA
55100      GOTO80
55300      WRITE(3,/)PHI,PR,PP,PVEL,UDA
55400  103 FORMAT(1H ,I3,5X,4F10.4,E10.4)
55500   80 CONTINUE
55600      V=V*1.0E-6
55700      GOTO 9
55800  111 VOLEF=(FLOI-FLOO)*RG*TO*1.0E+6/(PO*VV)
55850      VOLTR=(FLOI+FLEI-FLOO-FLEO)*RG*TO*1.0E+6/(PO*VV)
55900      WRITE(3,/)W/H2,VOLEF,VOLTR,FLOI,FLEI,FLOO,FLEO
56100      W=0.0
56200      FLOI=0.0
56300      FLOO=0.0
56350      FLEI=0.0
56360      FLEO=0.0
56400      PHI=0
56450      LLL=0
56500      NC=NC+1
```

```
66600     9 IF(NC.EQ.NCVLS) GOTO 5
66700       E0=0.0
66800       E1=0.0
66900       I0=0.0
67000       I1=0.0
67100       X1=0.0
67200       X1=0.0
67300       X0=0.0
67400       X0=0.0
67500       GOTO 1
67600     5 GOTO 270
67700       END
67800       FUNCTION CD1(A,A1,A2,A3,A4)
67900            CD1=A1+A2*A+A3*A**2+A4*A**3
68000       RETURN
68100       END
68200       FUNCTION FP1P2(P1,P2)
68300            P12=P1/P2
68400            IF(P12.GT.0.5283) GOTO 1
68500            P12=0.5283
68600     1      GK=1.4
68700            FP1P2=SQRT(P12**(2.0/GK)-P12**((GK+1.0)/GK))
68800       RETURN
68900       END
69000       FUNCTION Z(CD1,D,P,M,V,FCTN)
69100       CPG=1.005
69200       RG=0.287
69300            PI=3.14159
69400            A=PI*D**2/2.0E6
69500       Z=CD1*A*SQRT(2.0*CPG*P*M*1.0E5/(RG*V))*FCTN
69600       RETURN
69700       END
69800       FUNCTION Z1(CD1,D,P,T,FCTN)
69900       RG=0.287
70000       CPG=1.005
70100            PI=3.14159
70200            A=PI*D**2/2.0E6
70300       Z1=CD1*A*P*1.0E5*SQRT(2.0*CPG/(RG*RG*T*1.0E3))*FCTN
70400       RETURN
70500       END
70600       REAL FUNCTION LFT(THETA,YM,P,Q,RD,S,T,CP,CQ,CR,CS,CT)
70700            LFT=YM+THETA**P*CP+THETA**Q*CQ+THETA**RD*CR+THETA**S*CS+
70800      *       THETA**T*CT
70900       RETURN
71000       END
71100       FUNCTION FXY(RD,QD,V,CV,P,VD,K,E0,I0,E1,I1)
71200            FXY=RD*QD/(V*CV)-P*1.0E+5*VD*K/V+E0+I0+E1+I1
71300       RETURN
71400       END
71500       FUNCTION HCAL(X,B)
71600       HCAL=X*SQRT((B/2.0)**2-X*X)+(B/2.0)**2*ARCSIN(X*2.0/B)
71700       RETURN
71800       END
71900       FUNCTION ARCSIN(X)
72000       Y=SQRT(1.0-X*X)
72100       ARCSIN=ATAN(X/Y)
72200       RETURN
72300       END
72400       FUNCTION VCAL(Y,B,THETA)
72500       VCAL=2.*TAN(THETA)*(X/2.*(X*SQRT((B/2.)**2-X*X)
72600      *+(B/2.)**2*ARCSIN(2.*X/B))+(((B/2.)**2-X*X)**1.5)/3.0)
72700       RETURN
72800       END
```

```
72900       FUNCTION VOD(X,A,B,X2,THETA)
73000       VOD=-(2.*TAN(THETA)/3.)*(((B/2.)**2-X*X)**1.5
73100      *-((B/2.)**2-X2*X2)**1.5)-TAN(THETA)*X2*A
73200       RETURN
73300       END
73400       SUBROUTINE FLFRNT(XX,RAD,VF,RDS,BAREA,UBAREA)
73500       COMMON B3,PHR,THETA1,THETA2,HD,KK,K1,K2,K3,K22,B1,AB,
73600      *ARC1,ARCE,C,COD1,CODE,PIN,PEN,ED,ID,H1,SURFA
73650       VF=VF*1.0E+9
73700       PI=3.14159265
73800       V1=0.0
73900       VE=0.0
74000       AREA4=0.0
74100       AREA5=0.0
74200       DR=1.0
74300       RD=0.0
74400       V=0.0
74500       AREA=0.0
74600     5 R1=H1+(BB*B1/2.0)*TAN(THETA1)+K22*B1
74700       R2=BB/2.0-H1
74800       R3=(AB/2.0)/COS(PHR/2.0)
74900       R4=(BB/2.0)/COS(PHR/2.0)
75000       IF(XX.EQ.2) GOTO 10
75100       DO 170 RD=DR,RAD,DR
75200    10 DO 170 RD=DR,R4,DR
75300    20 RT=RD
75350 C     BASIC FLAME FRONT AREA.
75400       AREA=2.0*RD**2*(PI-PHR)
75450 C     BASIC BURNT ZONE AREA.
75500       AREA1=PI*RD**2
75600       IF(RD.GT.R1) GO TO 30
75700    70 IF(RD.GT.R2) GO TO 40
75800   110 IF(RD.GT.R3) GOTO 50
75900       GO TO 60
75950 C     INTERSECTION WITH PISTON.
76000    30 AREA=AREA-(RD-R1)*2.0*PI*RD
76100       AP=PI*(RD**2-R1**2)
76200       GOTO 70
76300    40 RT=R2
76350 C     INTERSECTION WITH CURVED REGION.
76400       IF(RD.GT.BB/2) GOTO 80
76500       DR1=H1*(1.0-SQRT(1.0-((RD-R2)/H1)**2))**2
76600       GOTO 90
76700    80 DR1=H1
76800    90 AA1=ARC1*DR1
76900       AA2=ARCE*DR1
77000       AA3=2.0*BB*B1*DR1
77100       AREA=AREA-(AA1+AA2+AA3)
77200       IF(RD.GT.BB/2) GOTO 100
77300       AR1=ARC1+B1*BB/2.0
77400       AR2=ARCE+B1*BB/2.0
77500       AREA2=(AR1*DR1/(H1-DR1)+DR1*SQRT(1.0+(AR1/H1)
77600      ***2))*DR
77700       AREA3=(AR2*DR1/(H1-DR1)+DR1*SQRT(1.0+(AR2/H1)
77800      ***2))*DR
77900       AREA4=AREA4+AREA2
78000       AREA5=AREA5+AREA3
78100       ADA=2.0*(AREA4+AREA5)
78200   100 GOTO110
78300    50 Z=SQRT(1.0-(R3/RD)**2)
78400       U=ATAN(Z/SQRT(1.0-Z**2))
```

```
      Y=4.0*(RD-R3)*RD*SIN(PHR/2.0)*U
      AREA=AREA+Y
   60 BAREA=AREA+2.0*RT*B1*B3+ADA+AP
      IF(RD.LT.H1) GOTO 130
      IF(CODE.GT.0.0) GOTO 140
      AV=0.0
      GOTO 120
  250 IF(CODE.GT.0.0) GOTO 140
      AV=0.0
      GOTO 120
  130 NN=0
      G=GAPI
      P=PIN
      II=ID
      CD=CODI
      T=THETA1
      GOTO 150
  140 NN=1
      G=GAPE
      P=PEN
      II=ED
      CD=CODE
      T=THETA2
      GOTO 150
  120 V1=(AREA+AV)*DR
      AV=0.0
      V=V+V1
      IF(VF.EQ.0.0) GOTO 160
      IF(V.GE.VF)GOTO 250
      GOTO 170
  160 IF(RD.GE.RAD) GOTO 250
  170 CONTINUE
  150 RC=SQRT(RD**2-H1**2)
      IF(P.LT.II) GOTO 180
C     FULL CUTOUTS.
      RR=(II/2.0)**2+(K3*II-CD*(2.0*P/II-1.0))**2
      DC=SQRT(RR-H1**2)
      R5=SQRT(DC**2+((C*BB+II)/2.0)**2)-II/2.0
      GOTO 190
C     PARTIAL CUTOUTS.
  180 Y1=SQRT(P*II-P**2)
      R5=SQRT(Y1**2+G**2)
  190 R6=SQRT((G+P/COS(T))**2+((II+C*BB)/2.0)**2)
      IF((RC.GT.R5).AND.(RC.LT.R6)) GOTO 200
      AC=0.0
      GOTO 240
C     VALVE POCKET AREA CALCULATION.
  200 E=(RC-G)/COS(T)-(P-II/2.0)
      IF(E.GT.II/2.0) GOTO 240
      YY=SQRT((II/2.0)**2-E**2)
      Z3=((II+C*BB)/2.0-YY)/RC
      AL=ATAN(Z3/SQRT(1.0-Z3**2))
      IF(P.LT.II) GOTO 210
C     FULL CUTOUT.
      PS=ATAN(((II+C*BB)/2.0)/(II/(2.0*COS(T))+G))
      AR=2.0*RC*(PS-AL)
      GOTO 220
```

```
C      PARTIAL CUTOUT.
  210  Z2=Q/RC
       BE=ATAN(Z2/SQRT(1.0-Z2**2))
       AR=RC*(PI/2.0-AL-BE)
  220  H3=(RC-Q)*CO*COS(T)/P
       AC=H3*AR
  240  IF(NN.EQ.1) GOTO 230
       AVI=AC
       VI=VI+AVI*DR
       GOTO 250
  230  AVE=AC
       VE=VE+AVE*DR
       AV=AVI+AVE
       NN=0
  250  RDS=RD
       VF=V/1.0E+9
       RETURN
       END
       FUNCTION VOM(PHI,BB,SS,CCR,L,PI)
       PHI=PHI+180.0
       PHIR=PHI*0.0174533
       VOM=PI*BB**2/4.0E+6*(SS/((CCR-1.0)*1000.0)+(SS/2000.0)
      **(1.0+COS(PHIR))+L/1000.0-L*SQRT(1.0-(SS/(2.0*L))**2
      **SIN(PHIR)**2)/1000.0)
       PHI=PHI-180.0
       END
       FUNCTION VDT(PHI,PI,BB,SS,N,L)
       PHI=PHI+180.0
       PHIR=PHI*0.0174533
       VDT=(PI**2*BB**2*N*SS/4.0E+9)*((SIN(PHIR*2.0)*SS/(4.0*L))/
      *(SQRT(1.0-(SS/(2.0*L))**2*SIN(PHIR)**2))-SIN(PHIR))
       PHI=PHI-180.0
       END
       FUNCTION HTFR(PT,TR,VP,TW,SURFA)
       HTCO=2.465044*(VP**0.33333)*SQRT(PT*TR)
       HTFR=HTCO*SURFA*(TW-TR)*1.0E-6
       END
       SUBROUTINE  INTE(XF,EQR,AA1,AA2,AA3)
       XX=140.0*XF*FARST
       AA1=-23.787+5.797*XX+0.8*XX**2
       AA2=0.798-0.00538*XX+0.0011996*XX**2
       AA3=(6.933+0.3283*XX+0.036*XX**2)*0.00001
       RETURN
       END
       FUNCTION U(EQR,TL)
       FI=4.69-8.72*(1.1-EQR)**2
       U=57.0*0.287*4.83E-7*TL**1.647*FI
       END
       FUNCTION GA(T)
       C1=-23.787+(1.085*T)+6.933E-5*T**2
       C2=-23.787+(0.7925*T)+6.933E-5*T**2
       GA=C1/C2
       END
```

APPENDIX A9

Schematic of mass fraction burned profile taken from Reference 53.

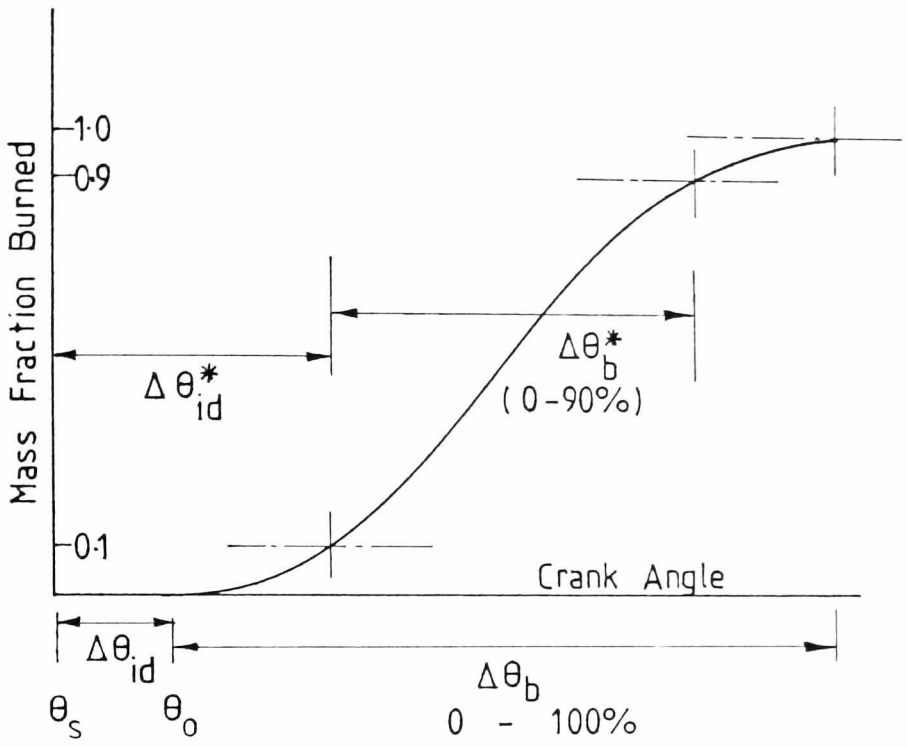

Schematic of mass fraction burned profile.
θ_s is spark timing, θ_o is start of combustion, $\Delta\theta_{id}$ is the ignition delay and $\Delta\theta_b$ is the combustion duration. $\Delta\theta^*_{id}$ and $\Delta\theta^*_b$ are the usual empirical definitions of ignition delay and combustion duration (0-100% and 10-90% burned respectively)